

# UNCLASSIFIED

AD NUMBER
AD296577
NEW LIMITATION CHANGE
TO Approved for public release, distribution unlimited
FROM Distribution authorized to DoD and DoD contractors only; Administrative/Operational Use; 15 Oct 1962. Other requests shall be referred to Director, Advanced Research Projects Agency, Washington, DC.
AUTHORITY
USNSSC ltr, 27 Mar 1970

THIS PAGE IS UNCLASSIFIED

UNCLASSIFIED

---

AD **296 577**

*Reproduced  
by the*

ARMED SERVICES TECHNICAL INFORMATION AGENCY  
ARLINGTON HALL STATION  
ARLINGTON 12, VIRGINIA



---

UNCLASSIFIED

**NOTICE:** When government or other drawings, specifications or other data are used for any purpose other than in connection with a definitely related government procurement operation, the U. S. Government thereby incurs no responsibility, nor any obligation whatsoever; and the fact that the Government may have formulated, furnished, or in any way supplied the said drawings, specifications, or other data is not to be regarded by implication or otherwise as in any manner licensing the holder or any other person or corporation, or conveying any rights or permission to manufacture, use or sell any patented invention that may in any way be related thereto.

296 577

GEST-2009  
RESEARCH AND  
DEVELOPMENT REPORT  
OCTOBER 15, 1962

ACCENT  
VALUE

296 577



2  
CATALOGED BY ASTIA  
AS AD NO. 1

# TECHNICAL SUMMARY REPORT THERMIONIC EMITTER MATERIAL PROPERTIES

FEB 23 1963  
TISIA

By  
L.N. GROSSMAN  
E.W. HOYT  
J.H. INGOLD  
A.J. KAZNOFF  
M.J. SANDERSON

PERIOD COVERED  
SEPTEMBER 15, 1961 THROUGH SEPTEMBER 15, 1962

PREPARED FOR  
DEPARTMENT OF THE NAVY  
BUREAU OF SHIPS, CODE 342B  
AND  
ADVANCED RESEARCH PROJECTS AGENCY  
WASHINGTON 25, D.C.

CONTRACT NO. 84289  
PROJECT SERIAL NO. SR0071201  
ARPA ORDER NO. 219-61, TASK NO. 2

SPECIAL PURPOSE NUCLEAR SYSTEMS OPERA

GENERAL  ELECTRIC

VALLECITOS ATOMIC LABORATORY  
PLEASANTON, CALIFORNIA

NO. OTS



GEST-2009

Research and  
Development Report

October 15, 1962

TECHNICAL SUMMARY REPORT

THERMIONIC EMITTER  
MATERIAL PROPERTIES

by

L. N. Grossman, E. W. Hoyt, J. H. Ingold,  
A. I. Kaznoff, M. J. Sanderson

Period Covered

September 15, 1961 through September 15, 1962

Prepared for

Department of the Navy

Bureau of Ships, Code 342B

and

Advanced Research Projects Agency

Washington 25, D. C.

Contract NObs 86289

Project Serial No. SR0071201

ARPA Order No. 212-61, Task No. 2

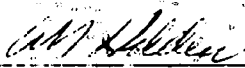
Special Purpose Nuclear Systems Operation

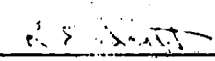
**GENERAL ELECTRIC**

VALLECITOS ATOMIC LABORATORY  
PLEASANTON, CALIFORNIA

866-TIO-21

APPROVED:

  
A. N. Holden  
Manager, Metallurgy and Ceramics

  
R. E. Scott  
Manager, Applications Engineering

## LEGAL NOTICE

This report was prepared as an account of Government sponsored work. Neither the United States, nor the Department of Defense, nor any person acting on behalf of the Department of Defense:

- A. Makes any warranty or representation, expressed or implied with respect to the accuracy, completeness, or usefulness of the information contained in this report, or that the use of any information, apparatus, method, or process disclosed in this report may not infringe privately owned right; or
- B. Assumes any liabilities with respect to the use of, or for damages resulting from the use of any information, apparatus, method, or process disclosed in this report.

As used in the above, "person acting on behalf of the Department of Defense" includes any employee or contractor of the Department, or employee of such contractor, to the extent that such employee or contractor of the Department of Defense, or employee of such contractor prepares, disseminates, or provides access to, any information pursuant to his employment or contract with the Department of Defense, or his employment with such contractor.

TABLE OF CONTENTS

	<u>Page No.</u>
I INTRODUCTION	1-1
II SUMMARY AND RECOMMENDATIONS	2-1
III ELECTRON EMISSION MEASUREMENTS	3-1
IV THERMOPHYSICAL PROPERTY MEASUREMENTS	4-1
V CESIUM COMPATABILITY WITH SELECTED THERMIONIC EMITTER MATERIALS	5-1
VI GRAIN GROWTH AND MICROSTRUCTURAL CHANGES IN REFRACTORY COMPOUND THERMIONIC EMITTER MATERIALS	6-1
VII THERMAL CYCLING OF SELECTED THERMIONIC EMITTER MATERIALS	7-1
VIII FLEXURAL STRENGTH APPARATUS FOR USE TO 2000°C	8-1
IX PHYSIOCHEMICAL PROPERTIES OF SELECTED THERMIONIC EMITTER MATERIALS	9-1
ACKNOWLEDGEMENTS	

## I. INTRODUCTION

On September 7, 1961, the General Electric Company submitted a proposal to the Advance Research Project Agency for a three-year program of experimental studies on thermionic converter materials. The work proposed consisted of a systematic and continuing effort to obtain the thermal, mechanical, chemical, and electrical properties of carbides and borides of rare earth and transition metals which might be used in thermionic converters. (1) The work schedule proposed was as follows:

	<u>1st Year</u>	<u>2nd Year</u>	<u>3rd Year</u>
Material Fabrication	XXXXXX	XX	
Property Measurements	XXX	XXXXXX	
Irradiation Tests		XXXXXX	XXX
Post-Irradiation Measurement		XX	XXXXXX

Subsequent to submission of this proposal, a contract for the first year's program was negotiated with the U. S. Bureau of Ships on November 15, 1961.

This final technical report describes experimental work conducted during the period July 1961 - September 1962 under Contract NObs 86289, ARPA 219-61, Task No. 2. Data obtained are discussed in the separate sections of this report. Quarterly reports (2), (3), (4), (5) prepared during the course of this program were issued on January 15, April 15, July 15, and September 15, 1962.

1. Proposal for Thermionic Converter Materials - GESP-62, September 7, 1961.
2. Progress Report #1, "Thermionic Cathode Material Properties".
3. Progress Report #2, "Thermionic Cathode Material Properties".
4. Progress Report #3, "Thermionic Cathode Material Properties".
5. Progress Report #4, "Thermionic Cathode Material Properties".

## II. SUMMARY AND RECOMMENDATIONS

To meet the needs of nuclear thermionic applications, fuel-emitter materials must possess a combination of specific chemical, nuclear, physical, and mechanical properties. Uranium and thorium-bearing carbides and two selected rare earth hexaborides,  $\text{EuB}_6$  and  $\text{YB}_6$ , have been studied to establish some degree of quantitative knowledge of these materials and the properties which they exhibit in the thermal and chemical environment in which they would most likely be employed in thermionic applications. The data obtained indicate the following:

1. Reproducible, routine fabrication techniques for the preparation of these materials requires further study to assure that control of stoichiometry and density are maintained, and that all shapes and sizes likely to be requested by the engineer, can, in fact, be produced. Fuel-bearing carbide fabrication technology is not as advanced as  $\text{UO}_2$  fabrication technology.
2. On the basis of fabrication and test experience, the thermal shock resistance of the uranium bearing carbides is, very probably, inadequate for applications which require that the fuel emitter retain structural integrity under thermal cycling and/or severe temperature gradient conditions, i.e. unclad applications.
3. The thermophysical properties, thermal conductivity, electrical resistivity, and emissivity of carbide materials are superior to corresponding oxide materials and approach properties exhibited by metallic materials. This is significant in that for clad fuel-emitter concepts both the maximum temperature of a carbide fuel and the temperature gradient in a carbide fuel will be lower for specific applications when compared with corresponding oxide systems.
4. The vapor pressure properties of the rare earth borides indicate that an upper temperature limit in the neighborhood of 1400 C exists for any application involving prolonged time at temperature.
5. The work functions of bulk carbides generally fall slightly below that of tungsten. In application involving thin coatings of carbides, the work function may be modified due to metallic uranium deposits on the emitting surface which result from reduction of the carbide by the substrate material.
6. The work functions of rare earth hexaborides have been reported, although not confirmed, to range from ~4.8 v for  $\text{EuB}_6$  to ~2.2 v for  $\text{YB}_6$ . The low value of  $\text{YB}_6$  may be the result of a surface phenomenon, since work by Kaznoff has disclosed that  $\text{YB}_6$  vaporizes incongruently with a boron-rich vapor. If the reported work function values are accepted as

valid, the low work function boride materials hold promise as emitter coatings for high output converters at temperatures approximately 400 degrees lower than converters employing tungsten or molybdenum.

7. Cesium compatibility tests have shown the very marked sensitivity of carbon-rich carbide materials to cesium attack in time periods less than 500 hours. Boride materials, on the other hand, appear resistant to cesium attack under conditions which produced severe attack and deterioration of the carbides. These results emphasize the importance of stoichiometry control in the preparation of the carbides for successful applications in cesium vapor environments. The mechanism of cesium attack in carbides needs elucidation.
8. Within the scope of the first year program, preliminary information on the grain growth characteristics of carbide and boride materials was obtained. In general, temperatures slightly in excess of those contemplated for thermionic applications was required to produce noticeable grain growth in short periods of time. Much more work is needed to determine the correlation and significance of grain growth phenomenon on electron emission as a function of time and grain orientation and on the mechanical properties after prolonged time at temperature.

#### Recommendations

Based on the above results obtained from screening tests on bulk carbides and borides, and considering the information available from related programs, we have reached certain conclusions concerning the emphasis for future thermionic materials work. These can be summarized as follows:

The development status of clad-oxide materials systems is far more advanced than for comparable carbide systems. However, some of the superior thermophysical properties of carbides such as higher thermal conductivity, lower electrical resistivity and lower emissivity make their continued development desirable.

We recommend the following programs for continued thermionic materials development for the reasons indicated below.

#### 1. Clad-Oxide Material Systems

Four critical items of information are needed to evaluate the application potential of clad-oxide nuclear thermionic materials. These items are:

- a. The kinetics and mechanism of oxide-metal diffusion or reaction at the fuel-emitter interface,
- b. The effect and nature of diffused species on the emitting surface of the clad material.
- c. The extent and effect of fission product release into the plasma volume and methods of minimizing fission gas pressures with minimum fuel transport due to the relatively high vapor pressure of  $\text{UO}_2$ .
- d. Laboratory endurance test experience using operational diodes to evaluate the performance-life characteristics of all elements of the converter system.

Extensive work is needed and recommended to obtain definitive information in the above areas.

## 2. Clad-Carbide Systems

As indicated previously, the thermophysical and nuclear properties of uranium carbides are such that significant advantages exist with these materials compared with clad-oxide systems. Greater knowledge of stoichiometry control in fabrication and clad material compatibility is needed. Additional work in these areas, rather than expensive, empirical development testing, is recommended.

## 3. Boride Materials

The results of investigations to date have not revealed any sound reasons for the dismissal of borides as coatings for emitter applications. Continuing work is needed to confirm or deny the reported work function properties of these materials and to develop coating techniques to candidate substrate or clad materials. Continuing activity of this nature is recommended.

## 4. Metallic Clad/Emitter Materials

The selection of suitable clad/emitter materials to use in conjunction with nuclear fuel oxide and carbide materials can be narrowed to a small number of materials such as: tungsten (electron beam melted, powder metallurgically prepared, or vapor deposited), tungsten-rhenium alloys, and molybdenum. A thorough study of the high temperature properties of the materials is recommended.



## SECTION III - ELECTRON EMISSION MEASUREMENTS - J. H. Ingold

SYMBOL AND NOMENCLATURE $\phi$  = work functions $\phi_{120}$  = effective  $\phi$  using  $A = 120 \text{ amp/cm}^2 \text{ deg}^2$  $A$  = emission constant $J_S$  = saturated thermionic current densityLIST OF ILLUSTRATIONS

<u>Figure No.</u>	<u>Title</u>	<u>Page No.</u>
1	Sample Support Stand	3-9
2	Emitter - Collector Assembly	3-10
3	Diagram of Test Circuit for Emission Measurements	3-11
4a	Current - Voltage Characteristic Obtained for Mo at 2170°K	3-12
4b	Current - Voltage Characteristic Obtained for FrC at 2213°K	3-12
5	Temperature Variation of Emission Current Density	3-13

### III. ELECTRON EMISSION MEASUREMENTS - J. H. Ingold

#### A. Introduction

The recent in-pile thermionic conversion experiments<sup>(1)</sup> at the Los Alamos Scientific Laboratory have sparked a wide interest in the thermionic properties of refractory compounds which might be mixed with a fissionable material to provide truly direct conversion of heat to electricity. A survey has shown that the most likely such compounds include the carbides and borides of the transition and rare-earth metals.<sup>(2)</sup> With this in mind, an experimental program aimed at measuring the thermionic emission properties of polycrystalline bulk samples of zirconium carbide, uranium carbide, uranium dicarbide, uranium-zirconium carbide, and the hexaborides of yttrium and europium was initiated at the General Electric Company, Vallecitos Atomic Laboratory.

Most of the thermionic emission data reported for polycrystalline refractory metal carbides have been obtained from thin coatings on filamentary substrates. For example, Goldwater and Haddad<sup>(3)</sup> investigated the emission properties of zirconium carbide in the form of a thin coating applied to a tungsten wire by electrophoresis. Wright<sup>(4)</sup> studied the emission properties of zirconium carbide powder coated on a tantalum strip, and Matskevich and Krachino<sup>(5)</sup> used an organic suspension to bond zirconium carbide powder to tungsten and to tantalum substrates. Finally, Haas and Jensen<sup>(6)</sup> investigated the emission properties of uranium carbide powder coated on a tungsten wire with an organic binder. Recently, however, Pidd, et al.,<sup>(7)</sup> reported the results obtained from bulk zirconium carbide, uranium carbide and uranium-zirconium carbide formed by arc-melting the appropriate metal and graphite together. They measured an emission current that was about an order of magnitude lower than that obtained from the thin coatings mentioned above. This difference may have resulted from the different measurement techniques used by these investigators, because Pidd, et al., used low collecting fields while the others used high collecting fields. Since low field measurements are probably more relevant to thermionic conversion, this method was chosen to obtain the data reported below.

Experimental data on the hexaborides of yttrium and europium are scarce. To the author's knowledge, the only measurements on these compounds are described in Russian references.<sup>(8,9)</sup> These data, as well as the other data mentioned above are summarized in Reference (2).

## B. Summary

A diode with a water-cooled, guard-ringed collector was designed and constructed for the purpose of measuring the low field thermionic emission properties of polycrystalline bulk samples of various refractory materials. To facilitate rapid interchange of samples and to reduce the cost per sample of the experiments, the diode was operated in a dynamic vacuum system composed of a water-cooled stainless steel belljar exhausted by a four-inch oil diffusion pump backed by a mechanical roughing pump and trapped with liquid nitrogen. The system was capable of maintaining a pressure below  $1 \times 10^{-5}$  torr at test temperature. The experimental apparatus was checked out using a disc of commercial grade molybdenum as the emitter. The effective work function ( $\phi_{120}$ ) obtained was 4.31 volts over the temperature range 2000 K to 2350 K; this is in good agreement with results obtained in previous investigations. Using the same apparatus, the thermionic emission from a vacuum hot pressed sample of zirconium carbide ( $\text{ZrC}_{0.84}$  according to X-ray diffraction analysis) was measured over the temperature range 1950 K to 2250 K. The effective work function obtained was 4.04 volts. This result is compared with results obtained by other investigators for ZrC samples prepared in various ways. No thermionic emission current was observed for yttrium hexaboride up to a temperature of 2000 K because of the buildup of a flaky deposit on the sample. Samples of europium hexaboride and uranium-zirconium carbide did not survive pre-experimental outgassing.

## C. Experimental Procedure

### 1. Sample Preparation

Zirconium carbide sample No. VHP-ZrC-Ta-A-01-I used in this experiment was formed by hot-pressing zirconium carbide powder onto a tantalum disc at about 2750 K for fifteen minutes with 7500 psi applied pressure. A metallurgical examination showed the sample to be well bonded and crack-free, with a density approximately 90 percent of theoretical density. The lattice parameter of this sample was determined to be  $4.6885 \text{ \AA} \pm 0.001 \text{ \AA}$  by x-ray diffractometry; this value corresponds to a carbon deficient composition described by the formula  $\text{ZrC}_{0.84}$ . Before incorporation in the measurement apparatus, each sample was outgassed in an induction heater to remove volatile impurities.

For checkout purposes, a disc of commercial grade molybdenum was used with no special preparation other than the outgassing operation in an induction heater.

## 2. Apparatus

In addition to the power supplies required to heat the sample and to collect the electrons emitted by a sample, the experimental apparatus consists of the following items: (1) sample supporting stand, (2) heater filament, (3) collector, (4) guard ring to minimize edge effects, (5) electric current measuring apparatus (oscilloscope, etc.), and (6) vacuum system. A photograph of the supporting stand, which incorporates the first four of the above items is shown in Figure 1. The coils are copper cooling tubes and the springs facilitate the adjustment of the electrode spacing. The details of the emitter-collector assembly are shown in Figure 2. The sample is supported on the end of a tantalum tube, and is heated from behind by electron bombardment from a pancake spiral tungsten filament. The collector consists of an inner water-cooled copper rod 0.25 inch in diameter, with a concentric water-cooled copper cylinder. The concentric cylinder is electrically insulated from the inner collector so that it can be used as a guard ring. The collector is removable so that evaporated deposits can easily be analyzed. Likewise, the sample can easily be removed after an experiment so that its weight loss can be determined. During operation, the entire assembly shown in Figure 1 is placed in a stainless steel water-cooled bell jar exhausted with a four-inch oil diffusion pump capable of maintaining a pressure below  $1 \times 10^{-5}$  torr with the emitter at test temperature.

## 3. Measurements

From the standpoint of thermionic emission, solid materials are usually characterized by two parameters called the emission constant  $A$  and the work function  $\phi$ . These parameters are related to  $J_s$ , the maximum thermionic current density which is spontaneously emitted by the material, by the Richardson-Dushman (10) equation,

$$J_s = AT^2 \exp(-e \phi / kT), \quad (1)$$

where  $T$  is the absolute temperature,  $e$  the electronic charge, and  $k$  the Boltzmann constant. Although the theoretical value of  $A$  is about 120 amps/cm<sup>2</sup>deg<sup>2</sup>, experimentally determined values range from  $10^{-1}$  to  $10^4$  amps/cm<sup>2</sup>deg<sup>2</sup>. This wide variation is not surprising, however, when the possibility of a temperature dependent work function is considered. For example, if the work function is a linear function of temperature, i.e.,

$$\phi = \phi_R(1 + \alpha T), \quad (2)$$

then Eq. (1) can be rewritten as

$$J_g = A^* T^2 \exp(-e\phi_R/kT), \quad (3)$$

where  $A^*$  is defined by the equation,

$$A^* = A \exp(-e\phi_R \alpha/k). \quad (4)$$

Hence, large positive and negative  $\alpha$ 's could account for anomalous values of the emission constant reported for different materials.

The various methods of determining the thermionic emission parameters of materials have been discussed thoroughly by Nottingham<sup>(11)</sup> and Hensley.<sup>(12)</sup> In particular, Hensley concludes that "For many purposes a satisfactory procedure is simply to take the emission data at a constant electric field of just sufficient value to ensure negligible space-charge effect." The "data," of course, consist of the variation of  $J_g$  with temperature, and are customarily displayed in the form of a Richardson plot of  $\ln J_g/T^2$  vs  $1/T$ . According to Eq (3), such a plot should give a straight line of slope  $(-e\phi_R/k)$  and intercept  $\ln A^*$ . However, Hensley contends that an effective work function plot is more useful, and this author agrees.

A refinement of the simple method proposed by Hensley for determining the emission properties of materials has been selected for the present investigations. This refinement consists of applying a 60-cycle sweep voltage to the collector and displaying the resulting current-voltage characteristic on an oscilloscope. A typical test circuit is shown in Figure 3; subscripts g and c refer to guard-ring and collector, respectively, and  $R_L$  denotes load resistance. In this way, the uncertainty of the effect of space-charge on the measurement of  $J_g$  is eliminated, because the saturation emission current is evident from oscilloscope trace.

A calibrated optical pyrometer was used to measure the emitter temperature. An estimate of the relative spectral emissivity at  $0.65\mu$  for the zirconium carbide sample was obtained by comparing the brightness temperature of a black body hole approximately 0.010 inch diameter by 0.060 inch deep with the brightness temperature of the sample surface near the hole. This method gave an emissivity which varied from 0.60 to 0.70 over the temperature range 1950 K to 2250 K.

#### 4. Results and Discussion

A disc cut from commercial grade molybdenum bar stock purchased from Fansteel Metallurgical Company was used to check out the apparatus. A typical current-voltage characteristic obtained for the Mo sample is shown in Figure 4a. Since the saturation current

continued to rise beyond the retarding voltage range, it was arbitrarily decided to take  $J_s$  to be the current density obtained at an accelerating voltage of 50 volts, which corresponded to an applied electric field of 5000 v/cm. The results obtained for this sample, which are presented in the form of a modified effective work function plot shown in Figure 5, gave an effective work function of 4.31 volts over the temperature range 2000 K to 2350 K. This work function is in good agreement with the values  $A^* = 115 \text{ amp/cm}^2 \text{ deg}^2$  and  $\Phi_R = 4.37$  volts obtained by Wright (13) for commercial grade molybdenum wire.

Similarly, a current-voltage characteristic typical of those obtained for the zirconium carbide sample is shown in Figure 4b, and the temperature variation of the emission current density measured at an applied electric field of 5000 v/cm is shown in Figure 5. The effective work function obtained from this curve is 4.04 volts. For comparison, the effective work functions obtained by previous investigators are listed in Table I.

**TABLE I**  
**Effective Work Function of ZrC at 2000 K**

Reference	$J_s$ (amp/cm <sup>2</sup> )	$\Phi_{120}$ (volts)	Form of Sample
3	4.000	3.20 (pulsed)	Thin coating on W
4	1.000	3.44 (DC)	Powder coating on Ta
	5.000	3.16 (pulsed)	
5	0.084	3.92 (pulsed)	Powder coating on W
	0.480	3.57 (pulsed)	Powder coating on Ta
7	0.130	3.79 (DC)	Bulk (arc-melted on Ta)
Present Result	0.030	4.04 (DC)	Bulk (hot-pressed on Ta)

Unfortunately, none of the previous investigators discuss the probable compositions of their samples, so a correlation between emission properties and stoichiometry is not feasible at the present time.

In addition to zirconium carbide, samples of yttrium hexaboride, europium hexaboride, and uranium-zirconium carbide were fabricated for emission measurements. The latter two samples did not survive the pre-experimental outgassing operation. Prior to heating the

uranium-zirconium carbide sample a few hairline cracks were visible on the emitting surface, but it appeared to be suitable for measurement purposes. However, during the outgassing operation, the cracks opened up considerably and the emitting surface became noticeably convex; this rendered the sample unsuitable for measurement purposes. The europium hexoxide sample was outgassed in an alumina crucible above 1900 K. The sample was mounted in a removable tantalum sleeve which is part of the emission apparatus. At the conclusion of this operation, reaction products which rendered the sample unsuitable for measurement purposes were observed on the tantalum ring and the sample. Two attempts to measure the emission from the yttrium hexaboride sample were unsuccessful because of the buildup of a flaky deposit on the sample during the test runs. A similar deposit was observed during the material property measurements on this material which are discussed elsewhere in this report. This deposit may have been due to the vacuum conditions of the equipment.

In conclusion, it is strongly recommended that future measurements of this kind be done in a sealed-off system (or one continuously exhausted by an ion pump) at a pressure as low as possible in order to obtain clean surfaces for measurement purposes.

## REFERENCES

1. G. M. Grober, *Nucleonics*, 17, 54 (1959).
2. P. Stephas, *Nucleonics* 19, 66 (1961).
3. D. L. Goldwater and R. E. Haddad, *J. Appl. Phys.* 22, 70 (1951).
4. D. A. Wright, *J. Inst. Elec. Eng. (London)* 100, 125 (1953).
5. T. L. Matskevich and T. V. Karchino, *Zhur. Tekh. Fiz.* 32, 220 (1962).
6. G. A. Haas and J. T. Jensen, Jr., *J. Appl. Phys.* 31, 1231 (1960).
7. R. W. Pidd, et al., *J. Appl. Phys.* 30, 1575 (1959).
8. G. V. Samsonov, *Uspekhi Khimii* 28, 189 (1959).
9. G. A. Kudintsev and B. M. Tsarev, *Radiotekhnika i Elektronika* 3, 428 (1958).
10. R. H. Fowler, *Statistical Mechanics*, (University Press, Cambridge, 1936) 2nd Ed., Chapt. XI.
11. W. B. Nottingham, "Thermionic Emission," published in *Handbuch der Physik*, E. Flugge, ed., (Springer-Verlag, Berlin, 1956) XXI, Page 1.
12. E. B. Hensley, *J. Appl. Phys.* 32, 301 (1961).
13. R. W. Wright, *Phys. Rev.* 60, 465 (1941).



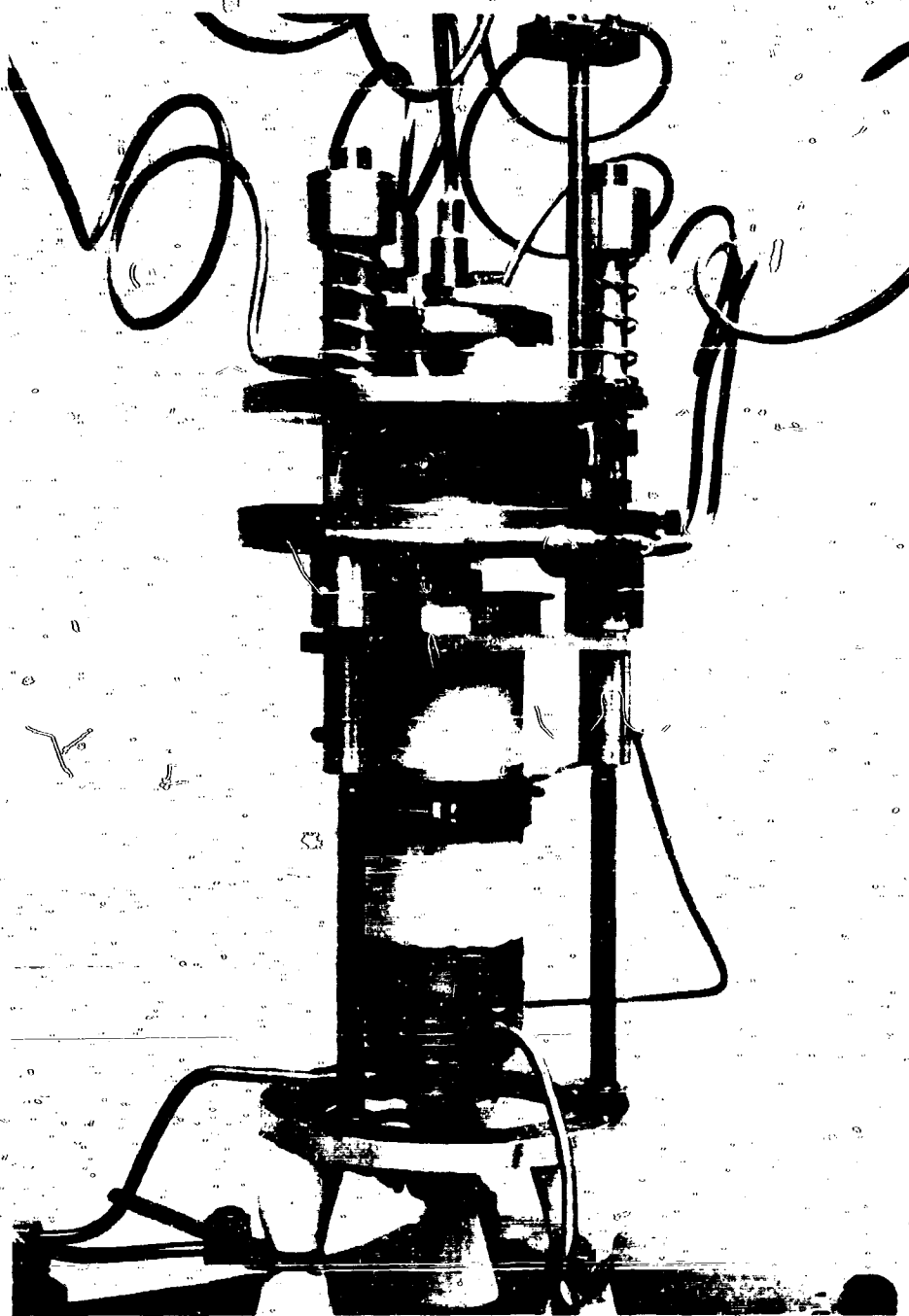
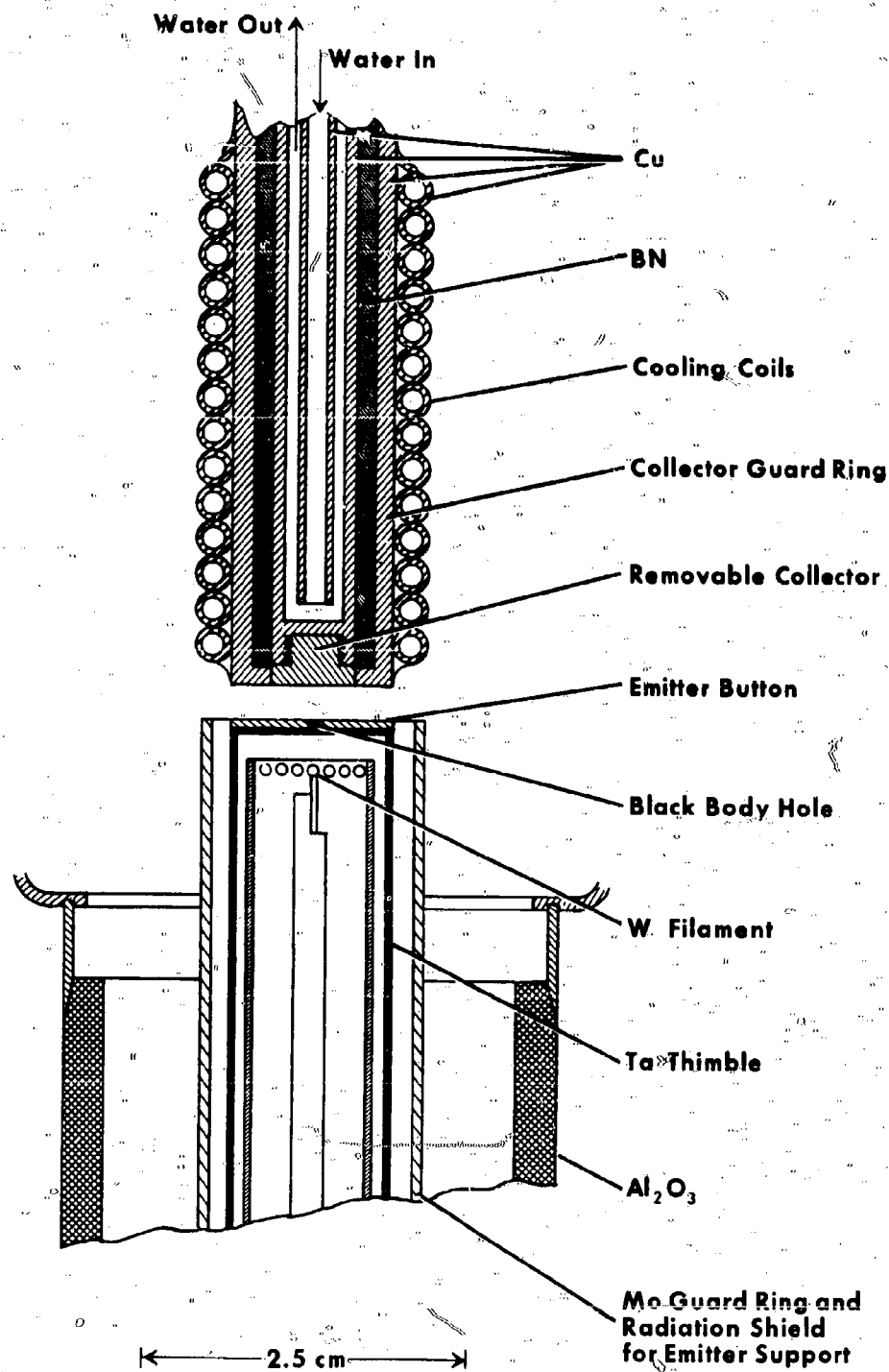
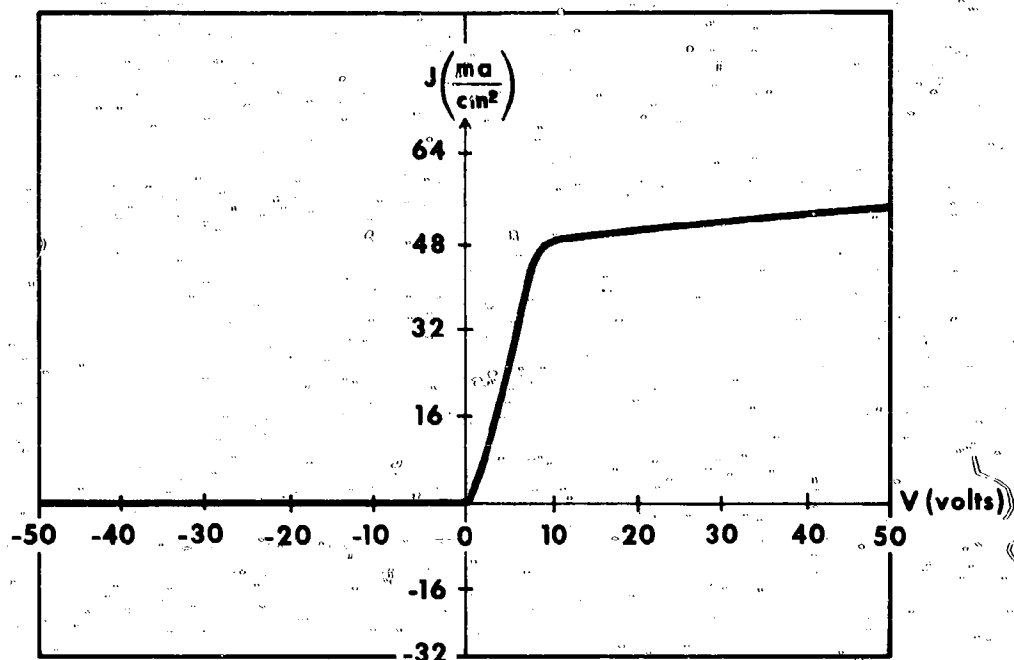


Figure 1. SAMPLE SUPPORT STAND



**Figure 2. EMITTER-COLLECTOR ASSEMBLY**





**Figure 4a. CURRENT-VOLTAGE CHARACTERISTIC OBTAINED FOR Mo AT 2170°K**

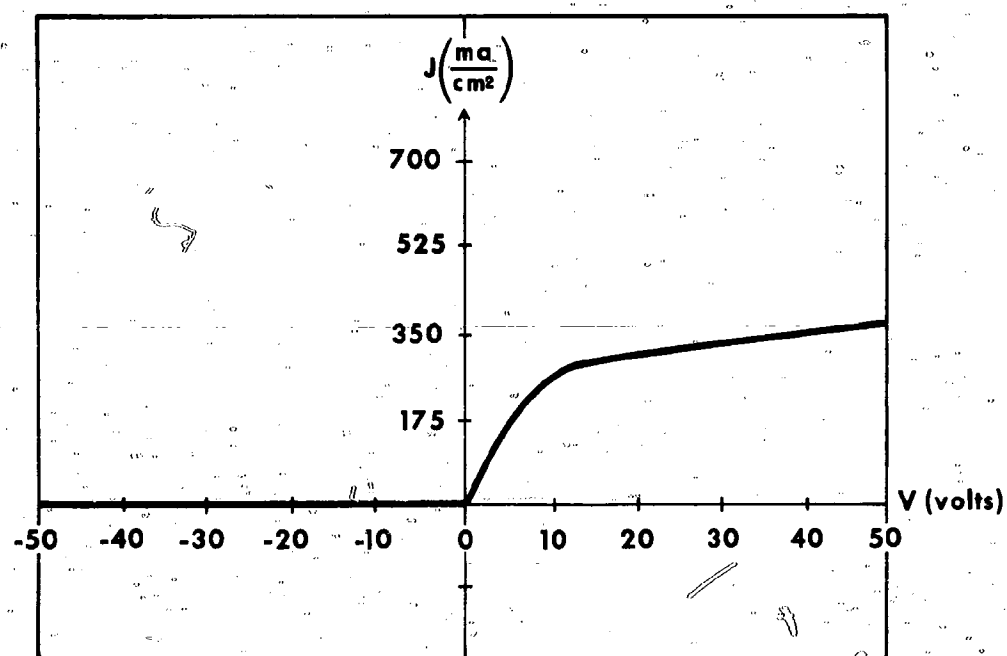


**Figure 4b. CURRENT-VOLTAGE CHARACTERISTIC OBTAINED FOR ZrC AT 2213°K**

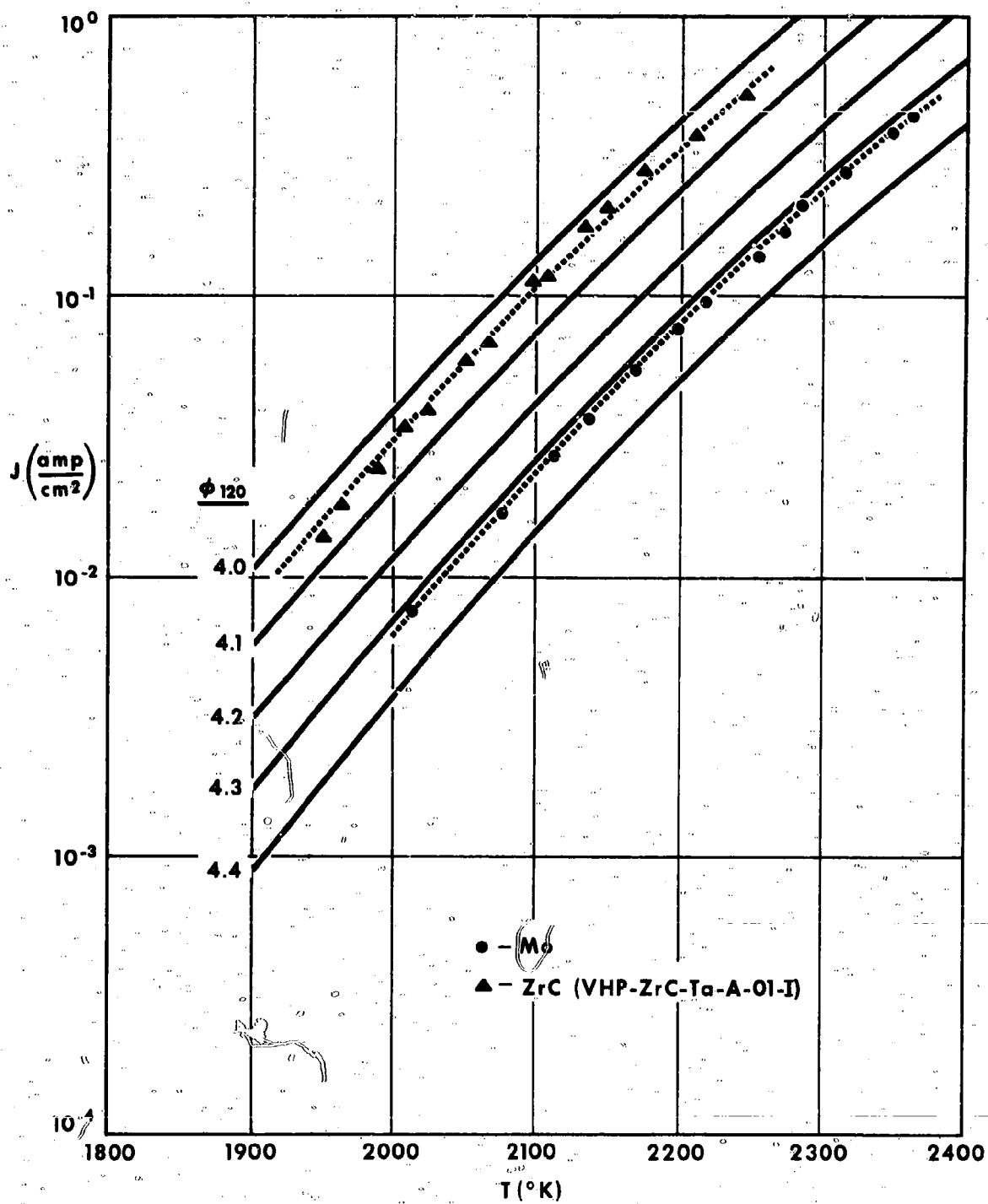


Figure 5. TEMPERATURE VARIATION OF EMISSION CURRENT DENSITY

## SECTION IV - THERMOPHYSICAL PROPERTY MEASUREMENTS - L. N. Grossman

SYMBOL AND NOMENCLATURE

$T_L$	= central temperature
$x_L$	= central position of specimen
$w$	= cross sectional area of specimen
$I$	= current
$\rho$	= electrical resistivity
$p$	= perimeter of specimen
$\epsilon_t$	= total hemispherical emission
$\sigma$	= Stefan's constant
$\kappa$	= thermal conductivity

LIST OF ILLUSTRATIONS

<u>Figure No.</u>	<u>Title</u>	<u>Page No.</u>
S-1	Thermal Conductivity Measurement Summary	4-25
S-2	Electrical Resistivity Measurement Summary	4-26
S-3	Total Hemispherical Thermal Emission Measurement Summary	4-27
1	Thermal Properties Apparatus	4-28
2	Electrical Resistivity; Experimental Points	4-29
3	Electrical Resistivity of UC (5.3 w/o Total Carbon)	4-30
4	Normal Spectral (0.65 $\mu$ ) Emission of UC (5.3w/o Total Carbon)	4-31
5	Total Hemispherical Emission of UC (5.3 w/o Carbon)	4-32
6	Thermal Conductivity; Experimental Points	4-33
7	Thermal Conductivity of UC (5.3 w/o Carbon)	4-34
8	ZrC Spectral Emission of (0.65 $\mu$ )	4-35
9	ZrC Spectral Emission Versus Time after Flashing	4-36

LIST OF ILLUSTRATIONS

<u>Figure No.</u>	<u>Title</u>	<u>Page No.</u>
10	Resistivity of ZrC	4-37
11	Total Thermal Emission of ZrC	4-38
12	Experiment Thermal Conductivity of ZrC	4-39
13	Photomicrograph of UC <sub>2</sub> Rod	4-40
14	Resistivity of UC <sub>2</sub> (8.7 w/o Total C)	4-41
15	Spectral Emission of UC <sub>2</sub> (0.65 $\mu$ )	4-42
16	Total Thermal Emission of UC <sub>2</sub>	4-43
17	Thermal Conductivity of UC <sub>2</sub> (8.7 w/o Carbon)	4-44
18	Resistivity of U <sub>0.5</sub> Zr <sub>0.5</sub> C	4-45
19	Spectral Emission at 0.65 $\mu$ of U <sub>0.5</sub> Zr <sub>0.5</sub> C	4-46
20	Emission of ThC and ThC <sub>2</sub>	4-47
21	Microstructure of ThC <sub>2</sub> Specimen	4-48
22	Resistivity of ThC <sub>2</sub>	4-49

#### IV. THERMOPHYSICAL PROPERTY MEASUREMENTS - L. N. Grossman

##### A. Summary

Four thermophysical properties (thermal conductivity, electrical resistivity, total hemispherical thermal emission, and normal spectral thermal emission at  $0.65\mu$ ) may be measured simultaneously on an apparatus designed and built partially under this program. The apparatus is useful in the temperature range from the onset of measurable thermal emission (about 1000 K) to an upper limit set by sublimation or decomposition of the specimen. The apparatus has been used to specimen temperatures of over 2500 K in the present investigation.

Table I summarizes all thermophysical property experiments undertaken for this program, together with the degree of success realized. Table II presents the values obtained for the various properties and the temperature range over which the values are valid. The error limits reported in Table II are very high confidence limits (95 per cent), valid over the temperature range reported. Electrical resistivity and thermal conductivity values are given for fully dense material. Some data outside of the temperature ranges indicated appear in the text, as well as some data for ThC and YB<sub>6</sub>.

Figure S-1 summarizes the thermal conductivity results obtained during this study, while Figure S-2 presents the electrical resistivity results obtained. Figure S-3 exhibits total hemispherical emission data obtained during the thermal conductivity measurements.

##### B. Conclusions - Thermophysical Properties

Thermal conductivity, electrical resistivity and total thermal emission are now known for UC, U<sub>0.5</sub>Zr<sub>0.5</sub>C, ZrC and UC<sub>2</sub> at temperatures of interest to nuclear thermionic and other high temperature nuclear systems. These materials are decidedly metallic with respect to those properties. The Wiedemann-Franz law may be used for these materials above 1000 K to determine thermal conductivity within 10 per cent. The electrical resistivity of ThC<sub>2</sub> has also been determined; a phase change may occur near 1550 K for this material.

There is a small but significant difference between the thermal conductivity of values measured for ZrC and those predicted by the Wiedemann-Franz law. The measured magnitude and slope are greater than predicted by the theory; also the  $1/T$  law for lattice conductivity is not obeyed. This observation has been previously noted by another investigator for ZrC and for ThC.



TABLE IHigh Temperature Property Measurement Summary

Material	Thermal Conductivity	Total Thermal Emission	Spectral Thermal Emission (0.65/l)	Electrical Conductivity
ZrC	A	A	A	A
UC	A	A	A	A
UC <sub>2</sub>	A	A	A	A
U <sub>0.5</sub> Zr <sub>0.5</sub> C	B*	B	A	A
YB <sub>6</sub>	B	B	A	B
EuB <sub>6</sub>	C	C	C	C
ThC	B	B	A	B
ThC <sub>2</sub>	B	B	A	A

Code: A Measurement completed during contract year.

B Measurement attempted, but not successful.

C Not attempted.

\* A good estimated value has been obtained.

**TABLE II**  
**Thermophysical Property Summary**

	ZrC	UC	$U_{0.5Zr0.5C}$	UC <sub>2</sub>	ThC <sub>2</sub>
Thermal Conductivity ( $\frac{\text{cal}}{\text{cm sec deg}}$ )	$0.040 \pm 1.7T \times 10^{-5}$ $1500 < T < 2400$ $\pm 10\%$ (1)	0.057 $1200 < T < 2050 \text{ K}$ $\pm 12\%$	$0.025(2) \cdot 3T \times 10^{-5}$ $1000 < T < 2400 \text{ K}$ $\pm 15\%$	$-0.035 + 4T \times 10^{-5}$ $1500 < T < 2000 \text{ K}$ $\pm 15\%$	--
Electrical Resistivity ( $\Omega \cdot \text{cm}$ )	$42.0 \times 10^{-6} + 73T \times 10^{-9}$ $300 < T < 2400 \text{ K}$ $\pm 2\%$	$20.4 \times 10^{-6} + 114.8T \times 10^{-9}$ $1100 < T < 2050 \text{ K}$ $\pm 2\%$	$106 \times 10^{-6} + 79T \times 10^{-9}$ $1100 < T < 1850 \text{ K}$ $\pm 2\%$	$189 \times 10^{-6} + 58T \times 10^{-9}$ $1550 < T < 2070 \text{ K}$ $\pm 3\%$	$68 \times 10^{-6} + 89T \times 10^{-9}$ $1700 < T < 2330$ $\pm 3\%$ (3)
Spectral Thermal Emission (0.65 $\mu$ )	0.63 $1100 < T < 2400 \text{ K}$ $\pm 3\%$	$0.539 - 0.02T \times 10^{-3}$ $1150 < T < 1890 \text{ K}$ $\pm 5\%$	0.7 (3) $1300 < T < 1900 \text{ K}$ --	0.54 $1400 < T < 2150 \text{ K}$ $\pm 5\%$	0.58 (3) $1500 < T < 2100$ $\pm 5\%$
Total Thermal Emission	$0.772 - 9T \times 10^{-5}$ $1500 < T < 2400 \text{ K}$ $\pm 5\%$	0.42 $1150 < T < 2050 \text{ K}$ $\pm 10\%$	--	0.5 $1650 < T < 2000 \text{ K}$ $\pm 12\%$	--

Notes: 1. Error limit values are 95 per cent confidence limits valid over the indicated temperature range.

2. Estimated as in text.

3. May be characteristic of a reacted surface.

4. Possible phase change in ThC<sub>2</sub> near 1550 K.

5. Possible phase change near 1550 K.

Normal spectral thermal emission has been measured at  $0.65\mu$  for UC, ZrC,  $U_{0.5}Zr_{0.5}C$ , ThC,  $ThC_2$ ,  $YB_6$  and  $UC_2$ . The often reported values of 0.7 - 0.95 for this type of material appear characteristic of reacted surfaces, i.e. oxidized, nitrided, or borated surfaces. The cleaned and polished metallic surfaces always emit less than 0.65 of black-body spectral emission over the temperature range investigated. For those materials forming stable reaction products with  $O_2$  or  $N_2$ , a vacuum of about  $10^{-7}$  torr is required to keep the surface clean with respect to spectral emission (at  $0.65\mu$ ) for a time of about 10 minutes.

Considerable difficulty was found in maintaining mechanically stable (U, Zr) C alloys under thermal gradients. The pure carbide, UC, is definitely superior to the alloyed material with respect to i) higher thermal conductivity, ii) lower electrical resistivity, iii) lower total thermal emission, and iv) greater thermal stress resistance. It appears advisable to re-appraise pure UC as a fuel in nuclear thermionic reactors, especially since its compatibility with tungsten has been reported for certain conditions.

Zirconium carbide has a solubility for carbon of at least 0.165 w/o above about 2300 C. The thermal conductivity of ZrC may be sensitive to the carbon content. However, electrical resistivity is not sensitive to carbon content between 11.0 to 11.8 w/o carbon over the temperature range studied.

#### C. Recommendations

The decidedly metallic behavior of UC and UC-ZrC alloys suggests that lower temperature gradients will exist across these fuel elements than corresponding oxide elements. In the clad fuel concept, this lowering of the maximum fuel temperature will have definite bearing on the successful venting of fission gases. It is recommended that vented carbide-fueled clad cathodes be considered for long-lived nuclear thermionic fuel elements.

In the unclad fuel-emitter concept, it is recommended that unalloyed UC be re-evaluated in light of its superior thermophysical properties. It is recognized that the vapor pressure of UC is greater than any of the (U, Zr)C alloys; however, the thermal shock resistance of pure UC may be essential in a reactor which is to be cycled. Recent advances in UC fabrication and stoichiometry control have caused the availability of UC specimens superior to those on which early decisions were based.

The high temperature properties of ThC,  $ThC_2$ ,  $YB_6$  and  $EuB_6$  are still not all known. It is recommended that a renewed effort be initiated to complete these property measurements. Existing equipment and techniques in this laboratory will allow these data to be readily obtained.

#### D. High Temperature Thermophysical Properties of Uranium Monocarbide

Uranium monocarbide is being considered for use as a fuel for nuclear power reactors and for the transformation of nuclear into electric energy by thermionic conversion. This interest in UC exists because of the material's high melting point, high uranium density, good thermal conductivity, and high thermionic electron emission. The present study reports high temperature values for some properties of considerable value in the design of nuclear systems.

Measurements of thermal and electrical conductivity have been previously reported (1, 2, 3) at temperatures up to about 1300 K, while no values for the thermal emission have been found in the literature.

#### 1. Experimental

##### a. Specimen

The UC measured in this investigation was an arc-cast rod 9 cm long and 0.900 cm in diameter supplied through the courtesy of Battelle Memorial Institute. It was 100 per cent dense with a composition of 94.7 w/o uranium and 5.3 w/o total carbon, (determined after the completed measurements), the oxygen content was < 200 ppm. Metallographic examination after the property measurements exhibited a slight second phase which is either  $UC_2$  or  $U_2C_3$ .

Specimen preparation included squaring of the rod ends and grinding to make it a right circular cylinder. Subsequent polishing through 600 mesh silicon carbide paper and finally 6 micron diamond produced a shiny metallic surface. All polishing was done in a calcium-gettered-argon glove box in the presence of  $P_2O_5$  powder to assure dry and oxygen-free conditions.

The measurement technique (described below) requires good thermal and electrical contact at the specimen ends. To achieve this, the ends of the rod were nickel electroplated and brazed in vacuum to copper end pieces.

A four-probe electrical continuity check at room temperature showed the braze to be of lower electrical resistance than an equivalent length of UC. The braze appearance was excellent. The rod was repolished in the glove box subsequent to brazing.

b. Thermophysical Properties Apparatus

The apparatus used for this investigation is described in detail elsewhere. <sup>(4)</sup> Figure 1 illustrates the main features of the apparatus. The rod specimen is attached to water-cooled electrodes and heated by 400 cycle, single-phase current in a vacuum (or inert gas) chamber. The specimen is free to radiate in all directions inside its enclosure; its environment is essentially a cold black-body.

c. Measurement of Resistivity

Resistivity was measured by symmetrically contacting the specimen with two spring-loaded tungsten voltage probes placed 0.63 cm apart about the specimen center. The probes led to a calibrated Tetrone 503 Oscilloscope. Current was measured by a Weston 327 current transformer coupled with a Weston 433 A-C ammeter. The overall probable error of resistance measurement was about  $\pm 2$  per cent.

d. Measurement of Temperature and Spectral Emission

Brightness temperature profiles of the specimen were taken with a Micro-Optical pyrometer mounted on a tripod. The profiles were used in the measurement of electrical and thermal conductivity, as described below. The distance along the rod was measured by a dial gauge attached to the tripod. Brightness temperature was converted to true temperature by a determination of the normal spectral emission of the surface. A 2 cm central portion of the rod specimen was cut out following the property determinations and a 0.02 inch diameter by 0.10 inch deep hole was drilled into it with a diamond drill. This rod was subsequently heated in vacuo with an induction coil and susceptor. The rod segment was allowed to radiate freely from the surface under observation. Temperature measurements were then taken of the black-body hole and of the surfaces adjacent to the hole. The hole and surface temperatures were converted to emission values utilizing a published tabulation. <sup>(5)</sup> A subsequent redetermination of spectral emission with an apparently identical sample was made in the properties apparatus under a vacuum of  $5 \times 10^{-7}$  torr. The results of the two determinations were essentially identical for temperatures above 1600 K.

Uranium carbide, when exposed to air, forms a tenacious surface skin of what may be an oxycarbide. <sup>(5)</sup> The thermal emission of the carbide with this surface layer is different than that of the cleaned carbide. It was found during the property determinations that this layer leaves the surface rapidly at temperatures above about 1800 K in a

vacuum of about  $10^{-6}$  torr. The exposed carbide surface retains its polish and gives reproducible emission values. If the temperature of the carbide is lowered to any temperature below about 1700 K in a vacuum of  $5 \times 10^{-7}$  torr total pressure, the spectral emission begins to rise slowly after about 10 minutes has elapsed. The spectral emission continues to rise until about 20-30 minutes has elapsed, when it reaches a constant value.

e. Measurement of Thermal Conductivity and Total Emission

Temperature profiles obtained from the specimen were fitted (using a computer) to the analytical expression

$$T - T_L = B(x - x_L)^2, \quad (1)$$

where  $T_L$  is the central temperature,  $x_L$  is the central position, and  $B$  is quadratic characteristic. Each profile then yielded a linear equation in which  $\epsilon_t$  and  $\kappa$  are the only unknowns: (4)

$$2 \kappa w B = \frac{I^2 \rho}{w} - p \epsilon_t \sigma T_L^4 \quad (2)$$

where  $\kappa$  is thermal conductivity,

$w$  is the cross-sectional area of the specimen

$B$  is the profile characteristic (defined above)

$I$  is the current through the rod

$\rho$  is the resistivity at temperature  $T_L$

$p$  is the perimeter of the rod

$\epsilon_t$  is the total hemispherical emission

$\sigma$  is Stefan's constant  $\left(5.67 \times 10^{-12} \frac{\text{watt}}{\text{cm}^2 \text{ deg}^4}\right)$  and

$T_L$  is the central temperature of the rod.

Each profile determination gave a linear equation in  $\kappa$  and  $\epsilon_t$  (equation 2) which is valid near  $T_L$ . Simultaneous solution of pairs of these equations was performed graphically as described below.

For temperatures below about 1800 K, the measurements were made with the specimen in a vacuum of about  $10^{-6}$  torr. Above 1800 K a cover gas of gettered argon at 100 torr was introduced to suppress vapor loss of the specimen. The cover gas introduced negligible errors in the property determinations because its thermal conduction is very low

compared to radiative transport above 1800 K, and because it does not noticeably affect the pyrometry.

## 2. Results and Discussion

### a. Resistivity

Figure 2 shows the measured electrical resistivity of uranium monocarbide between 1200 and 2050 K. Temperature is accurate to about  $\pm 20$  K for all points as discussed below. The measured points have been corrected for the thermal expansion of UC, assuming an expansion coefficient of  $10^{-5}$  per  $^{\circ}\text{C}$  at all temperatures. Linear extrapolation of the curve down to room temperature gives fair agreement with published room temperature resistivity values. (2) This indicates that a straight line temperature dependence of resistivity is not strictly valid from 300 to 1200 K; while it is probably valid at the higher temperatures (Figure 3). The analytic form of the linear region is

$$\rho = 20.4 \times 10^{-6} + 114.8T \times 10^{-9} \text{ ohm-cm, for } 1200 < T < 2050 \text{ K.}$$

The probable error of any point on the line is  $\pm 1.7 \times 10^{-6}$ .

The resistivity values reported by Accary and Caillat (3) are considerably lower than those observed in the present investigation. The work of Rough and Chubb (2) has shown room temperature resistivity to decrease with decreasing carbon content. Similarly, the work of Meerson and Kotelnikov (1) has shown room temperature electrical resistivity to decrease with increasing uranium content and thermal conductivity to increase with increasing uranium content. Therefore, it appears that the material studied by Accary and Caillat (3) was uranium rich.

### b. Spectral Emission and Temperature Measurements

Figure 4 presents the measured spectral emission values at 0.65 microns for uranium monocarbide. The upper curve represents the emission of the carbide with reacted surface. Other results with reacted surfaces indicate that the upper curve is not reproducible; the emission depends on the amount of reaction and on subsequent heat treatments. The lower curve is believed to be the true spectral emissivity of uranium monocarbide. However, since various polishing techniques were not tried, the lower curve is reported as an emission curve. The maximum observed emission value on the lower curve was 0.57, while the minimum was 0.46. The straight line through the measured points may be expressed analytically as

$$\epsilon_{0.65} = 0.539 - 0.02T \times 10^{-3} \text{ for } 1150 < T < 1890 \text{ K,}$$

where the probable error of any point of the curve is  $\pm 0.02$ . The reported slope is small compared to the error in the measurements and is therefore of no interpretational significance.

The observed slow rise of spectral emissivity after about 10 minutes at  $5.0 \times 10^{-7}$  torr is probably due to the build-up of a reaction product on the UC surface. The reaction product could be UN, or a U(C, N, O) solid solution; identification of the product has not been attempted. If one assumes that the product is formed from nitrogen (or oxygen), and that the "sticking coefficient" (reaction probability) of each nitrogen atom striking the UC surface is one, then kinetic theory can be used to calculate the reaction layer thickness. By this method the thickness of the reaction layer when a change in spectral emission is first noticed, is calculated to be between 100 and 1000 atomic layers.

The above equation for spectral emission ( $\epsilon_{0.65}$ ) was used in converting surface temperature measurements to true temperature. The probable error in emission corresponds to a probable temperature error of  $2^\circ$  at an observed temperature of 1000 K, and  $8^\circ$  at an observed temperature of 2000 K. The pyrometer was calibrated against a certified NBS tungsten strip lamp and was found to be reproducible to within  $10^\circ$  over the temperature range herein reported. An additional  $12^\circ$  was added to the observed values to correct for the absorption of the 1/2 inch thick silica window. Reported true temperature values should therefore be accurate to within  $\pm 20^\circ$ .

#### c. Total Hemispherical Emission

Figure 5 presents the results of simultaneous solutions for  $\epsilon_t$  of the experimental profile equations (equation 2). The total emission values are plotted for the average of the two  $T_L$ 's corresponding to the two profile equations from which they were solved. The two high values were obtained from the simultaneous solution of pairs of three profile equations obtained from the specimen when it had a reacted surface. Although the reacted surfaces are not reproducible, the points are of use in computing thermal conductivity at the lower temperatures. The data points shown in Figure 5 are best fitted by the straight line,  $\epsilon_t = 0.42$ , where the probable error of any point of the line is 0.02.



#### d. Thermal Conductivity

Figure 6 exhibits the experimental results of this investigation. The points were obtained by solving the experimentally determined linear equations (equation 2) in  $\kappa$  and  $\epsilon_t$  for  $\kappa$ , using  $\epsilon_t$  values from Figure 5 ( $c_t = 0.42$ ). The  $\kappa$  values at 1280 K and 1315 K were determined on the specimen with a reacted surface, while the others were determined on the cleaned specimen. The machined-calculated probable error is shown for the points: it is made up of the known probable error in  $B$ ,  $\rho$ ,  $\epsilon_t$ , and  $I$ , and estimated probable error in  $T_L$ . The error is primarily due to the difficulty in maintaining a clean, reproducible surface on the carbide.

The results of the present investigation together with some data obtained by other investigators, are presented in Figure 7. The data by Dayton and Tipton<sup>(2)</sup> were obtained on UC containing 5.3 w/o carbon, while that of Brown and Stobo<sup>(7)</sup> was obtained on 5.2 w/o carbon material. The electronic contribution to thermal conductivity was computed from the Wiedemann-Franz law using resistivity values from Figure 3:

#### 4. Conclusions

Uranium carbide exhibits typical metallic behavior in its thermophysical properties. That is, the temperature coefficients of  $\kappa$ ,  $\rho$ ,  $\epsilon_t$ , and  $c_{0.65}$  are of the same order as the refractory metals. In addition, the absolute values of these properties are typically metallic.

The thermal conductivity of UC with about 4 to 6 w/o carbon should not differ appreciably from that reported here for 5.3 w/o carbon since their electrical and thermal properties are quite similar in the temperature range between room temperature and 1000 K. (1, 2)

Linear extrapolation of the data herein reported is very likely valid to temperatures near the melting point of UC (~2700 K).

#### 5. Acknowledgments

Acknowledgment is extended to James Wilson and to Paul Waskevich who aided in data-taking and chemical analysis respectively. Walston Chubb is gratefully acknowledged for his efforts in supplying specimens for this investigation.

**REFERENCES**

1. Meerson, G. A., R. B. Kotelnikov, and S. N. Bashlikov, "Uranium Monocarbide", Atomnaya Energiya 9, 387 (1960).
2. Chubb, W. and R. F. Dickerson, "Properties of Uranium Carbides", Am. Cer. Soc. Bulletin, 41, 564 (1962).
3. Accary, A. and R. Caillat, "Development of Ceramic Fuels in France", in Nuclear Fuel Elements, ed. H. H. Hausner and J. F. Schumar, Reinhold Publishing Co., N. Y. (1959).
4. Grossman, L. N., "Thermal Properties Apparatus for Metallics at High Temperatures", APED-4002 (available from Technical Publications Unit; General Electric Co., Atomic Power Equipment Dept., San Jose, California).
5. Poland, D. E., J. W. Green and J. L. Margrave, "Corrected Optical Pyrometer Readings", NBS Monograph, 30 (1961).
6. Brown, D. J. and J. J. Stobo, "Preparation and Properties of UC", 4th Plansee Seminar, Plansee Metallwerk, Reutte, Austria (1961).

## E. High Temperature Thermophysical Properties of ZrC

Determination of the following properties have been made on two ZrC specimens:

- a. Thermal conductivity vs temperature.
- b. Spectral thermal emission vs temperature.
- c. Spectral thermal emission vs time in vacuum.
- d. Electrical resistivity vs temperature.
- e. Total thermal emission vs temperature.

The methods utilized in this investigation have been described previously.

### 1. Experimental

#### a. Specimen Descriptions

The specimens were rods, 0.607 cm in diameter and about 4 cm long. They were hot-pressed in graphite dies from -325 mesh high purity powder (Wah Chang Company) of 11.3 w/o carbon. Metallic impurities totaled less than 1000 ppm; the major impurity of the as-received powder was oxygen at 2600 ppm. The hot-pressing was accomplished in two steps: first a rod about 1-1/2 cm long was pressed, then another 1-1/4 cm was added to either end. The pressings were accomplished at about 2300 C and 6000 psi for one hour. No discontinuous grain growth was observed although some uniform growth occurred. The resulting specimens were 90 per cent of theoretical density. After fabrication and property measurements, the total carbon content was chemically analyzed to be 11.7 and 11.8 w/o for the two specimens, while the oxygen content was below 20 ppm.

Since the carbon content for stoichiometric ZrC is 11.635 w/o, it appears that a solubility of at least 0.165 w/o carbon exists at 2300 C. X-ray diffraction of the specimens after the property measurements showed a lattice parameter of  $a_0 = 4.699 \pm 0.002$  angstrom units. This corresponds to exactly stoichiometric carbide. (1) Chemical analysis of the test specimens showed the 11.8 w/o carbon sample to have about 0.3 w/o free carbon present, while the 11.7 w/o carbon sample had 0.18 w/o free carbon present after the property measurements. The free carbon content confirms carbon solubility of at least 0.165 w/o in ZrC at about 2300 C.

b. Temperature Measurement and Surface Condition

Temperature was measured with a micro-optical pyrometer operating at a wavelength of  $0.65\mu$ . Observed brightness temperature of the carbide was converted to true temperature utilizing spectral thermal emission data obtained during the properties measurements. A black-body hole, 0.020 inch in diameter by about 0.10 inch deep was drilled into the central portion of the ZrC rods. Spectral emission at  $0.65\mu$  was determined by comparing the hole temperature with adjacent surface temperatures. A published tabulation (2) yielded the emission value from these two temperatures.

The possibility of temperature error due to radial temperature gradients in the rod has been evaluated. The radial temperature profile has been calculated elsewhere. (3) The maximum radial temperature difference in the specimen rod under the present experimental conditions is  $45^\circ$  (at 2400 K), while the minimum is  $3^\circ$  (at 1100 K). The radial gradient introduces a small error at the highest temperatures which has not been taken into account in the following.

The measured spectral emission from ZrC at  $0.65\mu$  is shown in Figure 8. Each measurement below 2200 K was immediately preceded by flashing of the specimens to at least 2400 K. This was found to be necessary to avoid build-up of a reaction product layer on the surface of the ZrC as is discussed below. The specimen had been previously polished through 600 grit silicon carbide paper and was very metallic appearing. Upon insertion in the apparatus, the specimen was heated to 2400 K for one hour before any measurements were taken.

The rate of build-up of reaction product on ZrC in a dynamic vacuum of  $5 \times 10^{-7}$  torr can be qualitatively seen in Figure 9. To obtain this data, the specimen was flashed to 2400 K and then cooled in less than 10 seconds to about 1400 K. The increase in spectral emission with time is indicative of the formation of an optically thick layer of reaction product on the surface. Assuming that the reaction product is an oxide or nitride (or both), kinetic theory indicates that a reaction layer about  $10^3$  monolayers thick had formed in 60 minutes. At the end of the hour, the observed emission was from the reaction product layer, with negligible contribution from the metal substratum.

In subsequent measurement of temperature profiles for thermal conductivity and total thermal emission determination, all data was taken within a period of 10 minutes. It

can be assumed that negligible change in total emission occurred during this period as the profile did not change. After about 20 minutes at the low temperature settings, temperature profile changes consistent with an increase in total thermal emission were observed.

The data presented in Figure 8 is reported as spectral thermal emission values. The reproducibility of the data, together with the study reported in Figure 9, suggest that this data represents the true emissivity of ZrC. The lack of temperature dependence indicates that 0.65 micron is quite near the cross-over point in spectral emission vs wavelength. This conclusion is not supported by the study that Riethof reported. (4)

Riethof reported the cross-over to be at 2.3 microns and a decided temperature dependence at the shorter wavelengths. It is possible that Riethof's ZrC had surface contamination at the lower temperatures. It is also possible that the ZrC studied here was not identical in carbon content with Riethof's and that this might influence the spectral thermal emission. There is fair agreement in the absolute value of emission at 0.65  $\mu$  between these two studies; Riethof's data goes from about 0.67 to 0.55 between 2670 K and 2100 K, while the present study finds a near-constant value of 0.62 up to 2400 K.

#### c. Resistivity

Resistivity was measured by contacting the electrically heated rod specimen near its center with two tungsten voltage probes. The instrumentation for this measurement is described elsewhere. (3) Between the two voltage probes, the temperature profile of the rod was nearly flat. The difference between the rod temperature at the probes and the maximum central temperature never exceeded 100°. The temperature assigned to each resistivity measurement was obtained by averaging the known profile (a quadratic) over the distance between probes. This averaging resulted in a temperature no more than 30° below the maximum temperature.

Figure 10 presents the results of this study on two ZrC specimens, together with the data obtained by Taylor. (5) The data points reported here have been corrected for thermal expansion using values compiled by Goldsmith, et al, (6) and have been corrected to full density. The measured density, 90 per cent of theoretical, is in average density over each of the whole specimens. One central piece of a specimen measured 92 per cent of theoretical density. This uncertainty in density (about  $\pm 2$  per cent) is

the major error source in the reported resistivity values. The agreement between the present values at high temperatures and Taylor's data for temperatures below 1300 K is excellent. The elevated temperature resistivity of ZrO is apparently not sensitive to carbon content between 11.0 and 11.8 w/o total carbon within the accuracy of the two studies.

The data of Figure 10 is well fitted by a linear equation:

$$\rho = 0.42 \times 10^{-4} + 0.73 \times 10^{-7} T, \text{ for } 300 < T < 2400 \text{ K},$$

where the probable error in the linear fit to the experimental data is  $\pm 1.5 \times 10^{-7}$  ohm-cm. However, the uncertainties in specimen density place a limit of about  $\pm 2$  per cent on the data accuracy as discussed above.

#### d. Total Thermal Emission

Total thermal emission and thermal conductivity are determined simultaneously in the present thermophysical properties apparatus. Temperature profiles obtained from the electrically-heated specimen rods are computer fitted to a quadratic expression. Each profile then yields a linear equation in which total emission and thermal conductivity are the only unknowns.<sup>(3)</sup> The linear equations are valid near the central temperature of the rod. Total thermal emission values were obtained by simultaneous solution of pairs of these linear equations. The temperature assigned to each determination of total emission is the average between the central temperatures corresponding to the two linear equations in question.

Figure 11 presents the total thermal emission values obtained in this investigation. The straight line drawn through the points may be analytically expressed as

$$\epsilon_t = 0.772 - 9 \times 10^{-5} T, \text{ for } 1500 < T < 2400 \text{ K};$$

where the probable error in the line is  $\pm 0.02$  near 2000 K.

#### e. Thermal Conductivity

The linear equations in thermal conductivity and total thermal emission were solved for conductivity using emission values taken from the line in Figure 11. The emission value corresponded to the temperature characteristic of the linear equation. That temperature was also assigned to the resultant conductivity value. Porosity was corrected for utilizing the formula

$$\kappa_o = \kappa_p (1 - P)$$

where  $\kappa_p$  is the measured conductivity,  $P$  is the porosity, and  $\kappa_o$  is the conductivity at zero porosity. The above equation has been shown by Kingery<sup>(7)</sup> to be a good approximation for small  $P$  if the pore structure is discontinuous.

Figure 12 exhibits the experimental points from this study together with the curve reported by Taylor.<sup>(5)</sup> Taylor's scatter is comparable to that in the present study. The electronic contribution to thermal conductivity as given by the free electron value for the Lorenz number ( $2.45 \times 10^{-8}$  watt-ohm/deg<sup>2</sup>) and the resistivity data of Figure 10 is also shown in Figure 12.

## 2. Conclusions

There is a significant difference in the values for thermal conductivity obtained in this study and those reported by Taylor. No explanation for this difference is offered here, although it is noted that Taylor's specimens were carbon deficient and were probably single-phase, while the present specimens contained a small amount (about 0.2 w/o) free carbon. The slopes of the curves obtained by the two investigations are identical and are significantly above that predicted by the Wiedemann-Franz law. The  $1/T$  law which is predicted for the lattice contribution to thermal conductivity is not obeyed in either study. The failure of the total thermal conductivity to obey the equation  $K = K_e + \epsilon/T$  has been noted previously by Taylor<sup>(5, 8)</sup> for zirconium carbide and for titanium carbide.

## 3. References

1. Pollock, B. D., "The Vaporization Behavior and Thermodynamic Stability of Zirconium Carbide at High Temperatures", J. Phys. Chem., 65, 731 (1961).
2. Poland, D. E., J. W. Green, and J. L. Margrave, "Corrected Optical Pyrometer Readings", National Bureau of Standards Monograph 30 (1961).
3. Grossman, L. N., "Thermal Properties Apparatus for Metallics at High Temperatures", R62APE14 (1962). Available from: Technical Publications, General Electric Co., APED, San Jose, California.
4. Riethoff, "High Temperature Spectral Emissivity Studies", R61SD004 (1961). Available from General Electric Co., MSVD, Space Sciences Laboratory, Philadelphia 1, Pa.

5. Taylor, R. E., "Thermal Conductivity of Zirconium Carbide at High Temperatures", J. Am. Cer. Soc., 45, 353 (1962).
6. Goldsmith, A. E. Waterman, and H. J. Hirschhorn, editors, Handbook of Thermophysical Properties of Solid Materials, Vol. IV, MacMillan Co., N. Y. (1961).
7. Kingery, W. D., Introduction to Ceramics, John Wiley and Sons, N. Y. (1960), Pg. 504.
8. Taylor, R. E., "Thermal Conductivity of Titanium Carbide at High Temperatures", J. Am. Cer. Soc., 44, 525 (1961).

#### F. High Temperature Thermophysical Properties of UC<sub>2</sub>

##### 1. Experimental

Several attempts to fabricate UC<sub>2</sub> into rod shapes using graphite dies and plungers at high temperatures (2300 C) resulted in poorly bonded, low density specimens. Lineal density gradients occurred, with low central density and fairly high end densities. Addition of 1 per cent nickel to the UC<sub>2</sub> powder resulted in a rod 4.13 cm long and 0.623 cm in diameter. This specimen was hot-pressed in graphite for 15 minutes at about 1700 C and 6000 psi. A gross measurement of density immediately following fabrication showed it to be 95 per cent of theoretical density. A density check of the central one centimeter length of rod after property measurements showed it to be 90 per cent of theoretical density (10.5/11.7 gm/cm<sup>3</sup>).

Following the property measurements, metallographic examination, chemical analysis, and x-ray determination of the lattice parameters were performed. The specimen consisted of 8.7 w/o total carbon and had 0.3 w/o oxygen in it. The lattice parameters were  $a_0 = 3.515 \pm 0.002$  a.u. and  $c_0 = 5.976 \pm 0.002$  a.u. The x-ray pattern showed the UC<sub>2</sub> to be fairly well crystallized with a trace phase of UC present. (The last heat treatment before analysis ended with a rapid cooling from 2150 K).

Metallographic examination was performed both at the end of the rod (cold area) and at the center of the rod (hottest area). Nickel was found at the cold ends in the grain boundaries while none was observed at the center. The sample appeared to be of higher density than either density measurement indicated. The specimen exhibited considerable twinning and some UC precipitate as previously observed by Chubb and Phillips. (1) Figure 13 is a photomicrograph at 250X of the central section of the rod. The bright spots are voids.



The specimen was cleaned and polished in a gettered-argon glove box and then inserted into the thermal properties apparatus described previously. Temperature and other measurements were also performed as previously described. The initial heat up was done slowly, during which resistivity was often measured. Above 1500 C, nickel began to cook out rapidly so that further temperature measurements were in error due to a coated window. A final heating at 2070 K for one hour removed all traces of Ni from the central region of the specimen. Resistivity values during the initial heat-up are shown in Figure 14, they are labeled " $UC_2 + 1 \text{ v/o Ni}$ ". Subsequent heatings (after cleaning of the window) resulted in negligible nickel evaporation.

Figure 14 presents the resistivity of  $UC_2$  containing 8.7 w/o carbon. The upper points, labeled  $U_2C_3 + C$ , were obtained following a 30 minute soak at 1550 K and a 60 minute soak at 1450 K. The equilibrium phase composition at 1450 K is  $U_2C_3 + C$ , <sup>(2)</sup> however, the kinetics of the decomposition reaction at that temperature are quite slow so there is no assurance that only  $U_2C_3$  and C were present during the measurement. Heating above 2100 K caused the resistivity to approach that of  $UC_2$ , indicating that the " $U_2C_3 + C$ " was rapidly changing back to  $UC_2$  (the equilibrium phase at 2100 K). No analysis was made of the phase composition for the points labeled  $U_2C_3 + C$ . The data points in Figure 14 have been corrected for a porosity of 10 per cent and should be characteristic of the fully dense material. Due to uncertainty in density, the curve labeled  $UC_2$  is probably in error by  $\pm 5$  per cent.

Figure 15 shows the spectral emission values obtained at  $0.65\mu$  for the  $UC_2$  specimen. These data were used for temperature measurement during electrical resistivity, thermal conductivity, and total thermal emission measurements. The spectral emission values were very reproducible and did not change significantly even when the sample was soaked at the lower temperatures (1450 K) for 30 minutes in a vacuum of  $5 \times 10^{-7}$  torr. The implication here is that no noticeable reaction was occurring on the surface during the soaking period (the contrary was observed in the case of ZrC).

Figure 16 exhibits the results of the measurement of total thermal emission for  $UC_2$ . The straight line drawn through the points was used in calculating the thermal conductivity points in Figure 17 as described elsewhere. <sup>(2)</sup> The data shown here are not considered to be very accurate due primarily to the short length of the specimen rod and the resulting lack of resolution in determining the temperature profiles. Nonetheless, the data should be

accurate to  $\pm 20$  per cent at the worst. Figure 17 also shows the electronic contribution to the thermal conductivity of  $UC_2$  as given by the Wiedemann-Franz law and the resistivity values of Figure 14.

## 2. References

1. Chubb, W. and W. M. Phillips, "Constitution of the Partial System: Uranium Monocarbide-Uranium Dicarbide", Trans. ASM, 53, 465 (1961).
2. Grossman, L. N. "Thermal Properties Apparatus for Metallics at High Temperatures, R62APE14 (1962). Available from: Technical Publications, General Electric Co., APED, San Jose, California.

### G. High Temperature Thermophysical Properties of $U_{0.5}Zr_{0.5}C$

Property measurements were attempted on three specimens of  $U_{0.5}Zr_{0.5}C$ . In all three cases, failure of the sample (by fracture) occurred before the measurements could be completed. Data were obtained, however, on the electrical resistivity and the spectral thermal emission from specimens with reacted surfaces. The specimen preparation, characterization, and the measured properties will be discussed below, together with a thermal conductivity estimate.

Three  $1/4$  inch diameter rods about 2 inches long were hot-pressed from mixed, -325 mesh, UC and ZrC powders. An addition of 1 w/o Ni was made to the mixed powders to aid in densification. The powders were pressed in graphite at about 2000 K with 6000 psi applied pressure for 15 minutes at temperature. The resulting rods were of fully dense and well bonded. Metallographic and x-ray data obtained after the measurements will be presented below.

The first rod was heated to about 2000 K and remained at that temperature 2 hours while nickel cooked out of it (the vapor pressure of Ni is  $1.9 \times 10^{-4}$  atmos. at 2000 K). Upon slow cooling, a radial crack appeared near one cold end; examination after removal showed the break to be of the type one would expect from thermal stress. A similar break occurred in the second rod, also upon cooling. No useful data was obtained from either of these experiments.

A third rod, slightly longer than the first two, was inserted into the apparatus and resistivity was measured during the initial heat-up. The resulting data are reported in Figure 1 as  $U_{0.5}Zr_{0.5}C + 1$  w/o Ni. The specimen was then held at 2000 K for about two hours while nickel evaporated; the rapid evaporation of Ni at 2000 K was evidenced by a rapid plating out on the quartz view-port of the apparatus. The rod was then cooled and the window cleaned. Re-heating of the specimen yielded the

resistivity data for  $U_{0.5}Zr_{0.5}C$  reported in Figure 18. No nickel plated out on the window during the second heating. The sample broke (again apparently due to stresses arising from the steep thermal gradients at the rod ends) before further measurements could be taken.

Metallographic examination of the specimen central cross-section after the above measurements revealed a single-phase, well densified, solid solution. No trace of Ni was in evidence. The mean-intercept grain diameter was determined to be 5.4 microns. X-ray diffraction of the same surface showed a well-crystallized single phase with lattice parameter  $a_0 = 4.823 \pm 0.002$  Å. This parameter corresponds to the solid solution  $U_{0.50}Zr_{0.50}C$ . (1)

Temperature measurement of the rod was performed by observation with an optical pyrometer into a tapered hole 0.020 inch in diameter by about 0.050 inch deep. Comparison of the hole temperature with nearby surface temperatures yielded values for the spectral emission of the rod. No change in emission was observed after soaking at 2000 K for two hours; this observation together with the high emission values observed, indicates that the surface remained contaminated throughout the investigation. (The flashing temperature used for ZrC was about 2400 K, while UC was cleaned at about 2100 K; no attempt was made to find a minimum effective flashing temperature for these materials. Figure 19 presents this measured spectral emission at  $0.65\mu$  for  $U_{0.5}Zr_{0.5}C$  with a reacted surface. It appears that fully reacted surfaces (i.e. surfaces with optically thick reaction layers) of all of the materials examined in the present investigation have spectral emission values near 0.75.

The thermal conductivity of  $U_{0.5}Zr_{0.5}C$  could not be measured in the apparatus used in the present study due to the very low thermal stress resistance of the solid solution. An estimate can be made, however, utilizing the measured values of the Lorenz number ( $L$ ) for UC and for ZrC. These values are tabulated below:

Temperature (°K)	UC			ZrC		
	K ( $\frac{\text{cal}}{\text{cm sec deg}}$ )	$\rho$ ( $\Omega \cdot \text{cm}$ )	L ( $\frac{\text{watt } \Omega}{\text{deg}^2}$ )	K ( $\frac{\text{cal}}{\text{cm sec deg}}$ )	$\rho$ ( $\Omega \cdot \text{cm}$ )	L ( $\frac{\text{watt } \Omega}{\text{deg}^2}$ )
300	--	$0.4 \times 10^{-4}$	--	--	$0.64 \times 10^{-4}$	--
500	0.055	0.72	$3.32 \times 10^{-8}$	--	0.79	--
700	0.054	1.00	3.23	--	0.93	--
1000	0.054	1.38	3.12	--	1.14	--

Temperature (°K)	UC			ZrC		
	K $\left(\frac{\text{cal}}{\text{cm sec deg}}\right)$	$\rho$ ( $\Omega \text{ cm}$ )	L $\left(\frac{\text{watt } \Omega}{\text{deg}^2}\right)$	K $\left(\frac{\text{cal}}{\text{cm sec deg}}\right)$	$\rho$ ( $\Omega \text{ cm}$ )	L $\left(\frac{\text{watt } \Omega}{\text{deg}^2}\right)$
1250	0.056	1.55	2.91	--	1.33	--
1500	0.056	1.94	3.03	0.065	1.51	$2.74 \times 10^{-8}$
1730	0.056	2.24	2.86	0.069	1.71	2.83
2000	0.056	2.50	2.93	0.074	1.90	2.95
2100	0.056	2.60	2.90	0.075	1.98	2.96
2200	0.056	--	--	0.077	2.05	2.99

The above table shows the Lorenz numbers for UC and for ZrC to fall between about  $2.7 \times 10^{-8}$  and  $3.0 \times 10^{-8}$  above 1500 K; that is, the materials exhibit near-ideal metal characteristics ( $L = 2.45 \times 10^{-8}$ ). The lattice contribution of the solid solution  $\text{U}_{0.5}\text{Zr}_{0.5}\text{C}$  should be even less than that of the pure compounds. Therefore, a Lorenz number of  $2.8 \times 10^{-8}$  is probably accurate within  $\pm 10$  per cent for  $\text{U}_{0.5}\text{Zr}_{0.5}\text{C}$  above 1500 K. Between 1000 and 1500 K, a Lorenz number of  $2.8 \times 10^{-8}$  is probably accurate within  $\pm 15$  per cent; while nothing can be inferred about its behavior below about 1000 K. A tabulation of the estimated thermal conductivity of  $\text{U}_{0.5}\text{Zr}_{0.5}\text{C}$  is given in the following Table using the above estimated Lorenz number and the measured resistivity (Figure 18).

Temperature °K	K $\left(\frac{\text{cal}}{\text{cm sec deg}}\right)$
1000	0.036
1200	0.040
1400	0.044
1600	0.047
1800	0.049
2000	0.052
2200	0.053
2400	0.055

As is expected, the conductivity of the solid solution is lower than either of the pure carbides UC or ZrC. This low thermal conductivity may account for the observed cracking since higher thermal stresses will develop in  $\text{U}_{0.5}\text{Zr}_{0.5}\text{C}$  than in comparable UC or ZrC samples.

## REFERENCES

1. L. D. Brownlee, "The Pseudo-Binary Systems of Uranium Carbide with Zirconium Carbide, Tantalum Carbide, and Niobium Carbide", J. Inst. Metals, 87, 58 (1959).

H. ThC, ThC<sub>2</sub>, YB<sub>6</sub>, and EuB<sub>6</sub> Thermophysical Properties

Fabrication and experimental difficulties allowed only limited data to be obtained on these materials. No data was obtained on EuB<sub>6</sub> due to failure of all attempts to fabricate a suitable rod specimen. Spectral thermal emission values (some characteristic of reacted surfaces) were obtained for ThC, ThC<sub>2</sub>, and YB<sub>6</sub>. Electrical resistivity data was obtained for ThC<sub>2</sub> between 1300 and 2250 K. The materials will be discussed separately below.

Yttrium hexaboride was prepared in rod form by vacuum hot pressing in a molybdenum die using 1/4 inch diameter tungsten plungers. Fifteen minutes at 1500 C under 9000 psi produced an 85 per cent dense rod about 1-1/2 inch long. The starting material was -325 mesh YB<sub>6</sub> powder prepared at VAL from Y<sub>2</sub>O<sub>3</sub> and B. (1) During a subsequent brazing step, the sample was inadvertently exposed to air at about 500 C. Although no visible change occurred, its high measured resistivity (0.0346  $\Omega$ -cm at 10 C) indicated that some reaction had occurred. (The reported room temperature resistivity of YB<sub>6</sub> is  $10.4 \times 10^{-6}$   $\Omega$ -cm. (2)) Prior experience suggested that the borate, YBO<sub>3</sub>, had resulted from heating in air; x-ray diffraction confirmed a predominant phase of YBO<sub>3</sub>. Subsequent attempts to produce YB<sub>6</sub> rods in graphite dies were not successful.

Thorium monocarbide and thorium dicarbide bars were obtained from the Carborundum Co. They were 1/4 inch  $\times$  1/4 inch  $\times$  2 inches square bars. Due to the extreme reactivity between the carbides and air at room temperature, all handling of these bars was performed in a calcium-gettered argon glove box in the presence of P<sub>2</sub>O<sub>5</sub>. The routine methods of mounting the specimens in the thermal properties apparatus failed in this case. The method of mounting resorted to was pressure-fitting the carbide to the copper electrode using annealed gold foil in the interface. This technique provided greater electrical and thermal resistivity than brazing, but proved satisfactory.

The ThC specimen was heated up to 2335 K during which spectral emission values were obtained from hole vs surface temperature measurements. No resistivity or other data were obtained due to failure of the tungsten voltage probe. On cooling, the sample cracked badly, apparently due to thermal shock. No further studies on ThC were attempted, however the present techniques are adequate to determine the thermophysical properties of ThC. The emission data on ThC presented in Figure 20 is probably representative of a reacted surface at the lower temperatures, while the values above 1900 K may approach the true spectral emissivity of ThC.

The  $\text{ThC}_2$  specimen rod was pressure-contacted to the water-cooled copper electrodes of the thermal properties apparatus using annealed gold foil. The rod was 95 per cent dense ( $8.96 \text{ gm/cm}^3$ ). No chemical analysis is available at this time. The observed microstructure of the center of the rod after property measurements is shown in Figure 21. Considerable twinning is evident in the photomicrograph. The large and small non-metallic inclusions are isotropic and are believed to be  $\text{ThO}_2$ . The large uniformly grey areas are pores. The present powder-metallurgy product has very similar microstructure to the arc-fused material reported by Brett et al. (3)

Spectral emission values for  $\text{ThC}_2$  are shown in Figure 20. They were obtained using a hole 0.12 cm deep by 0.06 cm in diameter. The hole is not black-body, but no correction was made for its shallowness. The high values obtained below 1500 K are believed to be due to reaction product buildup on the surface of the carbide. The material was not initially highly polished, but high temperatures thermally polished it considerably. The values in Figure 20 are probably not true emissivity values as is indicated by the downward trend at very high temperatures. The data in Figure 19 was utilized in determining the resistivity vs temperature data discussed below.

Electrical resistivity of  $\text{ThC}_2$  was measured as previously described. The temperature profile between probes increased nearly linearly (due to poor thermal contact at the top electrode) so that a simple average could be employed accurately. The temperature difference between probes varied between 10 and 40 degrees. The observed resistivity values are shown in Figure 22. The somewhat abrupt change in slope near 1530 K may be due to a phase change in  $\text{ThC}_2$ . The points in Figure 22 were obtained over a variety of heating rates, both in the heating and cooling directions; the curve seems quite reproducible. The lattice for  $\text{ThC}_2$  has been reported as tetragonal, orthorhombic, and monoclinic as is recently reviewed by Kempter and Kikorian. (4) The apparent lack of agreement on lattice and parameters may be due to the existence of one or more high temperature phases whose existence at room temperature is dependent on cooling rate and/or impurity content.

No thermal conductivity or total emission data was obtained for the thorium carbides. The present apparatus is suitable for these materials; however, bonding techniques must be found to join the carbide to its water-cooled electrode.

#### References

1. Kaznoff, A. I., E. W. Hoyt and L. N. Grossman, "Physicochemical Properties of Boride Thermionic Cathode Materials", Advanced Energy Conversion 1, 1962 (in press).

2. Samsonov, G. V., L. Y. Markovski, A. F. Zhigach and M. G. Valiashko. "Boron. Its Compounds and Alloys", Akad. Sci. Ukr. SSR, Kiev (1960).
3. Brett, N., D. Law and D. T. Livey. "Some Investigations on the Uranium: Thorium: Carbon Systems", J. Inorg. Nucl. Chem., 13, 44 (1960).
4. Kempter, C. P., N. H. Krikorian, "Some Properties of Thorium Monocarbide and Dicarbide", J. Less-Common Met., 244, (1962).

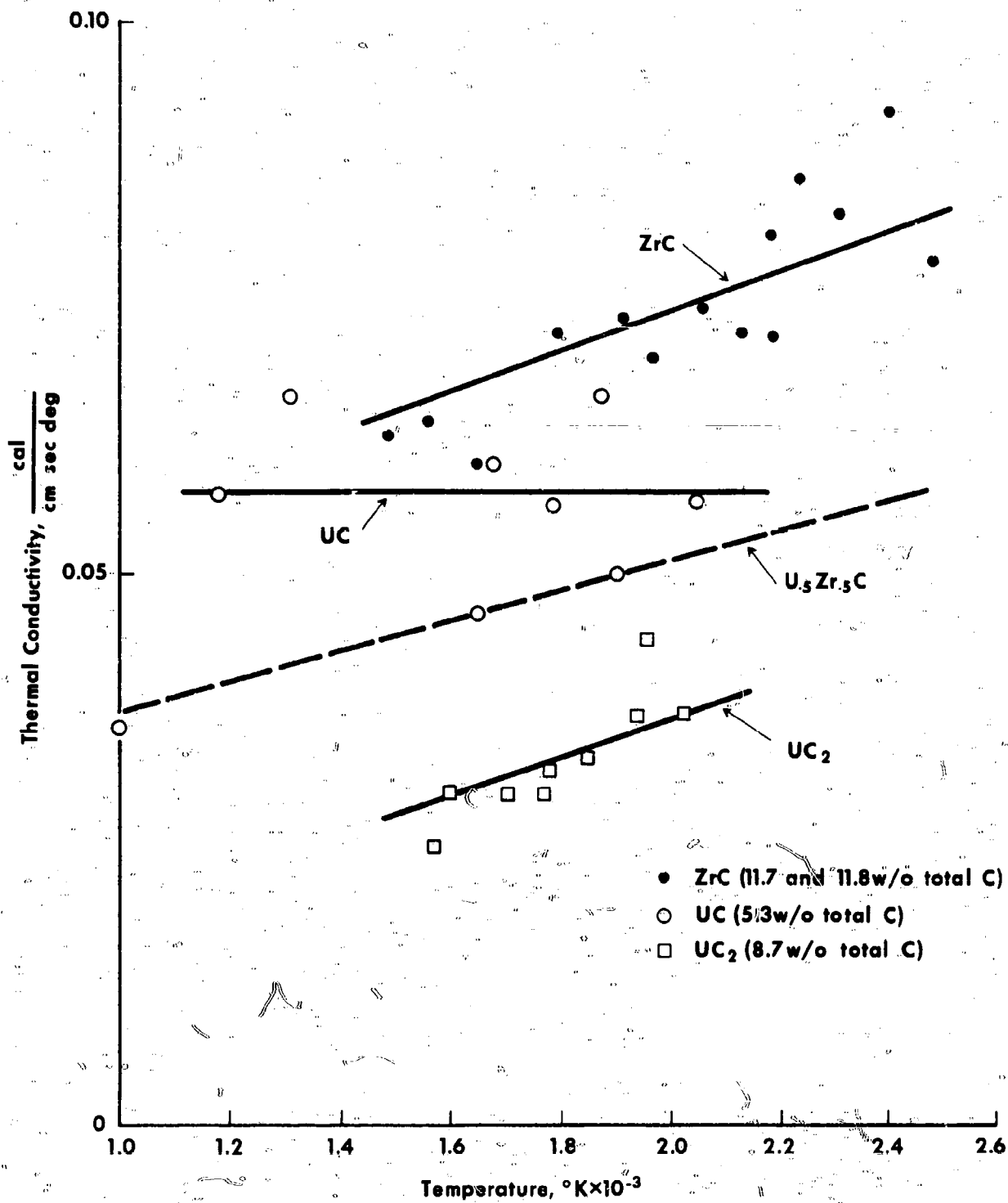


Figure S-1. THERMAL CONDUCTIVITY MEASUREMENT SUMMARY



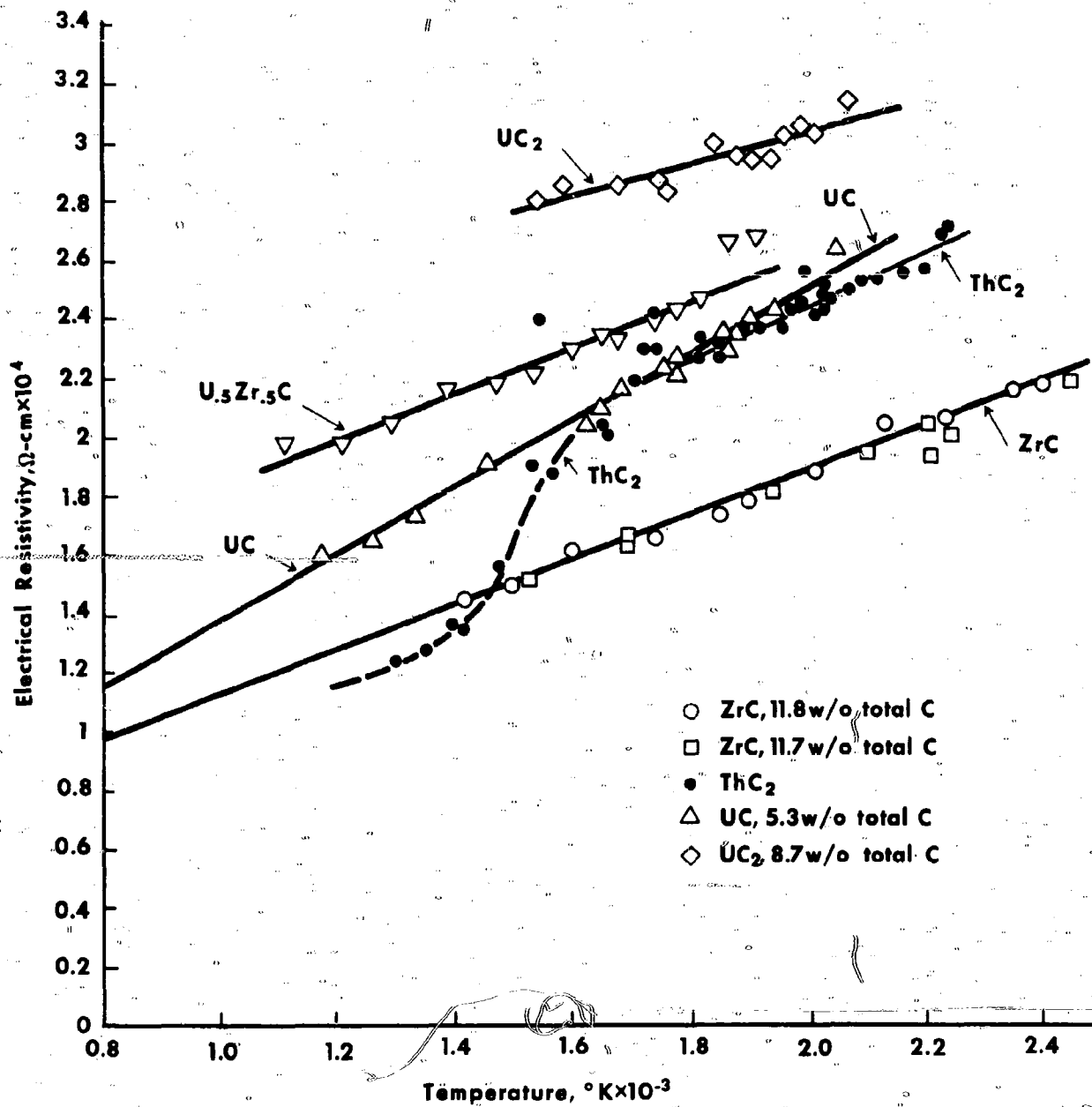


Figure S-2. ELECTRICAL RESISTIVITY MEASUREMENT SUMMARY

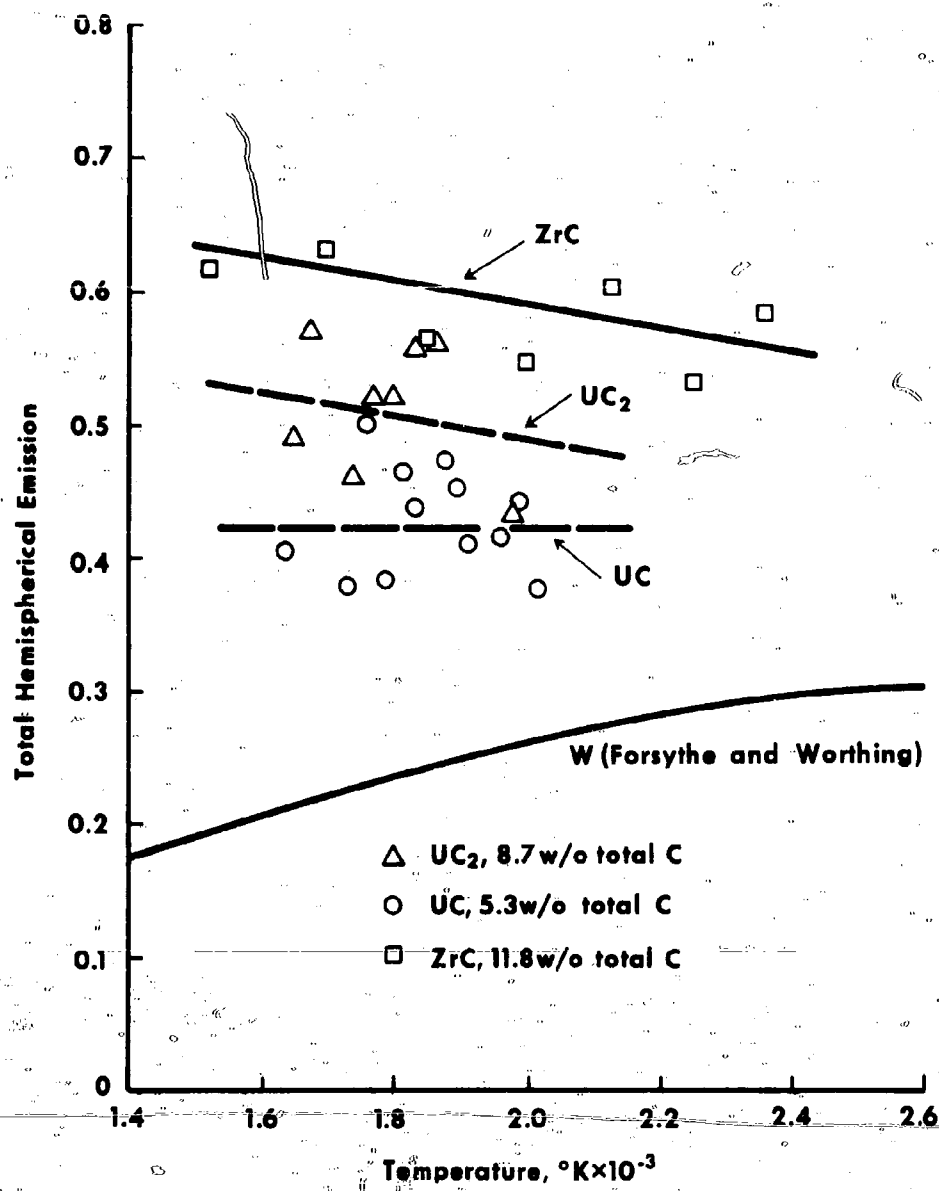


Figure S-3. TOTAL HEMISPHERICAL THERMAL EMISSION MEASUREMENT SUMMARY

Voltage Probes

Specimen

Water

Current

Vacuum

Figure 1. THERMAL PROPERTIES APPARATUS

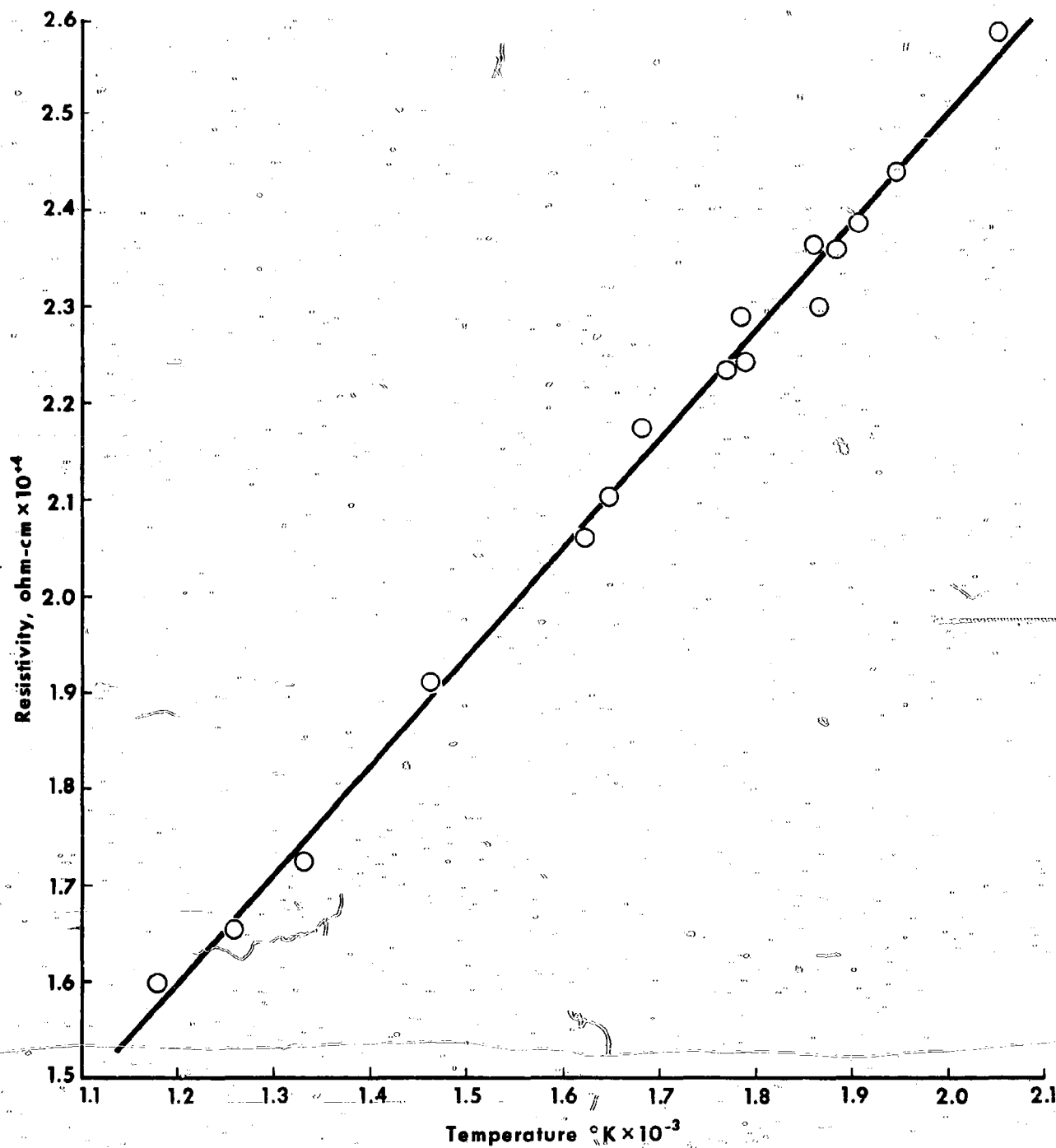


Figure 2. ELECTRICAL RESISTIVITY; EXPERIMENTAL POINTS

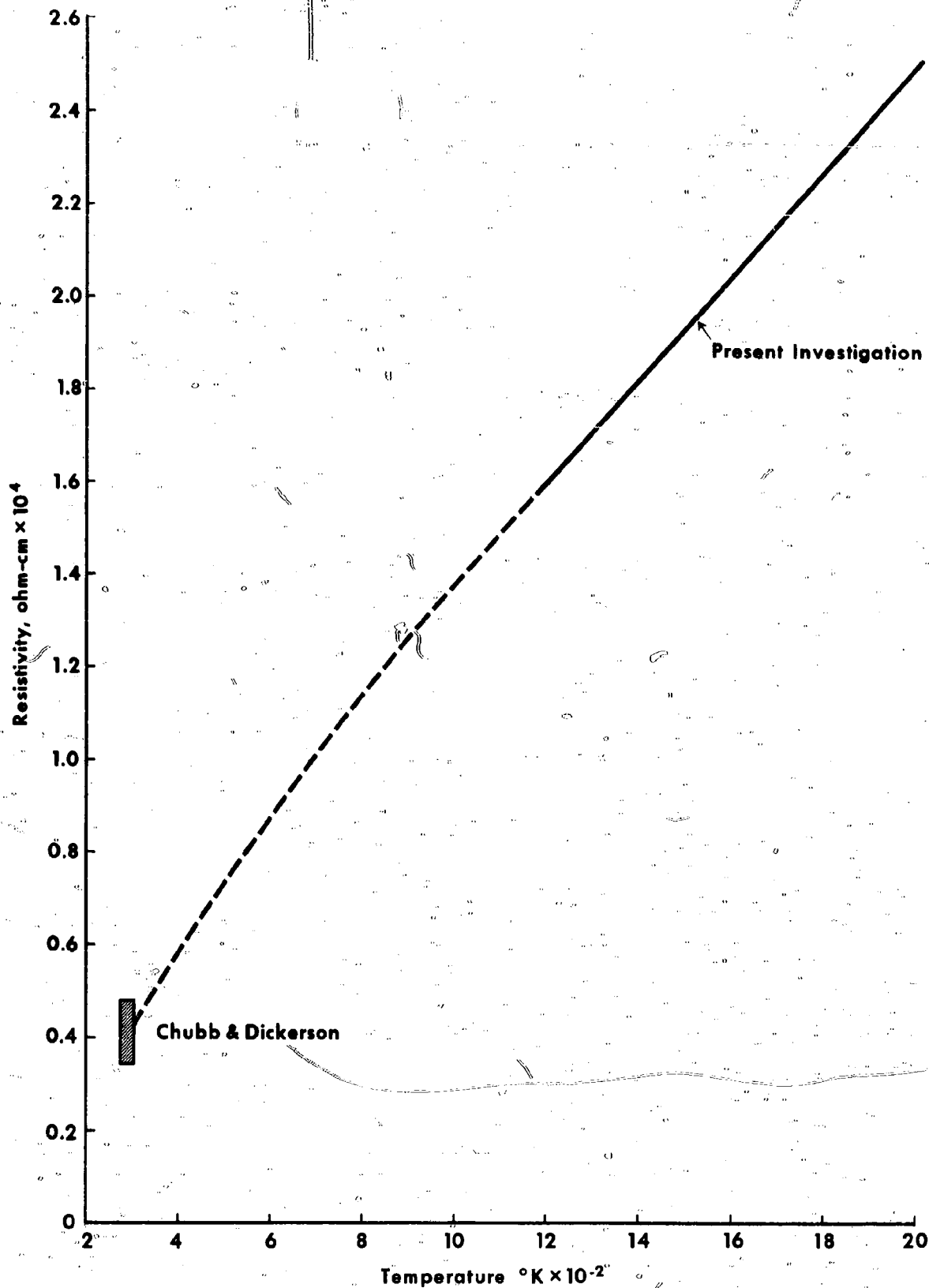


Figure 3. ELECTRICAL RESISTIVITY OF UC (5.3 w/o TOTAL CARBON)

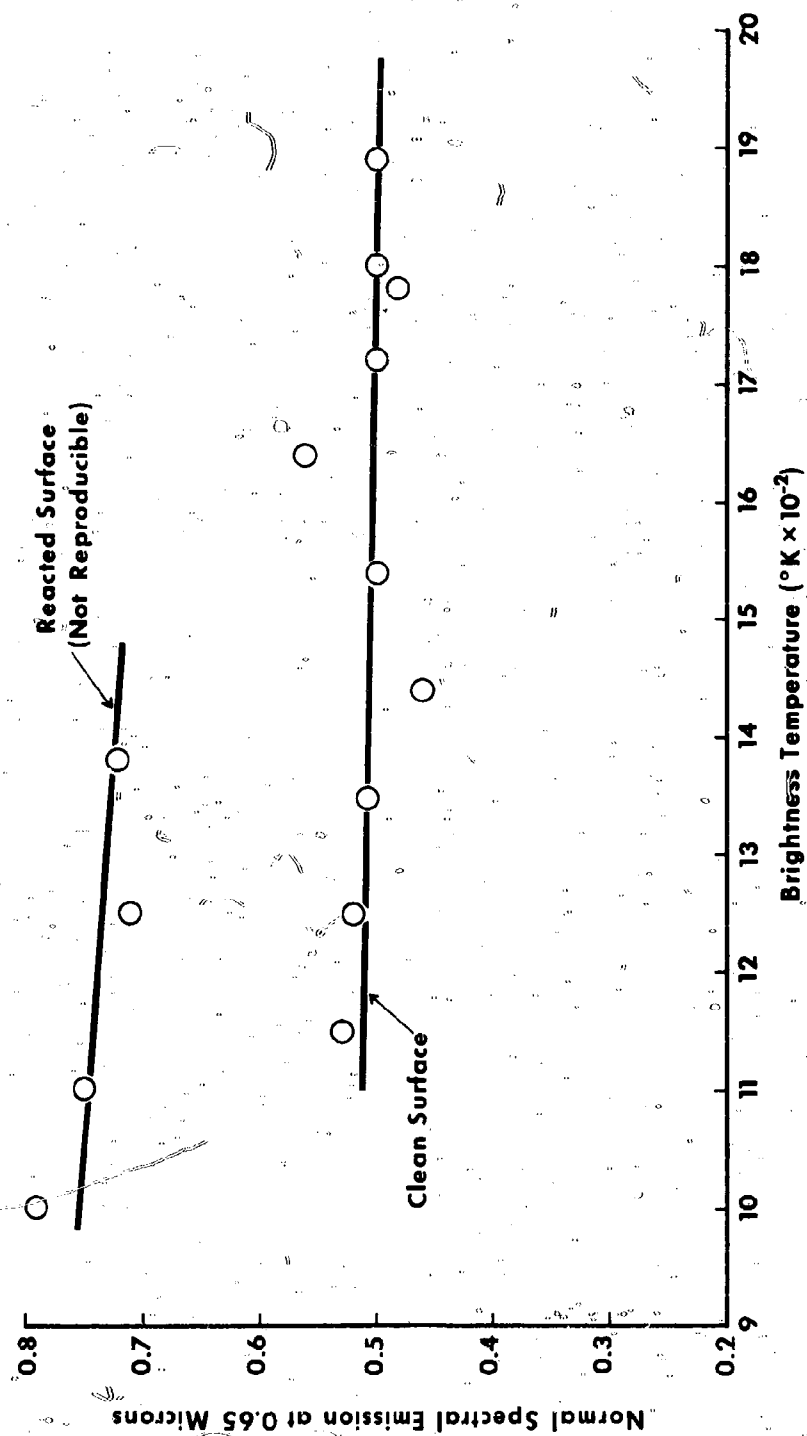


Figure 4. NORMAL SPECTRAL (0.65 $\mu$ ) EMISSION OF UC (5.3w/o TOTAL CARBON)

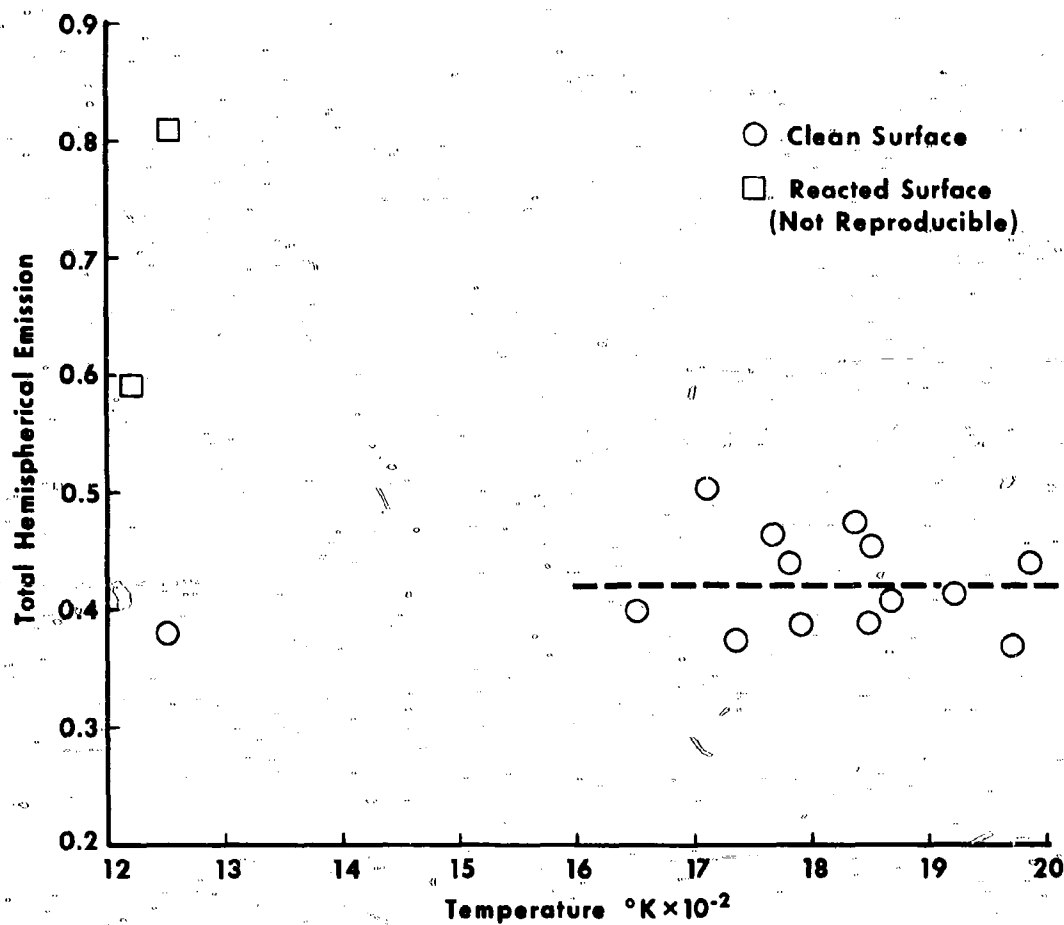


Figure 5. TOTAL HEMISPHERICAL EMISSION OF UC (5.3 w/o TOTAL CARBON)

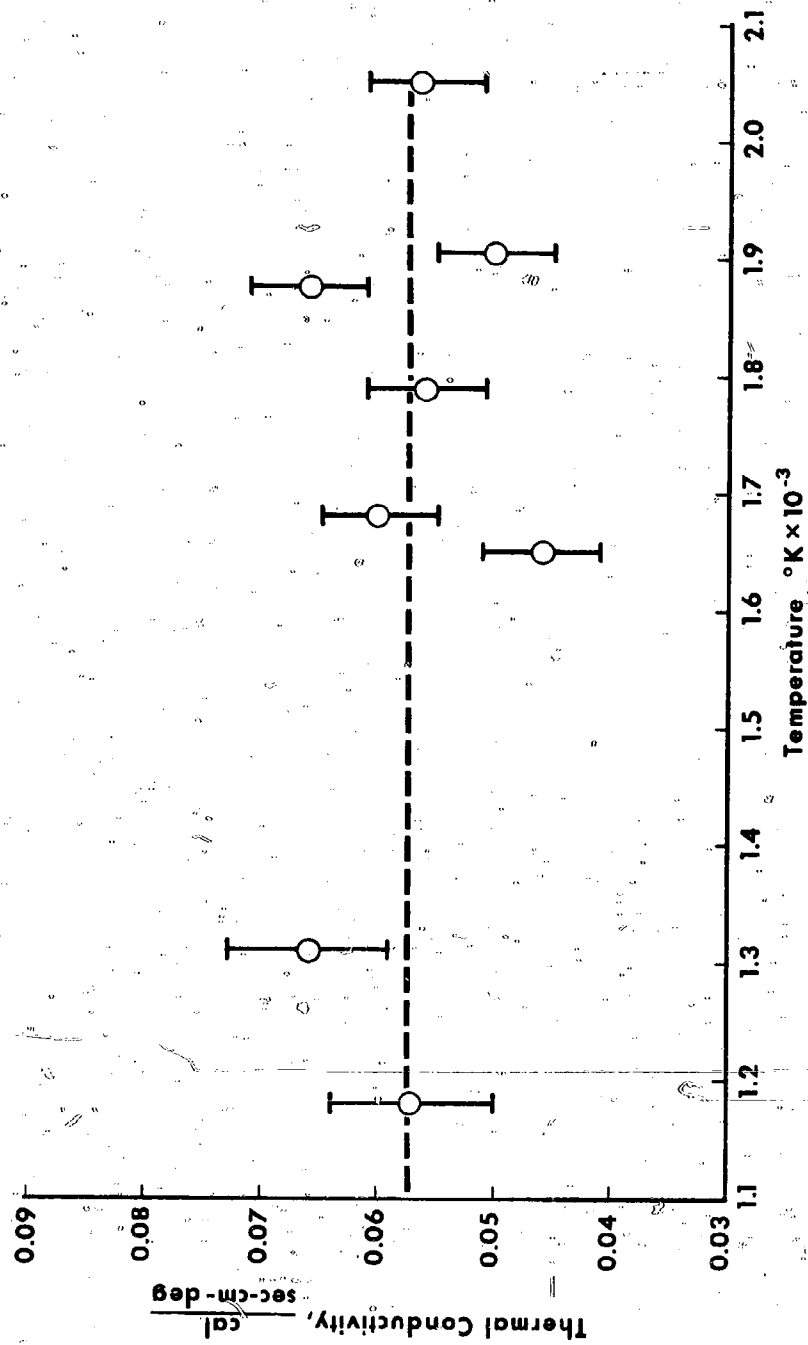


Figure 6. THERMAL CONDUCTIVITY; EXPERIMENTAL POINTS



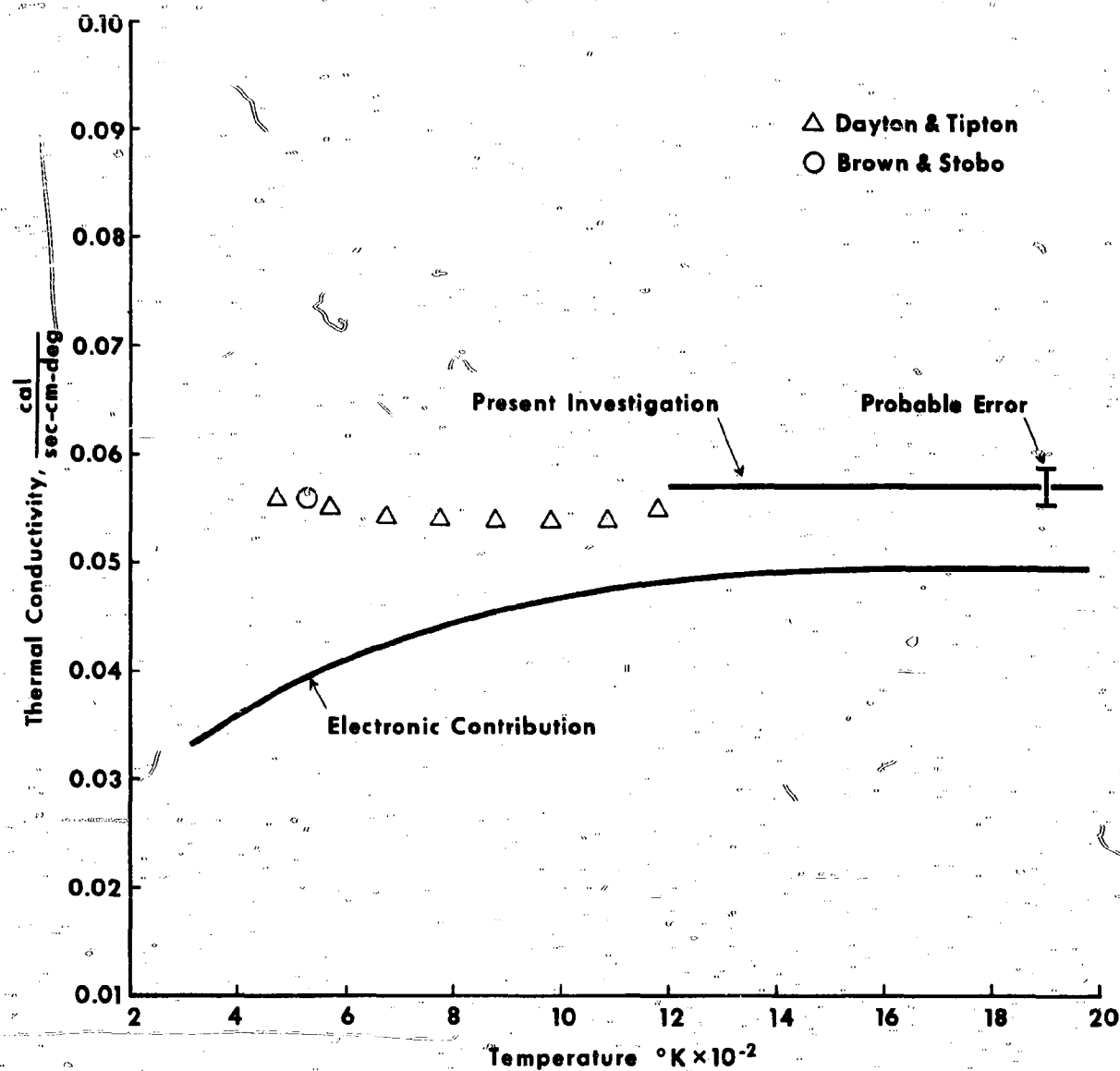


Figure 7. THERMAL CONDUCTIVITY OF UC (5.3 w/o TOTAL CARBON)

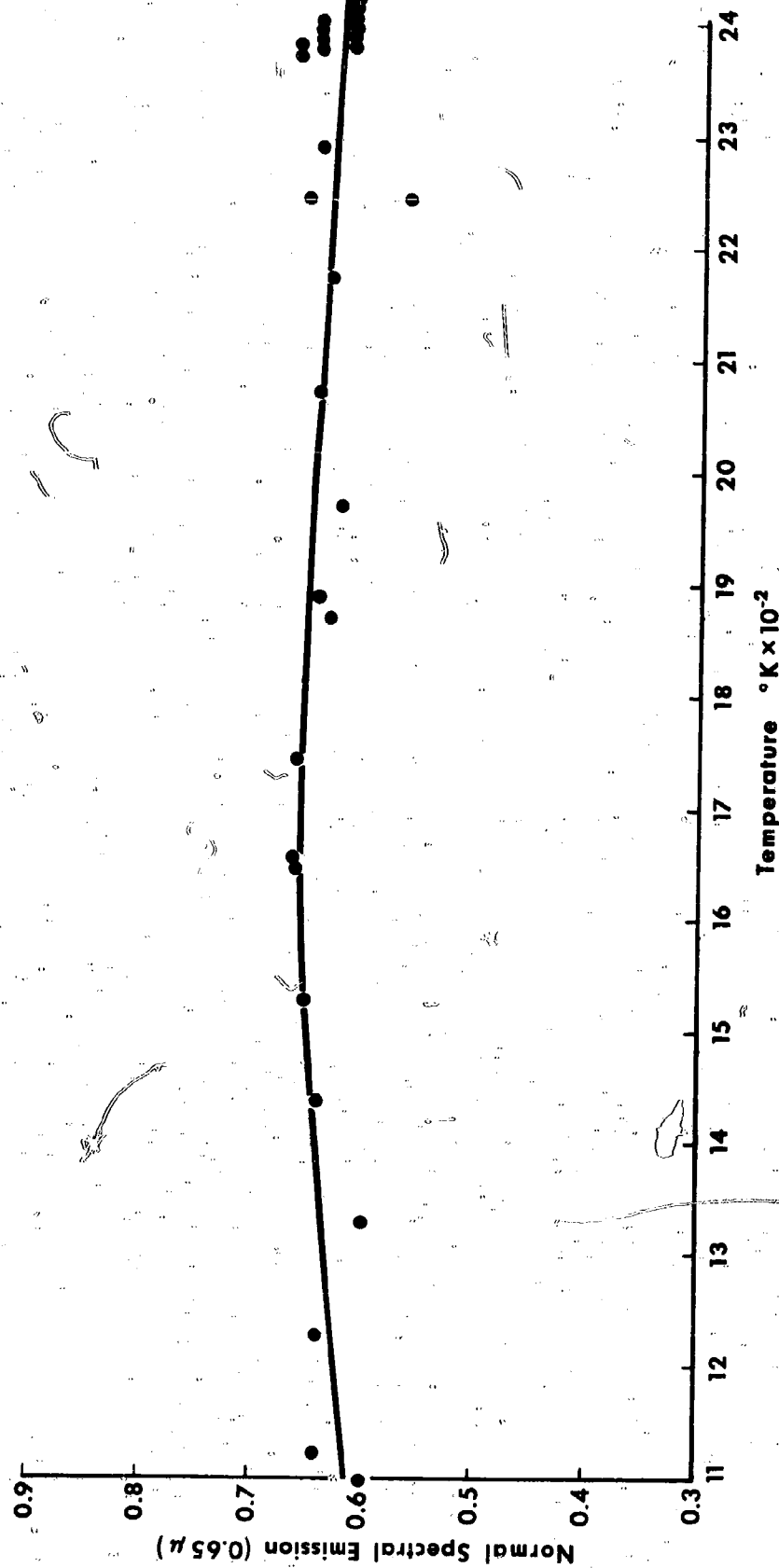


Figure 8. ZrC SPECTRAL EMISSION (0.65  $\mu$ )

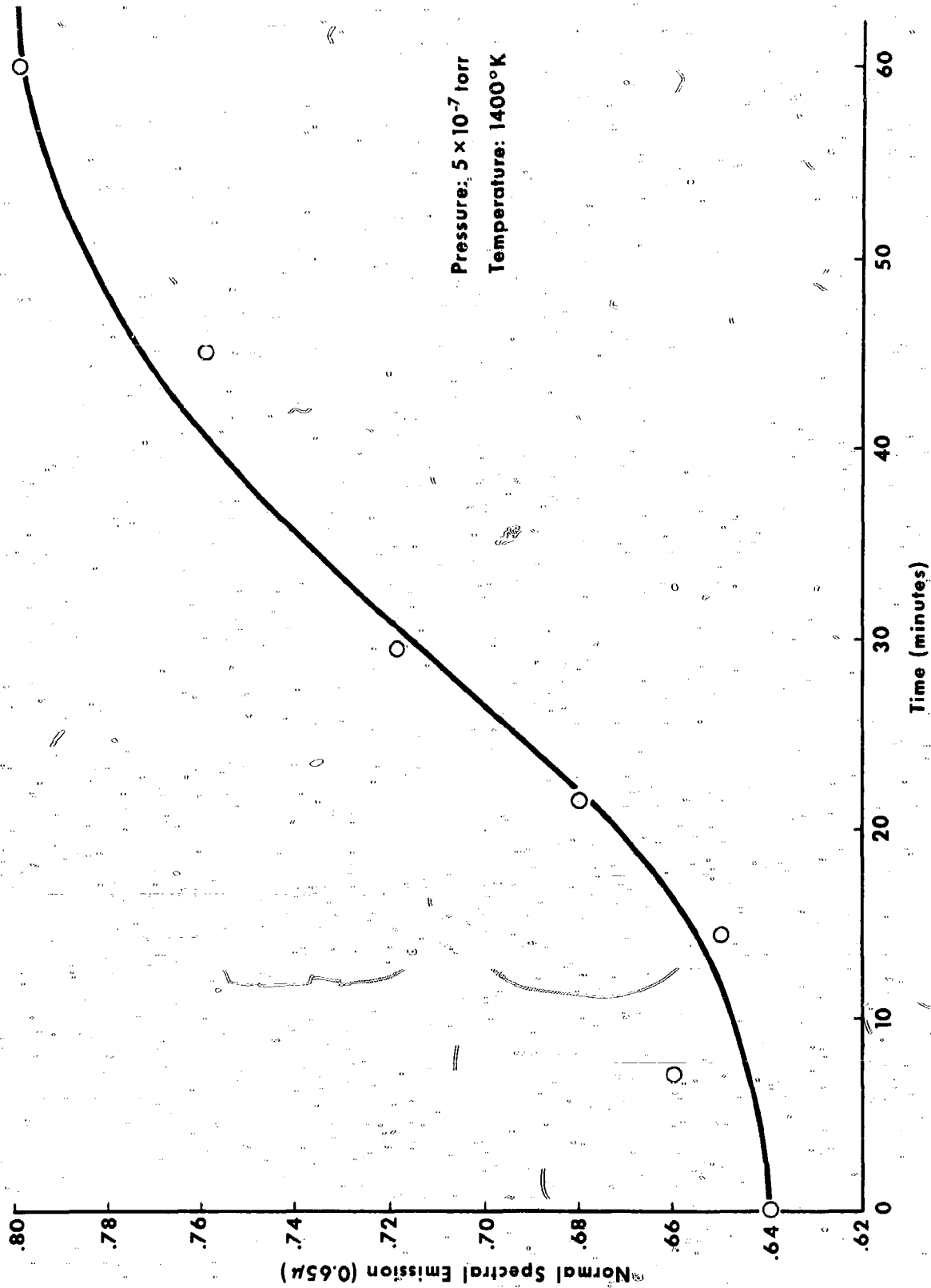


Figure 9. ZrC SPECTRAL EMISSION VERSUS TIME AFTER FLASHING

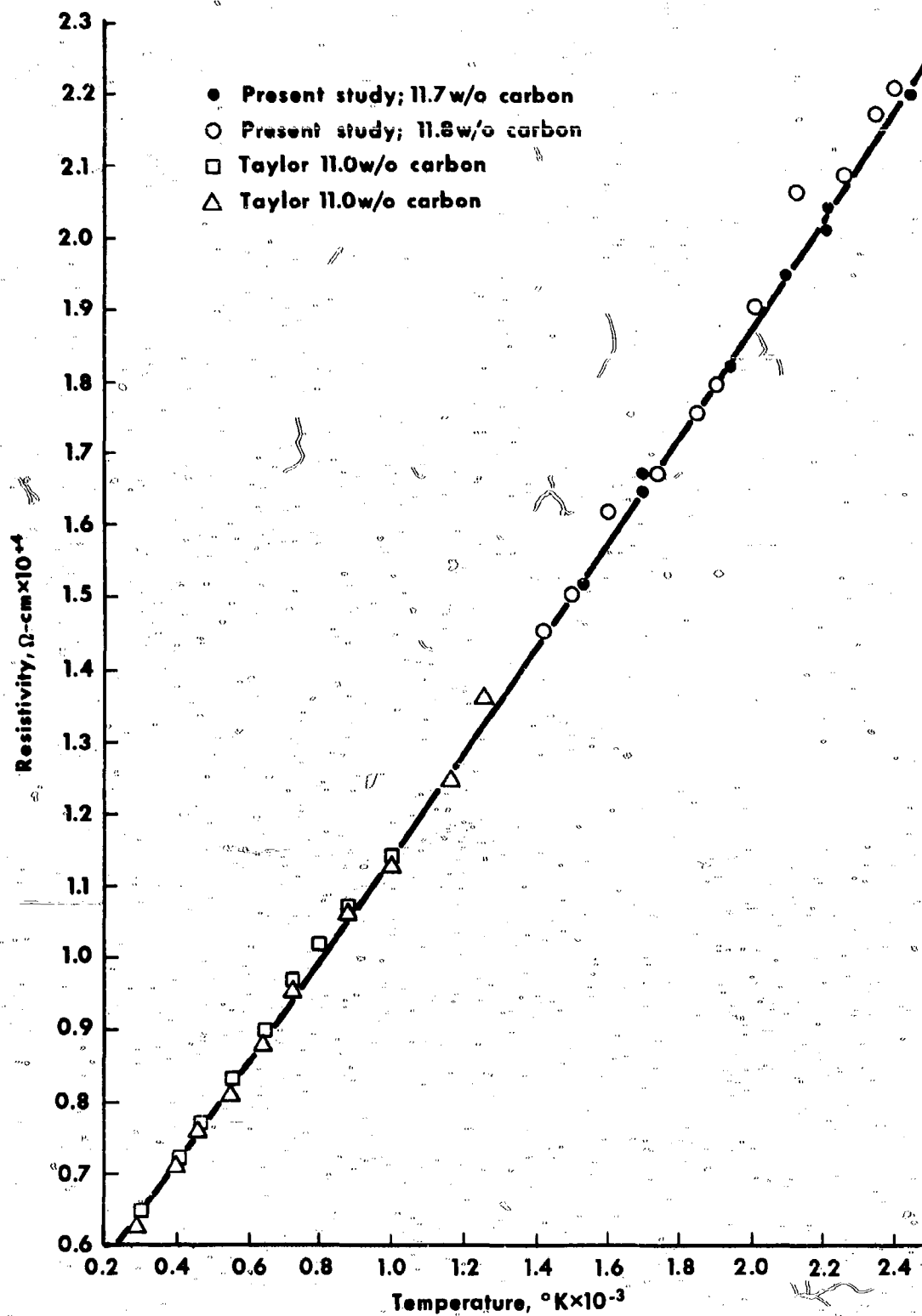


Figure 10. ELECTRICAL RESISTIVITY OF ZrC (11.8 w/o total carbon)

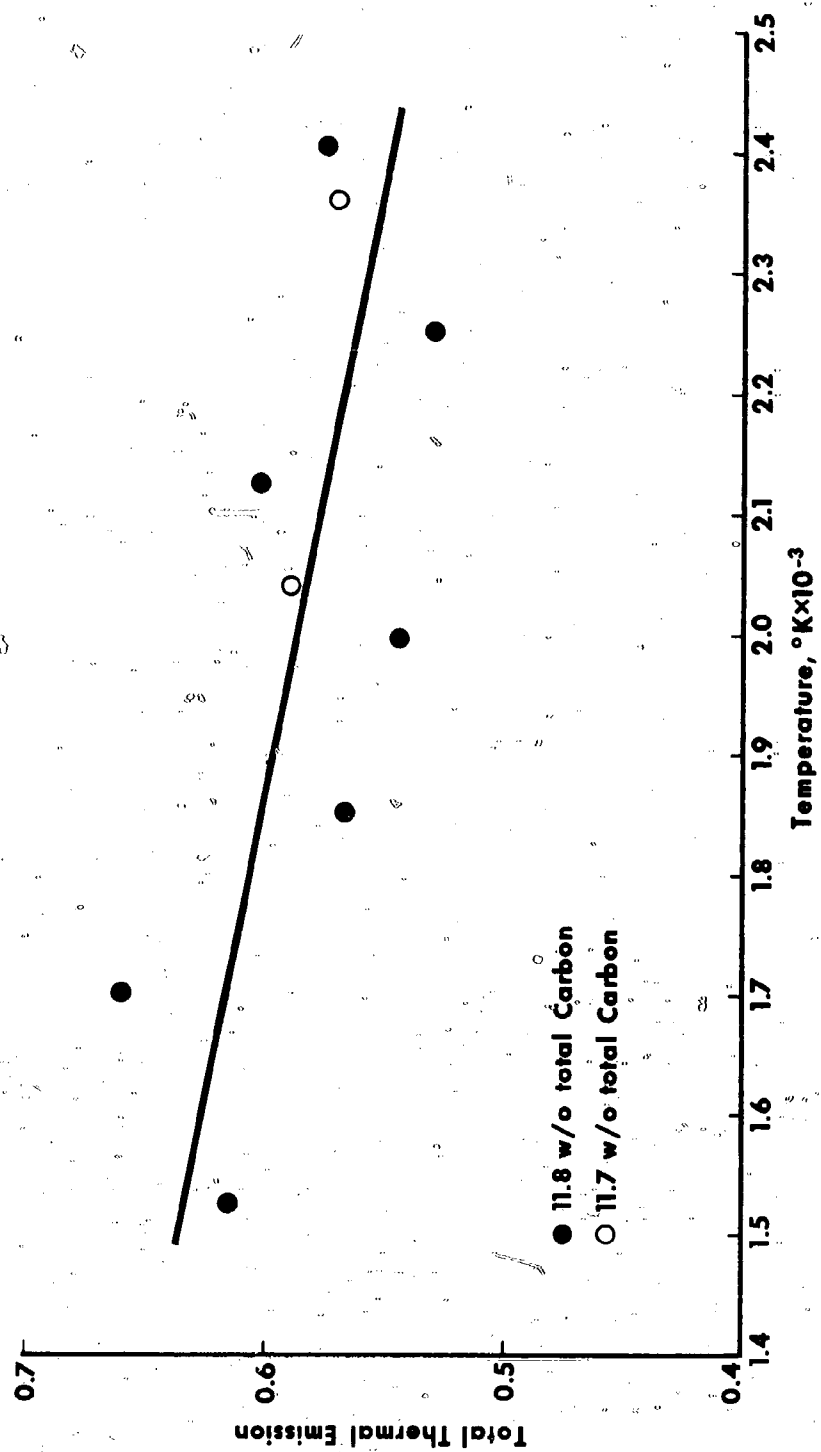


Figure 11. TOTAL THERMAL EMISSION FOR ZrC

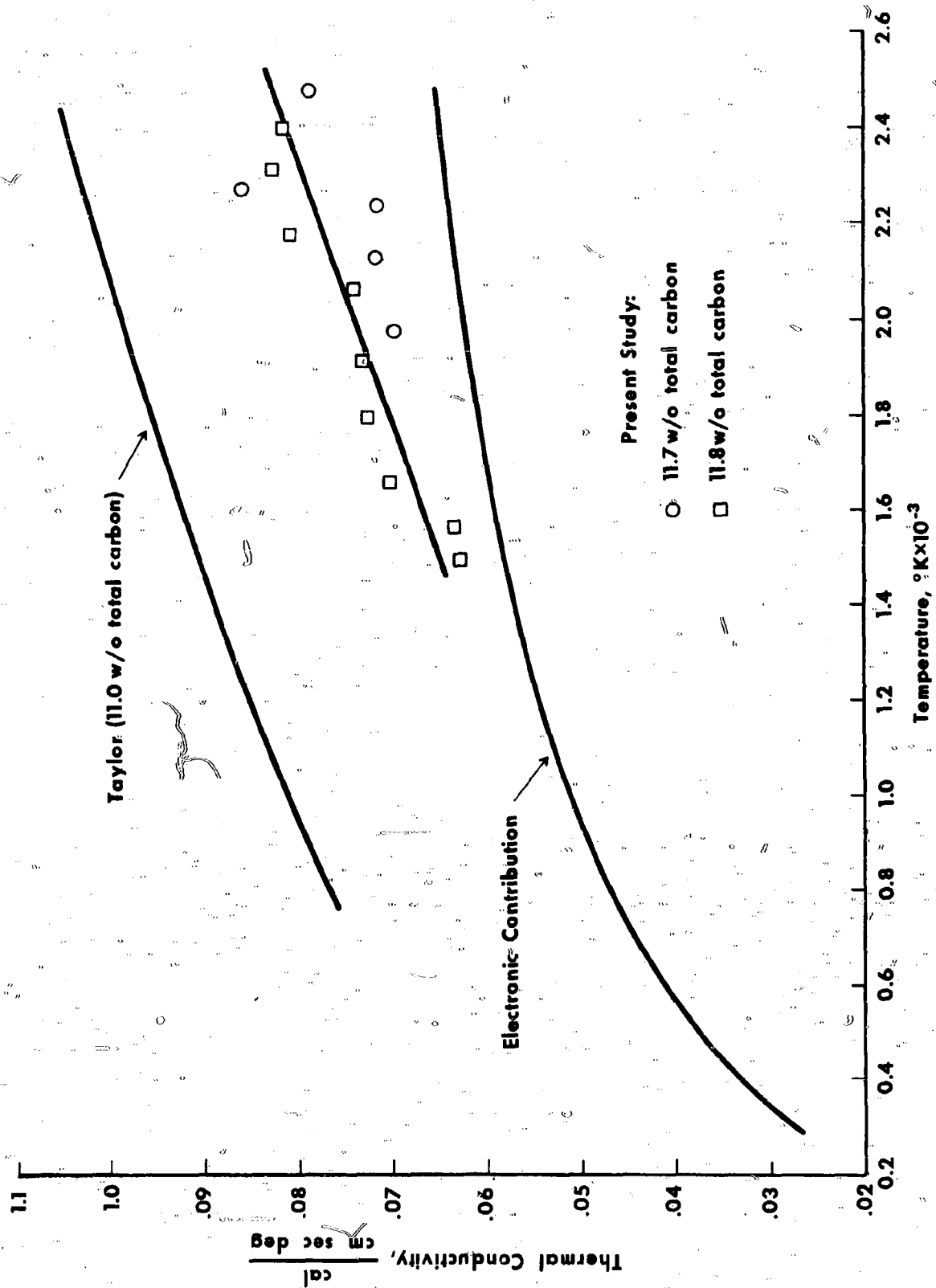


Figure 12. THERMAL CONDUCTIVITY OF ZIRCONIUM CARBIDE



**Figure 13. PHOTOMICROGRAPH OF UC<sub>2</sub> SPECIMEN (250 X)**

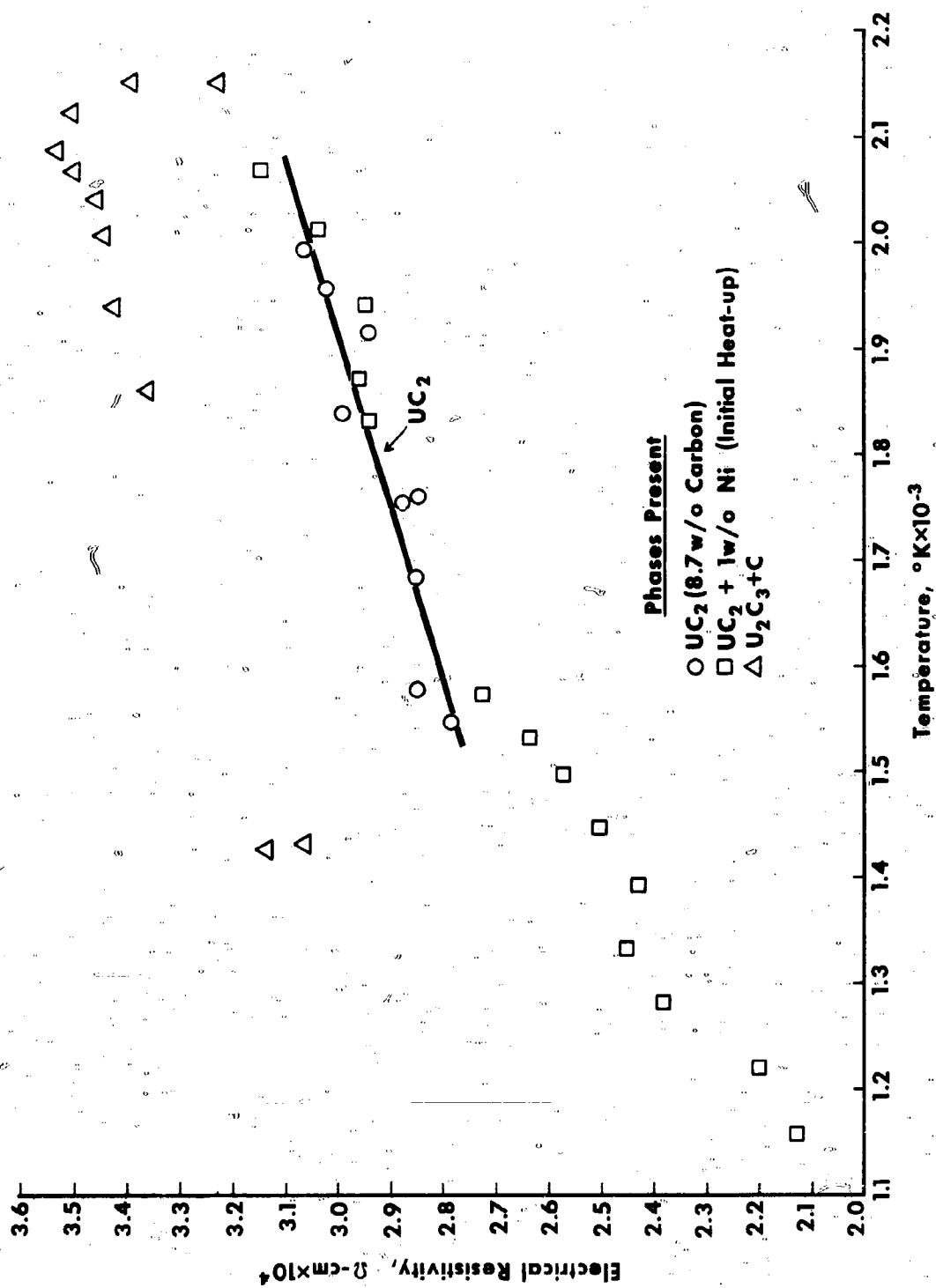


Figure 14. ELECTRICAL RESISTIVITY OF UC<sub>2</sub> (8.7w/o TOTAL C)



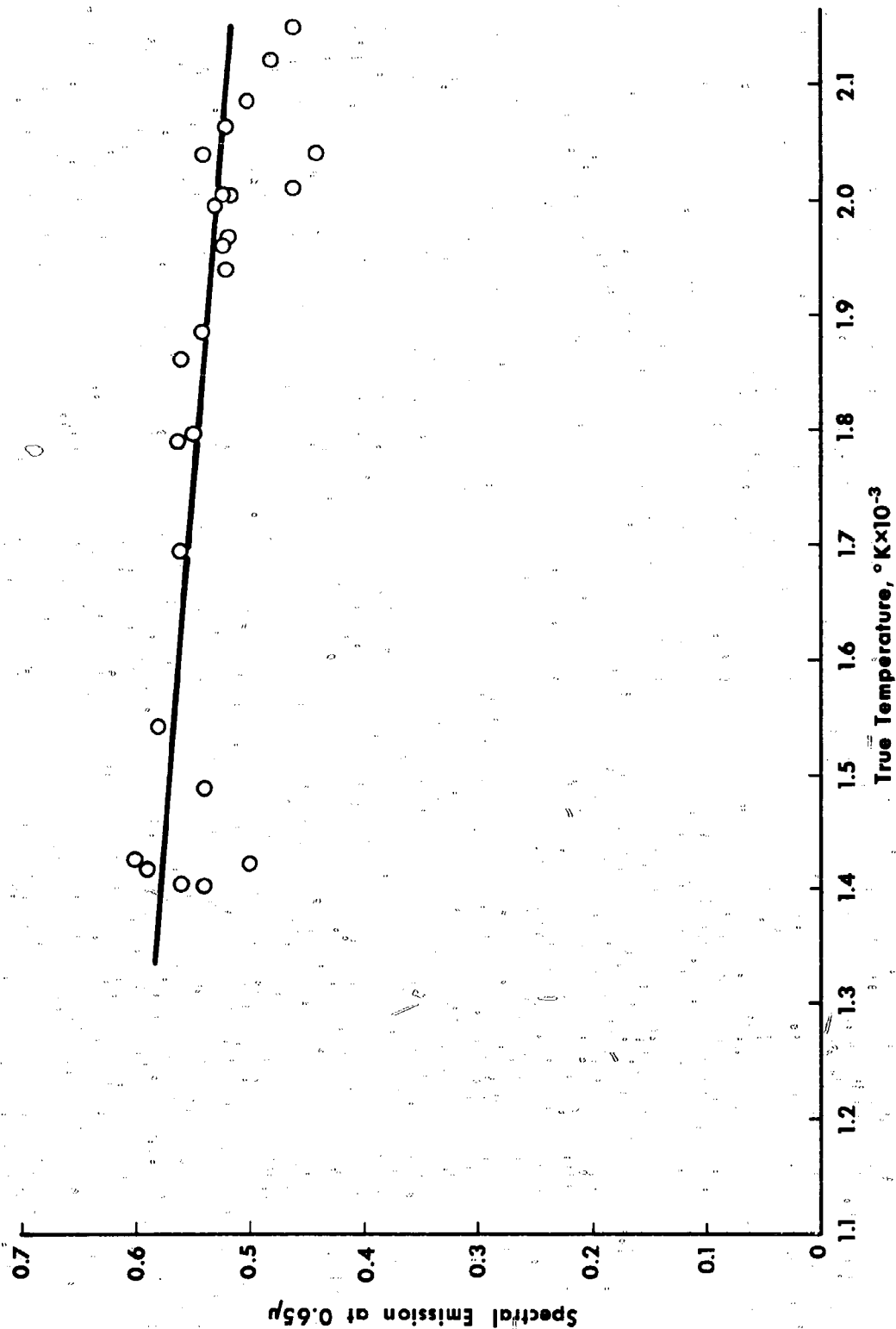


Figure 15. SPECTRAL THERMAL EMISSION OF  $\text{UC}_2$  AT  $0.65\mu$

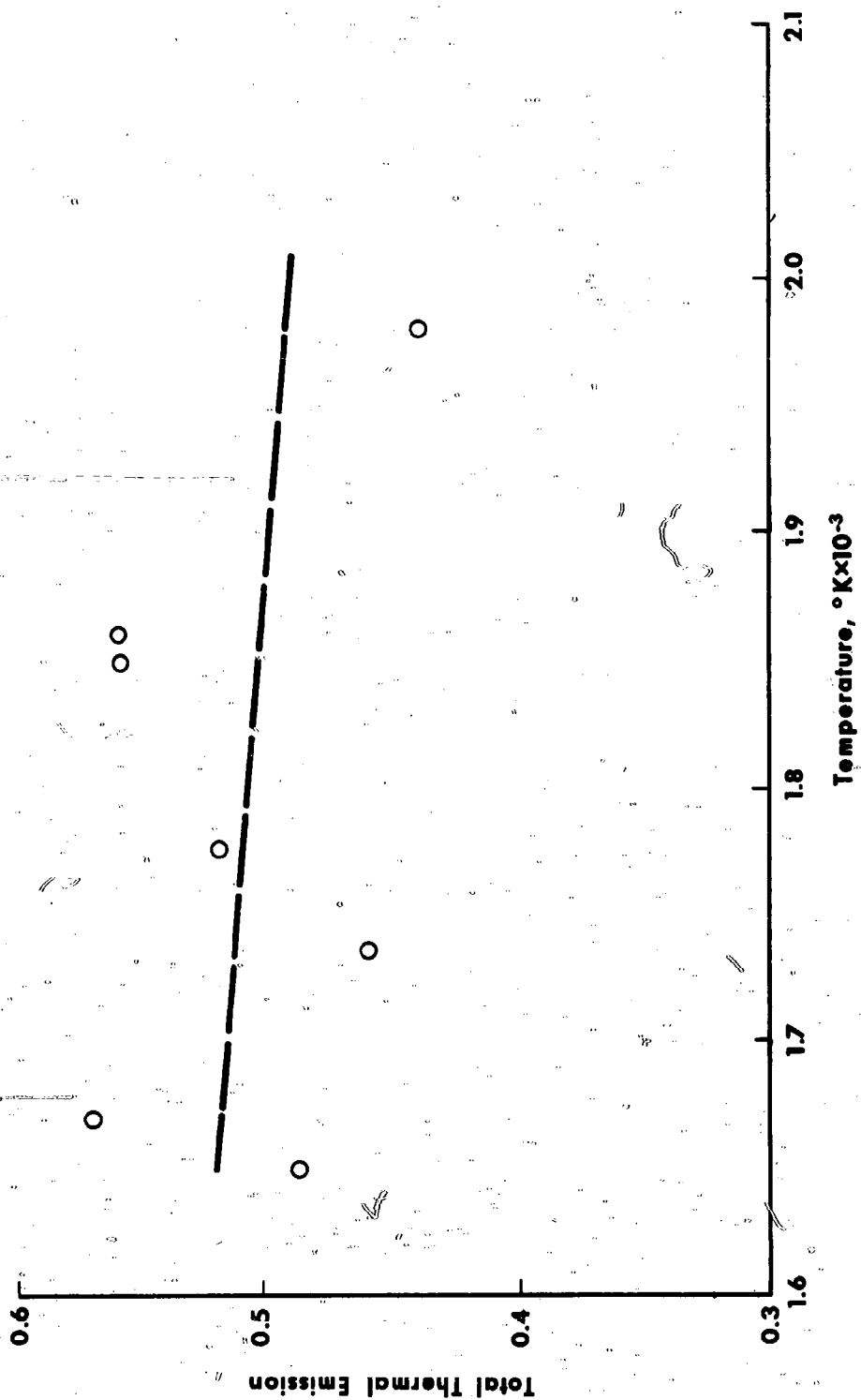


Figure 16. TOTAL THERMAL EMISSION OF UC<sub>2</sub> (8.7w/o total C)

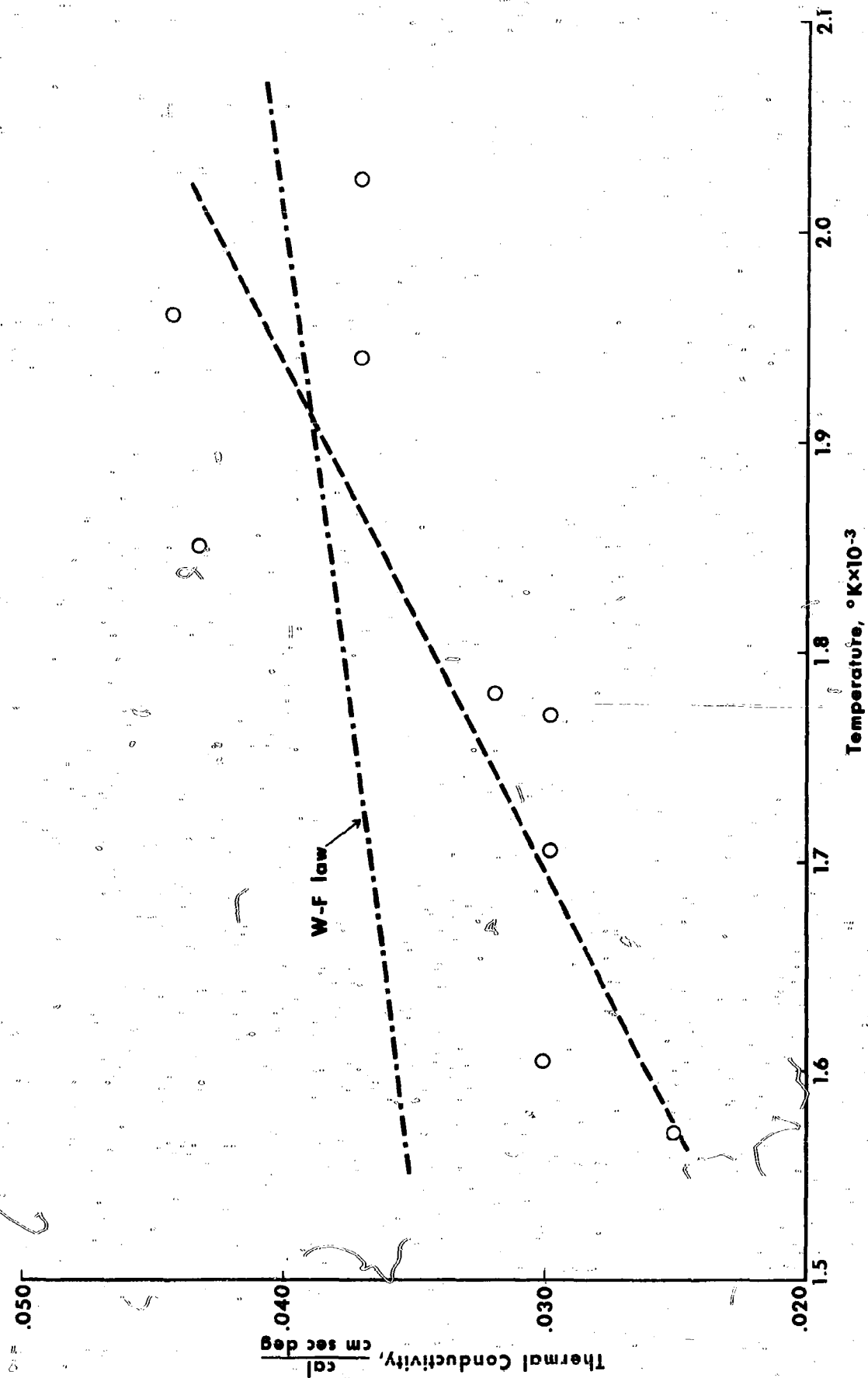


Figure 17. THERMAL CONDUCTIVITY OF  $\text{UC}_2$  (8.7 w/o CARBON)

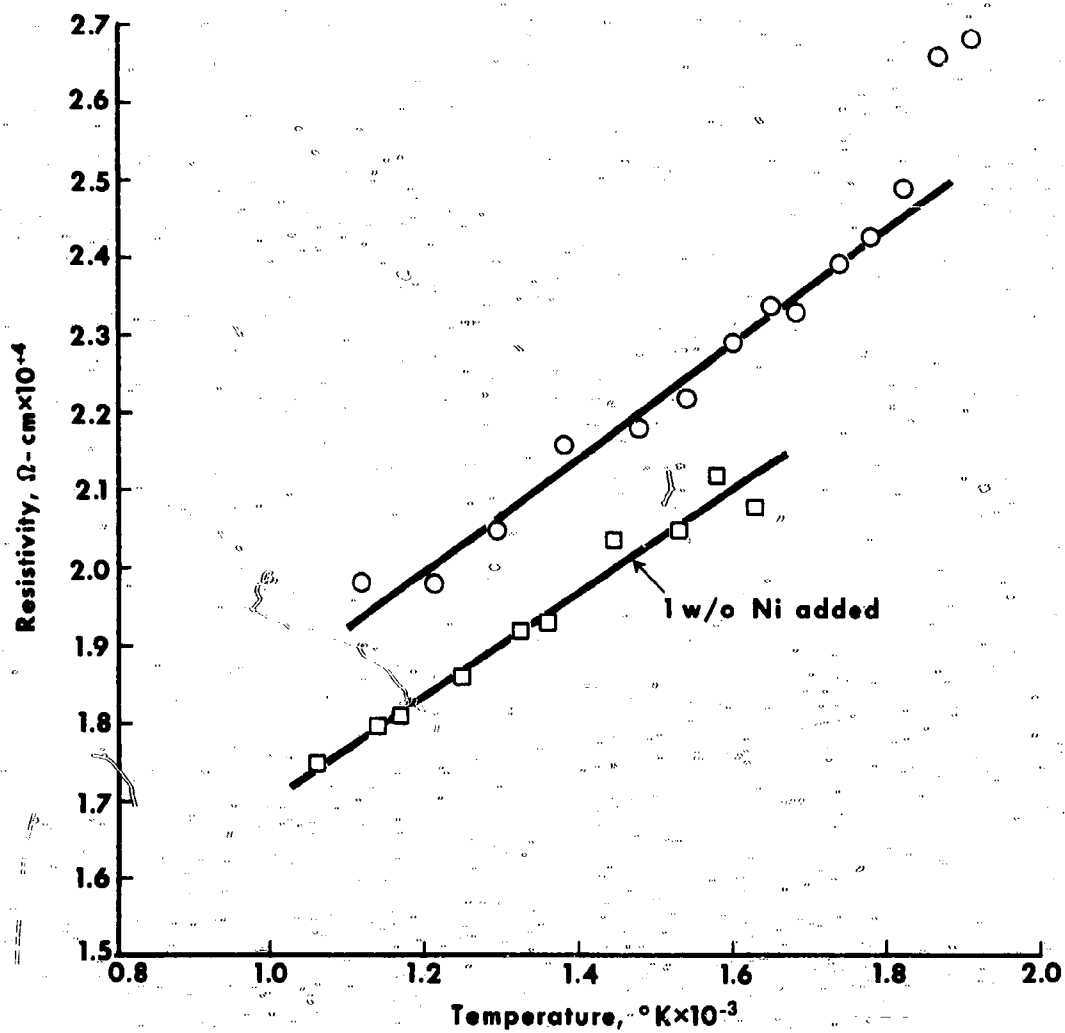


Figure 18. ELECTRICAL RESISTIVITY OF  $\text{U}_5\text{Zr}_5\text{C}$

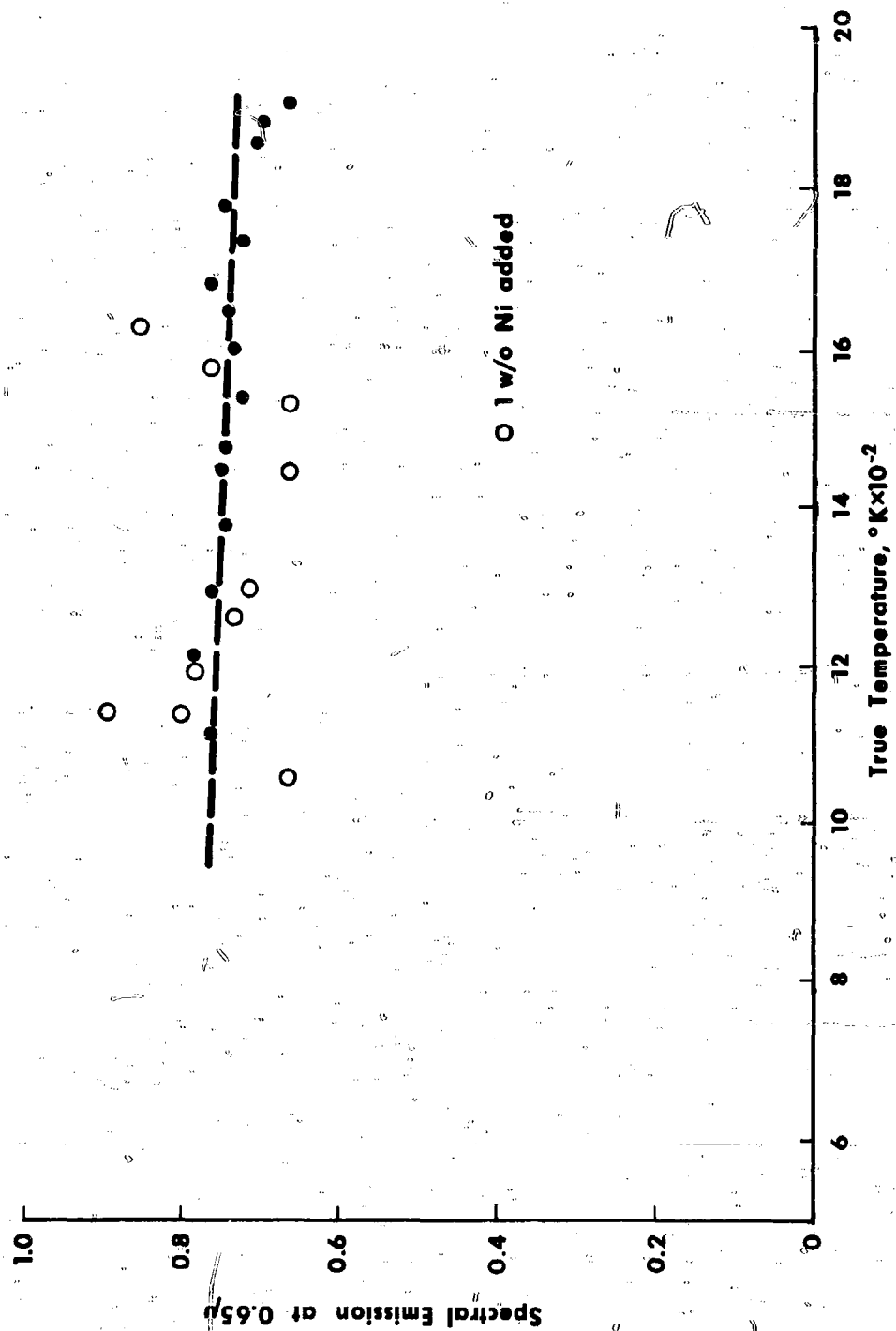


Figure 19. SPECTRAL EMISSION ( $0.65\mu$ ) OF  $\text{U}_5\text{Zr}_5\text{C}$  WITH REACTED SURFACE

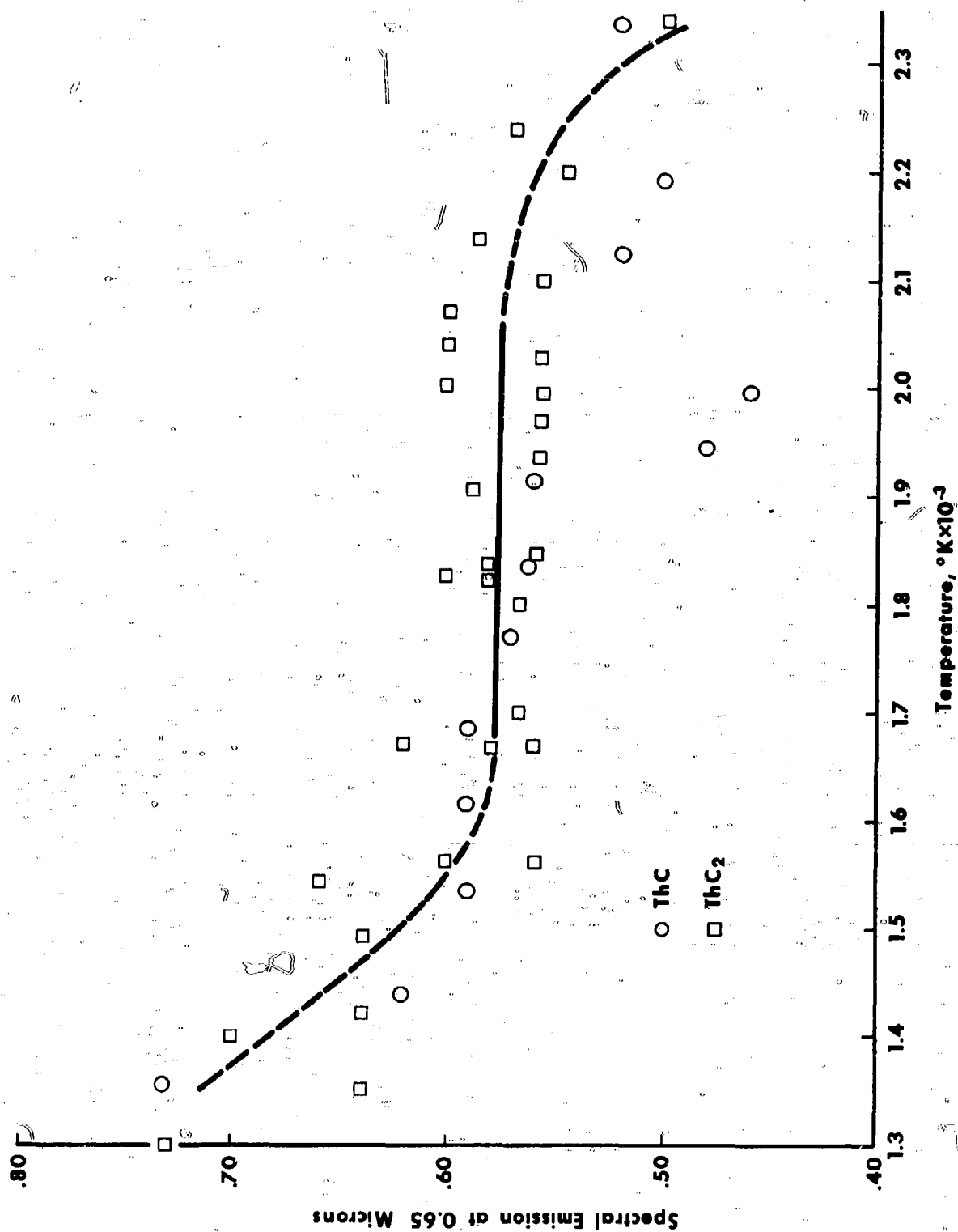
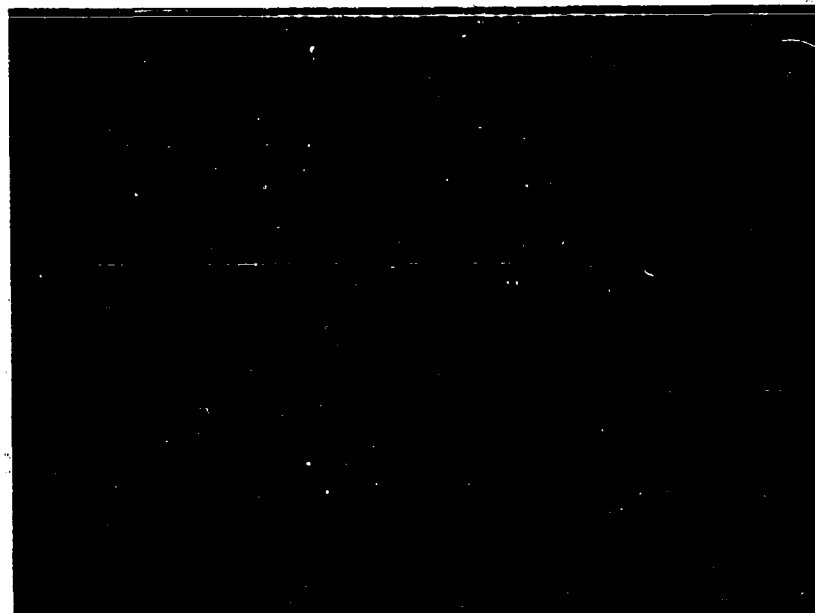


Figure 20. SPECTRAL EMISSION (0.65  $\mu$ ) OF ThC AND ThC<sub>2</sub>



**Figure 21. PHOTOMICROGRAPH OF  $\text{ThC}_2$**

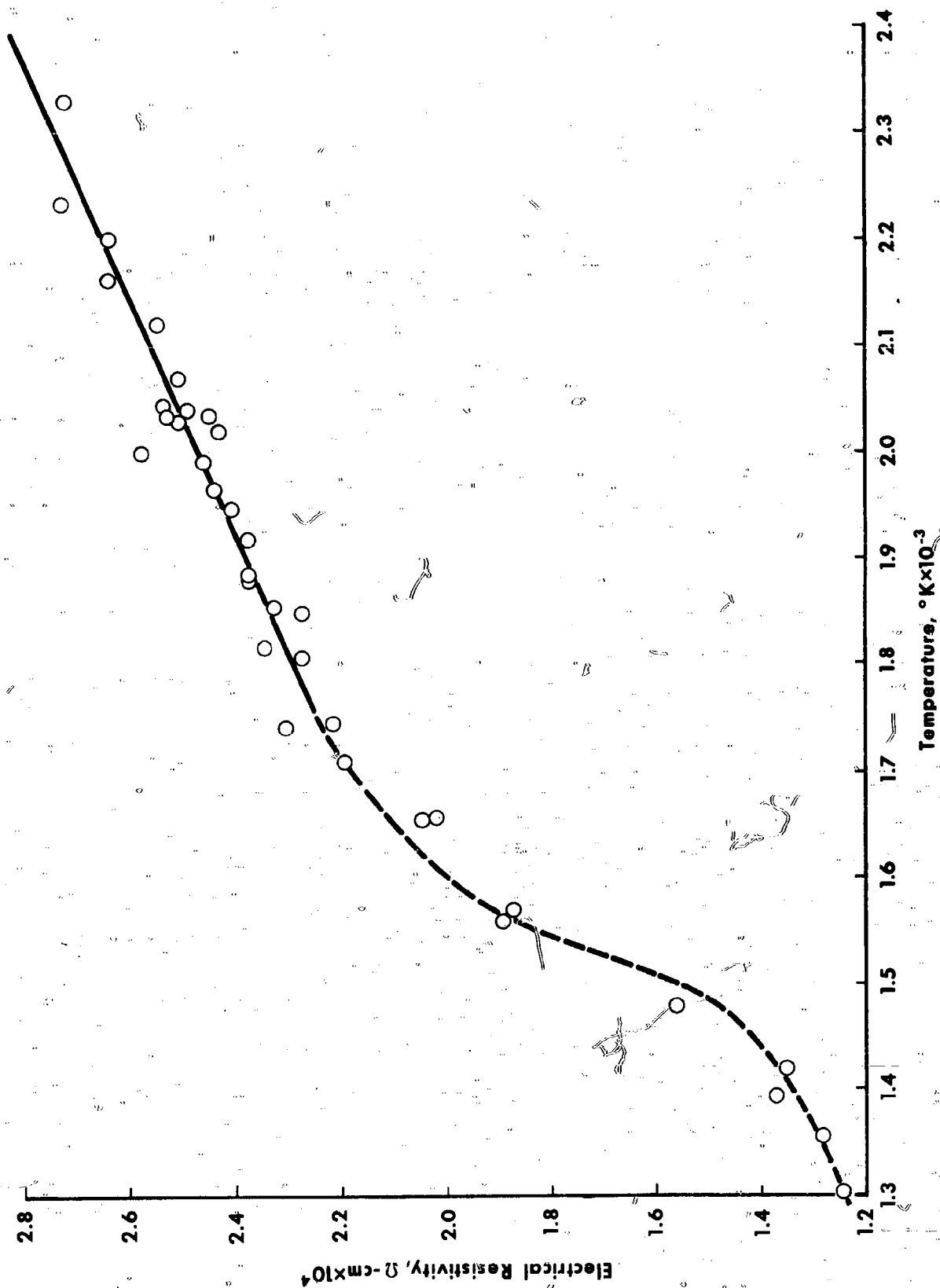


Figure 22. ELECTRICAL RESISTIVITY OF  $\text{ThC}_2$



**SECTION V - CESIUM COMPATABILITY WITH SELECTED THERMIONIC EMITTER MATERIALS****A. I. Kaznoff****E. W. Hoyt****LIST OF ILLUSTRATIONS**

<b><u>Figure No.</u></b>	<b><u>Title</u></b>	<b><u>Page No.</u></b>
<b>1</b>	<b>Cesium Vapor Pressure Range Encountered In Thermionic Converters</b>	<b>5-29</b>
<b>2</b>	<b>Total Vapor of Cesium as a Function of Re- ciprocal Temperature (16)</b>	<b>5-30</b>
<b>3</b>	<b>Volumetric Behavior of Liquid Cesium</b>	<b>5-31</b>
<b>4</b>	<b>View of Components of the Cesium Com- patibility Chamber</b>	<b>5-32</b>
<b>5</b>	<b>Cesium Compatibility Test System</b>	<b>5-33</b>
<b>6</b>	<b>Argon Dry Box</b>	<b>5-34</b>

**SYMBOLS AND NOMENCLATURES**

(Conventional thermodynamic symbols  
are used throughout this section.)

## V. CESIUM COMPATABILITY WITH SELECTED THERMIONIC EMITTER MATERIALS - A. I. Kaznoff,

E. W. Hoyt

### A. Introduction

The object of this report is to present some of the available information on the physico-chemical properties of elemental cesium and its chemical interaction with emitter materials. The physico-chemical properties discussed are primarily those of thermodynamic nature.

The chemical interactions are primarily discussed on the basis of binary systems with the elements occurring in the emitter materials studied: UC, UC<sub>2</sub>, (UC)<sub>0.5</sub>(ZrC)<sub>0.5</sub>, ThC, ThC<sub>2</sub>, YB<sub>6</sub> and EuB<sub>6</sub>. Consideration was also extended to the binary systems with oxygen, nitrogen, hydrogen, tantalum, iron, nickel and copper. This was deemed necessary because active gases such as O<sub>2</sub>, N<sub>2</sub> and H<sub>2</sub> can be present as a result of leakage, failure, etc. The other materials are structural materials used in compatibility testing. This study was made to supply background information for the cesium compatibility testing program at this laboratory.

As the field of cesium technology is experiencing a rapid growth it is possible that some of the material presented is dated and incomplete.

The results of a limited compatibility program are presented. The main emphasis in the first year's effort was the development of techniques for testing at elevated temperature. The principal results were of the nature of screening tests at 1000 C. The development of high temperature testing procedure and associated problems are discussed.

### B. Summary and Recommendations

1. A review of the cesium literature showed that many important areas have not been elucidated by investigators. Among some of the more important areas that need study are:

Cesium-Uranium System

Cesium-Oxygen System

Cs-Oxygen-Uranium System

Cs-Oxygen-Tungsten System

Although it was not considered in this report, the Cs-Pu and related systems are worth some consideration.

2. Techniques were developed for low temperature (1000 C) cesium compatibility testing. The primary objective of the testing program was the screening of emitter materials.
3. The results of 1000 C tests showed that borides are inert to cesium vapor. The specific borides tested were  $YB_6$  and  $EuB_6$ . Composite structure involving these borides with refractory metals showed interfacial failures which could not be attributed to cesium attack. The duration of the test was 350 hours.
4. A sample of  $UO_2$  at 1000 C (this material was not originally included in the work statement) was found to experience no attack by cesium after 350 hours. The test performed on  $UO_2$  is justified by increased importance of this fuel in nuclear thermionics.
5. Two tests at 1000 C were carried for 350 hours and 500 hours respectively. The second test was not totally successful as oxygen leakage occurred. It is postulated that leakage occurred through the nickel plated copper pinch-off tube. The resulting leakages, which was very small, contributed to the failure of carbide specimens during the test exposure. Borides were not affected.
6. The results of the tests suggest that further work can be performed with success if the test chamber is enclosed in a vacuum or operated in well-gettered inert gas (argon or helium). The furnace heating elements must be made of refractory metal (Ta or W).
7. An all tantalum testing system was developed for testing up to 1700 C and possibly higher. The testing chamber consisted of welded tantalum including a tantalum pinched-off cesium reservoir which was also welded shut in the final operation. The whole system was operated under argon in a purged alumina tube lined with molybdenum. The test had to be terminated because of the failure of the alumina tube which resulted in oxygen attack of the tantalum tube after about 115 hours of operation. No results could be salvaged from this experiment. Analysis of the test chamber showed that all tantalum welds were sound and that the oxidation attack occurred only in regions opposite the cracks that developed in the aluminum tube. Such failures can be obviated by using a vacuum furnace instead of rhodium tubular furnace used in this experiment.
8. It is imperative that techniques be developed to monitor cell conditions during the test period so that developing leakage could be ascertained when these occur so that test results may be saved for analysis.

9. Present state of knowledge of the physicochemical properties of cesium is inadequate but work in progress indicates that unknown areas are being rapidly filled up. At present a more urgent need is the determination of the chemical action of cesium on metals, particularly brazes, and insulators. Long term testing is desirable both for commercially available materials and for newer materials that appear to hold promise. It is of interest to determine the activity of oxygen in cesium as it is related to that of oxygen in refractory metal systems (as a function of temperature and cesium pressure).
10. It is important to establish phase diagrams, or partial phase diagrams (at least solubilities) in the following metal systems: U-Cs, Nb-Cs, (Zr-Cs), in the range of 300-1200 C as a start. Extension to higher temperature may be advisable after the suggested study is completed. The Cs-O system deserves more elucidation.
11. As there is a distinct possibility that oxygen deficient  $\text{UO}_2$  may result in metal clad fuel emitters, there is the possibility of loss of oxygen as  $\text{O}_2$  (gas), Mo or W oxides, and as  $\text{UO}_2$  (g). It is important to establish what happens to the elemental oxygen or that bound in volatile clad metal oxide in the presence of cesium and hot oxygen getters such as niobium. This is the same phenomenon that suggests the study of the U-Cs system since hypostoichiometry  $\text{UO}_2$ , if produced, may precipitate out metallic uranium on cool-down and revert to state closer to stoichiometry. The lowering of temperature, for whatever cause, will produce elemental uranium which will volatilize into the cesium atmosphere. The final disposition of this uranium is unknown. From the above discussion it is clear that thermal cycling may produce very undesirable effects by alternate losses of oxygen and uranium. The severity of these anticipated problems should increase with higher temperatures and temperature changes which may be necessary to increase efficiency of devices.
12. It is desirable that definitive corrosion data be obtained for metal systems in which cesium will be contained as a liquid. A close cooperation in this area must be established with the AEC and other agencies especially those active in cesium ion engine development. The target of the study should be the determination of specifications of container materials based on fundamental studies for the studies of mechanisms of attack.
13. It is desirable to establish the chemical interaction of cesium with fission products. Primary attention must be directed to electronegative species in the fission products (such as iodine, selenium, etc.). The study should cover gaseous interactions and interactions in liquid cesium. The reason for this study is to find what effects are produced by cesium

salts (say cesium iodide) on the rest of the system components. At least a paper study should be initiated at this time, followed by experimental work.

14. Alternative methods of cesium vapor generation could be given more attention particularly those that involve generation from solid compounds or solid state reactions.

### C. Physical Properties of Cesium

At present, a considerable number of physical constants are available for the metal cesium. A short summary of some of the basic properties is given below:

Atomic Number - 55	Atomic Radius ( $\text{\AA}$ ) - 2.62
Atomic Weight - 132.91	Ionization Potential (volts) - 3.87
Specific Gravity - (293.2 K)	Oxidation Potential (volts) - 2.923
in the solid state - 1.873	Electrical Conductivity (273.15 K) -
Melting Point ( $^{\circ}\text{K}$ ) - 301.8	(in mhos) $5.18 \times 10^4$
Boiling Point ( $^{\circ}\text{K}$ ) - 955	Brinell Hardness $\text{kg/mm}^2$ - 0.015

#### 1. Structure of Cesium Metal (Solid State)

Cesium metal crystallizes in a simple body-centered cubic structure (A-2). This structure exists from 1.2 K to the melting point (301.8 K).<sup>(1)</sup> No spontaneous phase changes below the melting point have been observed. The following x-ray parameters have been reported:

<u>Temperature (<math>^{\circ}\text{K}</math>)</u>	<u>Lattice Parameter</u>	<u>Reference</u>
5.00	$6.045 \pm 0.002 \text{ \AA}$	(2)
78.00	$6.067 \pm 0.002 \text{ \AA}$	(2)
263.15	6.13 (kX)	(3)
173.15	6.079 (kX)	(4)

Simon<sup>(5)</sup> has also measured a lattice constant but his figures are usually not quoted.

Brauer<sup>(4)</sup> has found that oxygen contamination increases the lattice parameters to 6.086 kX from the 6.079 kX value at 173.15 K. The level of oxygen was not determined.

#### 2. Electronic Structure, Radii and Related Properties

The cesium ion ( $\text{Cs}^+$ ) has the electronic configuration of xenon and the atom ( $\text{Cs}$ ) has the outer electron in  $6s$  state. The first ionization potential is 3.87 volts and the second is 23.4 volts.<sup>(6)</sup> The standard oxidation potential of Cs is 2.923 volts.<sup>(7)</sup>

The electron work functions are given below: (these all refer to solid crystalline cesium)

$\phi$ (e.v.)	Technique	Reference
1.81	Thermionic Work Function	(8)
1.90	Photoelectric Work Function	(9)
1.96	Photoelectric Work Function	(10)
1.93	Photoelectric Work Function	(11)

The work function of liquid cesium is believed to lie between 1.6 - 1.8 e.v. Work functions of cesiated surfaces can assume a variety of values from about 1.4 to 4.5 e.v. depending on the substrate work function, substrate temperature, and cesium pressure. References 11-13 should be consulted for some of the detailed information on the properties of cesiated substrates.

The atomic radius of a cesium atom is 2.62 Å. The normal covalent, single bond radius is quoted as 2.25 Å. (14) The ionic radius, according to Goldschmidt is 1.65 Å. (15)

### 3. Thermodynamic Properties of Cesium

A critical evaluation of the thermodynamic properties of cesium in solid, liquid and gaseous has been recently completed at the University of California. (16) The other principal sources of critically evaluated data are those of Kelley, (17) Kelley and King (18) and Stull and Sinke. (19) The more recent reference (16) must be considered to be the most reliable. However, there are several criticisms that can be leveled at this work.

- a. The data on the high temperature properties of cesium developed at Aerojet-Nucleonics (24) was not included because it was not available to the general public at the time of evaluation.
- b. The above probably precluded an evaluation of Cs(g) as a non-ideal gas (as in the case of Li, Na, K, Hg (16)) and the resulting treatment of the gas as being composed of Cs and Cs<sub>2</sub> leaves much to be desired.

Liquid properties are estimated, no high temperature vapor pressure results are available. (16) High temperature P-V-T data are completely lacking. Appraisal of the vapor pressure data (16) has shown that the diatomic species, as expected, increase in importance as the temperature (pressure) is raised. At 298.15 K the ratio of Cs to Cs<sub>2</sub> is  $3.32 \times 10^{-4}$  while at 1000 K it is  $9.6 \times 10^{-2}$ .

The data obtained by Aerojet-General Nucleonics<sup>(24)</sup> is primarily of the engineering type by contrast to more basic studies upon which the evaluation of R. Hultgren<sup>(16)</sup> rests. A general appraisal of the AGN work can be obtained from the similar work on rubidium reported in an unclassified report.<sup>(25)</sup>

The main contributions of the AGN work are in the following areas:

- a. Volumetric data on the liquid cesium at low pressures (to about 1 atm) between 500 and 1270 F. (532-960 K).
- b. Vapor pressure from 1000 to 1800 F (812-1255 K). This is the first investigation giving the pressure-temperature relationship considerably above the normal boiling point of liquid cesium.
- c. Specific heat ( $C_p$ ) of liquid cesium between 500 and 1650 F (532-1170 K).

The basic thermodynamic properties are tabulated at the end of this section. These are primarily drawn from reference 16 and reference 24.

There is no data on the critical temperature, pressure or volume of elemental cesium. Estimates indicate that the critical temperature lies probably in the range of 1600-2000 K. No serious basis can be given to these estimates especially to those (see for example reference 22) which have not been developed to cover the case of liquid metals. The paucity of data on the critical parameters of metals (only those of mercury are approximately known) hinders the development of confidence for these estimates. (20-23)

#### Estimates of Critical Parameters for Cesium

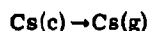
$T_c$ ( $^{\circ}$ K)	$P_c$ (atm)	$V_c$ ( $\frac{cc}{gm-mole}$ )	Reference
1780	46.7	900.7	(20)
1690	--	--	calculated according to (21)
1625	--	--	calculated according to (22)
2150	--	--	(23)
2520	--	--	calculated from ratio of $T_c/T_{B.P.}$ of Hg

If credence can be given to the above estimates then it appears that the experimental determination of the critical parameters of cesium is potentially feasible with existing technology.

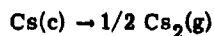
#### 4. Basic Thermodynamic Properties

The properties presented taken primarily from references 16 and 24. The symbols H and S refer to enthalpy and entropy respectively. The subscript "st" refers to 298.15 K. The thermodynamic properties are reported per gram-atom of cesium.

	Cs Crystal	Cs(g)	1/2 Cs <sub>2</sub> (g)	References
S <sub>st</sub> ( $\frac{\text{cal}}{\text{gm mole } ^\circ\text{K}}$ )	20.16 ( $\pm 0.5$ )	41.94	33.93	(16)



$$\Delta H_{V, \text{st}} (\text{sublimation}) = 18670 \pm (70) \frac{\text{calories}}{\text{gm-mole } ^\circ\text{K}} \quad (16)$$



$$\Delta H_{V, \text{st}} = 13,310 \frac{\text{calories}}{\text{gm-mole } ^\circ\text{K}} \quad (16)$$

The vapor pressure <sup>(16)</sup> is shown in Figure 1 for the range usually encountered in cesium thermionic converter (pressure in torr, temperature in  $^\circ\text{K}$ ); Figure 2 shows the vapor pressure over an extended temperature range. <sup>(16)</sup>

The vapor pressure equation presented in Reference 24 is as follows:

$$\log_{10} P(\text{atm}) = \frac{-7474.39}{T} - 7.59618 \log_{10} T + 30.4259$$

The number of significant figures is entirely misleading and is a result of curve fitting rather than actual precision. Temperature range of investigation was 810 - 1255 K. The boiling point in (24) was found to be 963.3 K while the one in reference 16 is 955 K.

#### 5. Condensed Phase Properties

Temp. $^\circ\text{K}$	C <sub>P</sub> (24) $\frac{\text{cal}}{\text{gm-mole } ^\circ\text{K}}$	H <sub>T</sub> - H <sub>st</sub> (16) $\frac{\text{cal}}{\text{gm-mole}}$	H <sub>T</sub> - H <sub>st</sub> (24) $\frac{\text{cal}}{\text{gm-mole}}$	S <sub>T</sub> - S <sub>st</sub> (16) $\frac{\text{cal}}{\text{gm-mole } ^\circ\text{K}}$
298.15	--	0.00	0.00	0.00
301.8(c)	--	3.00	--	0.09
301.8(1)	7.34	550	550	1.81
400	6.82	(1290)	1243	(3.95)
500	6.43	(2050)	1095	(5.95)
600	6.17	(2810)	2533	(7.03)



Temp. °K	$C_p$ (24) cal gm-mole°K	$H_T - H_{st}$ (16) cal gm-mole	$H_T - H_{st}$ (24) cal gm-mole	$S_T - S_{st}$ (16) cal gm-mole°K
700	6.06	(3570)	3134	(8.20)
800	6.08	(4330)	3479	(9.22)
900	6.24	(5090)	4364	(10.11)
1000	6.54	(5850)	5002	(10.92)

In reference 16 the heat capacity of the liquid was estimated as 7.6 cal/gm-mole °K. The data in reference 24 showed that the  $C_p$  had a minimum characteristic of all alkali metals that have been studied in detail. This gives rise to the discrepancy in the enthalpy values, and a corresponding one in the entropy. The scatter in reference 24 precludes any firm confidence in the heat capacity values but it represents an adequate result for engineering applications (actual range of data on  $C_p$  is from about 500 K to 1230 K). The density of liquid cesium is shown in Figure 3 as volume per gm-atom as a function of temperature (°K). (24) The authors report the data as a linear function of temperature while Figure 3 constructed with their data points shows considerable curvature. Temperature measurement may be also suspect as liquid cesium was studied below its melting point. The pycnometric technique as reported (24) proved to be quite troublesome and somewhat unreliable. Density determined by Andrade and Dobbs (24) does not extend beyond about 500 K, the results generally fail above the volumetric curve of reference 24.

The following is a summary of the properties for gaseous cesium at low pressures. the specific heat and heat content must be considered to be for an ideal gas at 1 atmosphere, i. e. the ideal properties associated with infinite attenuation are retained at 1 atm. (16)

T°K	Cs	$S_T - S_{st}$	1/2 Cs <sub>2</sub>	$S_T - S_{st}$	Partial Pressures (atm)	
	$H_T - H_{st}$		$H_T - H_{st}$		$P_{Cs}$	$P_{Cs_2}$
298.15	0	0.00	0	0.00	$1.23 \times 10^{-9}$	$3.4 \times 10^{-14}$
301.8	18	0.06	17	0.06	$1.79 \times 10^{-9}$	$5.8 \times 10^{-14}$
400	506	1.50	466	1.34	$2.88 \times 10^{-6}$	$1.83 \times 10^{-9}$
500	1003	2.57	926	2.37	$2.51 \times 10^{-4}$	$9.18 \times 10^{-7}$
600	1500	3.48	1389	3.21	$4.73 \times 10^{-3}$	$5.23 \times 10^{-5}$
700	1996	4.24	1854	3.93	$3.74 \times 10^{-2}$	$8.85 \times 10^{-4}$

T°K	Cs	$S_T - S_{st}$	1/2 Cs <sub>2</sub>	$S_T - S_{st}$	Partial Pressures (atm)	
	$H_T - H_{st}$		$H_T - H_{st}$		$P_{Cs}$	$P_{Cs_2}$
800	2493	4.91	2323	35.59	0.172	$6.87 \times 10^{-3}$
900	2990	5.49	2796	35.94	0.551	$3.23 \times 10^{-2}$
1000	3487	6.02	3273	36.28	1.38	0.109

## 6. References

1. C. S. Barrett, J. Inst. Metals, 84, 43 (1955).
2. C. S. Barrett, Acta. Cryst. 9, 671 (1956).
3. B. Bohm, W. Klemm, Z. Anorg. Chem., 243, 69 (1939).
4. G. Brauer, Z. Anorg. Chem. 255, 101 (1947).
5. F. Simon and E. Vohsen, Z. Phys. Chem. 133, 165 (1928).
6. Handbook of Chemistry and Physics, 42nd Edition.
7. W. Latimer, "Oxidation Potential".
8. H. H. Kingdon, Phys. Rev. 25, 892 (1925).
9. A. R. Olpin, quoted by Hughes and DuBridge in "Photoelectric Phenomena", 1932.
10. J. J. Brady, Phys. Rev. 41, 613 (1932).
11. A. F. Jaffe, quote in "Physics of Semiconductors", Academic 1960.
12. I. Langmuir, Collected Works, Pergamon 1960.
13. Symposium on Thermionic Power Generation, Colorado Springs, May 14-17, 1962.
14. Schomaher and Stevenson, quoted in American Potash and Chemical Corp. Bulletin No. TD-Cs/RC
15. Goldschmidt, ibid
16. R. R. Hultgren, Thermodynamic Lit. Survey, Dept. Mineral Tech., U. of Calif.
17. K. K. Kelley, USBM Bulletin 584 (1960), USBM Bulletin 383 (1935).
18. K. K. Kelley, E. G. King, USBM Bulletin 592 (1961).
19. D. R. Stull, G. C. Sinke, Thermodynamic Properties of the Elements.
20. D. S. Gates, G. Thodos, A. I. Ch. E. Journal 6, 50 (1960),
21. C. M. Guldberg, Z. Physick Chem. 5, 374 (1890),
22. H. P. Mussner and E. M. Redding, Ind. Eng. Chem. 34, 52 (1942).
23. A. V. Grosse, J. Inorg. Nucl. Chem. 22, 23 (1961).
24. P. F. Young et al, Cesium Corrosion and Physical Properties Evaluation Program, Report AGN-8041 (Classified). (Data reported is from the "Unclassified" Section of this report).
25. "Rubidium Corrosion and Physical Properties Evaluation Program", Report AGN-8034.

#### D. Binary Systems with Cesium

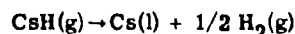
The objective of this section is not to present an exhaustive discussion on all the possible binary systems but to limit consideration to the elements encountered in the emitters investigated.

YB<sub>6</sub>, EuB<sub>6</sub>, UC, UC<sub>2</sub>, (UC)<sub>0.5</sub>(ZrC)<sub>0.5</sub>, ThC, ThC<sub>2</sub>, ZrC

Consideration is also given to other elements which may occur either as impurities in the cesium or as the basic materials used in the construction of test apparatus to contain cesium.

##### 1. Cesium - Hydrogen

The solubility limits of hydrogen in cesium are not known. CsH is known to exist and there are several references giving the preparative techniques. (1-4) The decomposition reaction



were studied by Herold (3) and Hackspill. (4) Hackspill has also studied the formation and decomposition of CsD.

The decomposition pressures are expressed as follows: (3)

$$\log P \text{ (torr)} = \frac{-5900}{T} + 11.79 \text{ (473-773 K)}$$

thus  $P = 1 \text{ atm}$  at 662 K.

The enthalpy of formation for CsH(c) is therefore -13,500 cal and its entropy is about 10 e.u. (in the temperature range of 473-773 K). The data of Hackspill (4) is at odds with that of Herold. (3) The results of this work show  $\Delta H_f$  of around -20,000 calories according to the author. (4)

Critical evaluation needs to be performed to establish the reliability of these investigations. Kelley (6) reports the entropy  $S_{298.15}^\circ$  of CsH(g) as 51.36 e.u. (see u). CsH is an ionic solid (the ions are considered to be  $\text{Cs}^+$  and  $\text{H}^-$ ). Its melting point is above 823 K and the material may only be melted under high pressures of hydrogen as seen from the data in the previous paragraphs. The crystals of CsH are white. CsH is not measurably dissolved by Cs up to 423 K. (5) This may indicate that the solubility of hydrogen in cesium metal is low. CsH is highly reactive. The reactions are generally more violent than for Cs. Exposure to air produces violent reaction; very energetic reactions are obtained, as expected, with fluorine and chlorine. Water is decomposed by CsH yielding hydrogen; alcoholates are formed with alcohols. Reaction with CO yields a salt of the formic acid. Undefined "carbides" (5) are formed with acetylene. E. Zintl and A. Harder (8) have determined the lattice parameters of f.c.c. CsH.

$$a = 6.376 \pm 0.001 \text{ kX}$$

Theoretical density is  $3.42 \text{ gm/cm}^3$ , experimental density is  $3.41 \text{ g/cm}^3$ . Structural analysis failed to give a definitive results. CsH may belong to the B1 or B3 type.

Recent work on low work function materials <sup>(9)</sup> indicates that hydriding of cesium will decrease the work function of the anode. The above data <sup>(3)</sup> on the decomposition of CsH indicates that high temperature, low work function anodes (with CsH) cannot be maintained. A partial pressure of hydrogen of about 10 torr is necessary to prevent CsH decomposition at 545 K (anode temperature); a partial pressure of 1 torr would be required at 461 K.

The vapor pressure of CsH must also be considered. Latimer has presented the data on CsH(g) <sup>(32)</sup> at 298.15 K.

	$\Delta F^\circ$	$\Delta H^\circ$	$S^\circ$
CsH(g)	29.0 kcal	24.3 kcal	51.25

The vapor pressure equation taking Herold's data for the solid can be written as

$$\log_{10} P(\text{atm}) = \frac{-9300}{T} + 9.02$$

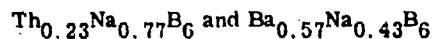
This shows that the vapor pressure will reach 760 torr at 1030 K. At 545 K and 461 K the corresponding vapor pressure will be  $7.6 \times 10^{-6}$  torr and  $5.65 \times 10^{-9}$  torr. (Cesium vapor pressure at 545 and 461 K is 0.82 torr and 0.048 torr).

## 2. Cesium - Boron

The solubility of cesium in boron and boron in cesium is not quantitatively known. The only reference to cesium borides is in the monograph of Perelman. <sup>(5)</sup> "Borides of rubidium and cesium ( $\text{Me}_3\text{B}$ ) have the ability of combining with the hydrides of the same metals to form quite stable borohydrides". No reference is made to the original source of work on cesium borides in (5). It is, of course, well known that  $\text{CsBH}_4$  does exist. <sup>(10)</sup> The calculated lattice energy is 150 kcal/gm mole and the enthalpy of formation is -63 kcal/gm mole at 298.15 K. <sup>(11)</sup> Samsonov <sup>(12)</sup> does not mention specifically any solubilities or compounds in the Cs-B system. His discussion on other alkali metals with boron is noteworthy. Early work by Moissan <sup>(12)</sup> indicated that boron could dissolve 3 to 6 per cent of alkali metals (such as K). Kroll's work <sup>(12)</sup> led that investigator to suspect that sodium borides existed because boron could contain from 3.8 to 6.4 per cent of Na. Andrieux's work <sup>(12)</sup> showed that mixed (one-phase) hexaborides could be produced by electrolysis. A typical material is the "hexaborides" of the following composition: (prepared at around 950 C)

23.6 per cent Ca 10 per cent Na and 65.6 per cent B

Bertaux and Blum<sup>(12)</sup> concluded that sodium was the only alkali metal that could substitute for other metals in hexaborides:



Investigations of Markovski and Kondrashev<sup>(12)</sup> indicated that boron could contain from 2-6 per cent of Li. Prolonged leaching with acids failed to remove the alkali metal from boron.

The above information leads to the following tentative conclusions:

- a. No definitely established phase or compound in the Cs-B system is known.
- b. There are indications that cesium could dissolve in boron under special conditions. It is doubtful that the solubility of boron in cesium is appreciable.
- c. Substitution of M in  $\text{MB}_6$  phases by cesium is a possibility.

Considering the volatility of cesium it is very unlikely that high temperature stable phases will be found in the Cs-B system unless a high partial pressure of Cs is maintained. This partial pressure will probably be much higher than that encountered in thermionic converters.

### 3. Cesium - Yttrium

No data exists on this system. In fact, there is a remarkable paucity in the knowledge of cesium interactions with the rare earths (including yttrium and lanthanum). The closest system reported is that of Al-Cs.<sup>(13)</sup> It is reported that almost complete immiscibility exists in the solid and liquid phases. Data on Al-Na and Al-K is substantailly the same. Solubility of Na in Al(c) is very low -- of the order of 0.002 wt per cent, immiscibility is always noted in the liquid states. Applicability of this data in guessing the characteristics of the Cs-Y system is difficult because of the differences in crystal structure of the Group 3B metals: Al is f.c.c. and yttrium is h.c.p.

There is only one system La-Na which has been studied among the lanthanide metal - alkali-metal system. This was studied by Mossenhausen.<sup>(14)</sup> This work is very inconclusive due to the impure lanthanum used (about 98 per cent purity) and difficulty encountered in the examination of specimens. It is tentatively established that a eutectic exists near the lanthanum-rich side. The addition of sodium to lanthanum was observed to produce very exothermic reactions. This could lead one to suspect that new phases are formed but since lanthanum was very impure the exothermic characteristics could be evidence of reaction with impurities.

#### 4. Cesium - Europium

No data exists on this system. The discussion in the preceeding system (Cs-Y) is applicable.

#### 5. Cesium - Zirconium

No data exists on the phase relationships of this system. The data in the Liquid Metals Handbook <sup>(15)</sup> indicates that zirconium is resistant to Na and K to about 600 C. Higher temperature behavior is unknown, however, it is known that titanium ceases to be resistant to alkali metal above 600 C and can only be exposed to their environment for short periods of time. Similar behavior may be expected for Zr.

#### 6. Cesium - Tantalum

No phase diagrams are available for this system. <sup>(13)</sup> Work in alkali metals <sup>(15)</sup> shows that tantalum should be inert to these materials. Work on niobium alloys and alkali metals <sup>(16)</sup> again points to the probable inertness of tantalum with alkali metals. Recent reports on the tantalum cathode thermionic converter by Wilson <sup>(17)</sup> shows that tantalum, when pure, is very stable in the presence of cesium vapor. In the field of thermionic energy conversion there has been ample evidence that between 800 and 2200 C no cesium attack on tantalum occurs. The observed attack on tantalum as reported by Slivka <sup>(18)</sup> cannot be considered to be definitive. The test was run at 900 C (281 hours). The mixed bright and matte surface and pores in tantalum may indicate that the tantalum specimen was impure.

#### 7. Cesium - Iron

Hansen <sup>(13)</sup> reports that cesium does not attack iron at 690 C and that cesium is not soluble in iron. Judging from the data on the Na-Fe iron system iron should be soluble in cesium above 200 C. It may be expected that iron solubility will be of the order of 0.001 wt per cent at that temperature.

#### 8. Cesium - Nickel

No phase diagram or other data is reported by Hansen. <sup>(13)</sup> In reference 15 it is noted that Ni is recommended for service in Na and K. It is also an established fact <sup>(15)</sup> that Ni dissolves in alkali metals but the rate of dissolution and solubility are apparently low. It can be expected that the behavior of nickel is not vastly different from that of iron and copper. Slivka noted vapor cesium attack on nickel <sup>(18)</sup> at 900 C.

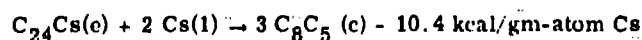
#### 9. Cesium - Copper

No phase diagrams or other data are reported by Hansen. <sup>(13)</sup> The Liquid Metals H-B reports that copper is considered for long term applications in Na and K up to about 450 C,

above this temperature and up to about 600 C the attack by liquid alkali metals is more pronounced. It can be expected that similar behavior will occur with cesium. Slivka reports cesium vapor attack at 900 C. Wilson's experience with liquid cesium in copper at around 300 C indicated no evidence of gross attack for hundreds of hours. No check on solubility of Cu in Cs has been made to date in spite of the fact that cesium pressures in thermionic diodes are usually established through the temperature of the cesium reservoir, and the most common reservoir material has been copper. Such faith in vapor pressure control can only be valid if the solubility of copper in cesium is very low, or if the reservoir temperature is low. Errors due to solubility effects may be larger at higher temperatures.

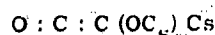
#### 10. Cesium - Carbon

Graphite is known to react with the alkali metals. <sup>(15)</sup> Cesium attack has been noticed at this laboratory and at others. Attack on some carbides has been noted at General Atomic. <sup>(19)</sup> Compound formation of K, Rb and Cs with graphite is well established. <sup>(20)</sup> Typical compounds are  $C_8M$ ,  $C_{24}M$ ,  $C_{36}M$ ,  $C_{48}M$  and  $C_{60}M$ . (M = alkali metal.) These compounds have distinctive color usually running from bronze to blue to black with increasing carbon content. At ordinary temperatures these compounds are stable in vacuo, but they decompose as the temperature is raised. It is doubtful if any are stable above 500 C. These compounds have a rather typical lamellar structure <sup>(20)</sup> found in many of the compounds formed with graphite. From the discussion in reference 20 it is evident that the alkali metal compounds have relatively low stability.  $C_4Cs$  probably has a  $\Delta H_f^\circ$  of about -4000 cal/gm-atom. It is doubtful if any of the compounds have a  $\Delta H_f^\circ$  lower than -50,000 cal/gm-atom. Herold <sup>(21)</sup> has studied the vapor pressures of some of these compounds. He reports the following:

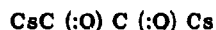


In air these compounds oxidize readily and spontaneous combustion may occur. They are relatively inert in boiling water although a limited amount of the metal can be leached out by this technique.

An interesting interaction exists between Cs and CO. <sup>(22)</sup> The compound is believed to have the following structure:



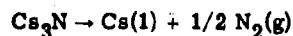
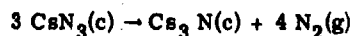
This carbonyl is explosive at around 250 C. If oxygen is present in CO the following yellow compound is formed:



Belozerski<sup>(41)</sup> presents a good summary of the properties of cesium carbonyl. It is known that cesium absorbs CO readily in the interval of 0-100 C and at higher temperatures (upper limit has been poorly defined in reported work). It is known that the carbonyl composition is such that Cs/CO ratio is unity. The degree of "Polymerization" of the carbonyl is not known. However, it is known that the carbonyls of all the other alkali metals are "dimers" so it is reasonable to suspect that cesium carbonyl is  $[\text{CsCO}]_2$ . Cesium carbonyl is a dark blue compound which is easily formed by an exothermic reaction of CO with Cs. The heat of formation is  $37.96 \pm 0.52$  kcal per Cs atom. It is stable in hydrogen up to 250 C.

#### 11. Cesium - Nitrogen

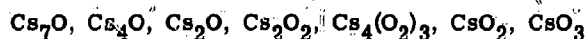
The solubility of nitrogen in cesium is not known. It is well established that  $\text{CsN}_3$  exists. (25, 26) The material decomposed readily at around 340 C to form Cs and  $\text{N}_2$ . This compound has an appreciable vapor pressure and it can be decomposed in vacuum. (5)  $\text{RbN}_3$  is known to decompose first to  $\text{Rb}_3\text{N}$ . Since  $\text{Cs}_3\text{N}$  has been reported, (24, 25, 27) it can be expected that the following decomposition steps occur



$\text{Cs}_3\text{N}$  is gray-green compound melting at 326 C and readily decomposing at 390 C. (28) It is hygroscopic and decomposes in moist air yielding  $\text{NH}_3$ . It is stable in hydrogen and dry air at room temperature. At high temperatures hydrogen replaces the nitrogen with the formation of the hydride. As expected, this material is very reactive with elements which produce stable cesium salts such as chlorine, fluorine and sulfur. Dilute acids decompose  $\text{Cs}_3\text{N}$  to form gaseous  $\text{NH}_3$ .  $\text{CsN}_3$  melts at 314 C. (28) In contrast to other alkali metal azides (with the exception of  $\text{RbN}_3$ )  $\text{CsN}_3$  is not explosive under impact. This azide is hygroscopic, but dissolves very slowly in ethanol.

#### 12. Cesium - Oxygen

Cesium forms a large number of oxides. (5) The following have been identified:



The solubility limits of oxygen in cesium is still unknown although the existence of  $\text{Cs}_7\text{O}$  indicates a limit for temperatures below 276 K.



The lowest of the sub-oxides  $\text{Cs}_7\text{O}$  melts at 276 K. Thermodynamic stability of this oxide is unknown. The x-ray studies have been unsuccessful in elucidating the structure but the pattern is quite distinct from Cs and  $\text{Cs}_2\text{O}$ . (29) Perelman (5) does not acknowledge the existence of any new phase between  $\text{Cs}_7\text{O}$  and  $\text{Cs}_2\text{O}$ . Brauer does mention  $\text{Cs}_4\text{O}$  but even less is known about this compound than in the case of  $\text{Cs}_7\text{O}$ . Perelman (5) advanced the hypothesis that oxygen can be taken up into the  $\text{Cs}_7\text{O}$  structure and this may result in the "intermediate" phases such as  $\text{Cs}_4\text{O}$ .

$\text{Cs}_2\text{O}$  is a well established compound with a relatively high melting point of 763 K.  $\text{Cs}_2\text{O}$  crystallized in rhombohedral,  $\text{CdCl}_2$  type structure with the following parameters. (31)

$$a = 5.85 \text{ kX } \alpha = 93.92 \quad D_m = 4.60 \text{ g/cm}^3 \quad M = 2$$

$$a = 6.74 \quad \alpha = 36.93 \quad M = 1$$

The thermochemical stability is given in reference 30. These data are given below for  $\text{Cs}_2\text{O}$  and the higher oxides at 298.15 K.

	$\Delta H_f^\circ$ (kcal)	$\Delta F^\circ$ (kcal)	S (e.u.)
$\text{Cs}_2\text{O}$ (c)	-75.9	-65.6	(29.6)
$\text{Cs}_2\text{O}_2$ (c)	-96.2	-78.2	(28.2)
$\text{Cs}_2\text{O}_3$ (c)	-111.2	-86.0	(28.7)
$\text{Cs}_2\text{O}_4$ (c)	-124.2	-92.5	(31.2)

The data on  $\Delta H_f^\circ$  is given in reference 5. The entropies were estimated by Latimer (32) from which  $\Delta F^\circ$  values were calculated.  $\text{Cs}_2\text{O}$  is the most frequently encountered oxide in the case of excess cesium or a limited availability of oxygen.

$\text{Cs}_2\text{O}_2$ , the peroxide, is an ionic crystal of the rhombic class; very little is known about this compound. (33) The oxide  $\text{Cs}_2\text{O}_2$  is probably formed by the step-wise oxidation of Cs, through the stages of  $\text{Cs}_2\text{O}_2$  and  $\text{Cs}_4(\text{O}_2)_3$  (or  $\text{Cs}_2\text{O}_3$ ). The structure of  $\text{Cs}_4\text{O}_6$  is b.c. cubic with  $a = 9.86 \text{ kX}$   $M = 4$ . (34) The salt is dark yellow in color and has not been studied in detail. (35)

$\text{CsO}_2$  is a yellow salt, with a b.c. tetragonal structure (36, 37)

for the f.c.c. unit cell  $a = 6.28 \text{ kX}$   $c = 7.20 \text{ kX}$

$$c/a = 1.145 \quad D_m = 3.80 \text{ g/cm}^3$$

An earlier study of the structure of this compound is also reported. <sup>(38)</sup> All of the oxides of cesium react with water to form  $\text{CsOH} \cdot \text{H}_2\text{O}$ . This monohydrate is quite stable, <sup>(5)</sup> melting at 180 C and decomposing at 400 C.

$\text{CsO}_3$  is reported by Perelman. <sup>(5)</sup> This compound is stable only at low temperatures (243-253 K) and decomposes readily at room temperatures



$\text{CsO}_3$  is usually observed as reddish brown crystals. <sup>(5)</sup> The structure has not been determined.

### 13. Cesium - Uranium

No data exists for this system. The only system that could be counted to resemble the one of interest is the U-Na system. <sup>(13)</sup> No intermediate phases are reported in this system at least up to 500 C. The solubility of U in liquid Na at 97.8 C was found to be between 0 and 0.005 wt. per cent. It is therefore surmised that uranium is not appreciably soluble in cesium and it is unlikely that stable compounds exist. It is clear that there is a need for experimental work on the Cs-U system.

### 14. Cesium - Thorium

This system has not been studied. Na-Th system is reported by Hansen. <sup>(13)</sup> It is claimed that a eutectic exists (92 C) at the sodium rich side (3.2 at. per cent). A phase  $\text{Na}_4\text{Th}$  is claimed to exist which decomposes peritectically at 121 C. The exhaustive studies by L. R. Kelman <sup>(39)</sup> failed to uncover this behavior of the Na-Th system. In the interval of 650-800 C thorium was found to be essentially inert to sodium. The behavior of Th is therefore quite close to that of U with Na. Kelman's results must be considered to be the most reliable at this time.

### 15. References

1. L. Hackspill, A. Boroceo, Chem. Rev. 204, 1475 (1937).
2. V. L. Hansley USA Pat. 2372670 1945  
USA Pat. 2372371 1945  
USA Pat. 2504927 1950
3. A. Herold, Ann. Chim. 6, 636 (1951).
4. L. Hackspill, A. Boroceo, Bu. Soc. Chim. 6, 91 (1939).
5. F. M. Perelman, "Rubidium and Cesium", Akad. Nauk, SSSR, Moscow (1960).

6. K. K. Kelley, E. G. King, USBM Bull. 592 (1961).
7. G. Herzberg, Spectra of Diatomic Molecules, D. Van Nostrand, N. Y. 1950.
8. E. Zintl, A. Harder, Z. Phys. Chem. 314, 265 (1931).
9. T. I. Symposium
10. Brit. Pat. 730263 (1955).
11. A. P. Altshuller, J. Amer. Chem. Soc. 77, 5455 (1955).
12. G. V. Samsonov, L. Y. Markovski, A. F. Zhigach, M. G. Vallashko, "Boron, Its Compounds and Alloys", Akad. Nauk. Uk, SSR, Kiev 1960.
13. M. Hansen, "Constitution of Binary Alloys", McGraw Hill 1958.
14. W. V. Massehausen, Z. Metallkunde 43, 53 (1952).
15. Liquid Metals H-B NAVEXOSP-733 (Rev)
16. Golden Gate Metals Conference, San Francisco 1962.
17. V. C. Wilson, personal communication (1962).
18. M. J. Slivka, Report No. 1 Contract NObs 86220, February 1962.
19. L. Yang, private communication, 1961.
20. A. R. Ubbelohde, F. A. Lewis, "Graphite and Its Crystal Compounds", Oxford 1960.
21. A. Herold, Bull, Soc. Chim. 999 (1955).
22. R. Setton, Chem. Revs. 238, 2323 (1954).
23. J. H. DeBrev, P. Clausing, G. Zecher, Z. Anorg. Allg. Chem. 160, 128 (1927).
24. K. Clusius, A. Znorg. Chem. 194, 48, 1930.
25. R. Suhrman, K. Clusius, Zeit, Anorg. Chem 152, 57 (1926).
26. T. Curtiss, J. Rissom, J. Pract. Chem. 58, 282 (1898).
27. H. Moissan, Comp. Rend. 136, 508 (1903).
28. A. E. Vol. "Structure and Properties of Binary Metallic Systems", Vol. 1 Moscow, 1959.
29. G. Brauer, Z. Anorg. Chem. 255, 101 (1947).
30. Selected Values of Chemical Thermodynamic Properties. Part 1. NBS Circular 500.

31. A. Helms, W. Klemm, Z. Anorg. Chem. 242, 33 (1939).
32. W. M. Latimer, "The Oxidation States of Elements and Their Potentials in Aqueous Solutions", Prentice-Hall, 1953.
33. H. Foppl, Angew.-Chemie, 67, 712 (1955).
34. A. Helms, W. Klemm, Z. Anorg. Chem. 242, 201 (1939).
35. J. Fischer-Hjalmars, B. Grabe J. Chem. Phys. 22, 1259 (1954).
36. A. Helms, Angew. Chem. 51, 498 (1938).
37. A. Helms, W. Klemm, Z. Anorg. Chem. 241, 97 (1939).
38. V. Kasatochkin, V. Kotov, Zh. Fiz. Khim. 8, 620 (1936).
39. L. R. Kelman, Argonne National Lab. Work done in 1947. Information secured through E. W. Hoyt.
40. G. P. Nicolsky, Z. A. Bagdasarian, I. A. Kazarnovski, Dokl. Akad. Nauk. SSSR 77, 69 (1951).
41. N. A. Belozerski, "Carbonyls of Metals", Moscow, 1958.

#### **E. Cesium Compatibility Test Program**

##### **1. Objectives**

The objective of this program was to make a screening study of the stability of selected thermionic emitters in cesium vapor. The materials to be tested were as follows:

UC, UC<sub>2</sub>, (UC) (Zr), ZrC, YB<sub>6</sub> and EuB<sub>6</sub>

The main objective was the development of suitable techniques and procedures for testing at moderate temperatures which would serve as a guide to high temperature testing procedures without resorting to actual construction of converters. The moderate temperature level was selected as around 1000 C and the high temperature objective was set at 1700 C. The cesium pressure was set between 2-10 torr as being representative of most thermionic converters.

##### **2. Design of Test Chambers for Moderate Temperatures and Experimental Technique**

The survey of alkali metal properties and corrosion indicated that inconel would be a suitable material for containment of cesium vapor up to 1000 C. It was further noted that inconel would afford a simplicity of operation due to its good resistance to atmospheric corrosion at

these temperature levels. The cooler sections of the test chamber could be constructed of stainless steel type 304 although type 304L is more desirable. Since it was desirable to isolate the specimens from each other, a plate and ring assembly was thought to provide physical separation while allowing cesium vapor circulation. Tantalum was chosen for this job because of its known inertness to cesium, ease of fabrication and good gettering properties with respect to oxygen and other active gases.

Copper (OFHC) was selected for the pinch-off section as copper was deemed to be the most reliable and proven material in cold welding. At the same time a limited amount of effort was applied to check pinch-off techniques on niobium and tantalum.

A photograph of the components is given in Figure 4. This represents the components in disassembly prior to testing. The assembly and joining of the test chamber involved only welding or direct fusion bonding. Hellarc welding was accomplished on SS 304 inconel, and inconel-to SS304. Copper was joined to stainless steel by direct fusion of the copper to that material. All components were leak tested as assembled so that certain key areas underwent several consecutive tests. The methods of fabrication deliberately skirted the use of brazes as these material are known to be potentially weak links as far as vac-tightness is concerned. Many brazes develop cracks, grain growth, and undergo cesium attack (particularly those based on noble metals).

When assembled, all the components were scrupulously cleaned following techniques adopted by the electron tube industry. After the specimens were loaded into the tantalum chambers, the chambers were assembled and placed in the main inconel chamber. The inconel chamber was welded (heli-arc) to the stainless steel-copper-stainless assembly for the introduction of cesium. Before the introduction of the cesium ampoule a filter made of tantalum foil was introduced to prevent glass particles from the ampoule to be introduced into the system. The cesium ampoule was then introduced and the system was pumped down to about  $10^{-6}$  torr. Figure 5 shows the best system as assembled. During the pump down operation the assembly, with the exception of the tube holding the cesium ampoule, was baked out at 600-700 C for about 2 hours. At the end of this period the system was cooled and the tube containing the ampoule was pinched and the glass ampoule crushed. A hot air blower melted the cesium and a stream of helium forced the liquid metal into the chamber. The copper tube was then heated with the same air blower and the system was pumped down. The copper tube was

pinched off using a pinch-off tool similar to that manufactured by Kane. Since helium was used to force the liquid metal into the chamber the pinched-off system was susceptible to a leak test on the pinched section by use of a Veeco MS-9 leak detector. This test showed that the system was tight. After this check-out the copper pinch-off tube was nickel-plated to prevent its oxidation in air.

The cesium test chamber was then ready for insertion into a vertical tube furnace. The tube of the furnace was made of high purity alumina with a rhodium heating element. The length of the tube was 16 inches, the tube diameter was 1-1/2 inches. Prior tests on this furnace were carried out to establish a constant temperature zone (to 5 C) and the power levels to operate the system at 1000 C (these turned out to be 0.9 kw). The cesium reservoir was surrounded by a massive jacket of copper which served to even out the temperatures in that section. A tape heater was used to maintain the cesium pool at a constant temperature. The furnace temperature was monitored by a chromel-alumel thermocouple, the same was used for temperature control on the cesium pool. Test observations showed that good control of furnace temperature could be maintained for 350 and 500 hour periods. Temperature variation never exceeded 10 C. The temperature of the cesium pool never varied more than 2-3 C.

Upon completion of the test period the chamber was cooled and then placed in an argon dry-box (Figure 6). This procedure was desirable from several standpoints:

- a. It allowed the observation of specimens as they appeared after the test and definitely with no appreciable levels of oxygen in the atmosphere during examination.
- b. It established unequivocally the presence and amount of cesium metal, and the appearance of attack if any on the internal surfaces of the test chamber.

Examinations without the benefit of dry-boxes is undesirable because of the oxidation of cesium and/or its decomposition by alcohols frequently obscures and confounds the analysis of results. After examination of the chamber components and specimens in the dry box the components were removed under mineral oil for further investigation. The residual cesium was removed from the pellets by use of higher alcohols (butanol used with care is quite satisfactory). The components and specimens were then analyzed by metallographic and x-ray techniques.

High purity (best available) cesium metal was used in the experiments. Dow Chemical was the supplier. Examination of other sources showed that the Dow material could be rated as high as any on the market. Furthermore, the use of this material was recommended by technical Air Force personnel supervising cesium compatibility test programs. Quantities of 5 grams of cesium metal were used in the tests. This large excess was considered to be desirable since any dissolution of impurities in cesium would very likely have a stronger effect the smaller the quantity of cesium present in the reservoir.

### 3. Observations of Test Results at Moderate Temperature (1000 C)

The conditions of the first test were as follows:

- a. Test chamber (with specimen) at 1000 C.
- b. Cesium reservoir temperature 300 C.
- c. Duration of test 350 hours.

The materials tested were:  $YB_6$ ,  $YB_6$ -Ta-1 (composite structure designated as CS),  $YB_6$ -Ta-2 (CS),  $YB_6$ -Mo(CS),  $EuB_6$ -Ta(CS),  $UO_3$  and  $Y_2O_3$ . The boride materials were made by hot-pressing the compounds in the form of powder (-325 mesh) in a vacuum induction hot press. The conditions of pressing usually had a range of 1500-2300 C and 4000-6000 psi.  $UO_2$  was also a hot pressed specimen of power reactor grade oxide fuel.  $Y_2O_3$  was hot-pressed into a pellet from the oxide powder. It was decided to include  $UO_2$  because of its growing importance in nuclear thermionics as a clad fuel.  $Y_2O_3$  was considered a very promising insulator with a high melting point and known inertness to a variety of environments. The composite boride-metal structures were made either by hot-pressing the boride powder onto a metal cup, or by pressing alternate layers of boride and metal powder.

The test procedures have been described in the previous section. It was possible to establish that metallic cesium existed throughout the test period. A large amount of it was evident in the cesium reservoir and as a coating on all the interior components. Nickel plating of the copper pinch-off reservoir was apparently satisfactory in the elimination of corrosion and leakage during the test period at 300 C. Metallographic and visual examination showed no noticeable attack on the interior of the inconel tube. Considerable corrosion was noted on the outside of the tube. All the tantalum specimen chambers were carburized to  $Ta_2C$  and  $TaC$ . It is believed that the carbon source was the stainless steel and tantalum served as a sink for it. The following observations were made:

<u>Material</u>	<u>Change In Wt.</u>	<u>Comments</u>
YB <sub>6</sub>	-0.0064 gm	No attack (metallography and x-rays)
YB <sub>6</sub> -Ta-1	+0.0024 gms	Interfacial separation between Ta and YB <sub>6</sub> . Ta outer surface carburized, YB <sub>6</sub> shows no attack.
YB <sub>6</sub> -Ta-2	0.0000 gms	No separation, YB <sub>6</sub> shows no attack. Ta carburized on surface.
YB <sub>6</sub> -Mo	-0.0252 gms	Separation at interface, no attack on YB <sub>6</sub> .
EuB <sub>6</sub> -Ta	-0.0028 gms	EuB <sub>6</sub> pressed into re-entrant cup. EuB <sub>6</sub> not attacked. Ta surface carburized (metallography and x-rays)
UO <sub>2</sub>	-0.0078	Unaffected by cesium
Y <sub>2</sub> O <sub>3</sub>	Specimen chipped in handling.	Unaffected by cesium

Weight loss or gain results are not subject to unequivocal interpretation since separation of composite materials, carburization and cleaning of specimens by means of alcohol, etc. may have affected the results. Presence of Y<sub>2</sub>O<sub>3</sub> at the interfaces of failed YB<sub>6</sub>-Ta composites may indicate that free yttrium metal was formed during pressing and subsequently oxidized during exposure to the atmosphere. Failure during the test is due, most likely, to thermal expansion mismatches at the interfaces.

The main conclusions of the first test were:

1. YB<sub>6</sub> and EuB<sub>6</sub> are inert to cesium vapor (and liquid) at 1000 C (2 torr cesium pressure) for a period of 350 hours.
2. The same applies to Y<sub>2</sub>O<sub>3</sub> and UO<sub>2</sub>.
3. Considerably more work is needed to produce mechanically stable composites of borides and refractory metals. Re-entrants cup design showed some promise.

The procedures developed for the first test at 1000 C were followed for the second moderate temperature test. The test conditions were:



Specimen Temperature	1010 C
Cesium Pressure	10 torr
Duration	500 hours

The use of higher cesium pressure required a higher temperature in the cesium pool (380 C). The duration of the run exceeded that of the first by 150 hours. Only carbides and one boride were exposed in this test.

Upon termination of the test run, it was observed that the cesium reservoir had experienced some attack as the surface was darkened. Examination in the dry box again showed the presence of elemental cesium. Some of the tantalum foil had the appearance of oxidizing attack and was found to be brittle.

Sectioning of the copper cesium reservoir tube showed that no gross corrosion occurred and if the leak occurred it was probably via a grain boundary migration of oxygen into system where the nickel plating was defective. In the presence of refractory metals, such as tantalum, the cesium oxide if formed does not have a chance of survival since the affinity of oxygen for tantalum would be much stronger. It appears that the following steps occur if an oxygen leak is present:

- a.  $1/2 O_2$  (atmospheres)  $\rightarrow$  O (in grain boundaries, probably as  $Cu_2O$ )
- b. O (in grain boundaries) + Cs  $\rightarrow$   $Cs_2O$  (and lower oxides)
- c.  $Cs_2O + Ta \rightarrow Ta (+O \text{ in solution or as oxide})$   
 $+ 2 Cs$

It is clear that an emitter material could function just as effectively as a gettering agent instead of tantalum.

In the second test the following materials were tested: UC,  $UC_2$ , (UC) (ZrC), and ZrC (a specimen of  $YB_6$  in the form of  $YB_6$  bonded on tantalum with a tungsten wire imbedded in the  $YB_6$  matrix was also tested). The carbides were hot pressed pellets produced in much the same way as the borides in the first experimental test. Upon completion of the test it was found that all the carbides were either reduced to a powder or broke into pieces. This circumstance again pointed to oxygen as the culprit. All the tantalum specimen chambers were lined with tungsten which was embrittled after the test. The starting materials were all characterized before the test. UC material was single phase,  $UC_2$  contained some UC, (UC) (ZrC) was single phase as was ZrC. Density range was between 80-92 per cent of

theoretical. Disintegration of the carbides precluded a comparison of weights before and after the test and precluded most of the metallographic examinations.

X-ray analysis confirmed oxidation as a result of a small leak that must have developed during the test,

<u>Material</u>	<u>X-Ray Results</u>
UC	Partially oxidized to $\text{UO}_2$ , UC present
$\text{UC}_2$	Partially oxidized to $\text{UO}_2$ , UC present
ZrC	Single phase ZrC
UC-ZrC	Evidence of oxidation
$\text{YB}_6 + \text{W}$ (on Ta substrate)	$\text{YB}_4$ , $\text{YB}_6$ and tungsten borides. No evidence of oxide or borates.

Only the boride showed no evident attack as a result of the test. The results of test showed that the reliability of the nickel plating procedure used in this study was poor. Apparently the (0-15 mil) plate had defects which permitted oxygen diffusion. Alternatives for the correction of this fault are:

- a. Development of reliable plating techniques.
- b. Development of stainless steel pinch offs or nickel pinch off techniques.
- c. Operation of the system under inert gas or in vacuum.

Alternative (1) speaks for itself, it is true that technique used have not been tested for expected reliability, i.e. statistics are lacking on the present procedure but it is known that good plating was achieved in a large number of instances. Alternative (2) was not pursued to any appreciable extent but it is known that the reliability of pinch-offs in stainless steel and nickel are lower than that for copper; the main effort, which was small, in the area of pinch-off techniques was concentrated on niobium and tantalum and the latter was found to be very successful. Alternative (3) was not possible due to the lack of availability of furnace space in the vacuum furnaces on the site and the need for extensive modification of these furnaces. It is also evident that the success of the first test was somewhat misleading and did not encourage a more extensive effort to render the testing procedure more reliable.

#### 4. Development of Testing Procedure for High Temperatures

The principal change suggested by high temperature testing (1700 C) was in the choice of material for the main test chamber which was made of inconel for the moderate temperature test. From the standpoint of strength, fabricability, availability, and resistance to cesium tantalum was chosen as the material of construction. The success of tantalum pinch-offs suggested the construction of the whole system out of tantalum. This was accomplished using commercial grade of tantalum (Fansteel) for the components required the development of welding techniques for the particular configuration in the laboratory where the assembly had to be accomplished. This was successfully accomplished. The handling of all the materials, assembly and welding were done in the argon dry box so that the exposure to the atmospheric conditions was minimal. The details of the test system were analogous to those used for moderate temperature testing. Tungsten lining was again used in the individual tantalum specimen chambers. Again no brazing and only welding was used in joining the component parts. The procedures followed in the pre-test procedure were similar to those already described.

The use of tantalum naturally precluded running the system in air. The test system was placed in an alumina tube with vac-tight water-cooled brass fittings at the ends. Argon was allowed to bleed through the system via the brass fittings and through an oil trap at the exit. The top fitting was equipped with a sight glass and prism for optical pyrometry through six tantalum radiation shields at the top of the assembly. The bottom had an accommodation for thermocouple monitoring of the cesium pool. Radiation shields were also placed at the bottom section to protect the cesium pool. Mock-up experiments established the geometry and conditions for maintaining the desired cesium reservoir temperature. Prior to this a new furnace supply was installed as there was some apprehension over power limitation. Mock-up and actual tests showed that power requirements at 1700 C were more than twice that at 1000 C.

In order to prevent the reaction of tantalum with alumina a molybdenum sheet lining was placed into the alumina tube. Mock-up experiments and other tests showed that the system was sound. The test was initiated and continued for about 115 hours when evidence of malfunction was noted. The test period to at least 98 hours did not show any indication of malfunction. It was observed that a deposit coated the sight glass and that an extremely large bleed of argon was necessary for the system. After a slow cool-down, it was observed

that the alumina tube had developed several cracks (3-4 inches long) in the central portion of the tube running along the length of the morganite tube. No chemical reaction in this portion was noted so that the cracking could not be blamed on solid state or other reactions.

The tantalum tube sections of the test system opposite the cracks were severely oxidized and cracked. All the specimens were oxidized to powder product and the test results were therefore lost. The weld sections of tantalum which were away from the cracked section of the alumina tube were intact and in good condition. The experience of this test strongly suggests the use of specially designed vacuum furnaces for the accomplishment of high temperature cesium compatibility tests because the reliability of test system would be much higher.

At present there is every indication that the tantalum test chamber system developed here would function adequately in a vacuum furnace with refractory metal heating elements.

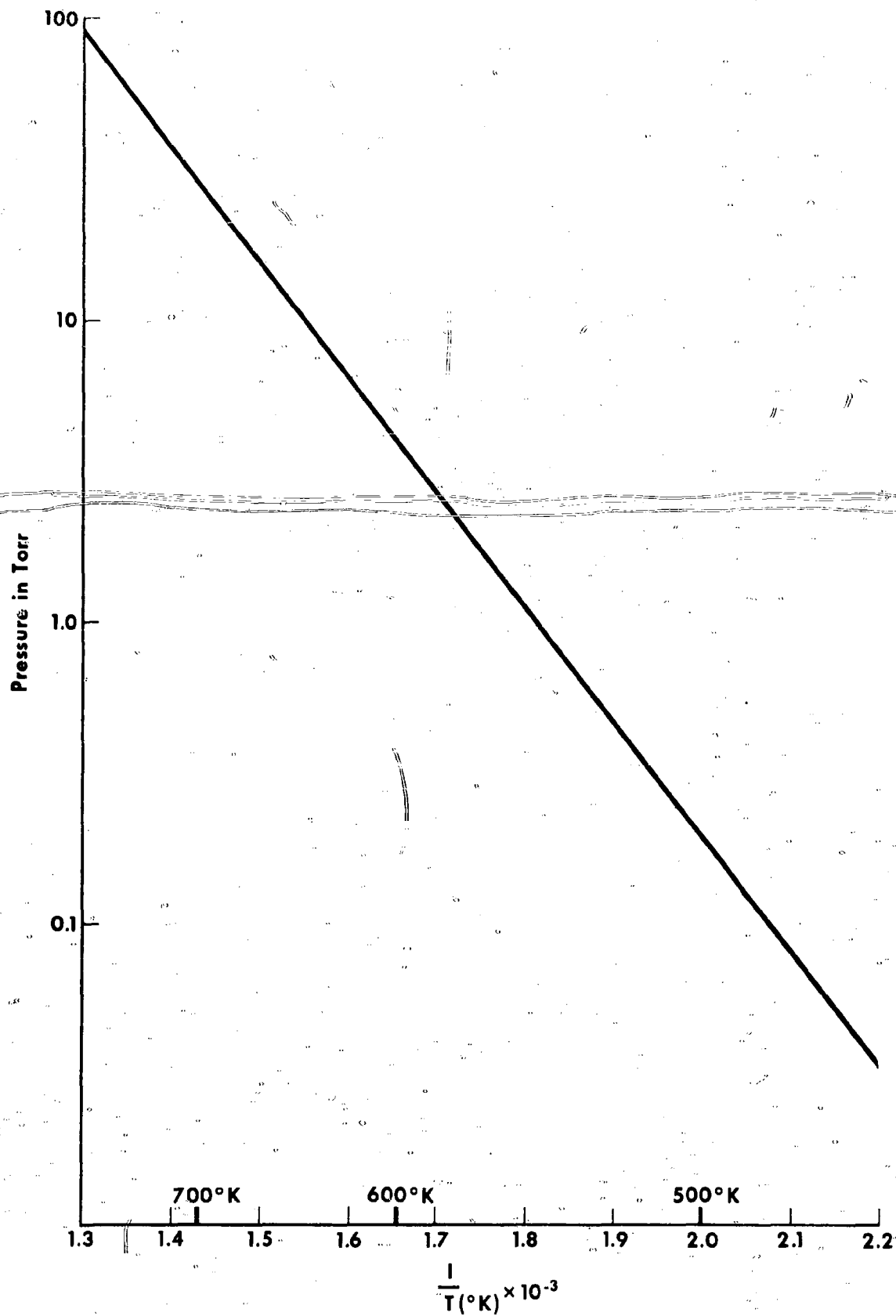


Figure 1. CESIUM VAPOR PRESSURE RANGE ENCOUNTERED IN THERMIONIC CONVERTERS

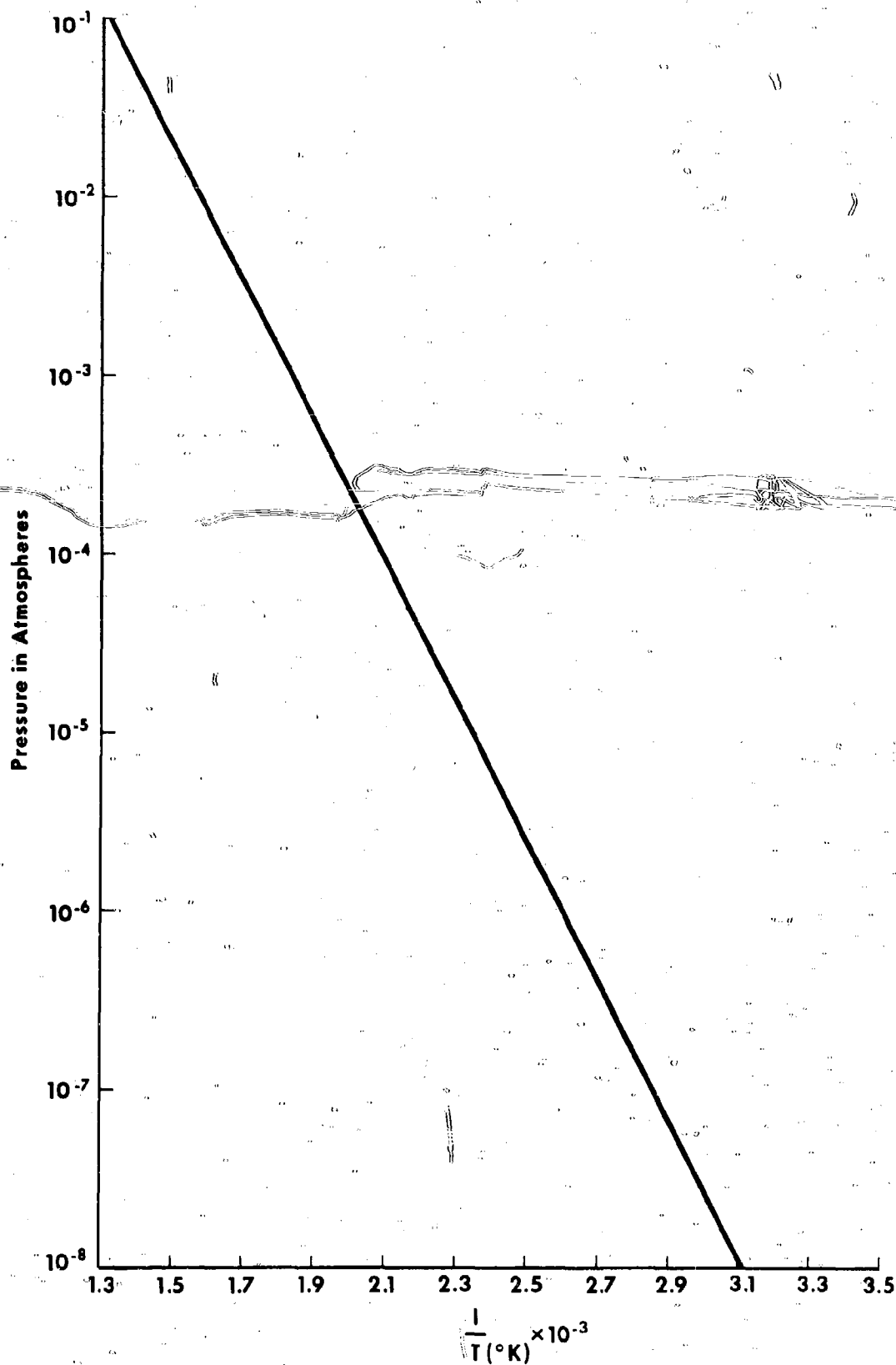


Figure 2. TOTAL VAPOR OF CESIUM AS A FUNCTION OF RECIPROCAL TEMPERATURE (16)

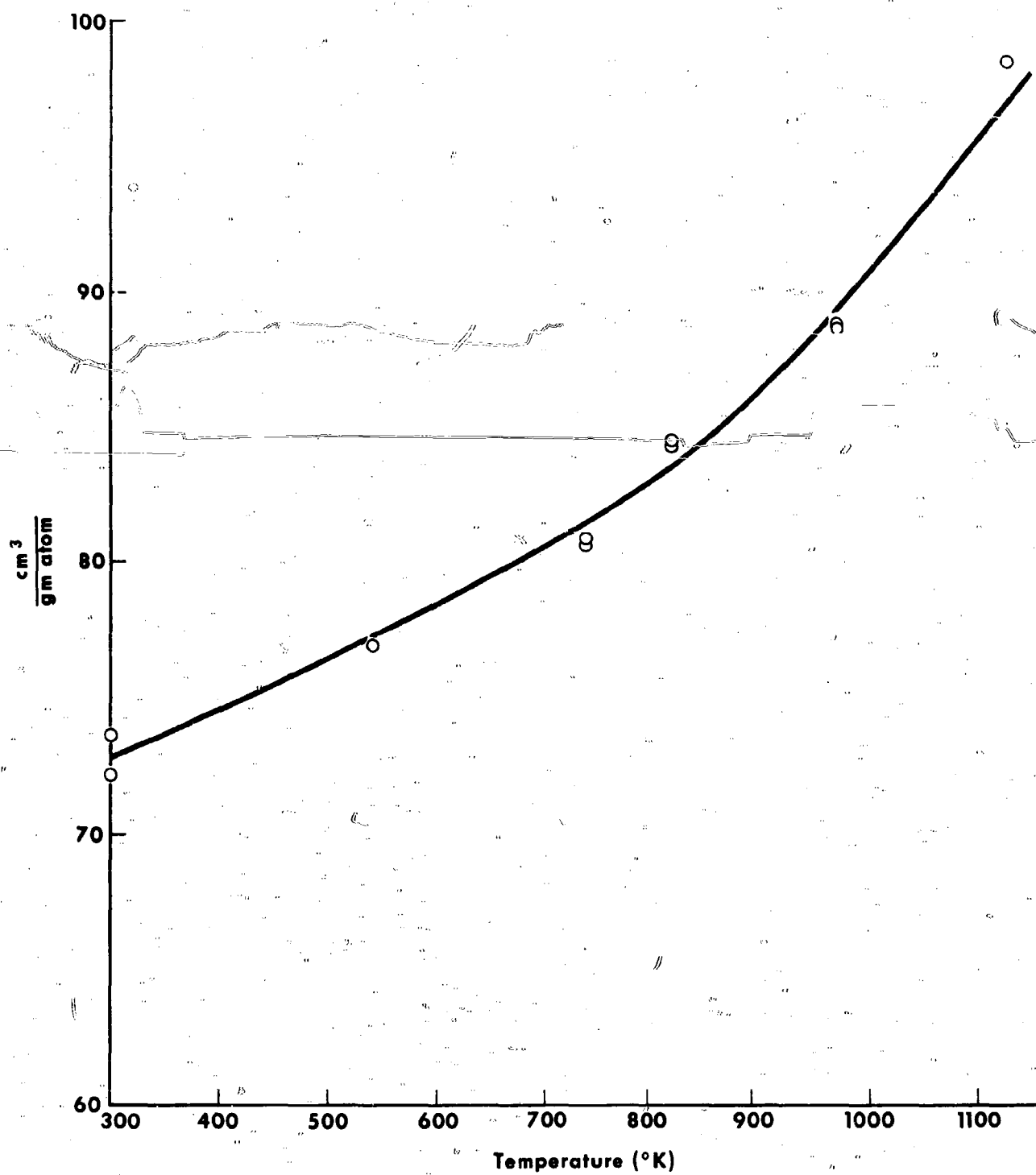


Figure 3. VOLUMETRIC BEHAVIOR OF LIQUID CESIUM

Figure 4. VIEW OF COMPONENTS OF THE CESIUM COMPATIBILITY CHAMBER



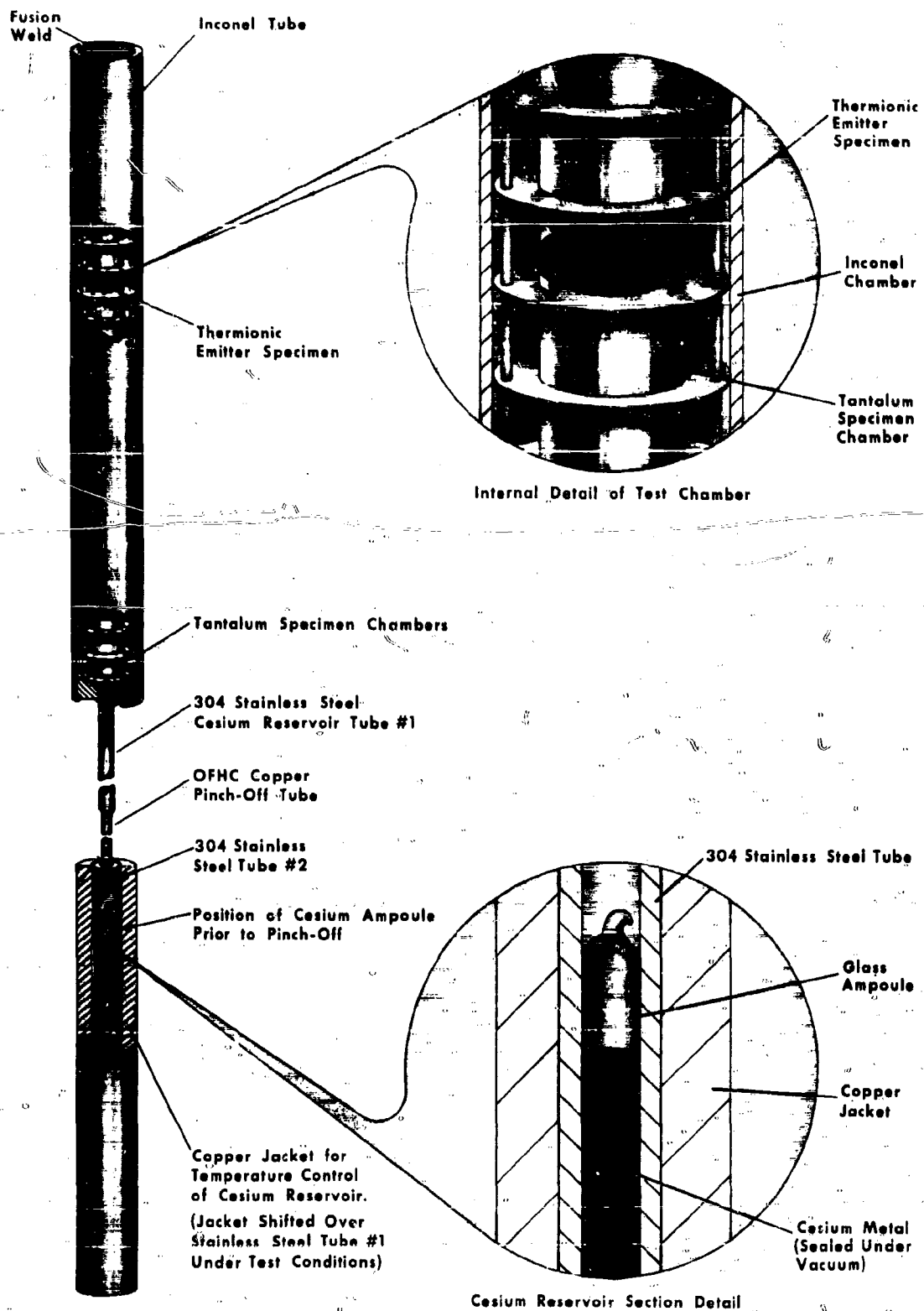


Figure 5. CESIUM COMPATIBILITY TEST SYSTEM

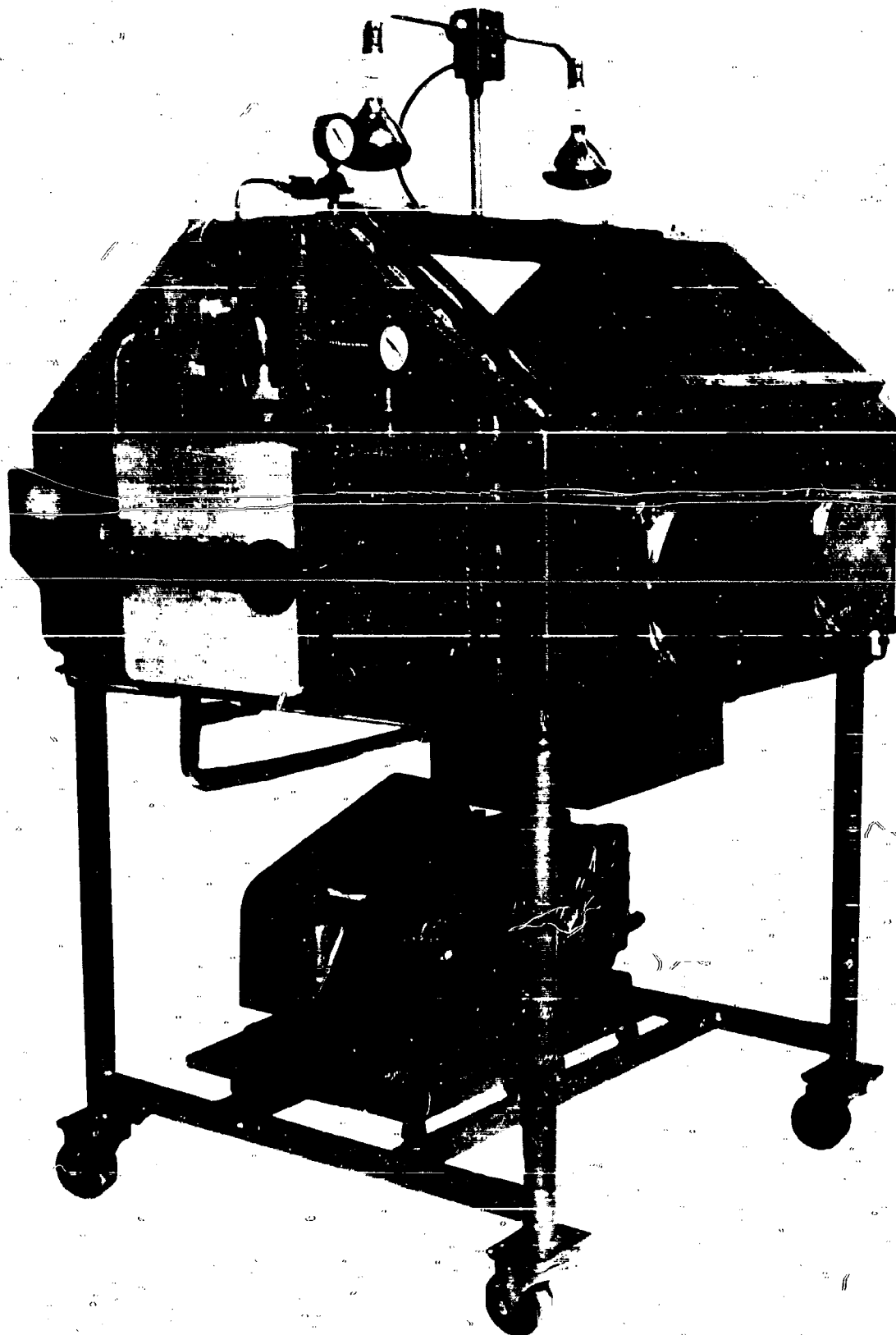


Figure 6. ARGON DRY BOX

**SECTION VI - GRAIN GROWTH AND MICROSTRUCTURAL CHANGES IN REFRACTORY THERMIONIC  
EMITTER MATERIALS    A. I. Kaznoff  
   J. G. Wilson**

**SYMBOL AND NOMENCLATURE**

$\sigma$	= strength
$\sigma_0$	= strength of 100% dense material
$p$	= volume fraction porosity
$n$	= constant
$D$	= grain size
$D_0$	= initial grain size
$r$	= average interfacial energy
$v$	= gram atomic volume

**LIST OF ILLUSTRATIONS**

<u>Figure No.</u>	<u>Title</u>	<u>Page No.</u>
1	Tantalum Resistance Furnace	6-19
2	Induction Furnace - pre-printed	6-20
3	ZrC-A-06 Starting Material (4904)	6-21
4	ZrC-A-06 1 hour at 200 C (4719)	6-21
5	ZrC-A-06 2 hours at 2000 C (4724)	6-22
6	ZrC-A-06 4 hours at 2000 C (4741)	6-22
7	ZrC-A-06 12 hours at 2000 C (4743)	6-23
8	ZrC-A-06 1 hour at 2200 C (4793)	6-23
9	ZrC-A-06 4 hours at 2200 C (4810)	6-24
10	ZrC-A-06 9 hours at 2200 C (4811)	6-24
11	ZrC-A-06 1 hour at 2400 C (4912)	6-25
12	ZrC-A-06 1 hour at 2400 C (4911)	6-25
13	ZrC-A-25 Starting Material (5074)	6-26
14	ZrC-A-25 1 hour at 2400 C (5196)	6-26
15	ZrC-A-25 2 hours at 2400 C (5194)	6-27
16	ZrC-A-25 3 hours at 2400 C (5198)	6-27

LIST OF ILLUSTRATIONS (Continued)

<u>Figure No.</u>	<u>Title</u>	<u>Page No.</u>
17	ZrC-A-25 1 hour at 2500 C (5205)	6-28
18	ZrC-A-25 2 hours at 2500 C (5202)	6-28
19	ZrC-A-25 3 hours at 2500 C (5207)	6-29
20	Grain Size in ZrC-A-25	6-30
21	(UC) (ZrC) A-08 1 hour at 2000 C (4914)	6-31
22	(UC) (ZrC) A-08 4 hours at 2000 C (4917)	6-31
23	(UC) (ZrC) A-08 9 hours at 2000 C (4920)	6-32
24	(UC) (ZrC) A-08 16 hours at 2000 C (4921)	6-32
25	(UC) (ZrC) A-06 1 hour at 2200 C (4828)	6-33
26	(UC) (ZrC) A-06 4 hours at 2200 C (4835)	6-33
27	(UC) (ZrC) A-06 9 hours at 2200 C (4866)	6-34
28	(UC) (ZrC) A-06 G. B. precipitate 4 hours at 2200 C (4838)	6-34
29	Grain Size in (UC) (ZrC)	6-35
30	(UC) (ZrC) Grain Growth at 2000 C	6-36
31	(UC) (ZrC) Grain Growth at 2200 C	4-37
32	UC-A-13 1 hour at 2000 C (5009) (Grey material is bakelite)	6-38
33	UC-A-13 1 hour at 2000 C (5010)	6-38
34	UC-A-13 2 hours at 2000 C (5026)	6-39
35	UC A-13 4 hours at 2000 C (5020)	6-39
36	UC A-13 6 hours at 2000 C (5029)	6-40
37	Grain Size of UC 2000 C	6-41
38	UC A-13 1 hour at 2200 C (5060)	6-42
39	UC A-13 4 hours at 2200 C (5180)	6-42
40	Grain Size of UC at 2200 C	6-43
41	UC <sub>2</sub> -A-02 Starting Material (4848)	6-44
42	UC <sub>2</sub> -A-01 1/2 hour at 1800 C (4937)	6-44
43	UC <sub>2</sub> -A-01 1 hour at 1800 C (4934)	6-45
44	UC <sub>2</sub> -A-01 6 hours at 1800 C (4962)	6-45
45	UC <sub>2</sub> -A-02 1 hour at 2000 C (4860)	6-46
46	UC <sub>2</sub> -A-02 1 hour at 2000 C (4898)	6-46

LIST OF ILLUSTRATIONS (Continued)

<u>Figure No.</u>	<u>Title</u>	<u>Page No.</u>
47	UC <sub>2</sub> -A-04 1/4 hour at 2000 C (4960)	6-47
48	UC <sub>2</sub> -A-04 1/2 hour at 2000 C (4959)	6-47
49	UC <sub>2</sub> -A-04 1 hour at 2000 C (4956)	6-48
50	UC <sub>2</sub> -A-04 2 hour at 2000 C (5006)	6-48
51	EuB <sub>6</sub> A-11 Starting Material (4798)	6-49
52	EuB <sub>6</sub> A-15 Starting Material (4994)	6-49
53	EuB <sub>6</sub> A-11 20 hours at 1800 C (4806)	6-50
54	EuB <sub>6</sub> A-15 1 hour at 2050 C (4985)	6-50
55	EuB <sub>6</sub> A-15 4 hours at 2050 C (4894)	6-51
56	EuB <sub>6</sub> A-15 9 hours at 2050 C (4896)	6-51
57	EuB <sub>6</sub> A-15 16 hours at 2050 C (4897)	6-52
58	Grain Size in EuB <sub>6</sub>	6-53
59	YB <sub>6</sub> A-19 1 hour at 2000 C (5083)	6-54
60	YB <sub>6</sub> A-19 2 hours at 2000 C (5086)	6-54
61	YB <sub>6</sub> A-19 4 hours at 2000 C (5092)	6-55
62	YB <sub>6</sub> A-19 6 hours at 2000 C (5098)	6-55
63	YB <sub>6</sub> A-19 (750X) Cracks (5099)	6-56
64	Edge YB <sub>6</sub> A-19 1 hour at 2000 C (5078)	6-56
65	Edge YB <sub>6</sub> A-19 4 hours at 2000 C (5090)	6-57

## VI. GRAIN GROWTH AND MICROSTRUCTURAL CHANGES IN REFRACTORY COMPOUND THERMIONIC EMITTER MATERIALS, A. I. Yaznoff; J. G. Wilson

### A. Introduction

The objective of this study was the determination of the microstructural changes occurring in thermionic emitter materials. The refractory compounds studied were:

1. ZrC
2. UC-ZrC
3. UC
4. UC<sub>2</sub>
5. EuB<sub>6</sub>
6. YB<sub>6</sub>

Although the primary objective was the study of grain growth it was also realized that other important changes can occur, e.g. compositional changes due to sublimation, development or disappearance of phases, and development of porosity. All of these have been observed on at least one of the materials studied. The extreme temperatures (1800-2500 C) used in this study were imposed by two considerations:

1. High temperatures are necessary for the efficient performance of thermionic converters.
2. High temperatures are necessary to observe changes in the structure of the material within reasonable time. Frequently it was necessary to raise the temperature above that which may be necessary for efficient converter operation to produce measurable changes in the microstructure within several hours.

There are several reasons why grain growth is a very important consideration in emitter materials. From the thermionic standpoint, it is well known that the work function is a function of crystalline orientation of the surface. These effects have been investigated primarily on refractory metals. The behavior of a thermionic device could be markedly different if the grain size of emitter was either small compared to the inter-electrode spacing or large compared to the spacing. This effect is true for both vacuum and cesiated converters. In the case of the latter it also is a well known fact that cesium absorption is also a function of crystal orientation (or work function). Experiments to date show that crystal faces with high work functions absorb cesium more strongly than those with low work functions.

Grain growth can influence other important properties. Greater strength is usually associated with fine-grained materials so the grain growth is usually deleterious from the standpoint of strength. This observation is frequently justified by invoking the concept of Griffith microcracks which are postulated to be limited to the grain size. Theoretically the fracture stress should be proportional to the square root of the grain size. Grain growth which is to be expected in nuclear thermionic converters will be at least, an undesirable effect from the strength and modulus of rupture criteria.

The development of porosity in the refractory emitters is also undesirable. The strength of a ceramic material showing a very strong dependence on porosity. An expression, that has found wide application, showing the strength decrease due to porosity can be written as follows:

$$\frac{\sigma}{\sigma_0} = \exp(-nP)$$

where  $\sigma_0$  = the strength for 100 per cent dense material

P = the volume fraction porosity

n = constant ranging usually from 4-7.

A 10 per cent porosity may cause the strength to decrease by 50 per cent.

The presence (or generation) of second phases also leads to lowered fracture stresses. This frequently occurs because boundary stresses are set up as a result of different thermal expansion coefficients. Equally important is of course the disappearance of second phases or the redistribution of the phases.

Theories covering normal grain growth under isothermal conditions have been formulated and presented by several authors. (1-3) Generally the following relationship is believed to hold:

$$D^2 - D_0^2 = K \gamma V t$$

when D and  $D_0$  are the final and initial average grain diameters after a time t of exposure in an isothermal regime; K is proportional to the rate constant for grain boundary migration,  $\gamma$  is the average interfacial energy and V is the gram atomic volume. The temperature behavior of K is expressed as

$$K = K_0 \exp(-G/RT)$$

where  $K_0$  is a constant, G is the "activation energy", R the gas constant and T is the absolute temperature. Actual experimental data frequently do not obey the above expressions and empirical fits are obtained by use of equations such as

$$D = K t^n$$

where  $n$  is generally lower than 0.5 (but is also known to exceed this value). This expression is only suitable if the following is true

$$D \gg D_0$$

i.e. if  $D$  and  $D_0$  are comparable one may not expect to obtain a suitable fit. It is also not unusual to obtain variable values for  $G_T$  dependent on  $T$  and in principle there is no physical requirement that  $K_0$  is strictly constant over a temperature interval. One of the most important variables, that of impurities, particularly in the grain boundaries, is extremely difficult to control especially in the less-developed and studied ceramics which are the subject of this study.

It is, therefore, not surprising that some of the results do not appear to follow the theories and semi-empirical equations that are found to be highly successful in pure phases and especially metals.

### References

1. Burke, J. E., D. Turnbull, Prog. Metal Physics, Vol. III, p. 220, 1952.
2. Burke, J. E. In "Ceramic Fabrication Processes", p. 120 (Kingery Ed.) Wiley, 1958.
3. Turnbull, D., Trans. Am. Inst. Mining Met. Engrs., 191, 661 (1951).

### E. Summary

1. Hot pressed ZrC does not show appreciable grain growth below 2300 C. Low density ZrC ( $\approx$  65 per cent theoretical density) shows very inhomogeneous grain growth. At 2400 C sintering is observed accompanied by very rapid growth. High density ZrC (92.5 per cent theoretical density) showed a lower rate of grain growth which followed a recrystallization step. The temperature range of 2400-2500 C was studied. Times of exposure did not exceed 12 hours.
2. Hot-pressed (UC) (ZrC) showed a very small growth rate after the first hour at 2000 C. A grain size of about 10 microns was developed after 16 hours. It is postulated that grain boundary impurities inhibited a more rapid growth. The results at 2200 C show a much more rapid growth which follows the theoretical relationship  $D^2 - D_0^2 = kt$ . The equation obtained shows that grain size of 32 and 324 microns may be expected after 10 and 1000 hours at 2200 C. The rapid grain growth in (UC) (ZrC) may be a contributing factor to the low strength of this material. "Blow-hole" porosity was noted particularly near the sample edges after exposure to 2200 C. Maximum time of exposure was 16 hours.



3. Grain growth in hot-pressed UC at 2000 and 2200 C was found to obey the theoretical relationship  $D^2 - D_0^2 = kt$ . This result is believed to be fortuitous. More rapid grain growth was observed at and near the exposed surface of the samples. Evidence of possible recrystallization was noted at 2000 C. Grain boundary metallic phases were observed. In a 100 hour, at 2000 C, a grain size of 375 microns could be expected, while at 2200 C a size of 3900 microns may be expected in only 10 hours. Maximum time of exposure was 6 hours.
4. No kinetic data was obtained for hot-pressed UC<sub>2</sub>. Nearly all of the microstructural changes occurred during the first hour at 1800 and 2000 C. Profuse twinning and highly irregular grain boundaries which were poorly delineated, were observed. Maximum time of exposure was 16 hours.
5. Both EuB<sub>6</sub> and YB<sub>6</sub> do not show grain growth at 1900 C within 10-20 hours of exposure. EuB<sub>6</sub> grain starts to grow appreciably at 2050 C. The growth law is not a linear one with respect to  $D^2$ . Tests at 2000 C showed that YB<sub>6</sub> shows grain growth at that temperature. Surface of YB<sub>6</sub> specimens become coated with a YB<sub>4</sub> layer while the interior is free of YB<sub>4</sub>. Large porosity increases were noted in EuB<sub>6</sub> and YB<sub>6</sub>. Both EuB<sub>6</sub> and YB<sub>6</sub> should not show appreciable grain growth in the temperature range 1400-1500 C. This range is considered to be the practical one for these materials due to their high sublimation rates. Maximum time of exposure was 20 hours.
6. The above results apply only to hot-pressed materials, and the results are largely exploratory and of short duration. Further tests are needed to verify the validity of relationships obtained for longer periods of exposure. Effects of the variables of purity and stoichiometry require extensive elucidation. All tests were made under a vacuum of  $10^{-6}$  torr in the presence of refractory metal getters, the results could be modified by the presence of cesium vapor.

### C. Recommendations

The statements made in this section are arranged in the order of decreasing importance. The evaluation of the priority reflects the judgement of the authors which may not be shared by other investigators.

1. Grain growth of the system UC-ZrC should be studied in greater detail over composition and temperature ranges of interest in thermionic converters. Strength and creep properties must be established along with thermal shock parameters. The importance of this

study cannot be over-estimated in the field of unclad fuel-emitter converters although the mechanical properties are of significance even for metal-clad emitters. Preference should be given to high UC content alloys. Effects due to the presence of clad material and cesium should also be investigated.

2. The same applies to pure UC phase although the extent and scope of work is much smaller.
3. Studies on ZrC should be extended to obtain definitive kinetics for grain growth particularly in configurations in which this material will be used. Extension of work on ZrC is dependent on the advantages this material may have as an emitter over metals.
4. No further work is deemed necessary for  $\text{EuB}_6$  and  $\text{YB}_6$  until an unequivocal recommendation based on electron emission data and bonding studies of  $\text{YB}_6$  to metal substrates can be made.

#### D. Experimental Procedure

The study of grain growth and related metallurgical factors was accomplished by isothermal annealing of test specimens at elevated temperature. Two furnaces were used:

Furnace A. A tubular (1 inch diameter) tantalum resistance furnace shown in Figure 1.

Furnace B. An induction furnace shown in Figure 2.

Both furnaces operate under vacuum of about  $10^{-6}$  torr. The vacuum is obtained with the help of a mechanical pump, diffusion pump and a nitrogen trap. The temperature was monitored by means of a micro pyrometer. It is estimated that the temperature was known to better than  $\pm 20^\circ\text{C}$  and that the over-all drift of the temperature during the test periods did not exceed  $20^\circ\text{C}$ . The tantalum furnace (A) had an upper temperature limit of  $2050^\circ\text{C}$  as a result of its power supply limitations. The induction furnace was tested up to  $2500^\circ\text{C}$  and power limitations were not encountered in the configuration used in these studies. Furnace A was therefore used for "low" temperature runs and those runs which needed long exposure while furnace B was used in the "high" temperature range for runs that did not require long exposure. Both furnaces were characterized by very low thermal impedance and B had a lower impedance than A. Both furnaces contained specimen chambers as shown in Figure 2; these were made of tantalum supported in a boron nitride stand. The tantalum chamber was lined with tungsten. Further precautions against solid state reactions were taken for the individual materials: Uranium bearing materials were supported on expendable specimens of the same material which in turn rested on zirconium carbide which was in contact with the tungsten lining. The borides rested on boride specimens in contact with tungsten lining. ZrC rested directly on the

tungsten. Examination of the surface of the test specimens did not indicate solid state reactions at the interface although possible vapor phase reactions could not be eliminated or controlled.

The specimen environment can be described as "reducing" due to the presence of metallic components and the absence of any oxidizing media in the form of oxides, etc. The presence of heated tantalum, especially the tantalum radiation shields has been shown to be very effective in gettering oxygen and other active components in the residual gases at  $10^{-6}$  torr.

The reducing atmosphere maintained in the tests comes close to representing the condition existing in thermionic devices except for the absence of cesium at a few torr pressure. The absence of cesium was unavoidable due to the extreme complications that would arise in its use. The presence of cesium, of course, could modify the high temperature processes in refractory materials to a very considerable extent. It can be anticipated that sublimation processes could be reduced perhaps by an order or orders of magnitude depending on the partial pressures of the cesium, work function of emitters, and the proximity of condensation sinks. For the high work function material the absorbed layer or layers of cesium on the surface and the capillary condensation in the cracks could influence material transport in much the same way as liquids do in sintering. It is also quite conceivable that reactions with cesium could occur although present limited information on these materials does not point to these reactions.

It is also important to note that the specimens used in this study were pellets or sections of pellets prepared by hot-pressing in graphite dies in an induction-heated hot-press. The results obtained undoubtedly apply to these compounds only if they are prepared in a similar fashion.

As the nature of this study was primarily an exploratory one it was not possible to obtain results as a function of starting material variables (e.g. fabrication, purity, etc.).

The conditions of fabrication are given in the table below.

**TABLE I**

Sample	Powder Mesh Size	Temperature (°C)	Normal Pressure psi	Density % Theoretical
ZrC A-06	- 325	2300	4,000	65.0
ZrC A-25	- 325	2300	5,000	92.5
(UC) (ZrC) A-08	- 325	1650	6,000	90.0

TABLE I (Continued)

Sample	Powder Mesh Size	Temperature (°C)	Normal Pressure psi	Density % Theoretical
(UC) (ZrC) A-06	-325	1700	6,000	90.0
UC A-13	-325	1500	6,000	83.0
UC <sub>2</sub> A-02	-325	1700	4,800	95.0
UC <sub>2</sub> A-01	-325	1700	4,800	95.0
UC <sub>2</sub> A-04	-325	1500	4,000	88.0
UC <sub>2</sub> A-17	-325	1700	5,000	97.0
EuB <sub>6</sub> A-15	-325	2300	6,000	98.0
EuB <sub>6</sub> A-11	-325	2300	5,000	89.0
YB <sub>6</sub> A-19	-325	1500	5,000	90.0

In the following paragraphs the starting materials are described briefly.

ZrC A-06 was originally pressed into a 1 inch diameter (1/4 inch thick) pellet. Limitations of the hot press did not allow the use of sufficiently high pressure so that the density of the final material was quite low. The material was single phase ZrC. The starting grain size was less than 4 microns. ZrC A-25 and ZrC A-24 was originally pressed into 1/2 inch diameter pellets (3/17 inch thick). Higher pressure and the smaller diameter of the die produced a very good densification. The material was single phase ZrC.

(UC) (ZrC) A-08 was a single phase material of high density (about 90 per cent of theoretical). The same description applies to (UC) (ZrC) A-06.

UC A-13 was found to contain a very minor amount of UC<sub>2</sub>. X-rays showed only UC lines. Some UC<sub>2</sub> specimens did not show presence of UC during x-ray examination. Metallography revealed that all UC<sub>2</sub> specimens contained some UC. UC<sub>2</sub> A-01 contained the least amount of UC.

EuB<sub>6</sub> specimens were all single phase samples.

YB<sub>6</sub> A-19 was found to have a very minor amount of YB<sub>4</sub>. As YB<sub>6</sub> was expected to sublime and form YB<sub>4</sub> as a result of boron loss this sample was considered to be satisfactory for this study as the formation of YB<sub>4</sub> is an unavoidable fact.

The method of testing consisted of placing the three or four specimens cut from the pellet into the furnaces. After a set period of time a sample was withdrawn and the test continued until the next specimen was to be withdrawn. The specimens were then examined by metallographic techniques at room temperature. No direct observations at temperature were made. In testing only one particular material was loaded into the furnace to prevent cross contamination of materials. No difficulties were encountered in maintaining the vacuum in the furnace system, although the UC-bearing samples did show de-gassing initially. Temperatures were achieved quite rapidly on heat-up of the furnaces because of the low heat capacity of furnace system. Furnace A (tantalum resistance element) could be heated to 1900 C in less than 10 minutes and the cool down cycle to room temperature was of the order of one hour. Furnace B (induction heated) could be brought to 2500 C in less than a minute although practically two to three minutes elapsed in this process, the cool-down to room temperature was less than 45 minutes. It is assumed that heating and cooling periods were reasonably short and the tests are therefore considered to be isothermal.

#### E. Experimental Observations

1. ZrC - The following tests were made on the various samples of this material.

<u>Sample</u>	<u>Temperature (°C)</u>	<u>Times of Isothermal Exposure in Hours</u>
ZrC A-06	2000	1
ZrC A-06	2000	2
ZrC A-06	2000	4
ZrC A-06	2000	12
ZrC A-06	2200	1
ZrC A-06	2200	4
ZrC A-06	2200	9
ZrC A-06	2400	1
ZrC A-25	2400	1
ZrC A-25	2400	2
ZrC A-25	2400	3
ZrC A-25	2500	1
ZrC A-25	2500	2
ZrC A-25	2500	3

As mentioned previously, ZrC A-06 was a relatively low density material. The starting material showed a grain size smaller than 4 microns. The starting material microstructure can be seen in Figure 3. The etching reagent used was: 25 H<sub>2</sub>O, 25 HNO<sub>3</sub>, 25 acetic, 2-3 HF. A light repolish was necessary to remove the gold colored stain after etching for seven seconds. The results of exposures at 2000 C showed that negligible grain growth occurred even after 12 hours test. Grain growth was highly inhomogeneous. Figure 4 shows the sample after 1 hour exposure. Areas of incipient grain growth are seen throughout the specimen. These areas are quite small and are frequently associated with large pores as can be seen in Figure 4. There were also some areas where clumps of larger grains were observed which leads one to suspect that at least some of the apparent pores rimmed with large grains were pull-outs made in polishing. The maximum grain size seen was 9.5 microns while the bulk of the specimen remained essentially unchanged (~4 micron grain size).

Figure 5 shows the same material after 2 hours at 2000 C. Again the large grains rimming a pore can be noted; the average grain size remained in 4-5 micron range. Largest grain seen was 15.4 microns and was not associated with a pore. Figure 6 shows the sample after 4 hours of exposure. No drastic changes had occurred. Figure 7 shows the sample after 12 hours at 2000 C. Even for this duration the average grain size remained in the range of 4-5 microns. No appreciable coarsening of the voids could be noted when the starting material was compared to the 12 hour specimen.

Figure 8 shows (UC) (ZrC) A-06 after 1 hour at 2200 C. The grain size is less than 5 microns. The largest grain observed was about 9 microns. Figure 9 shows the microstructure after 4 hours at 2200 C. Most of the grains are less than 5 microns but some around 9 microns are visible. More important, there is some densification of the ZrC areas and the voids are larger. Figure 10 shows the specimen after 9 hours at 2200 C. This was the first indication of clear-cut grain growth; most of the grains ranged between 5-10 microns while large ones of about 15 microns were also observed. Comparison with Figure 3, the starting material, clearly shows the larger grains, the densification of ZrC regions and the resulting large voids.

A further test was made for 1 hour at 2400 C on this material, ZrC A-06. The specimen showed large regions of "high" density in a "low" density matrix. Figure 11 shows the "low" density region which has a mean intercept grain diameter of 6.9 microns. Figure 12 shows

a "high" density region which has a mean intercept grain diameter of 8.9 microns. Other high density regions showed mean grain diameter of about 15 microns. Cracks separating "low" density regions from those of "high" density regions were observed. These cracks were intergranular. It appears that at 2400 C the low density materials sinter quite rapidly.

Further tests were made with the high density ZrC samples at more elevated temperatures.

The starting material ZrC A-25, is seen in Figure 13. The mean intercept grain diameter was around 5.4 microns. The results of exposure of this material for 1, 2 and 3 hours can be seen in Figure 14, 15 and 16 respectively. The mean intercept grain diameter was 4.6, 5.1 and 5.8 microns respectively. It appears then, that recrystallization was occurring in the initial stages of the test, probably within the first hour, and this was followed by the growth of recrystallized grains. After three hours at the temperature of 2400 C the smaller pores (voids) agglomerated into larger ones; this effect was not significant between the samples exposed to temperature but a marked difference could be seen between the starting material and the tested specimens especially in the "as polished" state before etching.

Figures 17, 18 and 19 show the microstructures of ZrC A-25 after exposure to 2500 C for 1, 2 and 3 hours respectively. It is observed that grain size (mean intercept value) change from 5.6 to 8.1 to 8.4 in the 1, 2, and 3 hour test respectively. The relatively small change in the first hour again suggests a recrystallization process during the initial period at temperature. Figure 20 is the graphical representation of the experimental results on high density ZrC A-25 specimens at 2400 C and 2500 C. The results at 2500 C again show the disappearance of small pores and the appearance of larger voids. It is interesting to note that the "low" density ZrC A-06 specimen had larger grains after one hour at 2400 C than any of the specimens of ZrC A-25, even those exposed for three hours (see Figure 20).

The testing of all ZrC specimens was accomplished in the induction furnace shown in Figure 2.

2. (Uc) (ZrC) - Two samples of (UC) (ZrC) used in this study were very close in their properties which is a result of almost identical fabrication conditions and experience with this carbide alloy. The starting materials were very difficult to etch and to reveal grain boundaries on film. In fact, even those exposed to 2000 C for 1 hour were difficult to etch. The starting material had a grain size of less than 3 microns and the density was better than 90 per cent.

The following tests were made on (UC) (ZrC).

Sample	Temperature (°C)	Times of Isothermal Exposure in hours
(UC) (ZrC) A-08	2000	1
(UC) (ZrC) A-08	2000	4
(UC) (ZrC) A-08	2000	9
(UC) (ZrC) A-08	2000	16
(UC) (ZrC) A-06	2200	1
(UC) (ZrC) A-06	2200	4
(UC) (ZrC) A-06	2200	9

Figure 21 shows the microstructure of (UC) (ZrC) A-08 after 1 hour at 2000 C. The grain size had more than doubled to 7.3 microns. Figure 22 shows a specimen held for 2 hours at 2000 C. The relative change in grain size is small to 8.6 microns. Figures 23 and 24 show the microstructures for 9 and 16 hour exposures to 2000 C. The respective mean intercept grain diameters were 9 and 10 microns. This heat treatment had a very profound effect on the etching characteristics. Samples exposed to higher temperature were easy to etch, while longer times at the lower temperature were needed to obtain the same result. The etch used was identical to that used for ZrC except that immersion was typically 15-30 seconds.

Studies on (UC) (ZrC) A-06 showed that extremely rapid growth occurred at 2200 C. The generally observed rapid rate of grain growth of (UC) (ZrC) at 2000 and 2200 C may contribute to its fragility. Figure 25, 26 and 27 show the microstructure of (UC) (ZrC) A-06 after exposure at 2200 C for periods of 1, 4 and 9 hours respectively. The mean intercept grain diameter increased to 16.9 microns, 20.4 microns and finally to 30 microns, after exposures of 1, 4 and 9 hours. Very large single grains were observed in all samples; the largest grain seen after 1 hour was 41 microns, after 4 hours 55 microns, and after 9 hour 86 microns (it should not be implied that the same large grain was studied). Although the material studied appeared to be single phase by x-rays and metallography at (250X) it was found that a very fine grain boundary precipitate was present, as observed at 1000X, after 4 hours at 2200 C (see Figure 28). The presence of the precipitate suggests that inhibiting effects could be observed in grain growth particularly at the lower temperature. Figure 29 shows grain size as a function of time for the two temperatures. It is clear that the growth characteristics



are different at the two temperatures studied. The tests at 2000 C show a sharp decrease in growth after the first hour at temperature. This may be accounted by the accumulation of the precipitate and other impurities in the grain boundaries. At 2200 C the grain size to temperature relationship appears to be close to the parabolic which is theoretically predicted for normal grain growth. Figure 30 tests the parabolic behavior for 2000 C. It is again clear that this relationship does not hold; the dashed line is a hypothetical line for the material in the absence of inhibitions in the grain boundaries. (The functional relationship of this hypothetical line is  $D^2 - D_0^2 = 65 t$  where D is in microns and t is in hours). Figure 31 shows that behavior at 2200 C did indeed follow the parabolic law

$$D^2 - D_0^2 = 105 t \text{ at } 2200 \text{ C.}$$

Using this equation, under the assumption that the relationship is valid for long time intervals, one may gain a rough appraisal of the grain of this material.

<u>Time (hrs)</u>	<u>Grain Size (microns)</u>
0	3
10	32
100	102
1000	324

The above table shows that the grain size of (UC) (ZrC) could become very large at high temperature. Further substantiation is, of course, necessary. The observation that normal grain growth occurs at 2200 C suggests that grain boundary impurities may be more soluble in the matrix at this temperature. No appreciable change in porosity was noted except the disappearance of small pores and the growth of large ones.

The data available from this study is too meager to evaluate a meaningful activation energy. It is doubtful if the activation energy exceeds two or three kilocalories at the elevated temperatures.

All the tests were accomplished in the induction furnace B (Figure 2).

3. UC - The starting material, as mentioned previously, contained some traces of  $UC_2$ , the mean intercept grain diameter was found to be 29.4 microns. The following tests were accomplished on UC A-13 samples.

Sample	Temperature °C	Times of Isothermal Exposure in Hours
UC A-13	2000	1
UC A-13	2000	2
UC A-13	2000	4
UC A-13	2000	6
UC A-13	2200	1
UC A-13	2200	2
UC A-13	2200	4
UC A-13	2200	6

As a result of the exposure of 1 hour at 2000 C the UC<sub>2</sub> was absent from the samples. It is believed that excess carbon was volatilized in the test and the sample was homogenized. With the disappearance of the UC<sub>2</sub> very minor amounts of metallic phase appeared in the grain boundaries. The presence of the metallic phase may be the result of reducing conditions existing in the study. This could result by vapor phase reactions. It is unlikely to have occurred by solid transport as the UC specimens rested on ZrC which in turn rested on tungsten. It is known that ZrC is a good barrier for solid state carbon diffusion. Furthermore, it was observed that grains grew much faster on the periphery of the sample than in the center of the pellet. This may be partially accounted by the sublimation clean-up of the grain boundaries on the outside surface of the specimen. Figure 32 shows UC on the outer surfaces of the specimen, note the metallic phase inclusions. Figure 33 shows the central portion of the pellet which was all one-phase and showed practically no metallic phase in the grain boundaries. The grain size in the outer surface was 52.6 microns while in the central regions it was 14.2 microns. Higher porosity was noted in the central region. Figure 34 shows the microstructure after 2 hours at 2000 C. The mean grain diameter is 47.4 microns. Regions with larger grains of 78 microns were again observed. After 4 hours the amount of the second phase increased. Figure 35 shows the typical appearance. Figure 36 shows the material after 6 hours. The six-hour sample did not appear to have as much of the metallic phase as the previous ones. A greater amount of large pores were noted but fine porosity persisted. In effect, two grain growths were noted; a) that of peripheral grains and b) that of the internal grains, see Figure 37. Both of these grain sizes were plotted parabolically, i.e.  $D^2$  vs time. It is apparent that probably some recrystallization occurred in the interior of the specimen while little or none of this occurred in the

surface layer grains. It is possible that the internal stresses and deformed regions in the interior of the hot-pressed pellet were quite different (and higher) than on the surface. This may have promoted a recrystallization in the interior prior to normal grain growth. Both of the grain growth plots show very similar slopes. It is possible that the differences of impurities in the grain boundaries may be a contributing factor. The following approximate expressions can be obtained from Figure 37.

$$D^2 - 900 = 1730 t \text{ for surface layer grains.}$$

$$D^2 - 200 = 1430 t \text{ } t \text{ measured in hours after 1st hour for interior grains.}$$

Thus, in a hundred hours the mean grain size of about 375 microns can be obtained even in the interior of the sample. In 1000 hours the grain size may be as 1260 microns provided the above relationship holds true for longer periods of time. The data in Figure 37 is primarily exploratory and is not a basis for design considerations, especially with respect to surface layer grains where considerable ambiguity exists in the determination of representative grain size.

The experiments at 2200 C showed a very large increase in grain growth. During the initial periods large amounts of metallic grain boundary material were noted under metallographic conditions at room temperature. Figure 38 shows a typical microstructure. "Blow-hole" porosity was noted in the specimen particularly in the edges. The sample for 2 hours exposure was lost in metallography. Figure 39 shows the typical appearance of grain after 4 hours at 2200 C. The specimen after 6 hours exposure showed a similar structure with some unidentified phase in the grain boundaries and very large grains. The increased porosity made the determination of grain size difficult and ambiguous especially for higher times of exposure. Figure 40 represents a very rough idea about the grain growth in UC at 2200 C. Further experiments are needed to establish grain growth characteristics in a definitive manner. The apparent growth can be expressed as

$$D^2 = 15000 t$$

In ten hours one could expect grains of 3900 microns.

The presence of grain boundary phases in all of the specimens indicates that the apparent parabolic growth law is obeyed fortuitously. The equations and plots are to be considered as empirical data. The present data is too meager for the determination of activation energy.

The induction furnace B was used in the UC studies.

4.  $UC_2$  - The following tests were accomplished on  $UC_2$ .

Sample	Temperature °C	Times of Isothermal Exposure (Hours)
UC A-01	1800	0.5
UC A-01	1800	1.0
UC A-01	1800	4.0
UC A-01	1800	6.0
UC A-04	2000	0.25
UC A-04	2000	0.50
UC A-04	2000	1.0
UC A-04	2000	2.0
UC A-02	2000	1.0
UC A-02	2000	4.0
UC A-02	2000	9.0
UC A-02	2000	16.0

$UC_2$  A-01 material had a fairly large initial grain size of about 20.1 microns.  $UC_2$  A-04 had a similar grain size of about 20 microns.  $UC_2$  A-02 had much smaller grain size of about 6.7 microns (see Figure 41). The results are, of course, complicated by the fact that  $UC_2$  undergoes a high temperature phase change around 1800 C from cubic to the tetragonal and is known to decompose at lower temperatures to  $U_2C_3$  and C. The final structures contain a very large amount of twins. The shapes of the grains are highly irregular making grain size determination very difficult. At the same time the delineation of the grain boundaries is very obscure at all times. A finely dispersed phase, probably C, is seen in all the specimens indicating that some decomposition was occurring to  $U_2C_3 + C$ . Figures 42, 43 and 44 show the results after 1/2, 1 and 6 hours. Most of the growth is completed in the first hour and insignificant changes are seen between 1 and 6 hours. The same general features are observed for samples of  $UC_2$  A-02 tested at 2000 C. Regions of large grain size were found next to those of much smaller size after 1 hour of exposure (Figure 46). The result of this was that runs for longer periods reflected these initial distributions and the over-all trends were obscured. Tests for shorter increments of time at 2000 C gave a better picture as to the progressive changes in  $UC_2$ . Figures 47, 48, 49 and 50 show the results after 1/4, 1/2, and 1 and 2 hours respectively.

The final microstructure of  $UC_2$  indicates that the high temperature transformation occurred for all of the samples tested.

5.  $EuB_6$  - Two sample batches were used for the studies  $EuB_6$  A-11 and  $EuB_6$  A-15 with grain sizes of 10.8 and 12 microns respectively (see Figures 51 and 52). The latter batch was considerably more dense (about 98 per cent) compared to former (89 per cent). The following tests were made:

Sample	Temperature °C	Time of Isothermal Exposure (Hours)
$EuB_6$ A-11	1900	1
$EuB_6$ A-11	1900	4
$EuB_6$ A-11	1900	20
$EuB_6$ A-15	2050	1
$EuB_6$ A-15	2050	4
$EuB_6$ A-15	2050	9
$EuB_6$ A-15	2050	16

All the tests were run in the resistance furnace A.

Tests at 1900 C showed that no appreciable grain growth occurs at this temperature even after 20 hours of exposure. Figure 53 shows the material after maximum exposure. Increase in pore size can be noted. The following mean intercept grain diameters were obtained for the tests at 1900 C.

Time (hours)	Grain Size Microns
0	12.8
1	12.4
4	11.8
20	11.5

Thus, no grain growth occurred within the error of the technique used in grain size determination.

Runs at 2050 C showed appreciable grain growth. Figure 54, 55, 56, and 57 shows the microstructure after 1, 4, 9 and 16 hours at temperature. The grain size did not follow the normal theoretical linear behavior of  $D^2$  vs t (time). It was found that plotting  $D^2$  vs t on log-log plot did produce a straight line. Figure 59 is the plot of the results obtained at 2050 C.

It must be emphasized that sublimation losses of  $\text{EuB}_6$  are quite severe at these temperatures and the grain growth studies were performed considerably above the temperatures that  $\text{EuB}_6$  should experience as a thermionic converter. These temperatures would probably not exceed 1400-1500 C due to the high sublimation losses. The study therefore shows that no appreciable grain growth can be expected for  $\text{EuB}_6$  at 1400-1500 C provided the presence of cesium will not produce any effect on the grain growth mechanisms.

6.  $\text{YB}_6$  - The  $\text{YB}_6$  starting material as mentioned previously had some  $\text{YB}_4$ . The starting grain size was around 11 microns. Since  $\text{YB}_6$ , like  $\text{EuB}_6$ , does not show unambiguous grain growth at 1900 C, higher temperatures were used in this study.

Sample	Temperature °C	Time of Isothermal Exposure (hours)
$\text{YB}_6$ A-19	2000	1
	2000	2
	2000	4
	2000	6

All the tests were done in the tantalum resistance furnace. Figures 60, 61, 62 and 63 show the microstructures after 1, 2, 4 and 6 hours at temperature. It is interesting to note that all of  $\text{YB}_4$  has left leaving only  $\text{YB}_6$ . There is also evidence of very large increases of porosity with time. After six hours cracks developed in the grains (see Figure 63). Figure 64 shows a 750X micrograph illustrating the cracks in  $\text{YB}_6$ . Very little grain growth occurred in the test period. 12.9, 10, 14.4 and 14.4 microns grain size was noted after 1, 2, 4 and 6 hours. The above results are applicable to the interior, or bulk  $\text{YB}_6$ . Observations were also made on the edge developments on  $\text{YB}_6$ . Figure 65 shows the development of the  $\text{YB}_4$  layer on the exposed surface and the  $\text{YB}_4$  phase around the grain near the exposed edge.

The  $\text{YB}_4$  layer continued to grow and the presence of  $\text{YB}_4$  around grains extended deeper into the material with longer periods of exposure. Figure 66 shows this effect for a sample exposed for 4 hours at 2000 C. These effects are very significant as these represent surface phenomena which are all-important in thermionic emitters.

As in the case of  $\text{EuB}_6$  the studies on  $\text{YB}_6$  indicate that little grain growth can be expected in vacuo at 1400-1500 C. This temperature range is the practical one for  $\text{YB}_6$  due to large

sublimation losses at high temperature. The results at higher temperatures show accelerated effects, i.e.  $YB_4$  surface layers will develop at both low and high temperature but they do so rapidly at elevated temperatures.

Specific comparison of the data presented with that of other investigators is reserved for the future publication of these results.

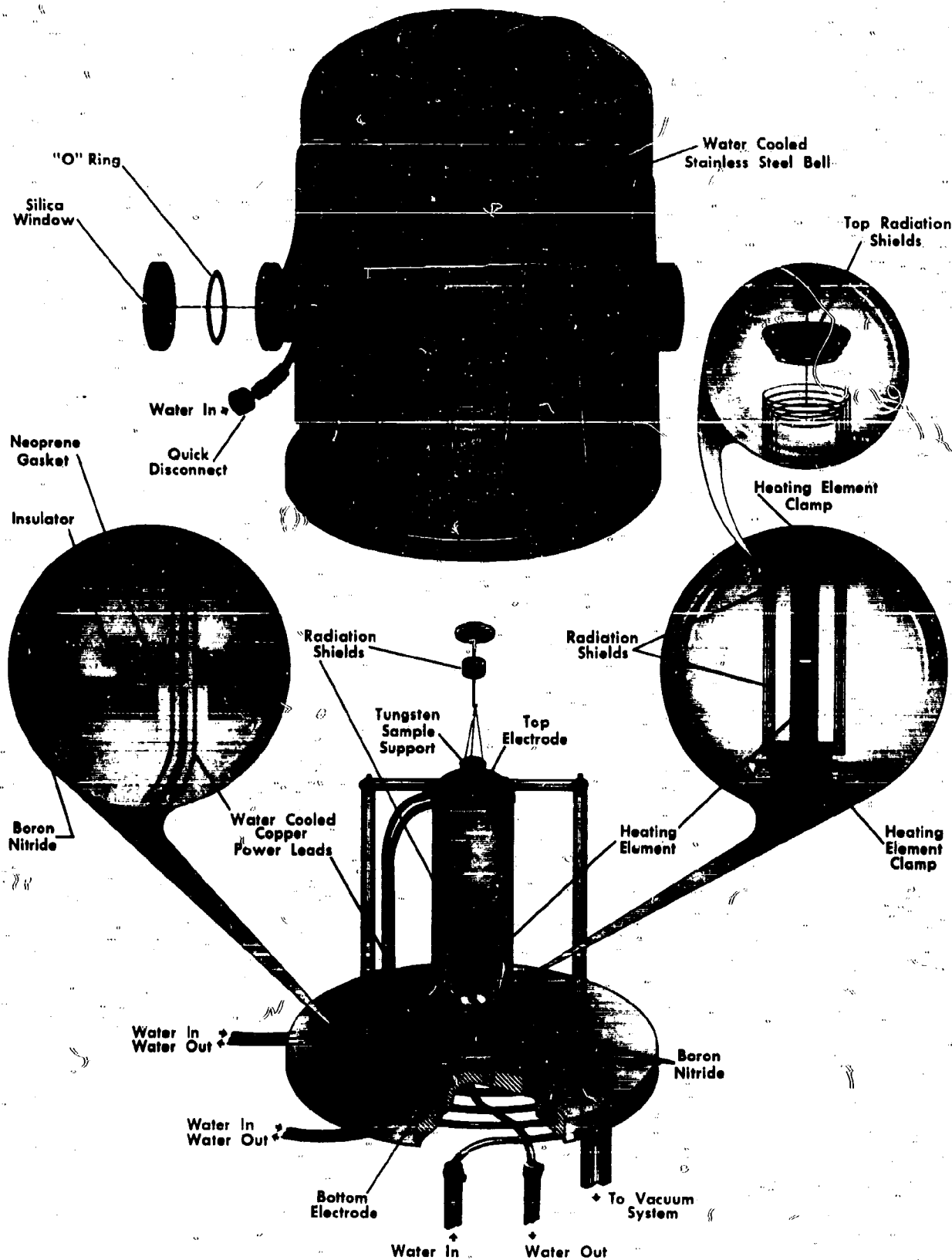


Figure 1. VACUUM RESISTANCE TUBE FURNACE



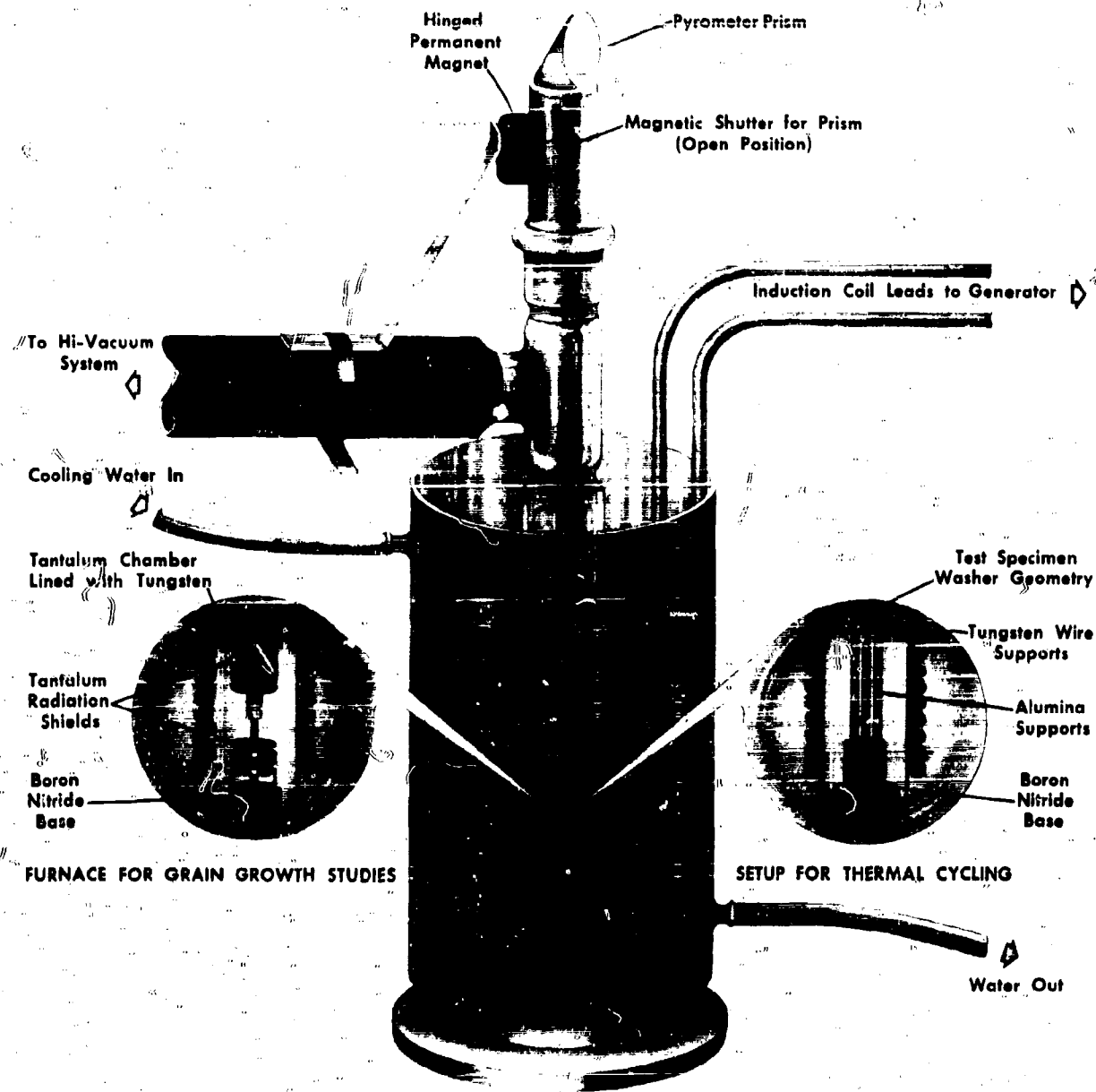
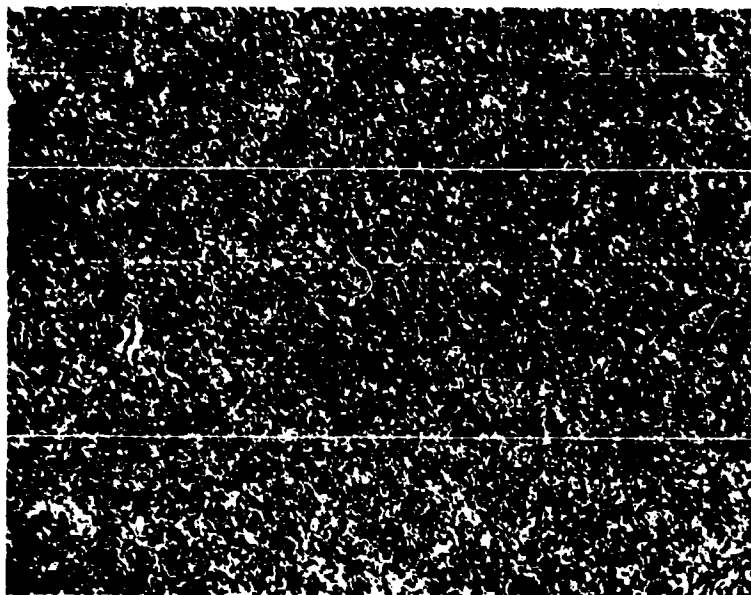
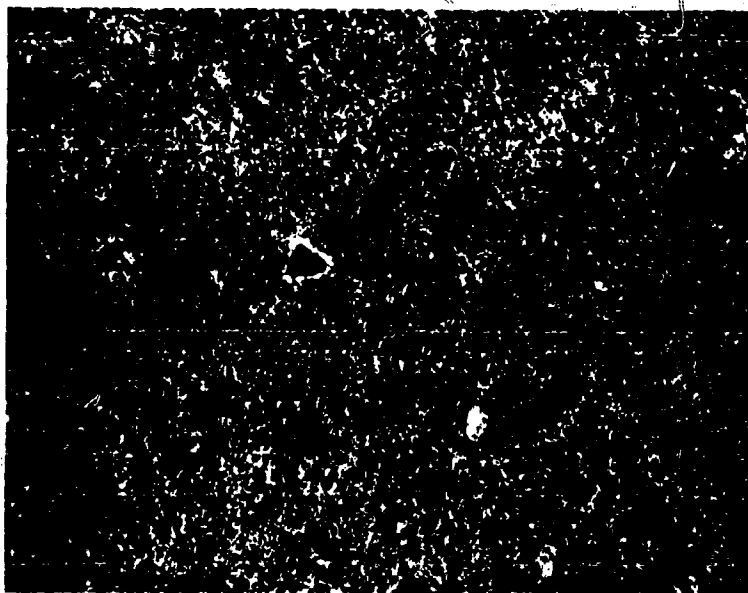


Figure 2. INDUCTION FURNACE FOR GRAIN GROWTH & THERMAL CYCLING



**Figure 3. ZrC A-06 (250X) ETCHED  
(250X) STARTING MATERIAL (4904)**



**Figure 4. ZrC A-06 (250X) ETCHED  
(250X) 1 HOUR AT 2000°C (4719)**

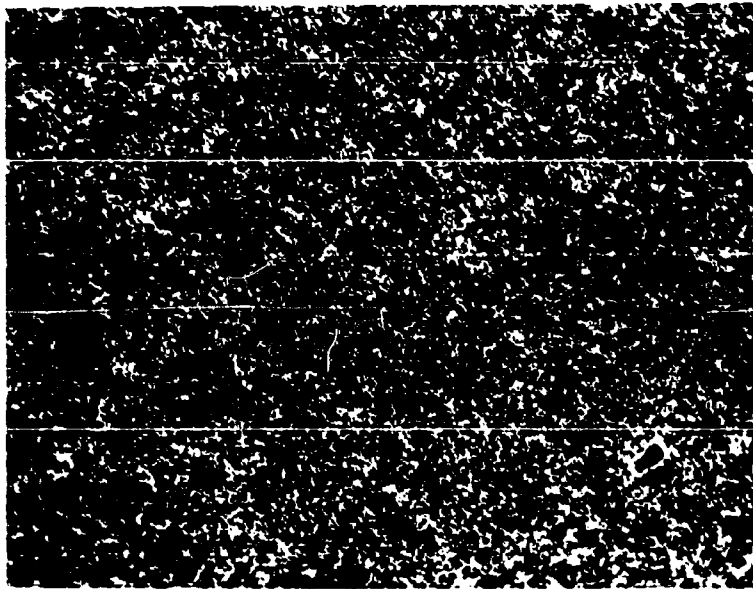


**Figure 5. ZrC A-06 2 HOURS AT 2000°C (4724) (250X)**

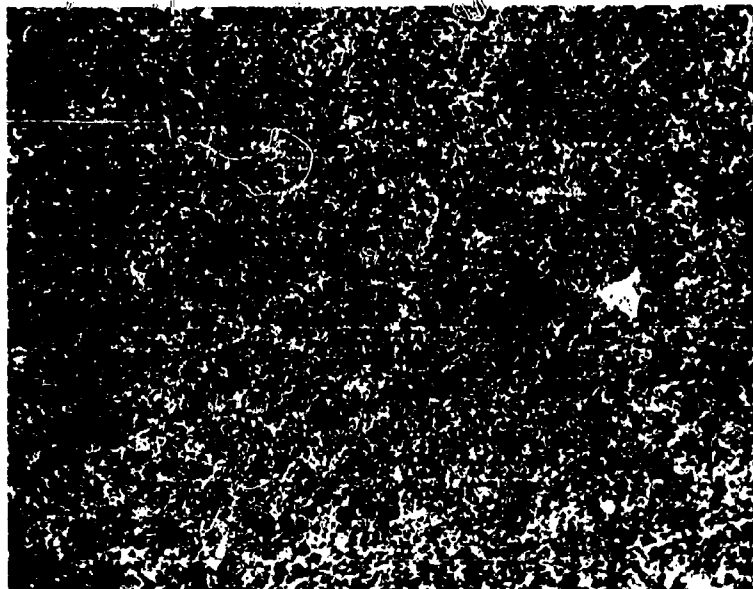


**Figure 6 ZrC A-06 4 HOURS AT 2000°C (4741) (250X)**

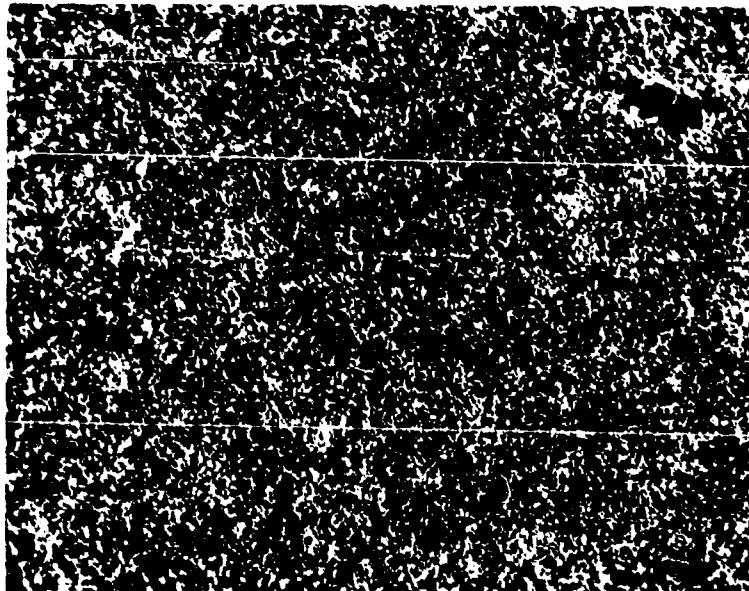


**Figure 7. ZrC A-06 12 HOURS AT 2000°C (4743) (250X)**

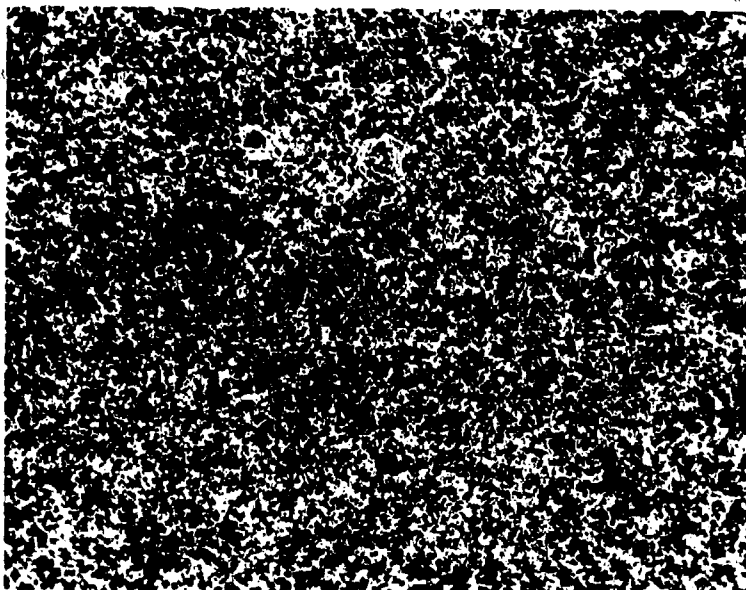


**Figure 8. Zr A-06 1 HOUR AT 2200°C (4793) (250X)**

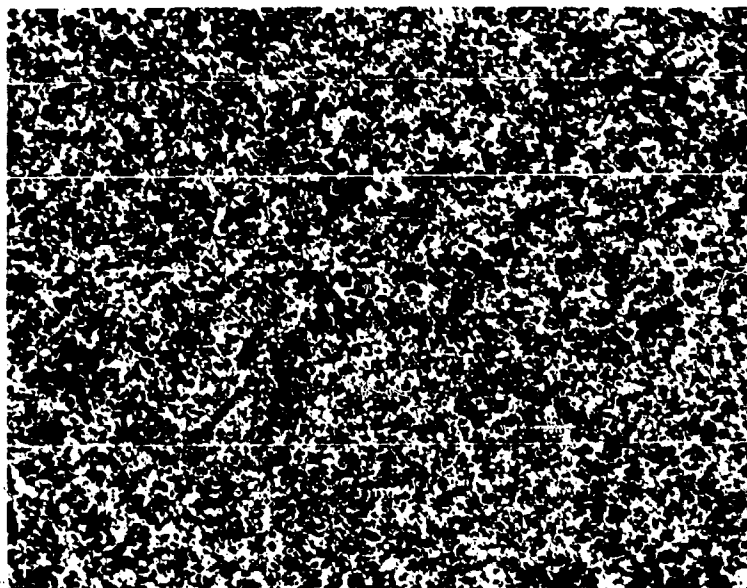


**Figure 9. ZrC A-06 4 HOURS AT 2200°C (4810) (250X)**

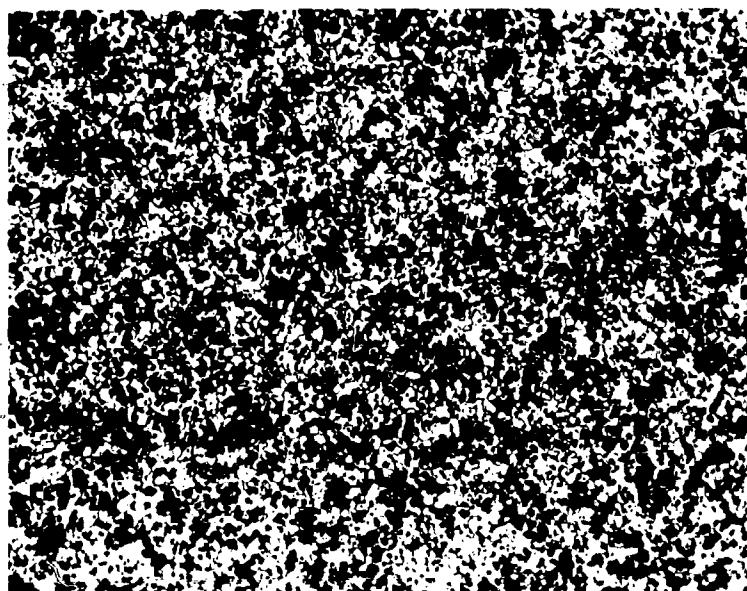


**Figure 10. ZrC A-06 9 HOURS AT 2200°C (4811) (250X)**

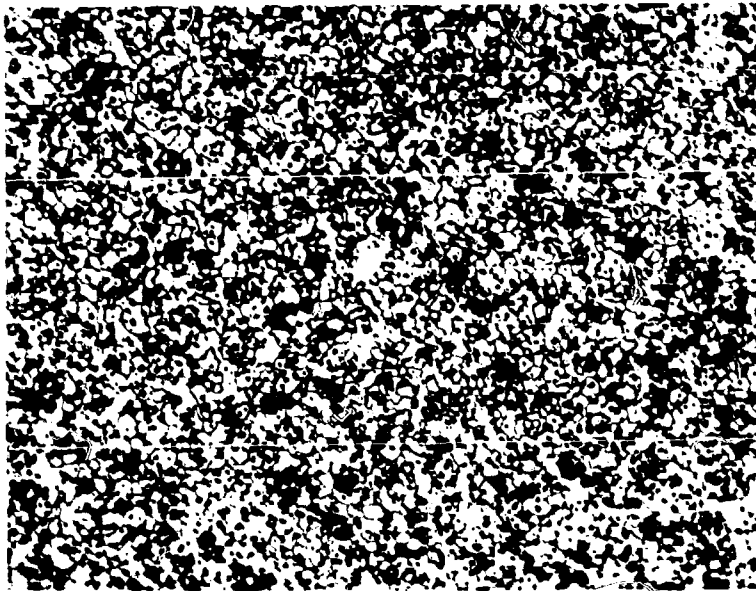


Figure 11. ZrC A-06 1 HOUR AT 2400°C (4912) (250X)

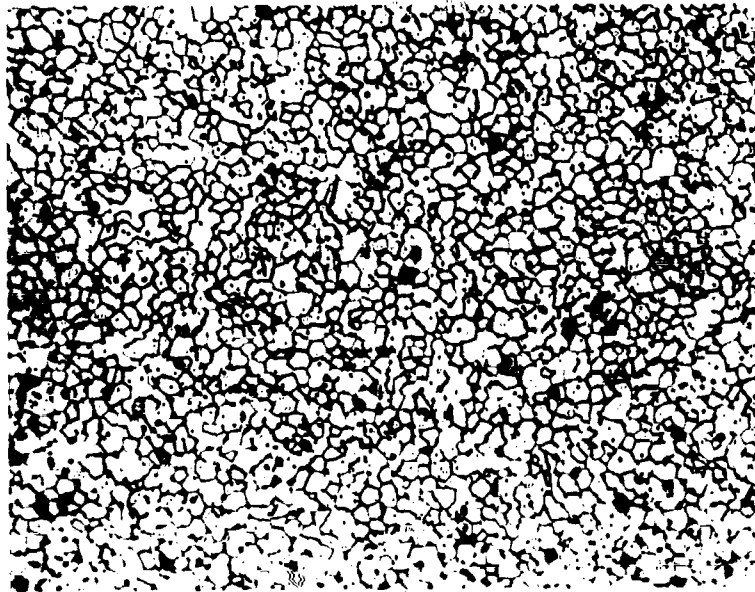
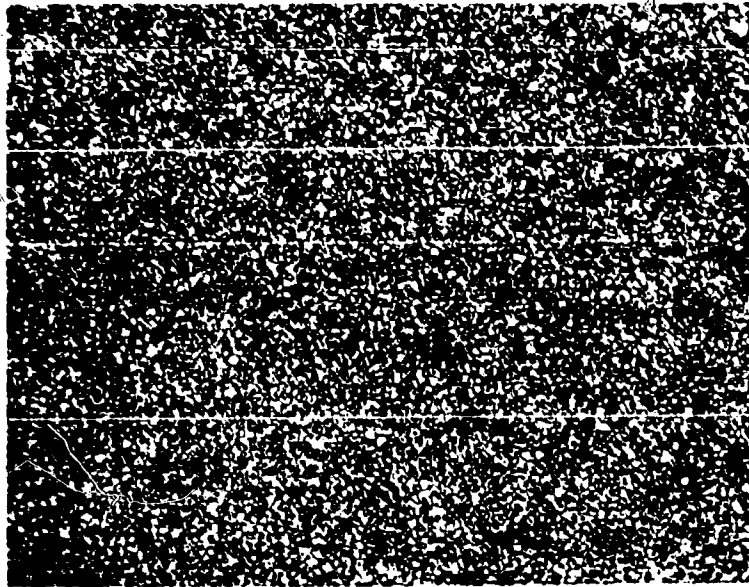
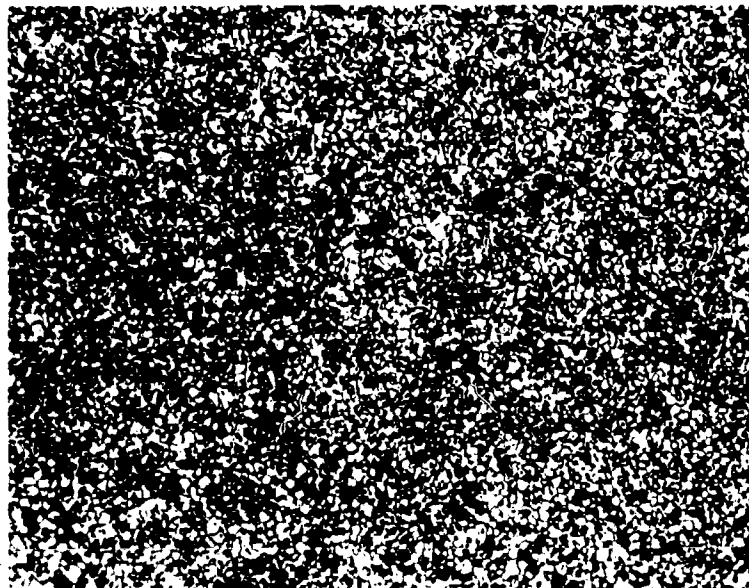


Figure 12. ZrC A-06 1 HOUR AT 2400°C (4911) (250X)



**Figure 13. ZrC A-25 STARTING MATERIAL (5074) (250X)**



**Figure 14. ZrC A-25 1 HOUR AT 2400°C (5196) (250X)**

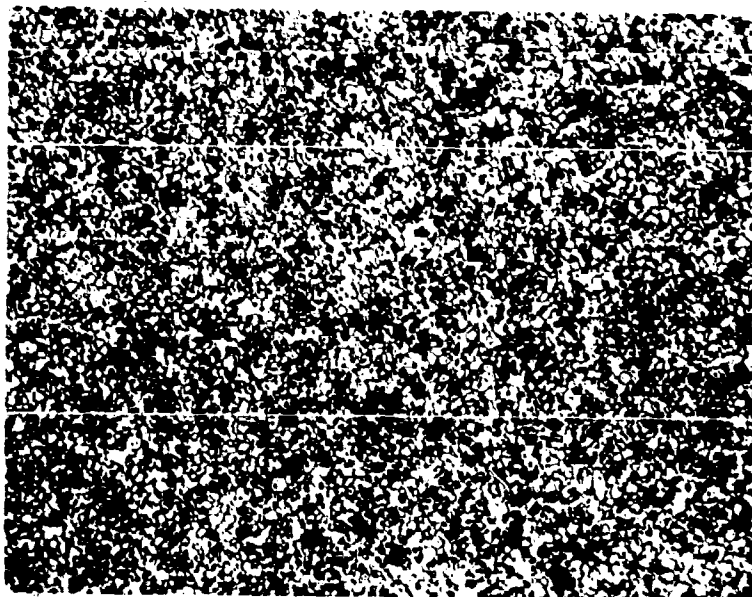


Figure 15. ZrC A-25 2 HOURS AT 2400°C (5194) (250X)

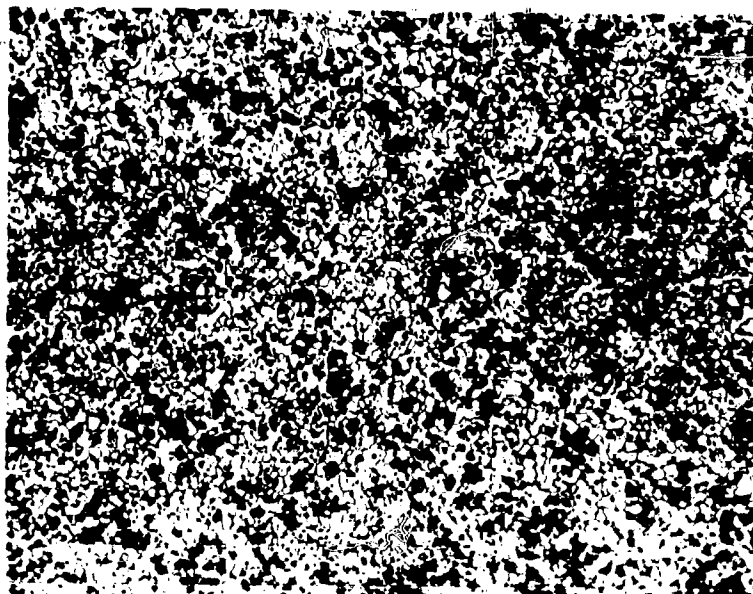
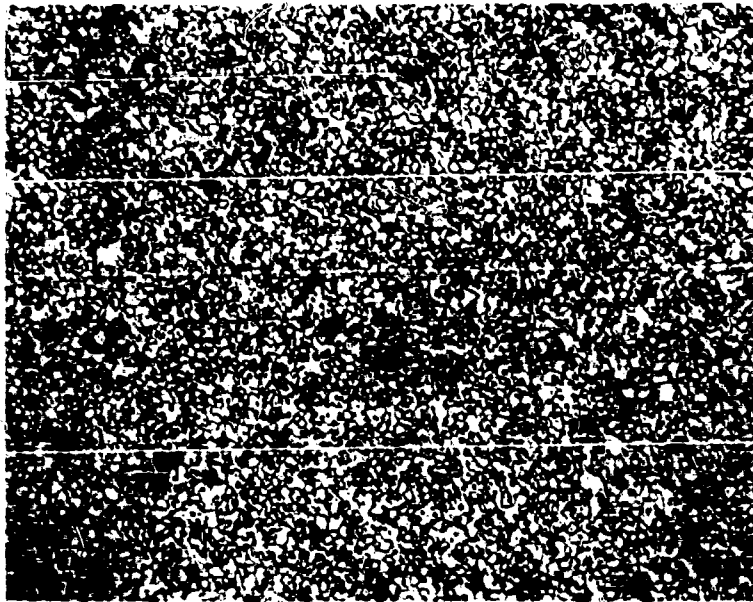
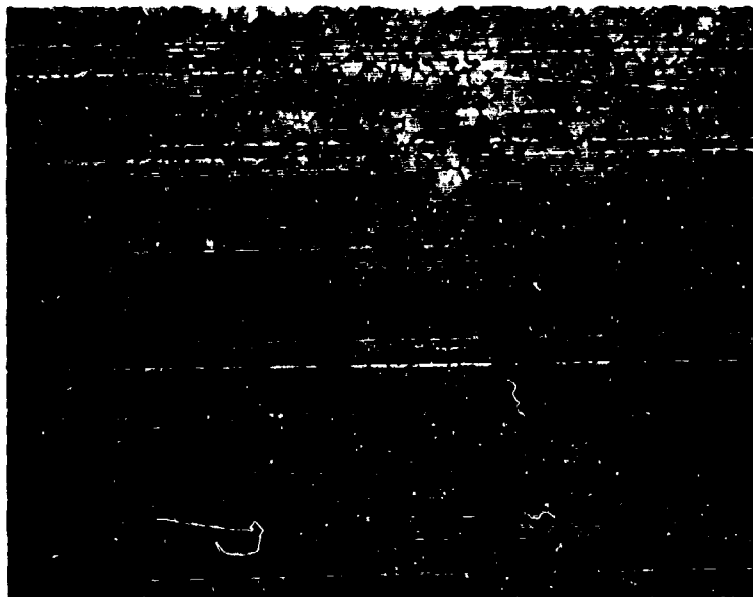


Figure 16. ZrC A-25 3 HOURS AT 2400°C (5198) (250X)





**Figure 17. ZrC A-25 1 HOUR AT 2500°C (5205) (250X)**



**Figure 18. ZrC A-25 2 HOURS AT 2500°C (5202) (250X)**

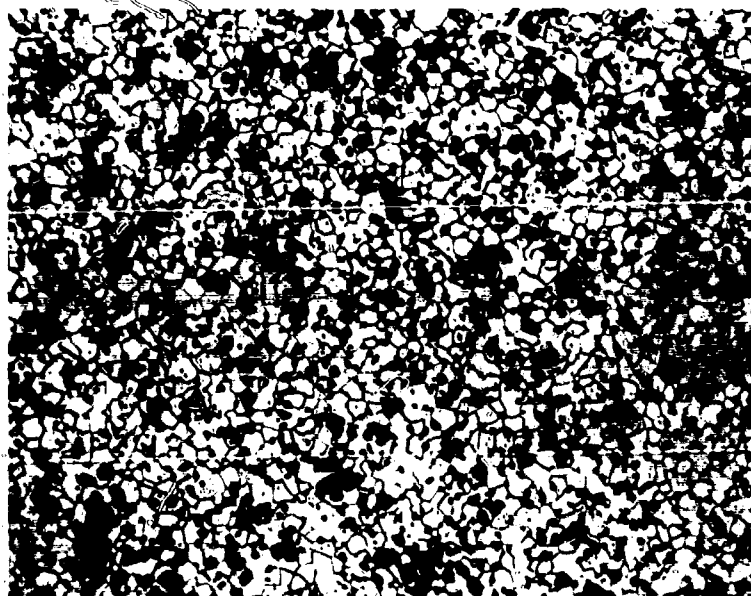


**Figure 19. ZrC A-25 3 HOURS AT 2500°C (5207) (250X)**

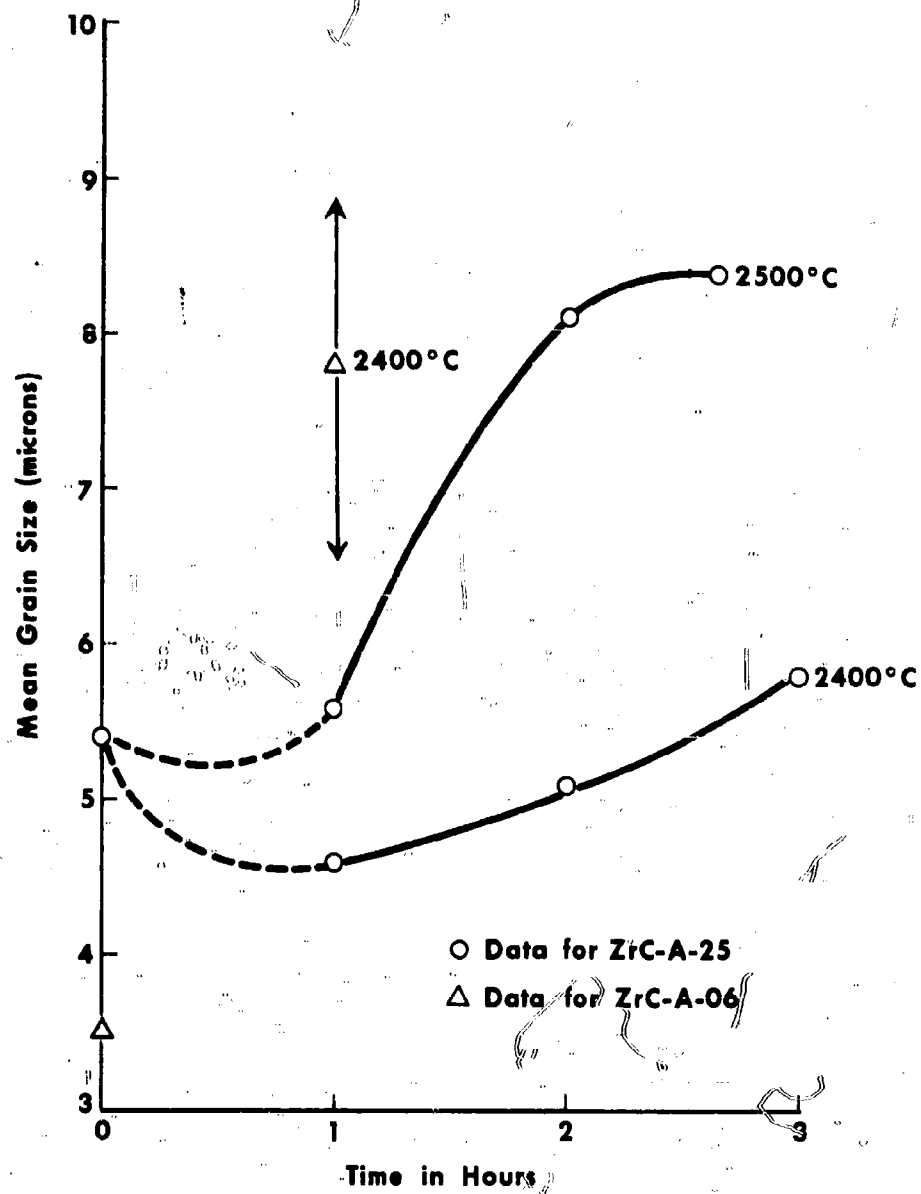


Figure 20. GRAIN SIZE IN ZrC-A-25

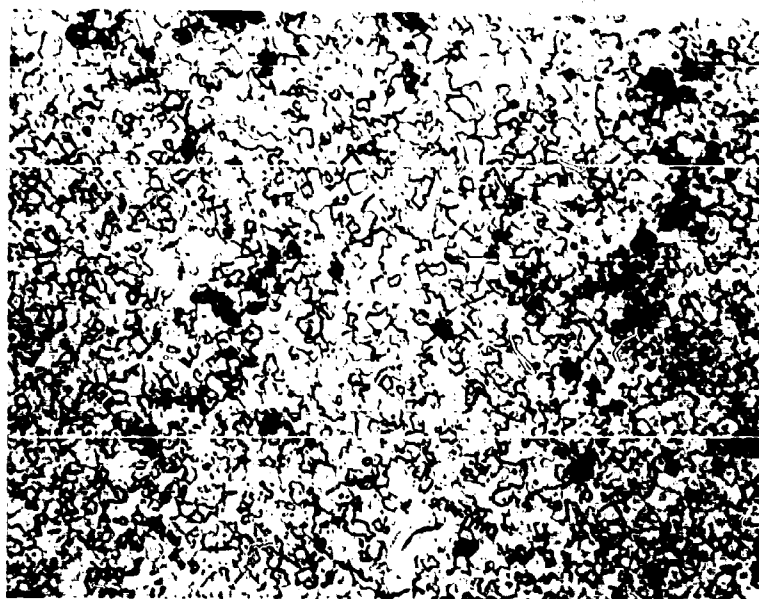


Figure 21. (UC) (ZrC) A-08 1 HOUR AT 2000°C (4914) (250X)

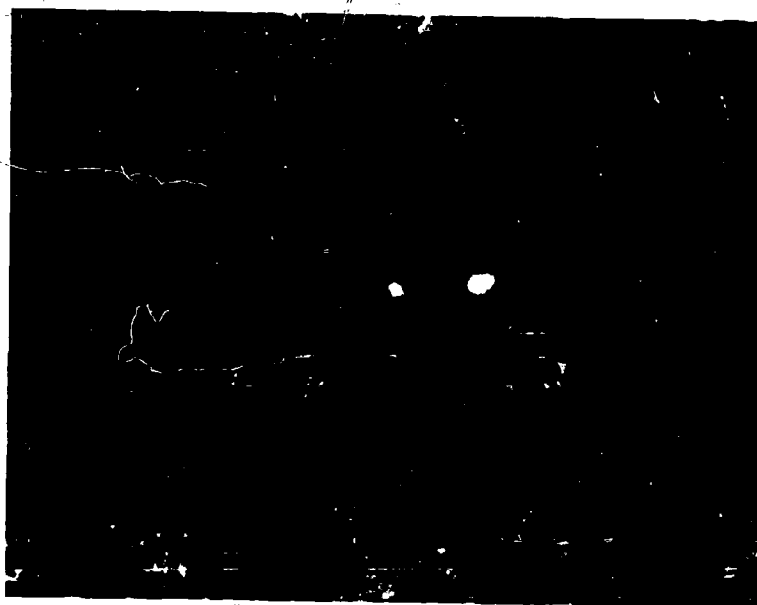


Figure 22. (UC) (ZrC) A-08 4 HOURS AT 2000°C (4917) (250X)

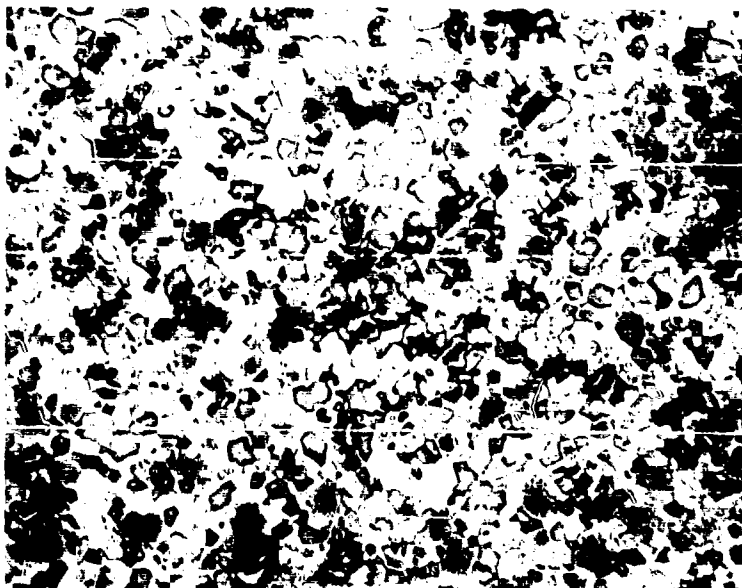


Figure 23. (UC) (ZrC) A-08 9 HOURS AT 2000°C (4920) (250X)

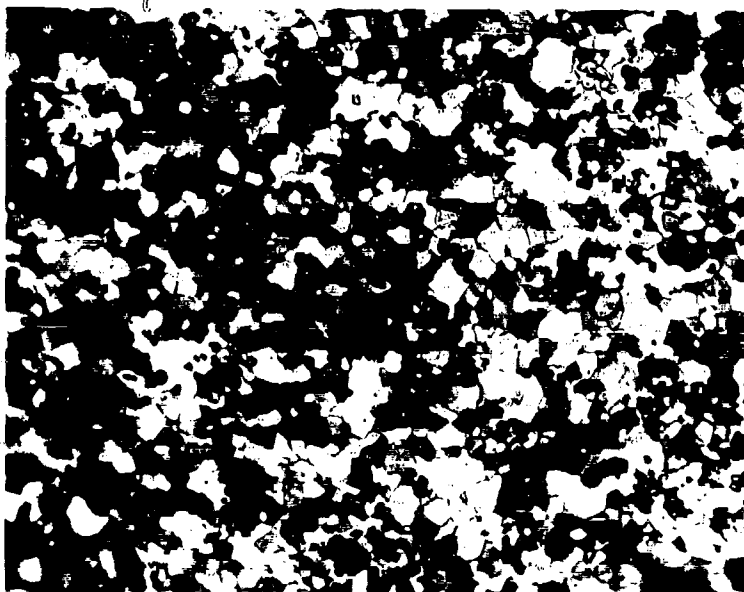


Figure 24. (UC) (ZrC) A-08 16 HOURS AT 2000°C (4921) (250X)

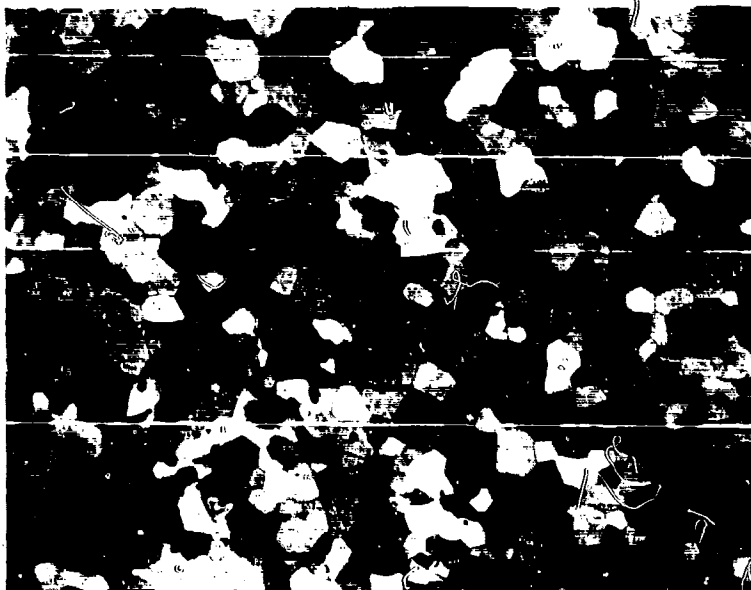


Figure 25. (UC) (ZrC) A-06 1 HOUR AT 2200°C (4828) (250X)

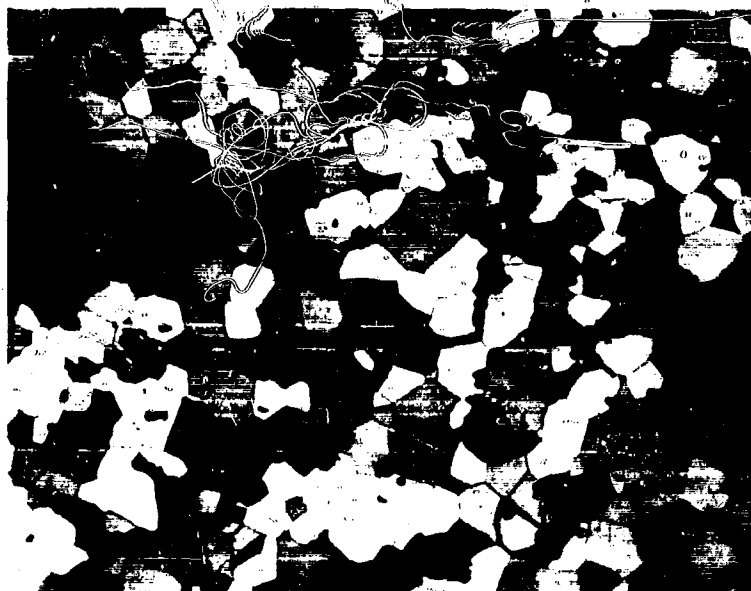


Figure 26. (UC) (ZrC) A-06 4 HOURS AT 2200°C (4835) (250X)

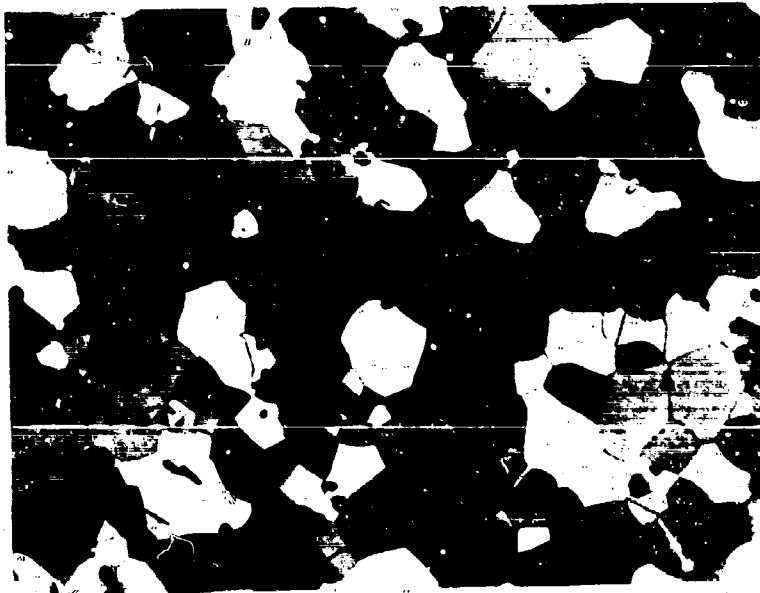


Figure 27. (UC) (ZrC) A-06 9HOURS AT 2200°C (4866) (250X)



Figure 28. (UC) (ZrC) A-06 G.B. PRECIPITATE AFTER  
4 HOURS AT 2200°C (4838) (1000X)

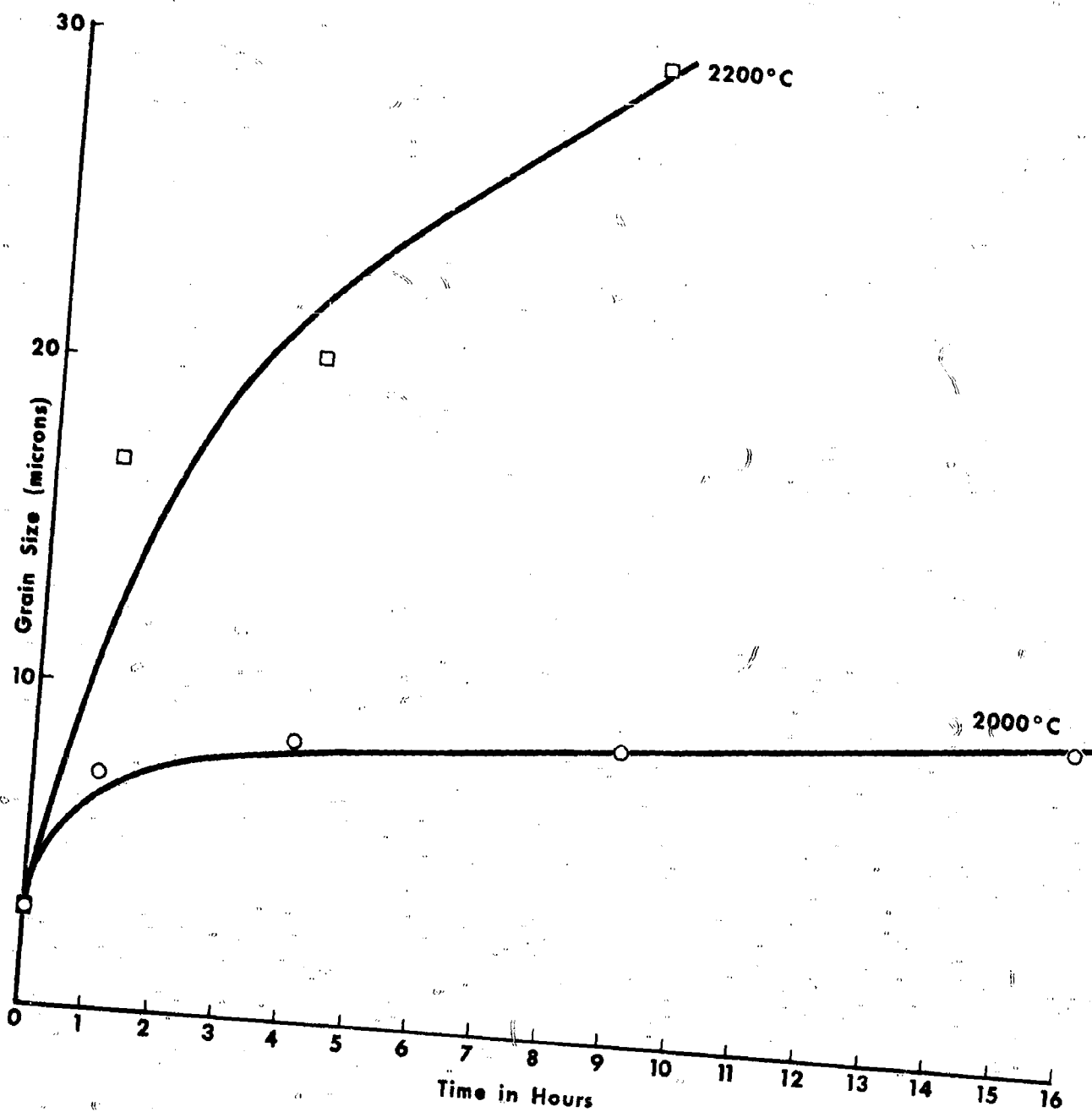


Figure 29. GRAIN SIZE IN (UC)ZrC



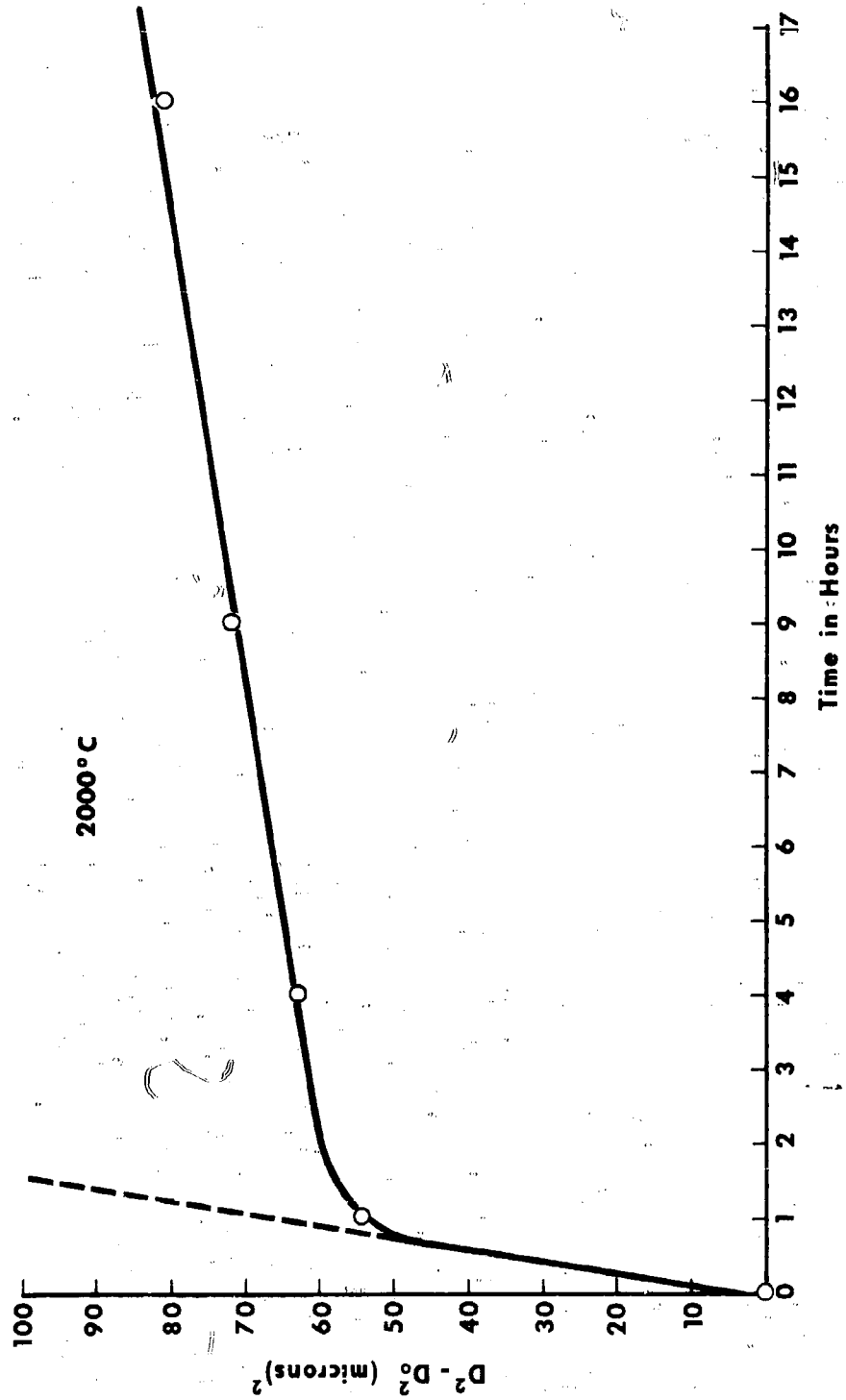


Figure 30. (UC)(ZrC) GRAIN GROWTH

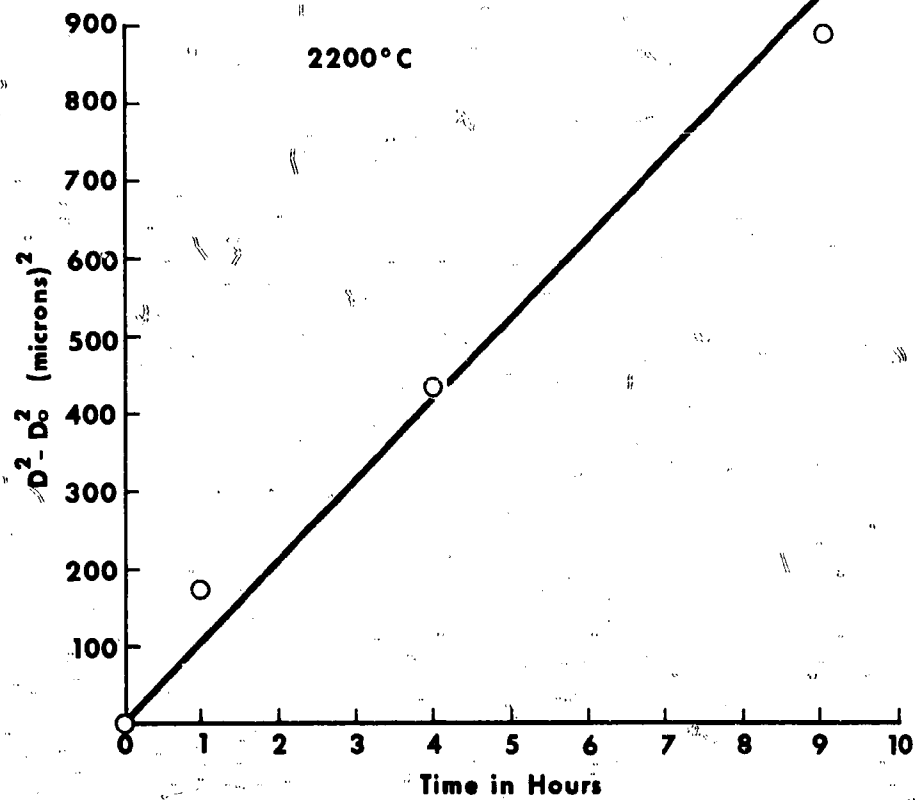


Figure 31. (UC) (ZrC) GRAIN GROWTH

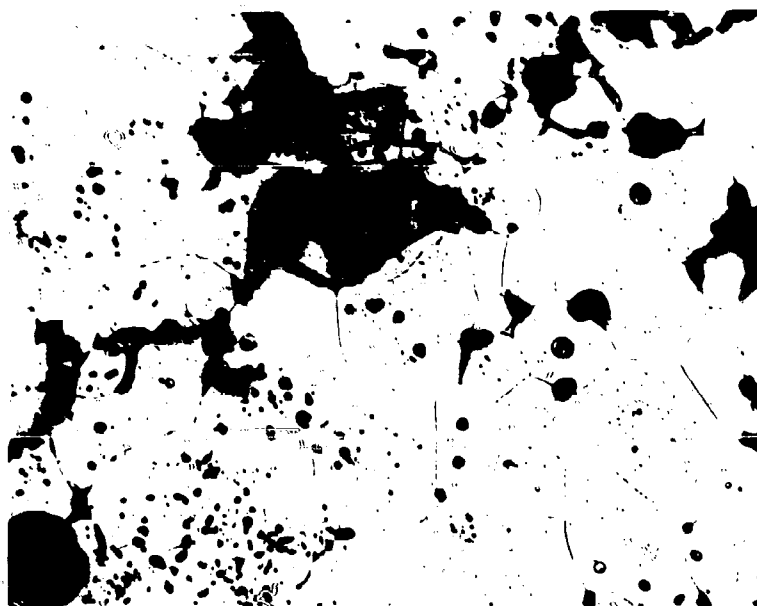


Figure 32. UC A-13 1 HOUR AT 2000°C (5009) (250X)

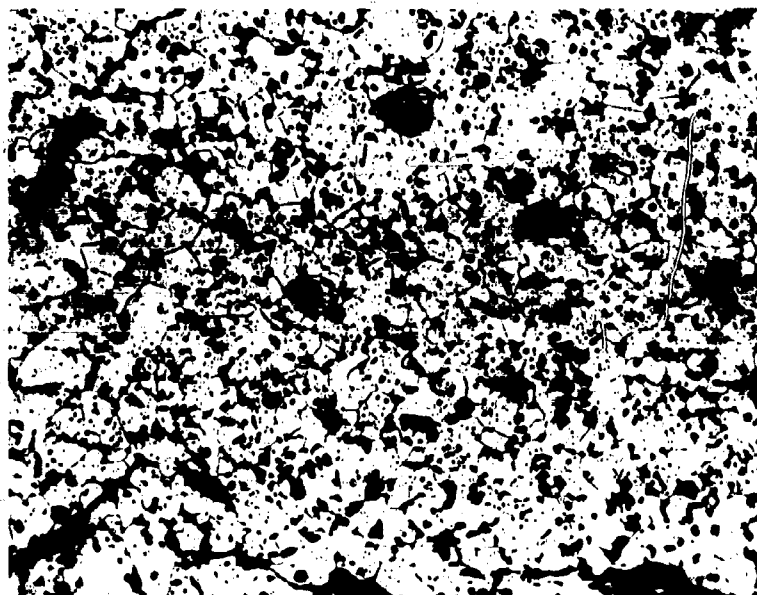
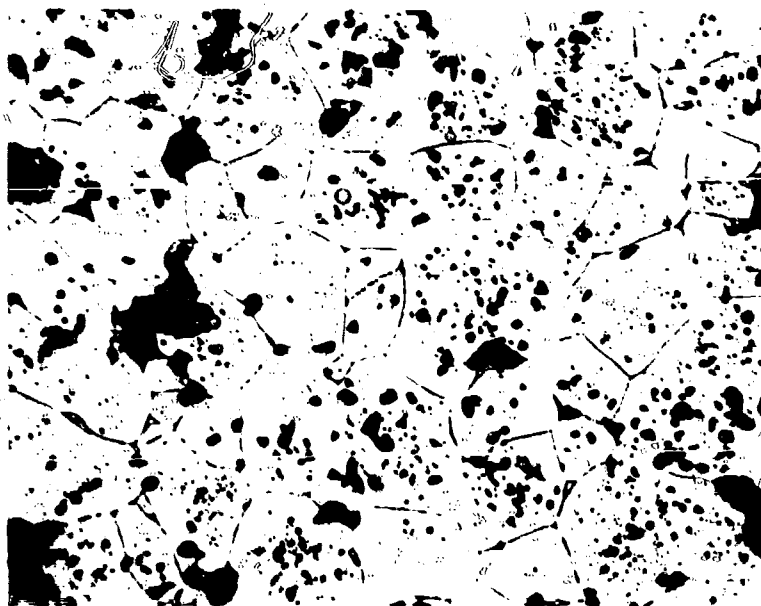
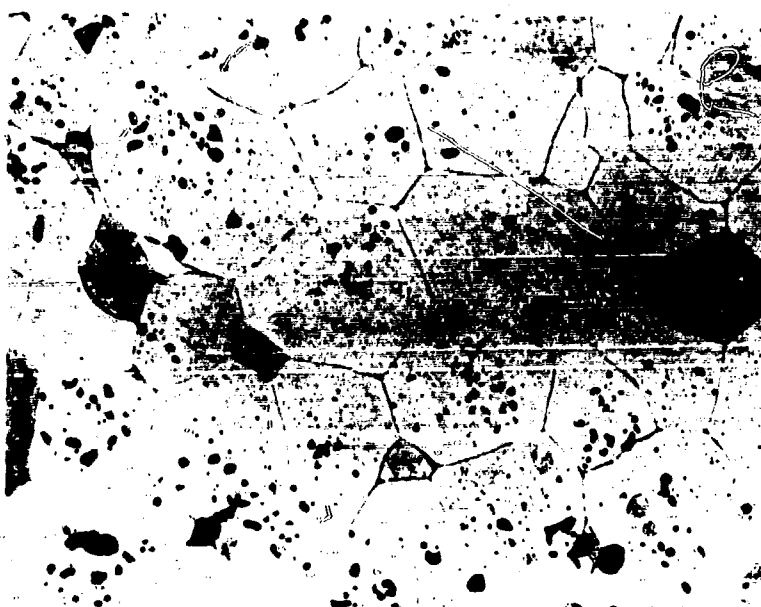


Figure 33. UC A-13 1 HOUR AT 2000°C (5010) (250X)



**Figure 34. UC A-13 2 HOURS AT 2000°C (5026) (250X)**



**Figure 35. UC A-13 4 HOURS AT 2000°C (5020) (250X)**

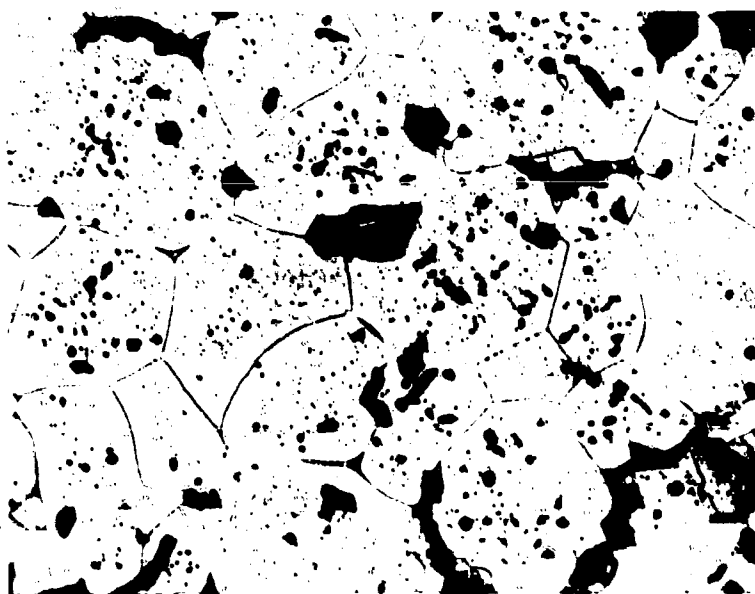


**Figure 36. UC A-13 6 HOURS AT 2000°C (5029) (250X)**

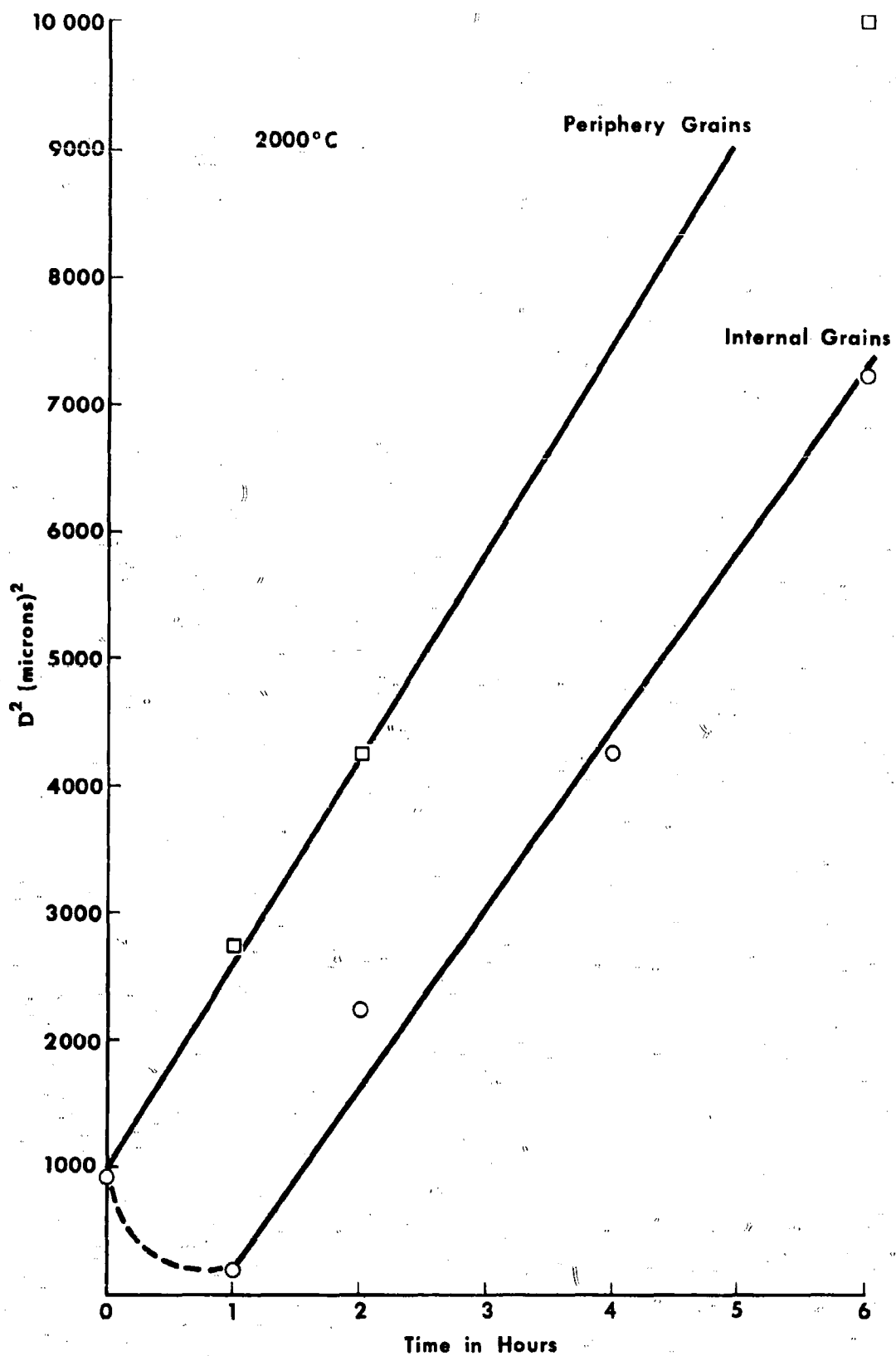
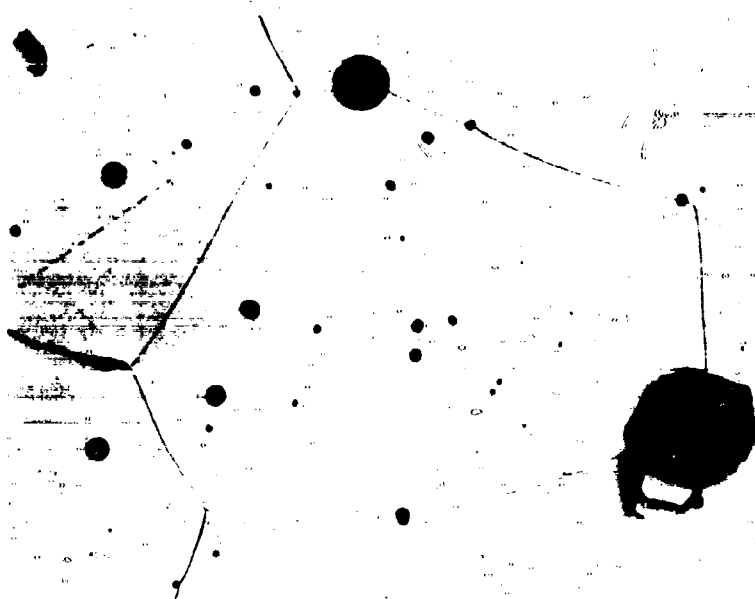


Figure 37. GRAIN SIZE IN UC.



**Figure 38. UC A-13 1 HOUR AT 2200°C (5060) (250X)**



**Figure 39. UC A-13 4 HOURS AT 2200°C (5180) (250X)**

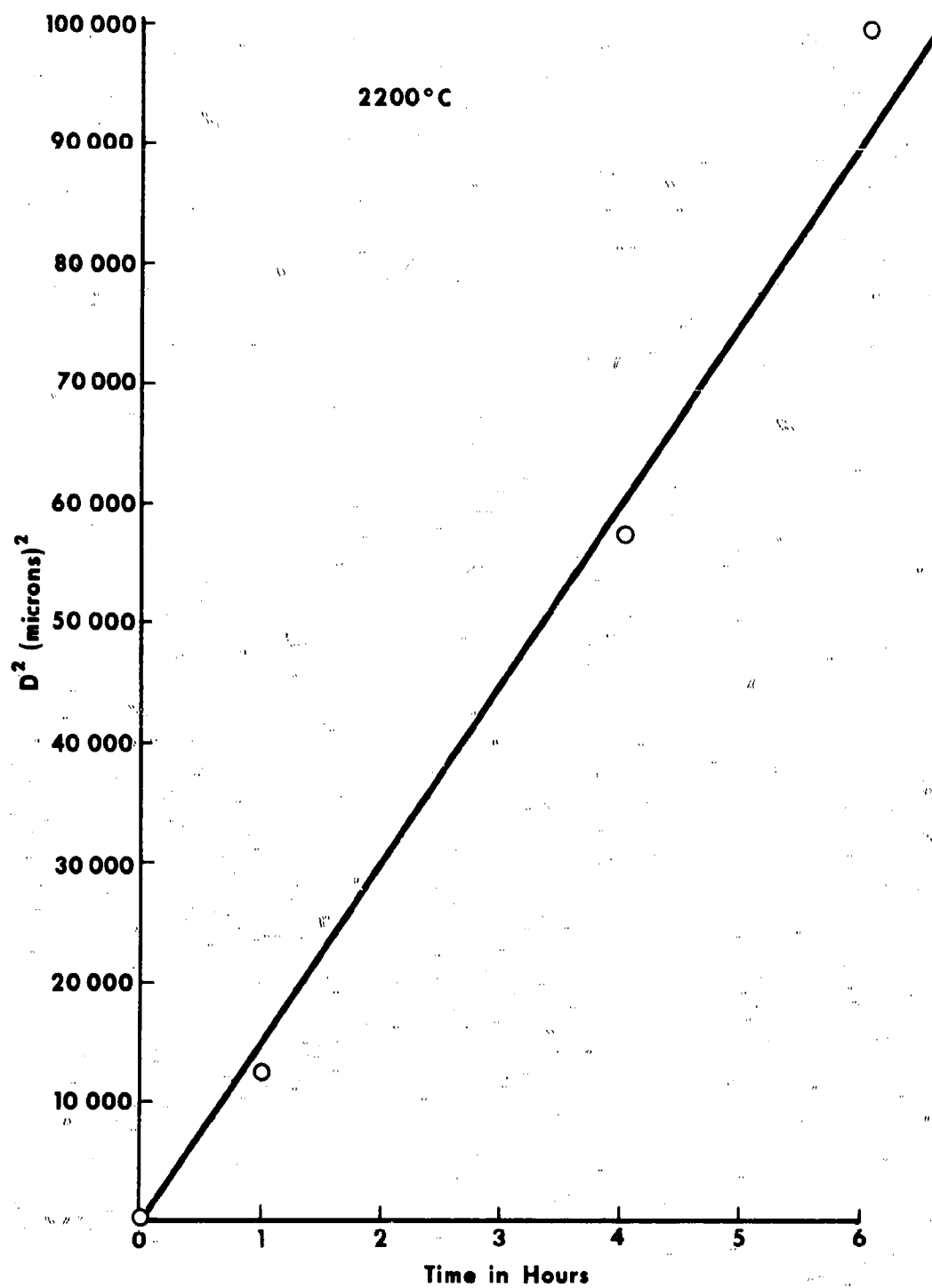
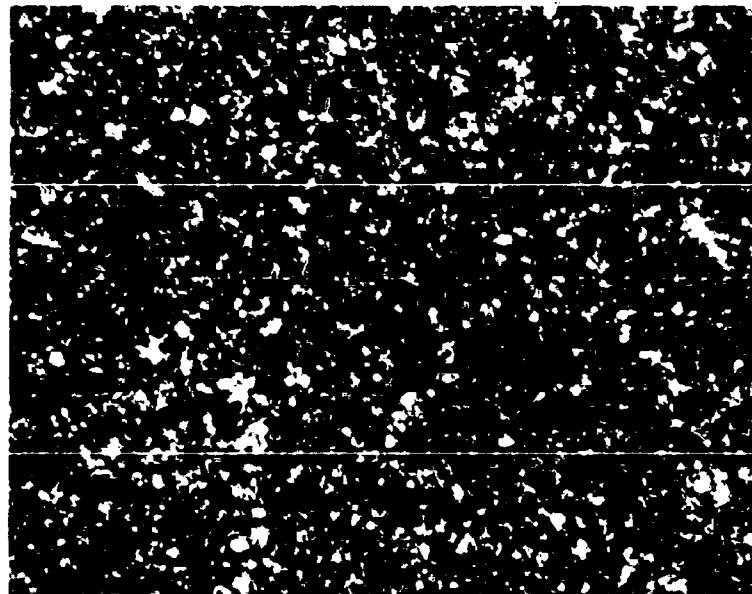
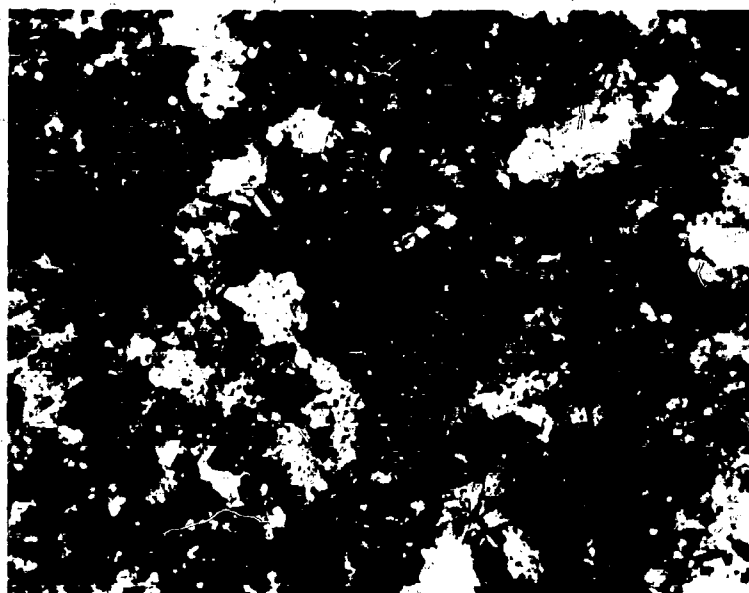


Figure 40. GRAIN SIZE IN UC





**Figure 41. UC<sub>2</sub> A-02 STARTING MATERIAL (4848) (250X)**



**Figure 42. UC<sub>2</sub> A-01 1/2 HOUR AT 1800°C (4937) (250X)**

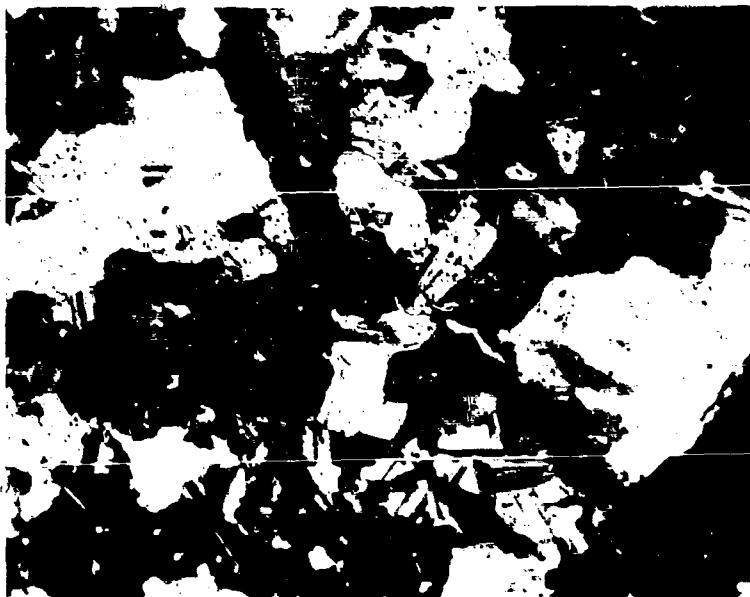


Figure 43.  $UC_2$  A-01 1 HOUR AT 1800°C (4934) (250X)

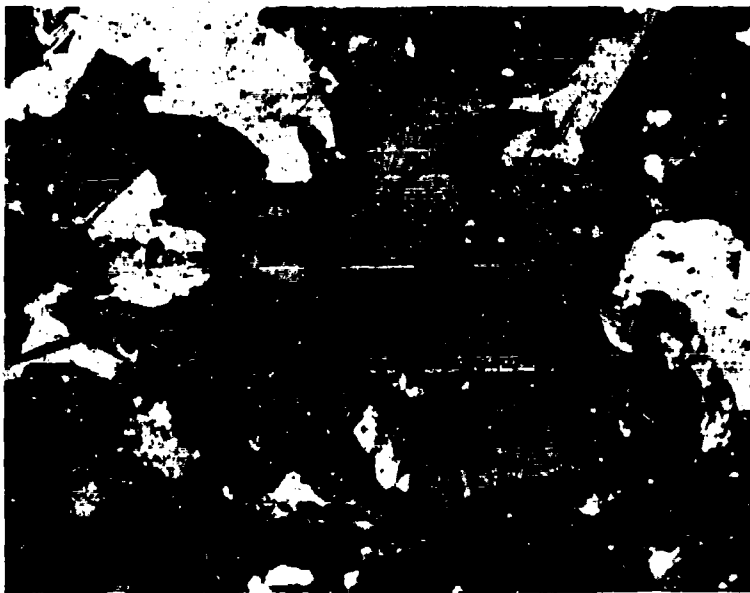


Figure 44.  $UC_2$  A-01 6 HOURS AT 1800°C (4962) (250X)

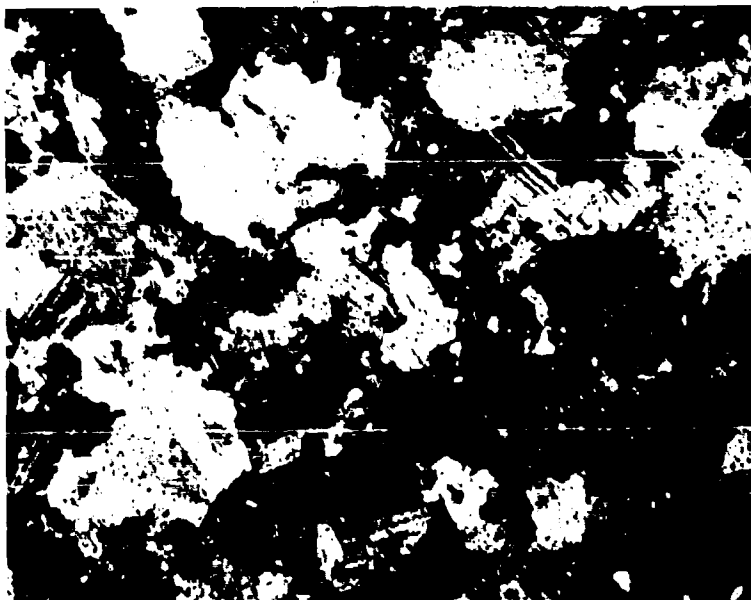


Figure 45.  $UC_2$  A-02 1 HOUR AT  $2000^{\circ}C$  (4860) (250X)

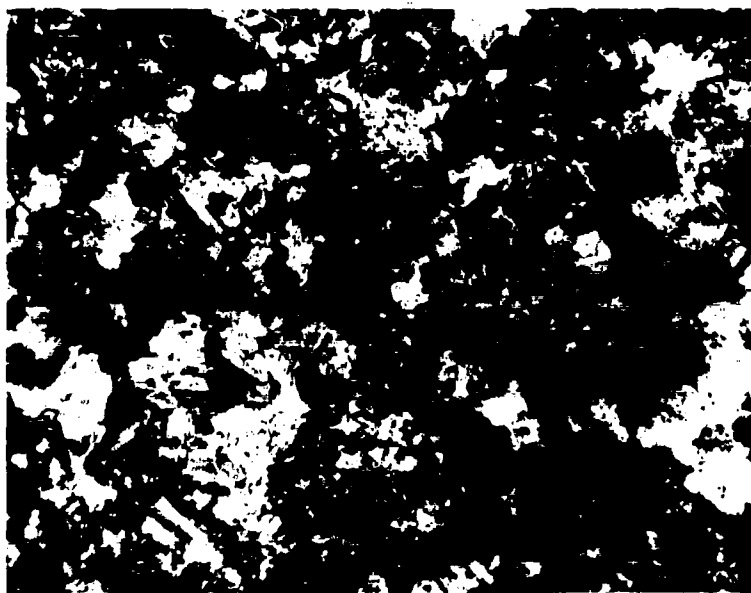
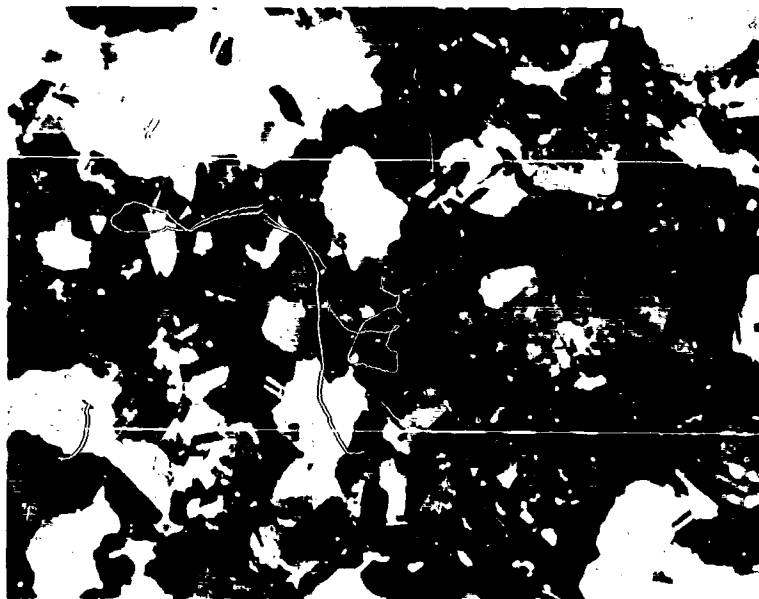


Figure 46.  $UC_2$  A-02 1 HOUR AT  $2000^{\circ}C$  (4898) (250X)



**Figure 47. UC<sub>2</sub> A-04 ¼ HOUR AT 2000°C (4960) (250X)**



**Figure 48. UC<sub>2</sub> A-04 ½ HOUR AT 2000°C (4959) (250X)**

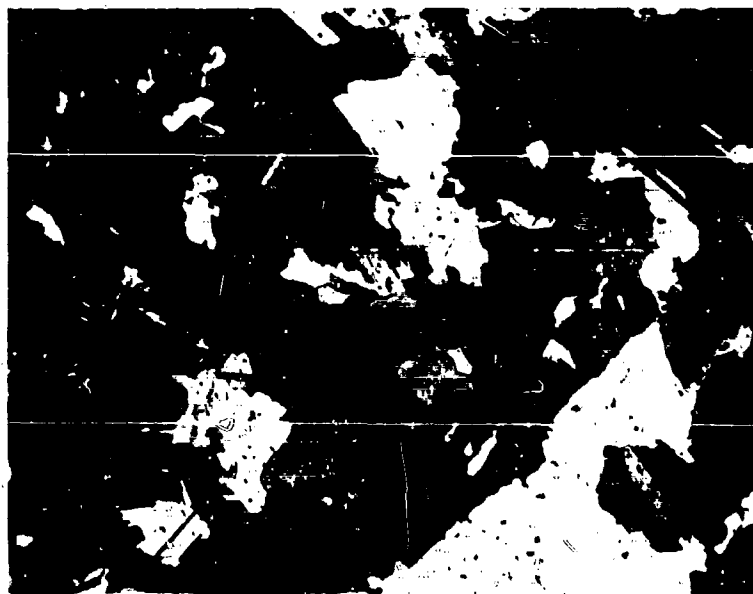


**Figure 49. UC<sub>2</sub> A-04 1 HOUR AT 2000°C (4956) (250X)**



**Figure 50. UC<sub>2</sub> A-04 2 HOURS AT 2000°C (5006) (250X)**

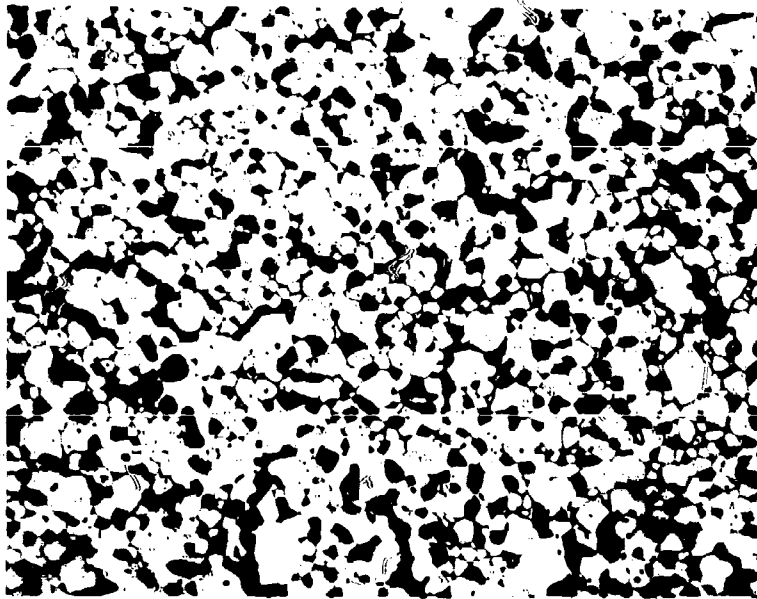


Figure 51.  $\text{EuB}_6$  A-11 STARTING MATERIAL (4798) (250X)

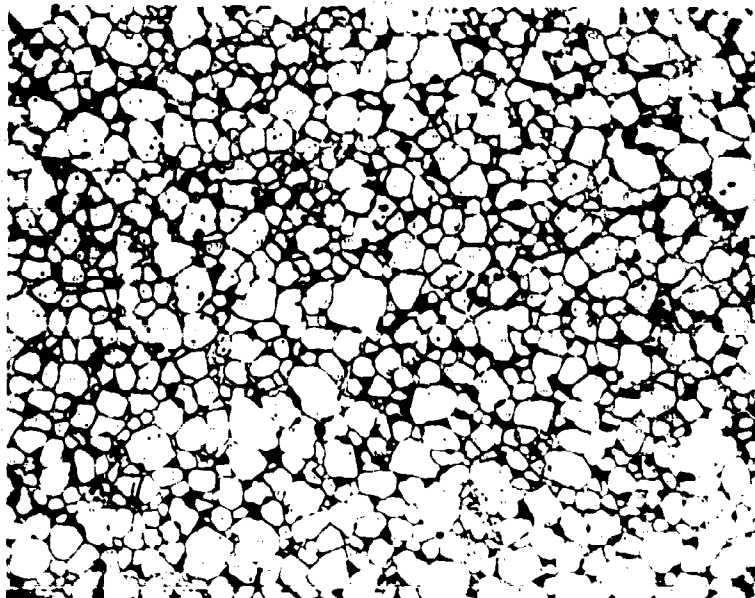


Figure 52.  $\text{EuB}_6$  A-15 STARTING MATERIAL (4994) (250X)

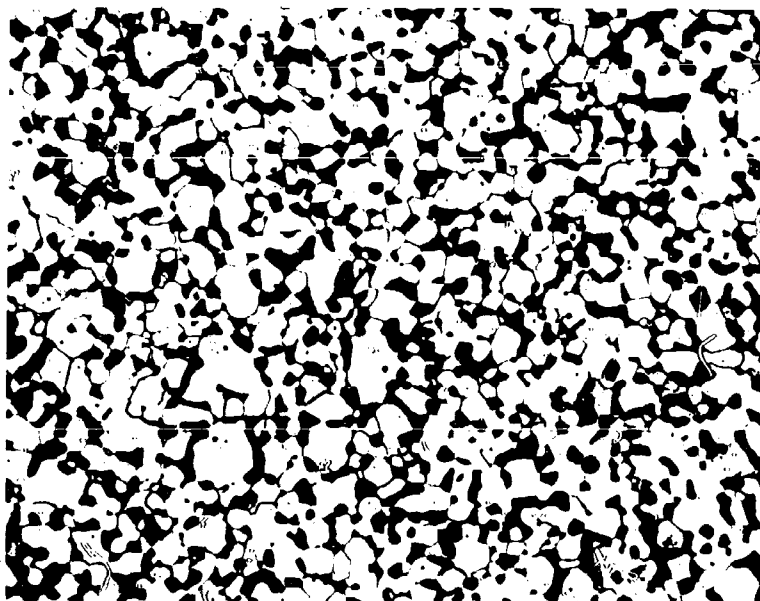


Figure 53.  $\text{EuB}_6$  A-11 20 HOURS AT  $1900^\circ\text{C}$  (4806) (250X)

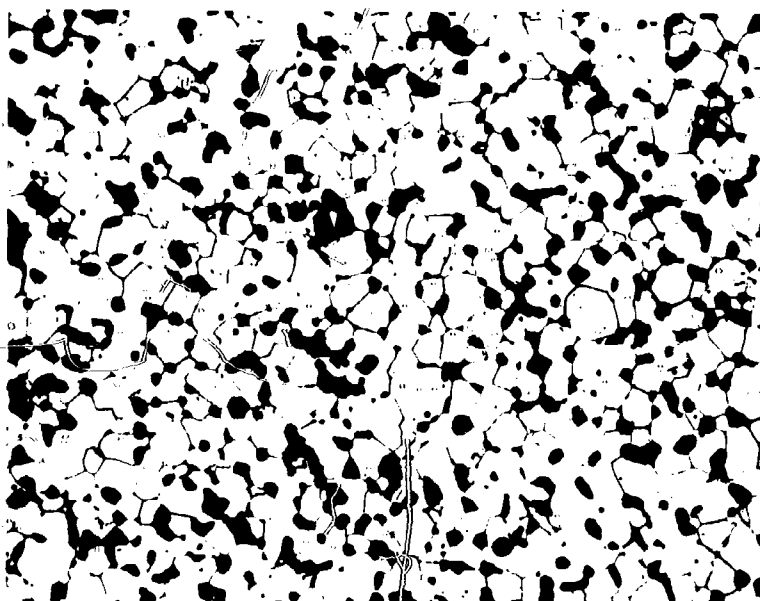


Figure 54.  $\text{EuB}_6$  A-15 1 HOUR AT  $2050^\circ\text{C}$  (4895) (250X)

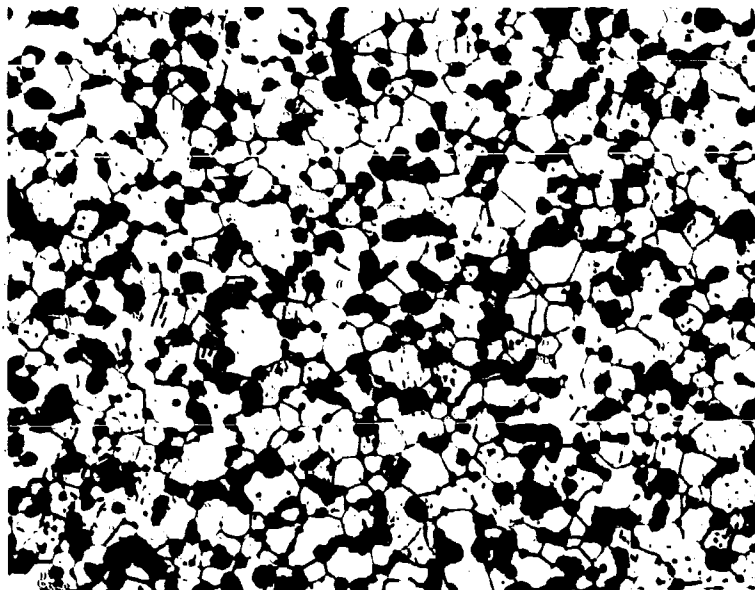


Figure 55.  $\text{EuB}_6$  A-15 4 HOURS AT  $2050^\circ\text{C}$  (4894) (250X)

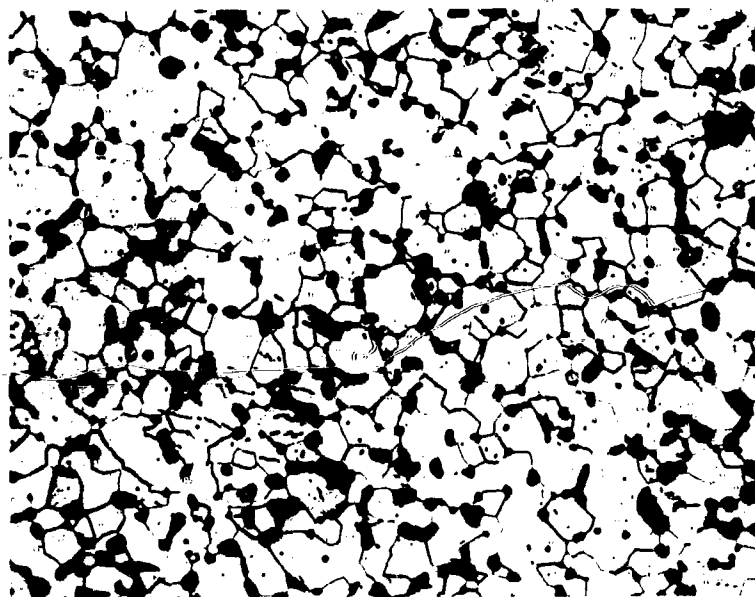


Figure 56.  $\text{EuB}_6$  A-15 9 HOURS AT  $2050^\circ\text{C}$  (4896) (250X)



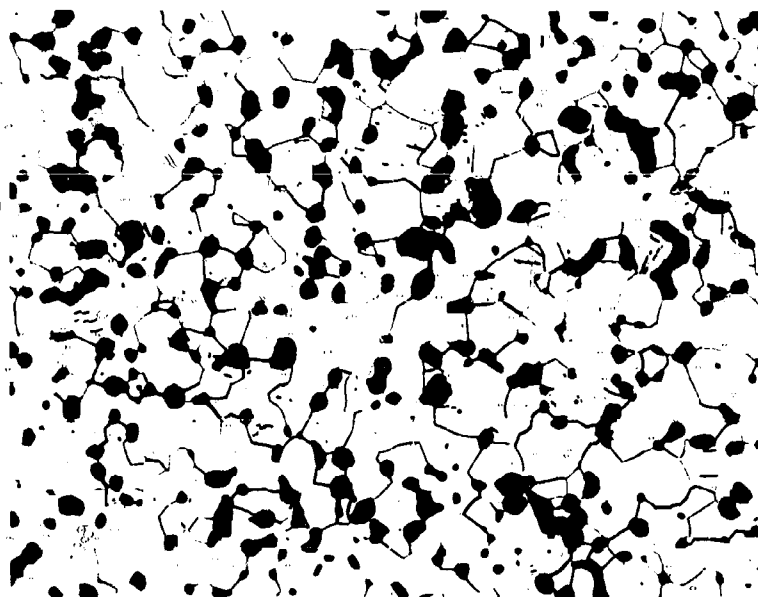


Figure 57.  $\text{EuB}_6$  A-15 16 HOURS AT  $2050^\circ\text{C}$  (4897) (250X)

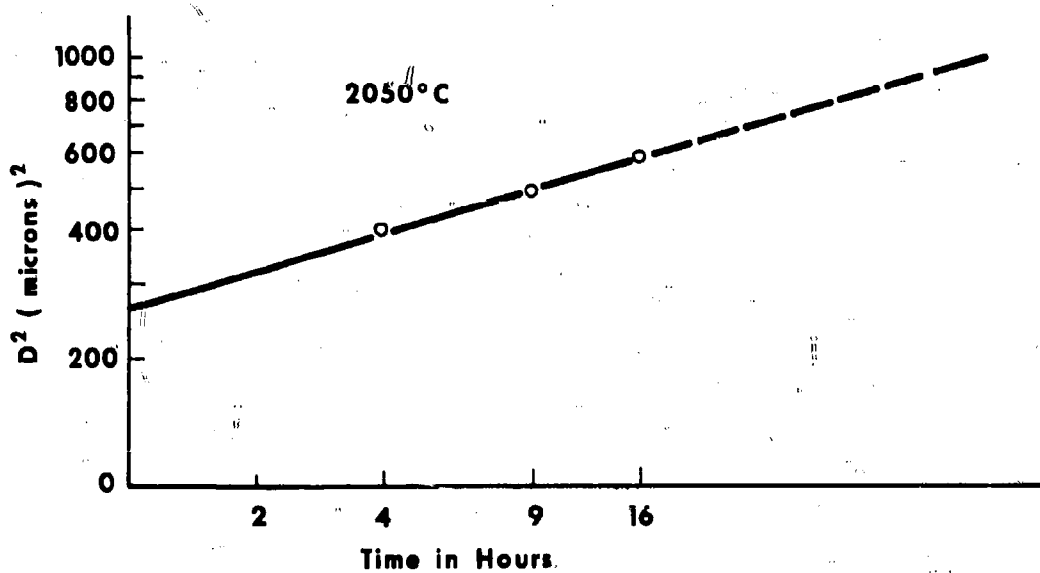


Figure 58. GRAIN SIZE IN  $\text{EuB}_6$

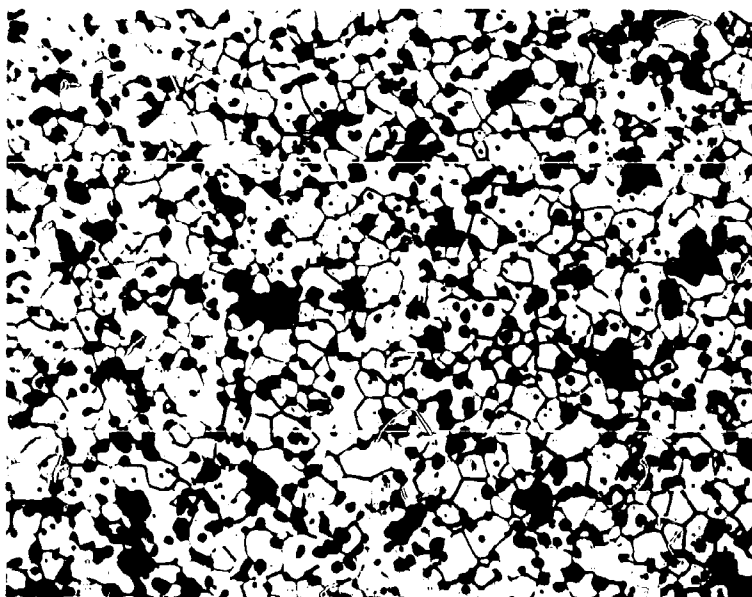


Figure 59. YB<sub>6</sub> A-19 1 HOUR AT 2000°C (5083) (250X)

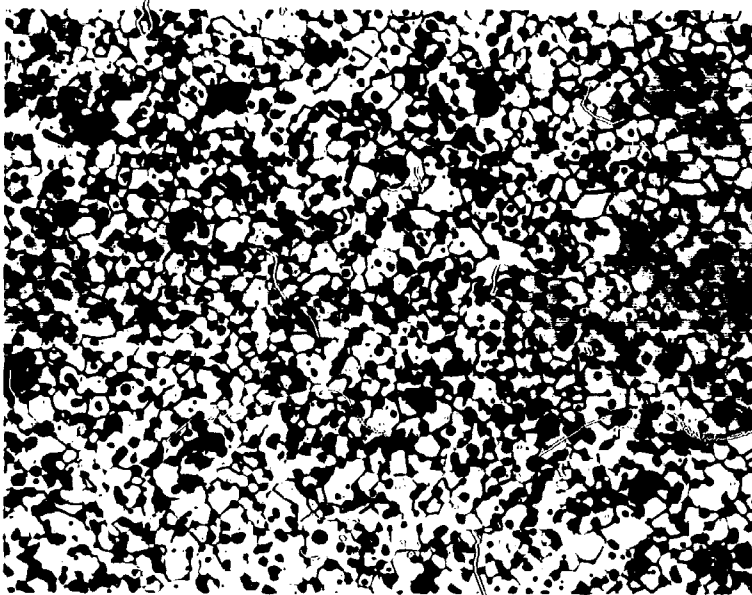


Figure 60. YB<sub>6</sub> A-19 2 HOUR AT 2000°C (5086) (250X)

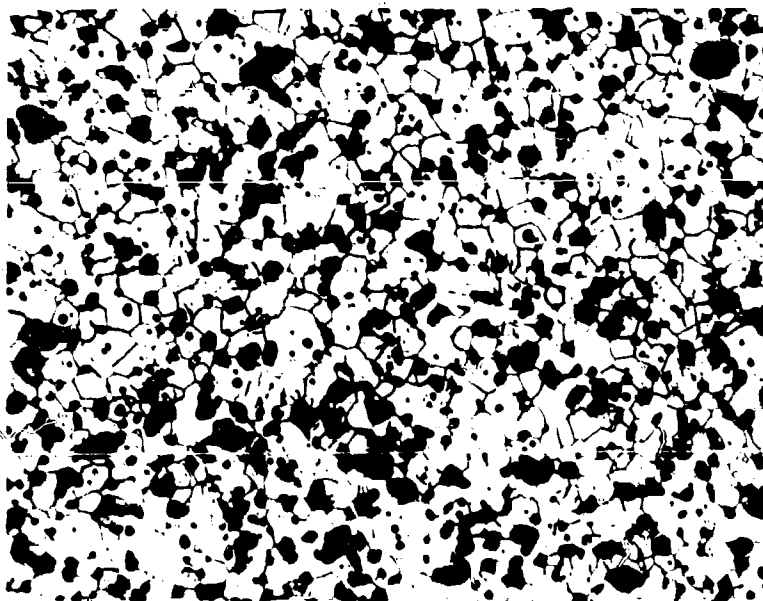


Figure 61. YB<sub>6</sub> A-19 4 HOURS AT 2000°C (5092) (250X)

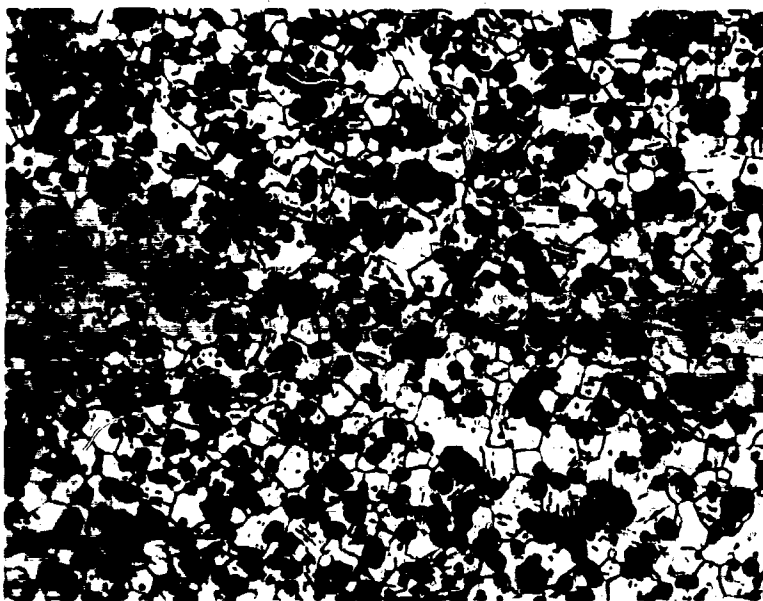
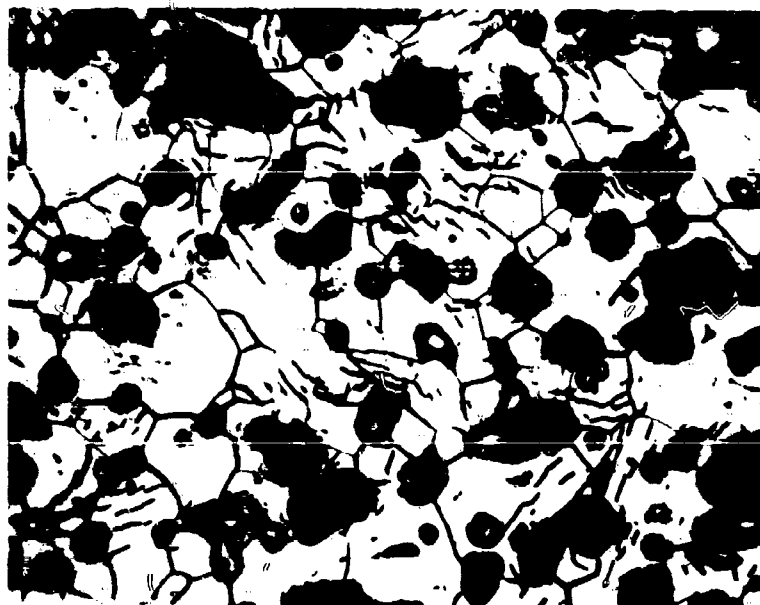
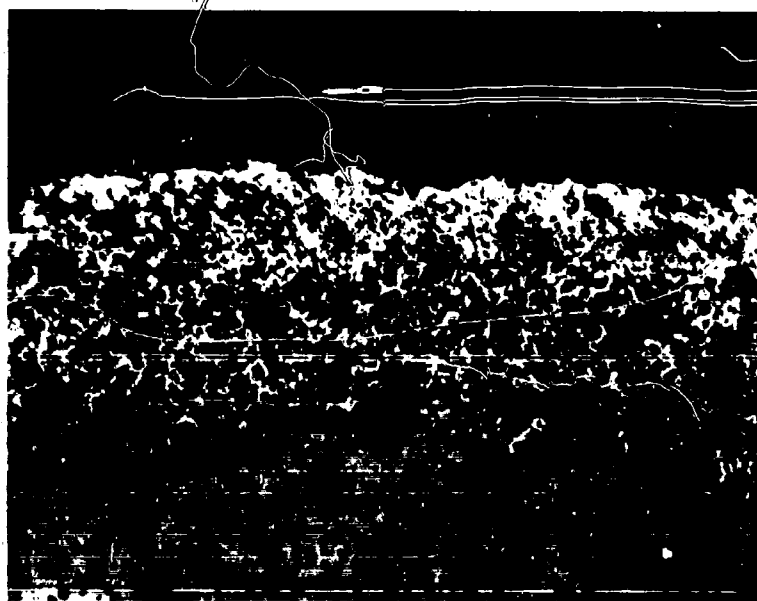


Figure 62. YB<sub>6</sub> A-19 6 HOURS AT 2000°C (5098) (250X)



**Figure 63. YB<sub>6</sub> A-19 SHOWING CRACKS (5099) (750X)**



**Figure 64. EDGE OF YB<sub>6</sub> A-19 1 HOUR AT 2000°C (5078)  
SHOWING YB<sub>4</sub> LAYER AND YB<sub>4</sub> IN GRAIN BOUNDARIES (250X)**

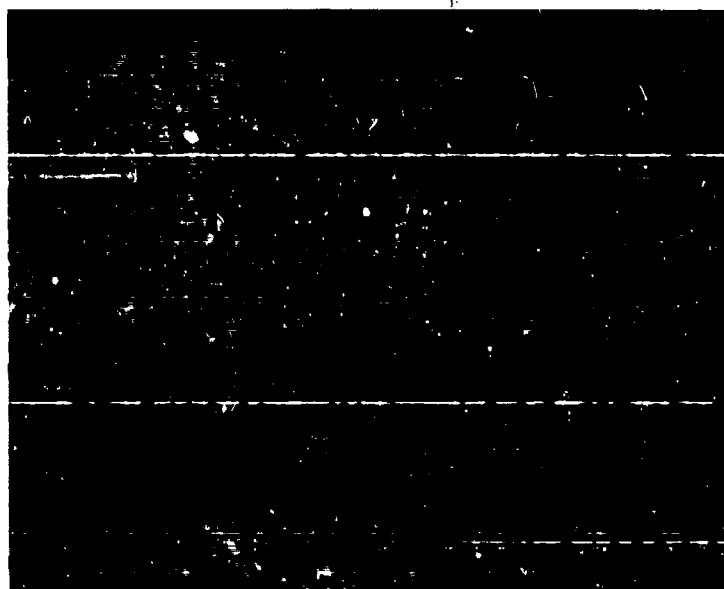


Figure 65. EDGE OF YB<sub>6</sub>A-19 4 HOURS AT 2000°C (5090) (250X)

**SECTION VII - THERMAL CYCLING OF SELECTED THERMIONIC EMITTER MATERIALS - A. I. Kaznoff  
J. G. Wilson**

**LIST OF ILLUSTRATIONS**

<b><u>Figure No.</u></b>	<b><u>Title</u></b>	<b><u>Page No.</u></b>
1	Vacuum Hot Press	7-15
2	Ultrasonic Drill	7-16
3	Thermal Cycling Specimens	7-16
4	Appearance of ZrC	7-17
5	As-polished YB <sub>6</sub>	7-17
6	Etched YB <sub>6</sub>	7-18
7	Etched EuB <sub>6</sub>	7-18
8	Etched EuB <sub>6</sub> (longer etching period)	7-19
9	As polished UC ZrC	7-19
10	UC ZrC After one hour at 2000 C	7-20
11	As polished UC	7-20
12	Etched UC	7-21
13	Etched UC <sub>2</sub> , Sample A-04	7-21
14	Etched UC <sub>2</sub> , Sample A-01	7-22
15	Etched UC <sub>2</sub> , Sample A-02	7-22
16	Thermal Cycling Apparatus	7-23
17	Temperature Cycle for ZrC	7-24
18	Temperature Cycle for YB <sub>6</sub>	7-25
19	Fracture Surface of EuB <sub>6</sub>	7-26
20	Fracture Surface of UC <sub>2</sub>	7-26

## VII. THERMAL CYCLING OF SELECTED THERMIONIC EMITTER MATERIALS - A. I. Kaznoff, J. G. Wilson

### A. Introduction

Thermionic cathodes are generally exposed to very high temperature levels. If the source of heat is a nuclear fuel or even if fossil fuel is used, it is evident that high heating rates can and will be encountered by the emitter materials in the start-up operation, change of power level, or excursions of the system supplying the thermal power. It is for these reasons that thermal cycling information is necessary since the stresses set up by the heating and cooling may cause the mechanical failure of the emitter body.

There is a general paucity of data on thermal stress resistance of the materials studied. Their elastic-plastic behavior is poorly known, their coefficients of thermal expansion at elevated temperature are not known, and their thermal emission is poorly ascertained. Thus, the determination of thermal shock parameters for UC, UC<sub>2</sub>, ZrC, (UC) (ZrC), YB<sub>6</sub> and EuB<sub>6</sub> presents a very large and difficult task. It was, nevertheless, interesting to determine the stability of these materials when subjected to thermal cycling and note the qualitative and semi-quantitative differences in these materials in order to gauge their potential as thermionic emitters and to ascertain the problems that can arise in their use.

This report is concerned with results of thermal cycling testing performed on the above materials. The specimens were subjected to the same test conditions. The materials were all prepared by hot-pressing powdered compounds at this laboratory and the results must be construed to be valid only for the conditions similar to the ones maintained and for the materials prepared and processed by the particular technique described in this report.

### B. Summary

1. Hot-pressed ZrC samples proved to be stable in thermal cycling experiments between about 500 and 2000 C for 50 cycles with a cycle period of 2 minutes.
2. The same results were observed with hot-pressed "YB<sub>6</sub>" with the exception that the upper temperature was 1700 C. The presence of YB<sub>4</sub> apparently had no deleterious effects.
3. Hot-pressed EuB<sub>6</sub> lasted an average of 35 cycles (maximum temperature 1700 C). Two of the four specimens tested survived the full 50 cycle test. An apparent correlation with density of the material was noted: specimens of the highest density are desirable. The fact that some specimens did survive the full test indicates that further development and control of variables should lead to EuB<sub>6</sub> resistant to thermal cycling.



4. Hot-pressed UC did not show good resistance to cycling and the results show considerable scatter. Three of the four sample tests did not last for over 3 cycles. Identical test samples, from the same batch of fabricated material, showed divergent results: one lasted the full 50 cycles (2000 C max), the other only 3 cycles. A very large amount of work needs to be done on UC to ascertain the conditions necessary to obtain the material resistant to thermal cycling.
5. Tests on hot-pressed  $UC_2$  specimens shows this material to be inferior on the average to UC (for  $UC_2$  average number of cycles to failure was 10, while for UC it was 15). A very large scatter in results was noted: 1 cycle (to failure) to 22 cycles (to failure). No apparent correlation to density could be observed.
6. All of the samples of hot-pressed (UC) (ZrC) failed after 1 cycle (2000 C max). This material proved to be the most inferior of those tested.
7. A method for thermal cycling was developed which allows a rapid testing procedure for refractory compound specimens. Methods of fabrication of the best specimens of ZrC,  $YB_6$ ,  $EuB_6$ , UC,  $UC_2$  and (UC) (ZrC) were developed. Heating rates of several thousands of degrees (centigrade) per minute were achieved.

#### C. Recommendations

The results of this exploratory testing for thermal cycling resistance has led the authors to the following recommendations:

1. The intrinsic stability of ZrC and  $YB_6$  during thermal cycling which was quite severe shows that these materials need no further testing in this area. Should these materials be attractive as emitters they can only be used as emitter coatings as they are not fuels; therefore, further studies, if deemed necessary, should be oriented to the development of bonding of these materials to structural (refractory) metals and the testing of these composites for chemical and mechanical stability in the regions projected in their application.
2. Further work in fabrication of  $EuB_6$  is necessary. No work is necessary for stoichiometry control. Once this is accomplished bonding studies similar to ones suggested in (1) are in order provided  $EuB_6$  is considered to hold promise in applied thermionic conversion.
3. A very considerable amount of work is needed for UC.
  - a. Further testing is necessary to determine effects of composition and density.

- b. Testing should be extended to UC fabricated by means other than hot pressing.
  - c. The effects of surface preparation must be investigated.
  - d. A definitive program to determine, quantitatively, the thermal shock parameters of UC fabricated by a variety of methods should be initiated. This should be supplemented by other basic studies such as: high temperature mechanical properties, thermal expansion, etc. Temperature range of 1400-2400 C should be covered.
4. There appears to be little incentive to study UC<sub>2</sub> as this material does not appear to offer any important advantages in nuclear thermionics.
  5. The recommendations for UC-ZrC are essentially the same as those of UC. It is recommended that several alloy compositions be investigated with special emphasis based on part (d) of the recommendations in 3.

The most urgent need for technical information appears to lie with UC and UC-ZrC fuels.

#### D. Experimental Procedures

##### 1. Sample Preparation

The materials were prepared by hot-pressing the respective powders in a vacuum hot-press. (Figure 1.) The dies were made by precision machining of Graphite G. Spacers in the die were of the same graphite. The conditions for pressing and other results are given in Table I.

After the hot-pressing operation the dies were opened and the pellets were cleaned to remove graphite and extraneous material. The pellets were then reduced to a washer geometry with the following dimensions:

Outside Diameter	0.5 inches
Inside Diameter	0.25 inches
Thickness	0.20 inches

This was accomplished by means of a Mullard Ultrasonic Drill (Figure 2) or by conventional drilling with diamond drill. Black-body holes were then made by the same techniques. Typical black-body holes were 10 mil in diameter and 60-70 mils deep. The specimens were then polished. Figure 3 shows a typical specimen.

TABLE I

Material	Powder Size	Temp C	Pressure (Nominal)	Sintering Aids	Achieved Density, % (Theoretical)	X-Ray Examination Results
ZrC A-05	-325 mesh	2300 C	5,000 PSI	None	92%	Single phase
ZrC A-20-1	-325 mesh	2200 C	6,000 PSI	Initial Ni 1% wt.	100%	Single phase
ZrC A-20-2	-325 mesh	2200 C	6,000 PSI	Initial Ni 1% wt.	100%	Single phase
YB <sub>6</sub> A-10-1	-325 mesh	1800 C	4,800 PSI	None	~99%	Some YB <sub>4</sub> present
YB <sub>6</sub> A-10-2	-325 mesh	1800 C	4,800 PSI	None	~99%	Some YB <sub>4</sub> present
YB <sub>6</sub> A-16	-325 mesh	2300 C	4,000 PSI	None	~99%	Some YB <sub>4</sub> present
EuB <sub>6</sub> A-10	-325 mesh	2300 C	4,800 PSI	None	83%	Single phase
EuB <sub>6</sub> A-14	-325 mesh	2300 C	6,000 PSI	None	90%	Single phase
EuB <sub>6</sub> A-15	-325 mesh	2300 C	6,000 PSI	None	100%	Single phase
(UC) (ZrC) A-06-1	-325 mesh	1700 C	6,000 PSI	None	90%	Single phase
(UC) (ZrC) A-06-2	-325 mesh	1700 C	6,000 PSI	None	90%	Single phase
(UC) (ZrC) A-08-1	-325 mesh	1650 C	6,000 PSI	None	90%	Single phase
UC A-08-1	-325 mesh	1760 C	6,000 PSI	None	75%	Very minor UC <sub>2</sub> present
UC A-08-2	-325 mesh	1100 C	6,000 PSI	None	75%	Very minor UC <sub>2</sub> present
UC A-13-1	-325 mesh	1500 C	6,000 PSI	None	83%	Single phase UC
UC A-13-2	-325 mesh	1500 C	6,000 PSI	None	83%	Single phase UC
UC <sub>2</sub> A-05	-325 mesh	1500 C	6,000 PSI	None	90%	Some UC <sub>2</sub> present
UC <sub>2</sub> A-02-III	-325 mesh	1700 C	4,800 PSI	None	95%	
UC <sub>2</sub> A-01	-325 mesh	1700 C	4,800 PSI	None	95%	Minor amount of UC Present
UC <sub>2</sub> A-04	-325 mesh	1500 C	4,800 PSI	None	88%	Single phase

The specimens were examined by metallographic and x-ray techniques and their densities were determined. All these operations were carried out at room temperature. Table I shows some of the results obtained. In the following paragraphs a more detailed appraisal of the specimens prior to testing is given.

Metallographic examination of ZrC confirmed that the material was single phase. Even the specimens to which nickel was added to promote densification did not reveal the presence of a second phase. This may be accounted by the fact the high temperature (2200 C) and the time at temperature during hot-pressing was sufficient to volatilize the nickel. In other studies it was found that nickel when present was always concentrated in the grain boundaries. A typical appearance of ZrC is seen in Figure 4. This particular specimen was ZrC A-20; the mean intercept grain diameter was 34.4 microns. Lower density specimens were similar except for a higher porosity and lower grain size (smaller than 8 microns).

All of the  $YB_6$  specimens contained some  $YB_4$ . The high densities obtained reflect the presence of the lower boride. Since  $YB_6$  at high temperature will always produce  $YB_4$  as a result of sublimation processes it was deemed to be more realistic to use specimens containing this second phase. Figure 5 shows a  $YB_6$  A-16 as-polished specimen. The light colored phase is  $YB_4$ . Figure 6 shows the same specimen after it has been etched.

X-rays all showed that  $EuB_6$  was single phase. Very small amounts of a second phase which is probably accounted by impurities in the starting materials, were revealed by metallography. Figure 7 is a photomicrograph of  $EuB_6$  A-15 and Figure 8 is for  $EuB_6$  A-13 which was a sister pellet of  $EuB_6$  A-14. Both of these specimens were etched, that in Figure 8 was etched for a longer period (10 seconds) which removed the minor second phase material.

(UC) (ZrC) was found to be single phase by x-rays with the exception of (UC) (ZrC) A-05 which showed presence of  $UC_2$ . Examination by metallographic techniques revealed the presence of a second phase which was isotropic (see for example Figure 9 for (UC) (ZrC) A-06 as polished). Grain size was quite small (less than 3 microns) and the samples were generally quite difficult to etch. A sample of (UC) (ZrC) A-08 which was heated for one hour at 2000 C was still difficult to etch but showed a single phase material with a mean intercept grain diameter of about 7 microns (Figure 10). Grain growth accounts for the larger grain size.

UC A-08 showed some  $UC_2$  present in very minor quantity. X-rays indicated that UC A-13 was single phase but metallography showed an isotropic second phase. Figure 11 shows UC A-13 as polished and Figure 12, as etched.

Although x-rays did not always indicate UC in  $UC_2$  samples, metallography showed that all the samples contained some UC. Figures 13, 14, and 15 shows the etched grain structure of  $UC_2$  A-04,  $UC_2$  A-01 and  $UC_2$  A-02 respectively. Figure 14 shows the structure of  $UC_2$  which was maintained for a longer period at the higher temperatures. This picture was taken under polarized light.

The following is a summary of the etchants and their application in the metallographic investigations.

ZrC	25 $H_2O$ , 25 $HNO_3$ , 25 Acetic, 2-3 HF. Four to seven seconds by immersion. Repolish very lightly to remove gold colored stain that forms.
$YB_6$	20 $H_2O$ , 15 HF, 10 $HNO_3$ . Immersion. Time varies. Best to start with no more than 15 seconds and continue at 15 second intervals to prevent overetching. Sometimes it is necessary to repolish and re-etch depending on whether fine polishing scratches are visible after the first etch.
$EuB_6$	Same as $YB_6$ except that repolish is seldom necessary.
UC	25 $H_2O$ , 25 $HNO_3$ , 25 Acetic, 2-3 HF. Immersion 10-60 seconds. Sometimes necessary to repolish lightly to remove stain.
UC-ZrC	25 $H_2O$ , 25 $HNO_3$ , 25 Acetic, 2-3 HF. Immersion 15-30 seconds.
$UC_2$	25 $H_2O$ , 25 $HNO_3$ , 25 Acetic, 2-3 HF. Immersion 30-90 seconds. Usually necessary to examine under polarized light since this is a stain etch and not a grain boundary etchant.

## 2. Thermal Cycling Procedure

The thermal cycling was accomplished in the apparatus shown in Figure 16. The sample was supported on three tungsten wires which were held in alumina tubes resting in a boron nitride support. The power was supplied by a 5 KW General Electric induction unit. The vacuum system consisted of an oil diffusion pump with a nitrogen trap and a mechanical pump with a capability of maintaining the system below  $10^{-6}$  torr. The test chamber was made of vycor. Calibrations were made on the quartz window and prism to provide

corrections for optical pyrometry. A micro pyrometer was used in all temperature measurements. In order to provide regular periodic cycling, a 2 rpm motor with a microswitch was interconnected to the induction power supply. The period of the cycle was 2 minutes with 30 seconds at full power and 90 seconds at zero power.

After a sample was introduced and the system was pumped down, the power was gradually raised to the setting which would heat the specimen to the required temperature and maintain it at that level indefinitely. Prior to attaining this level it was necessary to de-gas the samples in situ, so that no arcing would occur in the system and a good vacuum could be maintained. The degassing operation was not necessary or very brief for all the specimens of  $\text{ZrC}$ ,  $\text{YB}_6$  and  $\text{EuB}_6$ . Considerable outgassing was necessary for  $\text{UC}$ ,  $\text{UC}_2$ , and  $(\text{UC}) (\text{ZrC})$ , the periods rarely exceeded 5-10 minutes. The outgassing was carried out above 1500 C, the exact temperature was largely determined by the rate of evolution of gas from the sample. In practice it was possible to start degassing at say 1400 C and follow this with a gradual increase in the temperature to 2000 C.

The upper temperature for the cycle was 2000 C for all the material except  $\text{YB}_6$  and  $\text{EuB}_6$ . The latter two have very appreciable vapor pressures which would limit their use to about 1400 C. Since it is of interest to cycle materials above this temperature an upper temperature of 1700 C was selected for the borides. The rest of the materials were cycling to the same temperature limit for the sake of test uniformity; it is realized that  $(\text{UC}) (\text{ZrC})$  and  $\text{ZrC}$  could be operating as emitters at temperatures above 2000 C.

The typical heating cycles were as follows:

- 15-20 seconds to heat to 2000 C for carbides and to 1700 C for the borides
- Power on for total of 30 seconds.
- Samples at constant upper temperature for about 10-15 seconds.
- Power off for total of 90 seconds.

Figure 17 shows the temperature as a function of time for the cycling of  $\text{ZrC}$ . Figure 18 shows the same for  $\text{YB}_6$ . These representations are typical for all the materials and specimens tested. The solid lines represent measured temperatures. Dashed lines represent portable temperature profiles in time. The test consisted in cycling until the specimen cracked (or split apart) or until 50 cycles were completed. If the specimen cracked but

still maintained its integrity on the supports, the effect was noticed by a very large drop in the temperature of the specimen. Typically a power setting suitable for heating a specimen to 2000 C would not raise a cracked specimen above 1300-1400 C. In almost all cases the disintegration was sufficient to displace the specimen from the tungsten supports so that no ambiguity as to the termination of the test was possible. Some of the specimens were examined, in situ, during test at 1 cycle, 25 cycles and 50 cycles (where feasible). It was not possible to detect any small cracks that could be developing through a drop in observed temperature, therefore, the test could be terminated only when a crack clear through the specimen occurred or when the specimen broke into two sections. These spot checks on the specimens did demonstrate that the original temperature regime was maintained throughout the test period. These checks were, of course, feasible only on specimens that could be cycled many times.

The materials that showed stability and integrity for 50 cycles were not given more than three tests. At least four tests were given to the other materials.

### 3. Discussion of Results

A summary of results obtained on the materials tested are given in Table II.

Disregarding the variables from sample to sample and bearing in mind that only a limited number of samples were tested for each material, one may still gain some qualitative insight as to the mechanical stability of these materials from the arithmetic average of cycles to failure:

#### Average No. of Cycles to Failure

1. ZrC	50+ (2000 C)
2. YB <sub>6</sub>	50+ (1700 C)
3. EuB <sub>6</sub>	35 (1700 C)
4. UC	15 (2000 C)
5. UC <sub>2</sub>	10 (2000 C)
6. UC-ZrC	1 (2000 C)

It is significant that the first (best) four materials, ZrC, YB<sub>6</sub>, EuB<sub>6</sub> and UC had at least one sample that lasted the full 50 cycle test, this indicates that with careful control of variables of stoichiometry and fabrication and the understanding of these variables as they relate to thermal cycling resistance it may be possible to develop materials that could take considerable temperature excursions.

TABLE II

Sample	No. of Cycles to Failure	Remarks
ZrC A-05	50+ (2000 C max)	Sample remained intact after 50 cycles
ZrC A-20-1	50+ (2000 C max)	as above
ZrC A-20-2	50+ (2000 C max)	as above
YB <sub>6</sub> A-10-1	50+ (1700 C max)	as above, surface covered with YB <sub>4</sub>
YB <sub>6</sub> A-10-2	50+ (1700 C max)	as above
YB <sub>6</sub> A-18	50+ (1700 C max)	as above
EuB <sub>6</sub> A-10	7 (1700 C max)	Broke into two pieces
EuB <sub>6</sub> A-14-1	50+ (1700 C max)	Sample intact after 50 cycles
EuB <sub>6</sub> A-14-2	24 (1700 C max)	Broke into two pieces
EuB <sub>6</sub> A-15	50+ (1700 C max)	Sample intact after 50 cycles
(UC) (ZrC) A-06-1	2 (2000 C max)	Broke into two pieces
(UC) (ZrC) A-06-2	1 (2000 C max)	as above
(UC) (ZrC) A-08-1	1 (2000 C max)	as above
(UC) (ZrC) A-08-2	1 (2000 C max)	as above
UC A-08-1	1 (2000 C max)	as above
UC A-08-2	3 (2000 C max)	as above
UC A-13-1	50+	remained intact
UC A-13-2	3	Broke into two pieces
UC <sub>2</sub> A-02-III	22	Cracked but did not break into two pieces
UC <sub>2</sub> A-01-1	9	Broke into two pieces
UC <sub>2</sub> A-01-2	1	Broke into two pieces
UC <sub>2</sub> A-04	1	as above
UC <sub>2</sub> A-05	17 (2000 C max)	as above



Examination of the fracture surfaces indicate that "brittle" fracture occurred in all the specimens that failed. There was no evidence of fatigue processes in the post-examinations. This is supported by observation in situ during the tests, since starting cracks would have appeared as bright lines on the surface of the specimen. If cracks formed they were micro-cracks and not visible at the magnification of the optical pyrometer. Figure 19 shows the fracture surface of  $\text{EuB}_6$  and Figure 20 that of (UC) (ZrC). These fractures are typical of the ones encountered in this study. The planes of fracture ran roughly parallel to the axis of radial symmetry of the washers. Cracking of the specimens frequently occurred on heating cycle but it was not established if preliminary cracking did not occur below 900 C, i.e. below the temperature at which pyrometric observations were conducted. Judging from the fractured surfaces one may assume that most of the failures occurred at lower temperatures before the onset of appreciable plastic deformation. In the case of UC it is conceivable that the fracture occurred below 1000 C. The onset of appreciable plasticity in the materials as obtained from hot-pressing studies is as follows:

UC	about 1100 C
$\text{UC}_2$ , UC-ZrC	about 1500 C
$\text{YB}_6$	about 1500-1800 C
$\text{EuB}_6$	about 1800-2300 C
ZrC	about 2300 C

Originally it was suspected that black-body holes may serve as crack initiation centers. The results showed this to be false, no specimen showed a crack passing through the black-body hole. Non-uniformity of temperature was also resolved to be a very minor effect. Gradients exceeding 10 C were not observed across the specimens. Temperature uniformity was achieved without special precautions about centering the specimen inside the induction coil, as the test device was self-centering (see Figure 16), the coil fit tightly over the vycor tube and the boron nitride support in the tube was fitted tightly to the container, thus the geometry was fixed sufficiently well in all the tests.

In the following paragraphs the materials tested are discussed separately. ZrC proved to be very stable material. It was originally suspected that ZrC, with nickel added as a sintering aid during hot-pressing may prove to be weaker due to the possible presence of nickel in the grain boundaries and larger grain size. Metallography revealed no nickel in the grain boundaries and the grain size apparently did not affect the results within the test limit of

50 cycles. The duration of the cycling test and the temperature of the cycling could not produce appreciable grain growth.

It was anticipated that the presence of  $YB_4$  in  $YB_6$  may weaken this material but this was not the case. The results indicate that  $YB_6$  could function satisfactorily while developing the  $YB_4$  phase as a result of sublimation losses of boron. It was observed that all the surfaces of  $YB_6$  specimens were coated with a loose  $YB_4$  layer similar to the ones observed in sublimation studies with this material. The specimen,  $YB_6$  A-10-1 developed "whiskers" during the test. These "whiskers" had many kinks and were shown to be polycrystalline  $YB_6$ . The other two  $YB_6$  specimens did not exhibit this behavior. Although a lower maximum temperature of 1700 C was chosen mainly on the basis of excessive sublimation losses of  $YB_6$  at higher temperature levels, it was observed that at 2000 C and higher  $YB_6$  specimens generally break apart and their structures show many micro-cracks in the grains.

$EuB_6$  was a single-phase material and unlike  $YB_6$  does not develop any second phase as a result of sublimation processes. Two of four specimens survived the full 50 cycles (1700 C max). The failure of two of the specimens at 7 and 24 cycles may be correlated to the higher porosity of these samples, although factually it is only one of many variables which could influence the results. The following is the comparative table indicating the correlation with the measured density of the starting material:

<u>Material</u>	<u>No. of Cycles</u>	<u>Density (% theoretical)</u>
$EuB_6$ A-10	7	83%
$EuB_6$ A-14-1	24	90%
$EuB_6$ A-14-2	50+	90%
$EuB_6$ A-15	50+	100%

Specimens of  $EuB_6$  A-14 and  $EuB_6$  A-15 were prepared under identical nominal conditions of temperature and pressure, but the resulting density was quite different. Moreover, one of the  $EuB_6$  A-14 specimens did last through the full test of 50 cycles so that the correlation with density may be accidental. In general, lower temperatures and pressure in the fabrication step produce higher porosity in the sample. The temperatures encountered in the test would not produce appreciable grain growth as temperatures exceeding 1900 C have to be reached to obtain measureable grain growth effects within a few hours.

UC specimens in common with all the uranium bearing materials required considerable out-gassing. One specimen survived the full test of 50 cycles. Again it appears that higher density specimens had a better resistance to cycling. Specimens of UC A-08 besides being less dense, contained more  $UC_2$  than UC A-13.

	<u>Hot-Pressing Conditions</u>	<u>Density</u>	<u>Cycle to Failure</u>
UC A-08-1	1100 C, 6000 psi	75%	1
UC A-08-2	1100 C, 6000 psi	75%	3
UC A-13-1	1500 C, 6000 psi	83%	50
UC A-13-2	1500 C, 6000 psi	83%	3

It appears to be feasible to develop UC which could survive the rigor of the full test but considerably more information is needed on the effects of the variables.

It is remarkable that some of the  $UC_2$  specimens were able to withstand several cycles (one lasted through 22 cycles) since the material could pass through two phase transitions. At 1800 C it is known to change crystal structure from cubic to tetragonal and below 1300 C it decomposes under equilibrium conditions, to  $U_2C_3 + C$ . The ability to withstand such drastic conditions may be tied to its ability to twin. Exposure to temperatures of 1800 C or higher always produces very rapid grain growth as was shown in grain growth studies. The following is a comparative table of observations on  $UC_2$ :

	<u>Hot Pressing Conditions</u>	<u>Density</u>	<u>No. of Cycles</u>
$UC_2$ A-04	1500 C, 4000 psi	88%	1
$UC_2$ A-01-2	1700 C, 4800 psi	95%	1
$UC_2$ A-02-1	1700 C, 4800 psi	95%	9
$UC_2$ A-02-III	1700 C, 4800 psi	95%	22
$UC_2$ A-05	1700 C, 4800 psi	90%	17

(UC) (ZrC) turned out to be the least satisfactory material with respect to thermal cycling. None of the samples tested lasted more than 1 cycle. In thermal conductivity experiments, such as those conducted by L. N. Grossman, it was always observed that a large temperature gradient caused cracking in (UC) (ZrC) rod specimens. One may only speculate that lower thermal conductivity and lack of ductility of this solid solution may cause these rapid failures. L. N. Grossman has measured and estimated (those values marked\*) the values of thermal conductivity for UC, ZrC, and (UC) (ZrC) (K given in cal/cm sec deg).

	<u>UC</u>	<u>ZrC</u>	<u>(UC) (ZrC)</u>
727 C (1000 K)	0.054		0.035 *
1227 C (1500 K)	0.056	0.069	0.042 *
1727 C (2000 K)	0.056	0.073	0.048 *

In conclusion it is interesting to point out that very high heating rates were used in these studies. Mean heat-up rates on carbides were about 6000 C/minute and 3500 C/minute on the borides. Since the power supplied was set to reach the steady state temperature of 2000 C and 1700 C the heating rate was more rapid at the lower temperature (above the mean quoted) and a lower rate prevailed at the higher temperature where the materials were more plastic. Although such rates are lower than those encountered in nuclear reactor excursions they are much higher than those encountered in the start-up of power reactors. The heating rates encountered represent fairly closely changes from 50 per cent power to 100 per cent power in a power reactor. Since it appears to be reasonable to assume that brittle fracture was the mode of failure it is interesting to compare the cooling rates of the various materials below the level of temperature where appreciable plasticity is shown. In UC-ZrC and UC<sub>2</sub> one sees that at 1000-1200 C a very plausible temperature range at which failure could have occurred, a cooling rate of about 1200 C/min was encountered. Similarly for UC, at 800 C, the cooling rate was approximately 480 C/minute. For ZrC the temperatures covered were essentially those over which brittle behavior dominated but, of course, no failures were encountered. Similar analysis could be made for YB<sub>6</sub> and EuB<sub>6</sub>. These are naturally estimates as the exact temperatures at which failure occurred were not observed and the high temperature mechanical properties of the materials, as fabricated in this study, are not adequately known. This study could be criticized on the basis of "unrealistic" cycling conditions as these heating and cooling rates may not represent those associated with some particular thermionic system. One must bear in mind that the present study is not related or oriented to any particular system and it is known that the number of systems under consideration is large. The cycling rate chosen was "intermediate" between the relatively slow start-ups and changes of power level in power reactions and the well known excursions and scrams that are encountered in test reactors. There is another significant point in the fact that thermionic devices are tested in reactors which are considerably different from the projected thermionic system reactors and test reactors are known to have periods when very large rates of temperature change occur. The objective of this study was primarily a comparative evaluation.

of the stability of some materials to a particular type of thermal cycling. It is obviously more desirable to perform further cycling experiments which have a closer correspondence to hypothetical reactor systems in the materials configurations that would be used in those systems. It is equally obviously that low rates of change of temperature are desirable in a practical system especially if potentially brittle refractory compound emitters are used.

It can not be over-emphasized that the results of these tests are primarily exploratory. They refer only to the materials as fabricated and prepared for this study and the results should not be extrapolated to materials of different origin, for instance, it would be incorrect to assume that cast UC will behave similarly to hot-pressed UC. Some of the more important facets need exploration for definitive conclusions. These are:

1. Effect of preparation and fabrication.
2. Chemical composition.
3. Surface preparation (and composition)
4. Geometry
5. Residual gases in the test apparatus and in the samples.
6. Heating rates and cycle frequency.

Another important facet is the bonding and support structure (for these emitter materials) as cycling results could be quite different if one studied a composite structure of say a carbide bonded to a refractory metal.

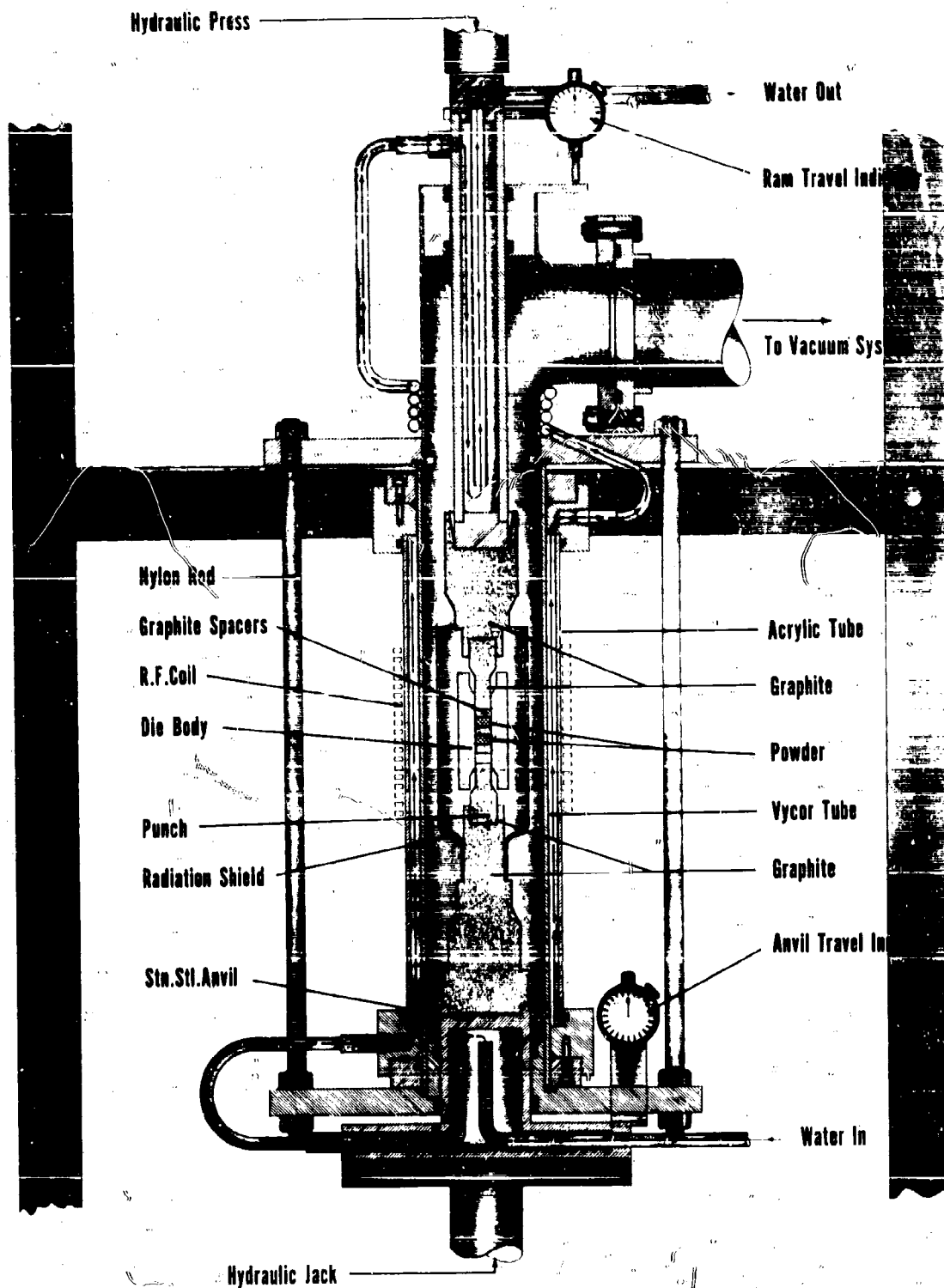


Figure 1. VACUUM HOT PRESS

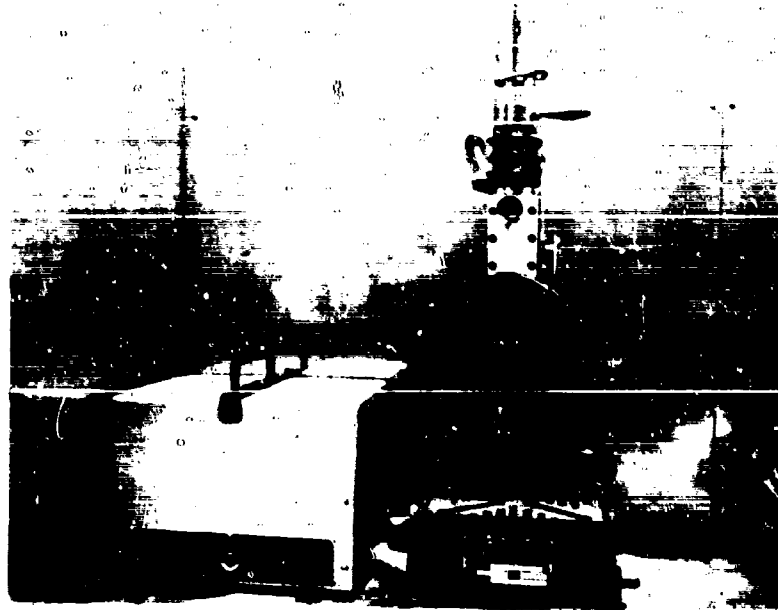


Figure 2. ULTRASONIC DRILL

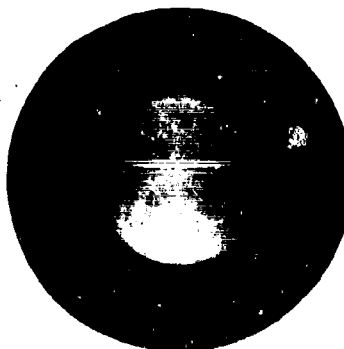


Figure 3. ZrC SPECIMEN

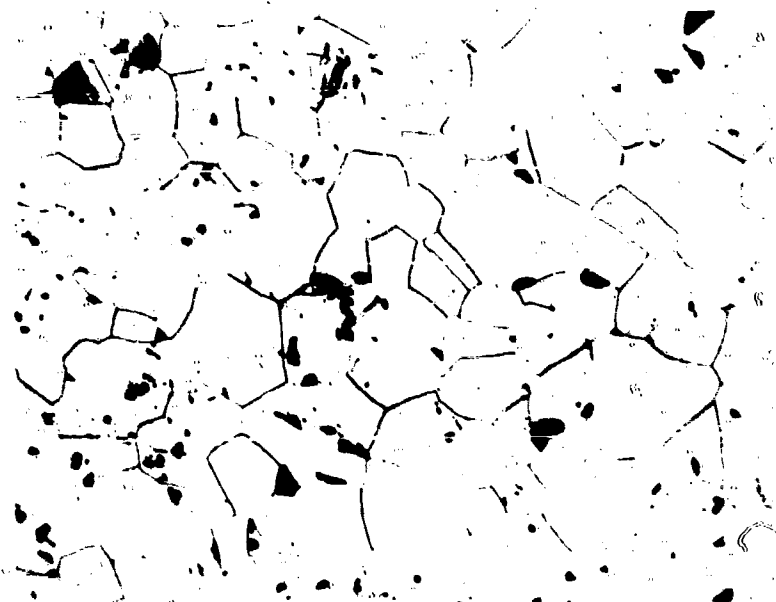


Figure 4. ZrC (250X)

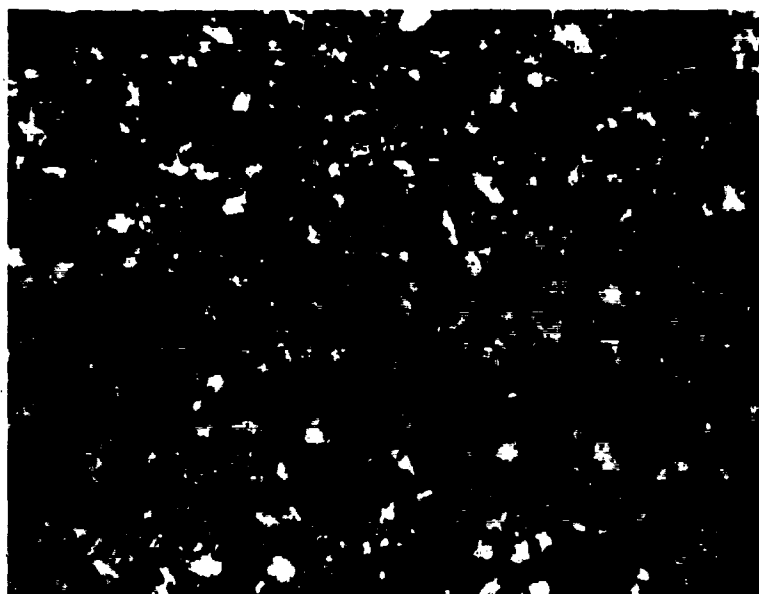


Figure 5. YB<sub>6</sub> (250X)



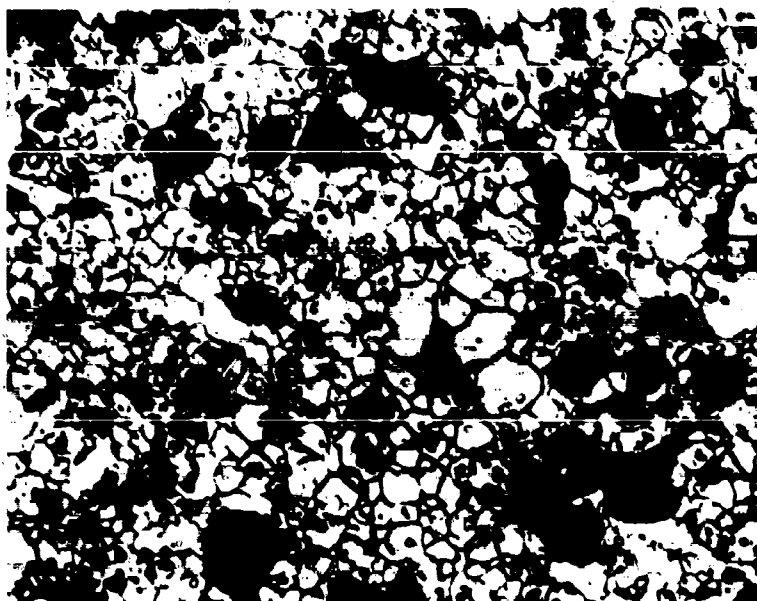


Figure 6.  $YB_6$  (500X)

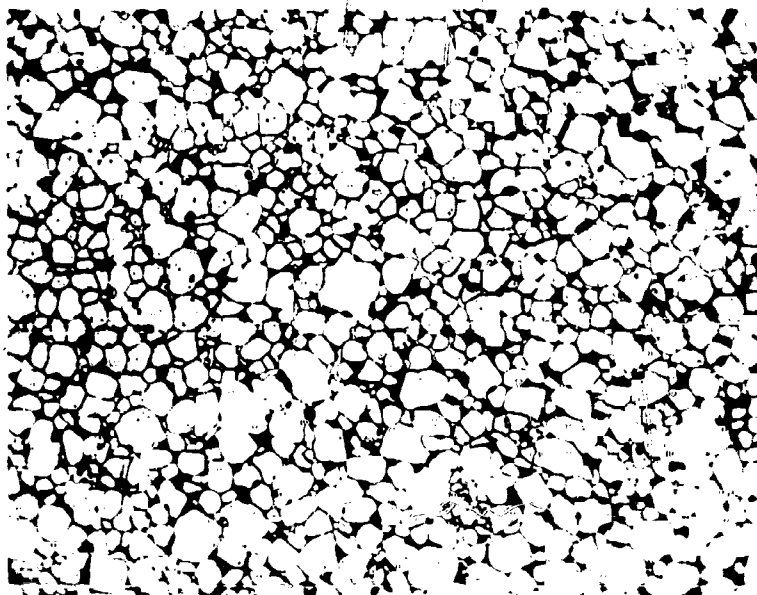


Figure 7.  $EuB_6$  (250X)

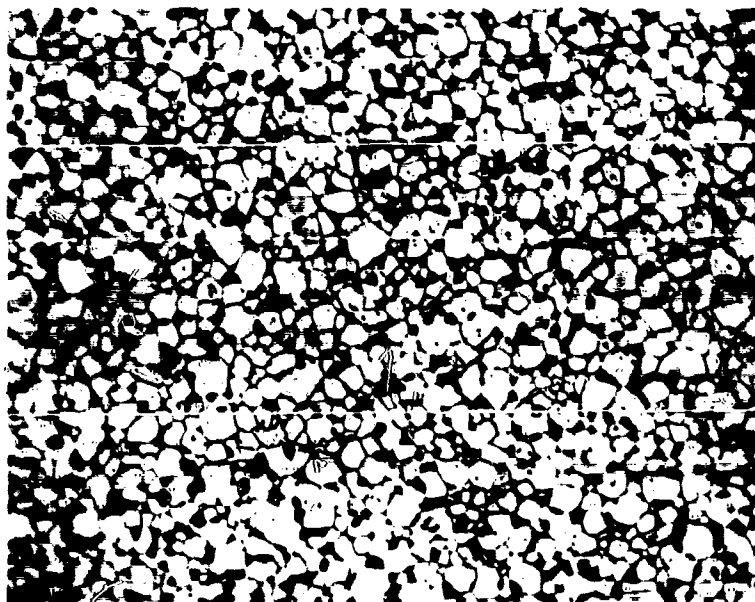


Figure 8. Eu B<sub>6</sub> (250X)

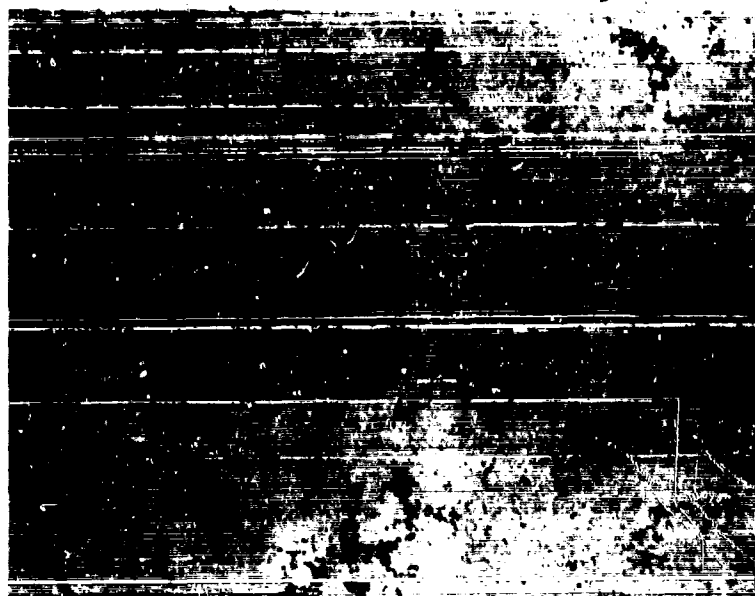


Figure 9. (UC) (ZrC) (250X)

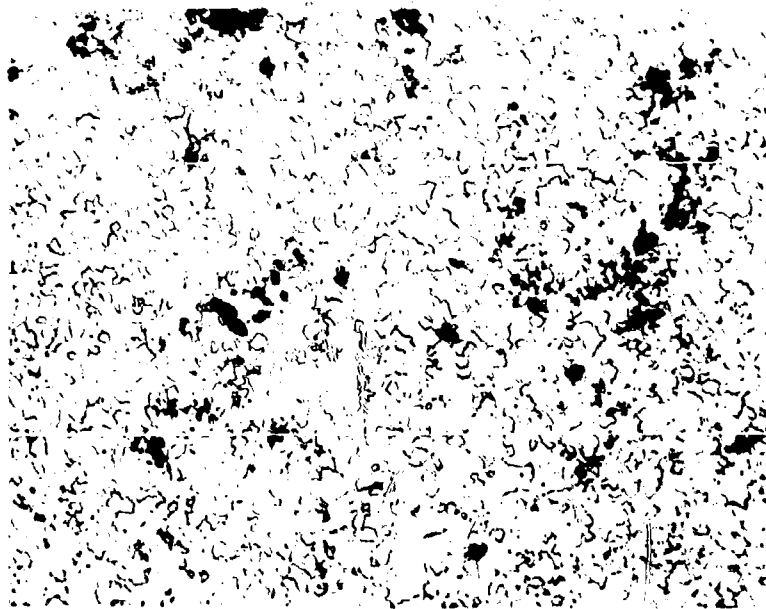


Figure 10. (UC) (ZrC) (250X)

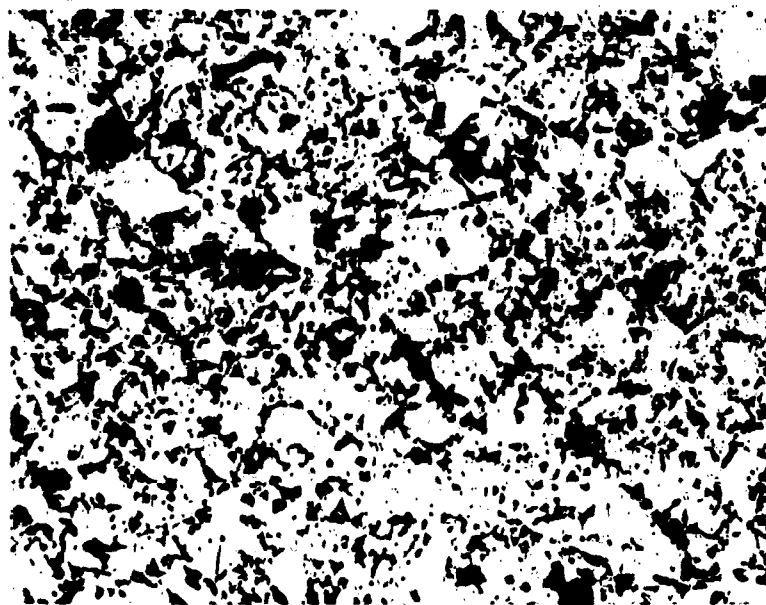


Figure 11. UC (250X)

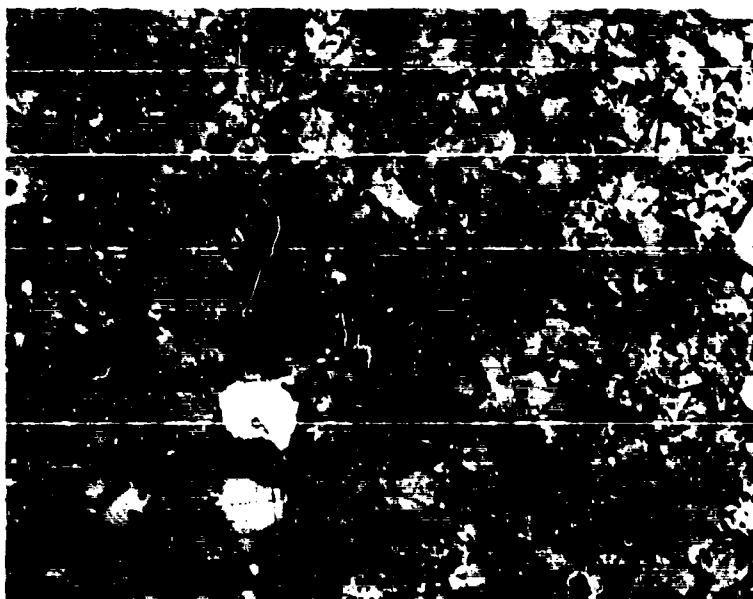


Figure 12. UC (250X)

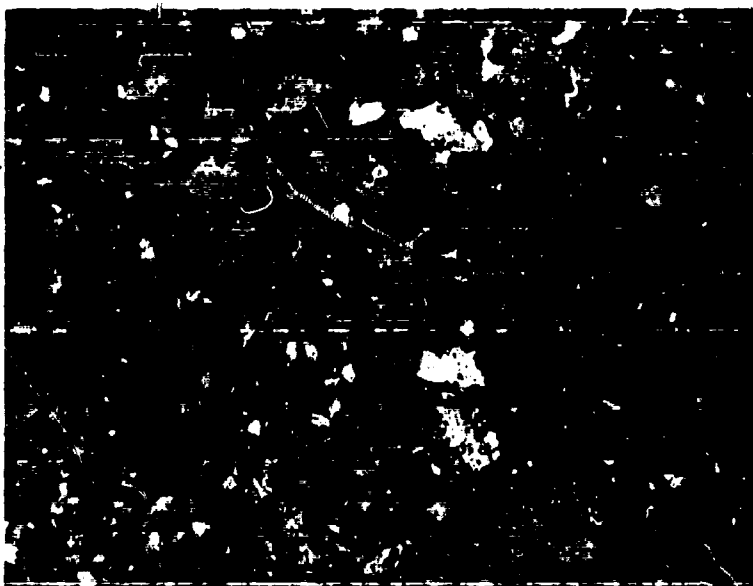


Figure 13. UC<sub>2</sub> (250X)

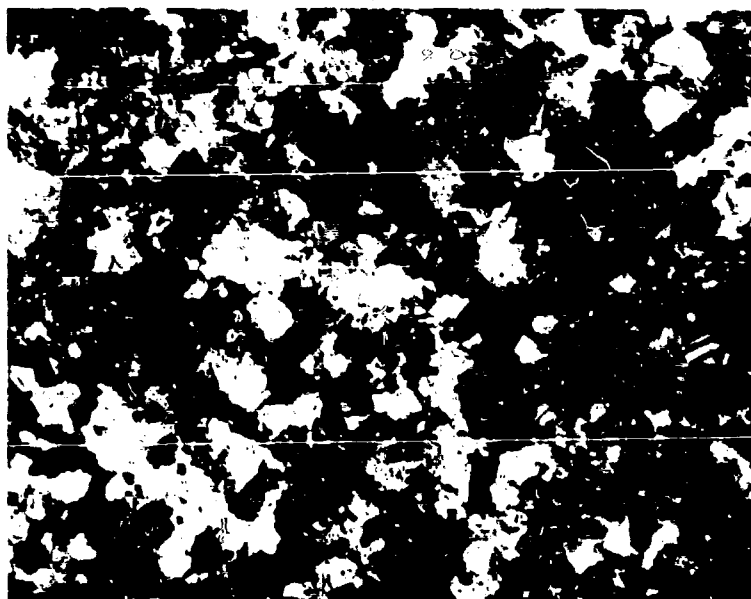


Figure 14.  $UC_2$  (250X)

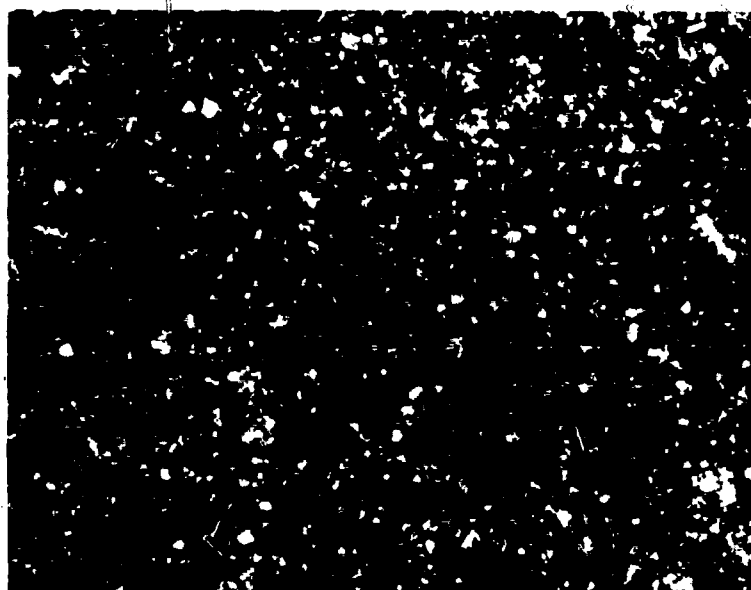


Figure 15.  $UC_2$  (250X)

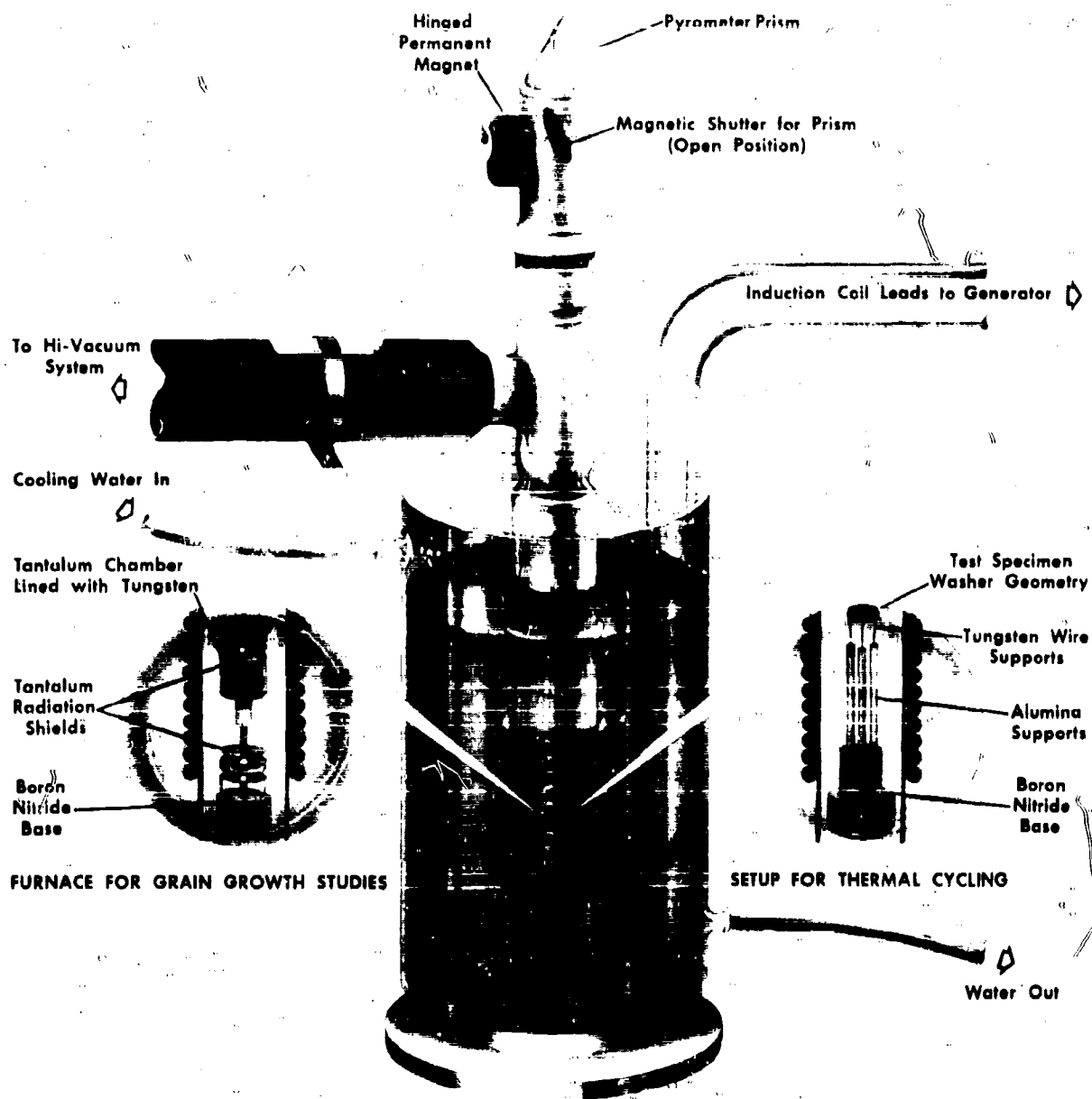


Figure 16. INDUCTION FURNACE FOR GRAIN GROWTH & THERMAL CYCLING

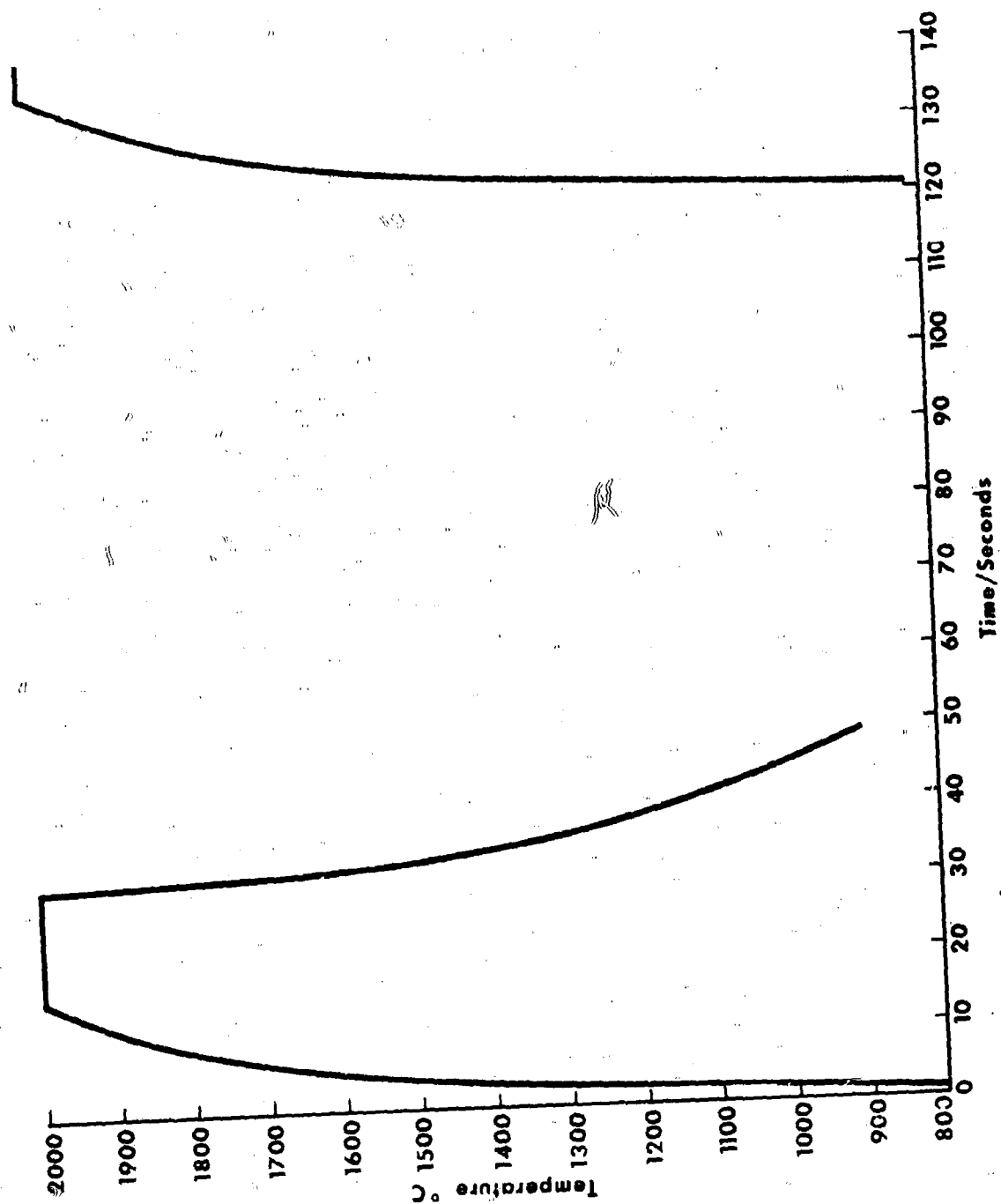
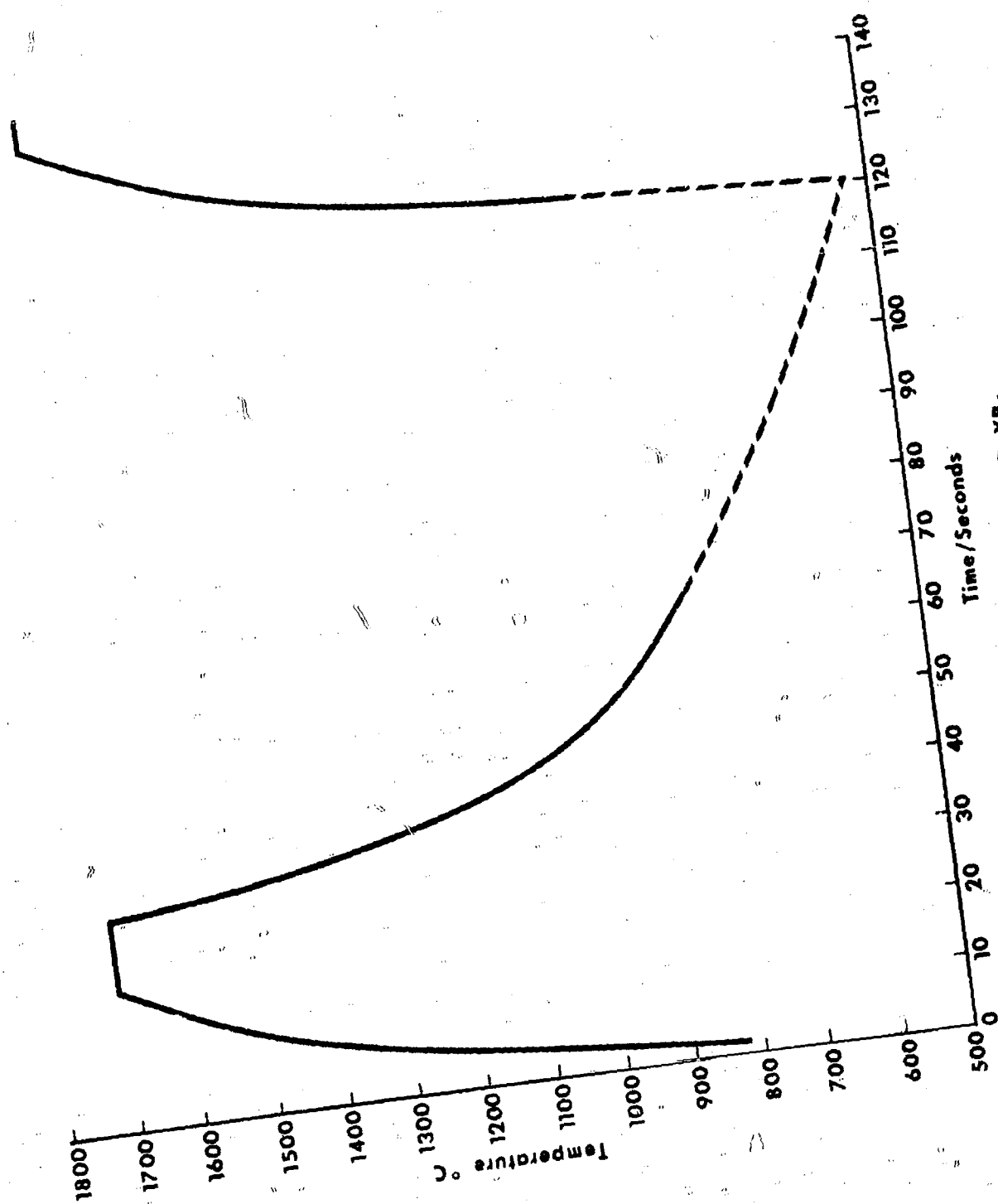
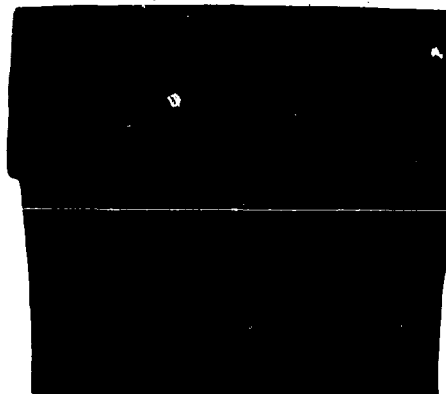


Figure 17. CYCLE FOR ZrC

Figure 18. CYCLE FOR YB<sub>6</sub>





**Figure 19. FRACTURE SURFACE OF Eu B<sub>6</sub>**



**Figure 20. FRACTURE SURFACE OF UC<sub>2</sub>**

SECTION VIII - FLEXURAL STRENGTH APPARATUS FOR USE TO 2000 C. - L. N. Grossman  
R. Ross

SYMBOL AND NOMENCLATURE

$\sigma$  = rupture modulus  
 $\sigma_0$  = rupture modulus at zero porosity  
 $P$  = volume fraction porosity

LIST OF ILLUSTRATIONS

<u>Figure No.</u>	<u>Title</u>	<u>Page No.</u>
1	Flexural Strength Apparatus	8-6
2a	Photoelastic Model of 3 Point Loading	8-7
2b	Photoelastic Model of 4 Point Loading	8-7
3	Millivolt Output vs Load	8-8
4	Plot of Cooling Conditions of Equipment	8-9
5	Rupture Modulus	8-10

### VIII. FLEXURAL STRENGTH APPARATUS FOR USE TO 2000 C - L. N. Grossman, R. Ross\*

#### A. Introduction

Transverse testing to determine the fracture strength of brittle bodies is generally preferred over tensile testing due to the difficulty of setting up a purely tensile load on a non-ductile specimen. Various methods have been employed and described; (1-6) however, none accommodate small reactive specimens at high temperatures. The need for testing small specimens has arisen from fabrication limitations on many interesting materials which are not readily formed into large, dense bodies. The present apparatus was designed and built for application to testing refractory intermetallics, borides, oxides, and carbides.

Three unique features have been incorporated in the apparatus: 1) hydrostatic balancing of the loading bars to assure symmetric loading; 2) accommodation of small specimens ( $3/4$  inch  $\times$  0.2 inch  $\times$  0.02 inch); and 3) direct reading load data from a pressure transducer in hydraulic balancing system. In addition, the specimen environment may be either vacuum or inert gas at temperatures up to 2000 C. All materials in the hot zone are refractory metals (W, Ta, or W-Ta alloys) so that reaction with furnace components or their vapors is minimized.

#### B. Summary

A hydrostatically balanced, 4-point flexural strength apparatus has been constructed for use with small, brittle specimens. Accurate temperature control, variable loading rate, and vacuum or inert gas atmosphere are features of this device. Results are presented for the porosity dependence of flexural strength for zirconium carbide.

The flexural strength apparatus has been proven usable to 1200 C. The furnace assembly has been heated to 1700 C with no specimens present. The sensitivity of the loading system is about 0.3 pounds while the maximum load is about 35 pounds per knife edge.

Data on the porosity dependence of the rupture modulus of ZrC has been obtained. The scatter in the data are comparable with that obtained by other investigators. The extrapolated value for the flexural rupture modulus of 100 per cent dense ZrC of grain size 3-4 microns is 50,000 psi.

The ZrC specimens appear well suited to further basic studies on the effects of temperature, porosity, grain size, and grain size distribution on strength. Studies at this laboratory have shown that control

---

\* Pyxis Automatic Control Systems, Berkeley, California

of grain size and porosity is possible by variation of the hot-pressing parameters. The lack of quantitative experimental and theoretical data on this subject require further exploitation of the equipment and technology developed for this program.

### C. Description of Apparatus

Figure 1 illustrates the major features of the flexural strength apparatus. The hydrostatically balanced loading heads are located in the hot zone of a tungsten hair-pin furnace which is enclosed in a water-cooled bell jar. The environment of the specimen may be either vacuum or inert gas. Temperature is measured by a W-W, 26 Kc thermocouple which is imbedded in a hole in the massive loading block immediately below the specimen. Probing of the hot zone with Pt. Pt - 10 Rh thermocouples has shown the sample to be within 30 C of the block temperature up to 1600 C.

Loading is of the four-point type. The advantages of this over three-point loading have been described considerably. (1, 7) and are illustrated in Figures 2a and 2b. Figure 2a is a photoelastic model of 3-point loading while 2b is the 4-point case. It is clear that 4-point loading results in a constant stress plateau between the two center knife edges. In the present apparatus, the upper knife edges are connected to two identical copper bellows. The bellows are filled with oil and connected hydraulically so that the load is equal on each of the knife edges regardless of the sample shape. The hydraulic system is also connected to a visual load indicator and to a pressure transducer (Schaevitz type PRBT-A-75). The output of the transducer may be read on a millivolt recorder. Figure 3 shows the millivolt output vs load on one knife edge. The minimum observable load is about 0.3 pound while the maximum load tolerable is about 35 pounds per knife edge. The lower load sensitivity limit is set by the elastic constant of the bellows, while the upper limit is set by the pressure limit of the bellows (60 psi). The knife edges are pivoted to provide a degree of rotational freedom to minimize torsion that may arise due to warped samples.

The knife edges are 1/8 inch rods which may be replaced without disturbing the loading members. Knife edge inserts used in this investigation were tungsten carbide. The loading members are machined tantalum or tantalum-tungsten alloy. An aluminum oxide thermal barrier exists in each loading member, located outside of the furnace proper. The barrier provides about 500 C temperature drop at sample temperatures near 1600 C. The upper and lower bearings are press-fitted into water-cooled brass fixtures.



Loading is accomplished by driving the pedestal at a predetermined rate through a copper bellows seal. The rates 0.025, 0.0125, and 0.0063 inches/min are obtainable by changing gears on the drive motor. Maximum temperature can be achieved in about 15 minutes using a kw power supply. The sample may be replaced with 30 minutes after maximum temperature is reached in vacuum and within 15 minutes of inert gas is present. Figure 4 shows a portion of the cooling curve for vacuum conditions.

### 1. Experimental

The long-range objective of this study is to examine the effect of temperature, grain size and porosity on the rupture modulus of some refractory borides and carbides. Determination of the temperature onset of ductile deformation will also be made, and some tensile deformation data obtained above that temperature. The present paper will describe results obtained on the porosity effect on the flexural strength of zirconium carbide.

Hot pressed ZrC discs 1 inch diameter by 1/4 inch thick were sliced on a thin blade diamond saw into 6 to 12 bars measuring about 1/4 inch  $\times$  0.4 inch  $\times$  3/4 inch. Surfaces were polished through 600 grit silicon carbide paper. The microstructure of the ZrC specimens showed them to be fine grained (3-4 $\mu$  average grain diameter), with uniform connected porosity throughout. By varying the fabrication pressure, the porosity could be controlled between 10 per cent and 40 per cent with no noticeable change in grain size. Chemical and x-ray analysis showed the specimens to be ZrC<sub>x</sub>, where  $x = 1.00 \pm 0.01$  mole fraction.

Figure 5 exhibits the results of breaking tests for ZrC specimens of differing porosity. The straight line drawn between the average moduli can be represented by

$$\sigma = \sigma_0 e^{-bP}$$

where

- $\sigma$  is the rupture modulus at any porosity,
- $\sigma_0$  is the modulus at zero porosity,
- $e$  is the natural logarithm base,
- $b$  is a constant, and
- $P$  is the volume fraction porosity.

The above equation for the strength dependence of porosity was proposed by Duckworth<sup>(8)</sup> and has been shown by Knudsen<sup>(9)</sup> to apply to much of the literature data. For the present investigation, the constant  $b = 3.25$ , while  $\sigma_0 = 50,500$  psi:

$$\sigma = 50,500 e^{-3.25P} \text{ psi.}$$

Limited elevated temperature studies have been completed on ZrC at this time. No significant decrease in modulus has been observed up to 700 C. Sparse data at 1200 C indicate some decreased strength at that temperature. These studies are continuing.

**REFERENCES**

1. J. P. Roberts and W. Watt, "Determination of Bend Strength and Bend Creep of Ceramic Materials", Trans. Brit. Ceram. Soc. 48, 343 (1949).
2. E. Ryshkewitch, "Modulus of Elasticity of Sintered Oxide Refractories", Ber. dent. Keram. Ges. 23, 243 (1942).
3. S. D. Mark, Jr., "An Apparatus for the Determination of the Moduli of Rupture and Elasticity in Cross Bending to 1500 C", Bul. Am. Ceram. Soc. 34, 203 (1950).
4. P. T. B. Shaffer, "Compact Apparatus for High Temperature Modulus of Rupture Measurement", Rev. Sci. Inst., 32, 794 (1961).
5. E. A. Bush and F. A. Hummel, "High Temperature Mechanical Properties of Ceramic Materials: 1. Magnesium Dilitanate", J. Am. Ceram. Soc., 41, 119 (1958).
6. M. C. Smith, D. M. Olson and H. L. Brown, "Testing Machine for Short-Time Creep and Stress-Rupture Testing at 2000 to 2500 C", Rev. Sci. Inst. 28, 543 (1957).
7. W. H. Duckworth, "Precise Tensile Properties of Ceramic Materials", J. Am. Cer. Soc., 34, 1 (1951).
8. W. Duckworth, "Discussion of the Ryshkewitch Paper", J. Am. Cer. Soc., 36, 68 (1953).
9. F. P. Knudsen, "Dependence of the Mechanical Strength of Brittle Polycrystalline Specimens on Porosity and Grain Size", J. Am. Cer. Soc., 42, 376 (1959).

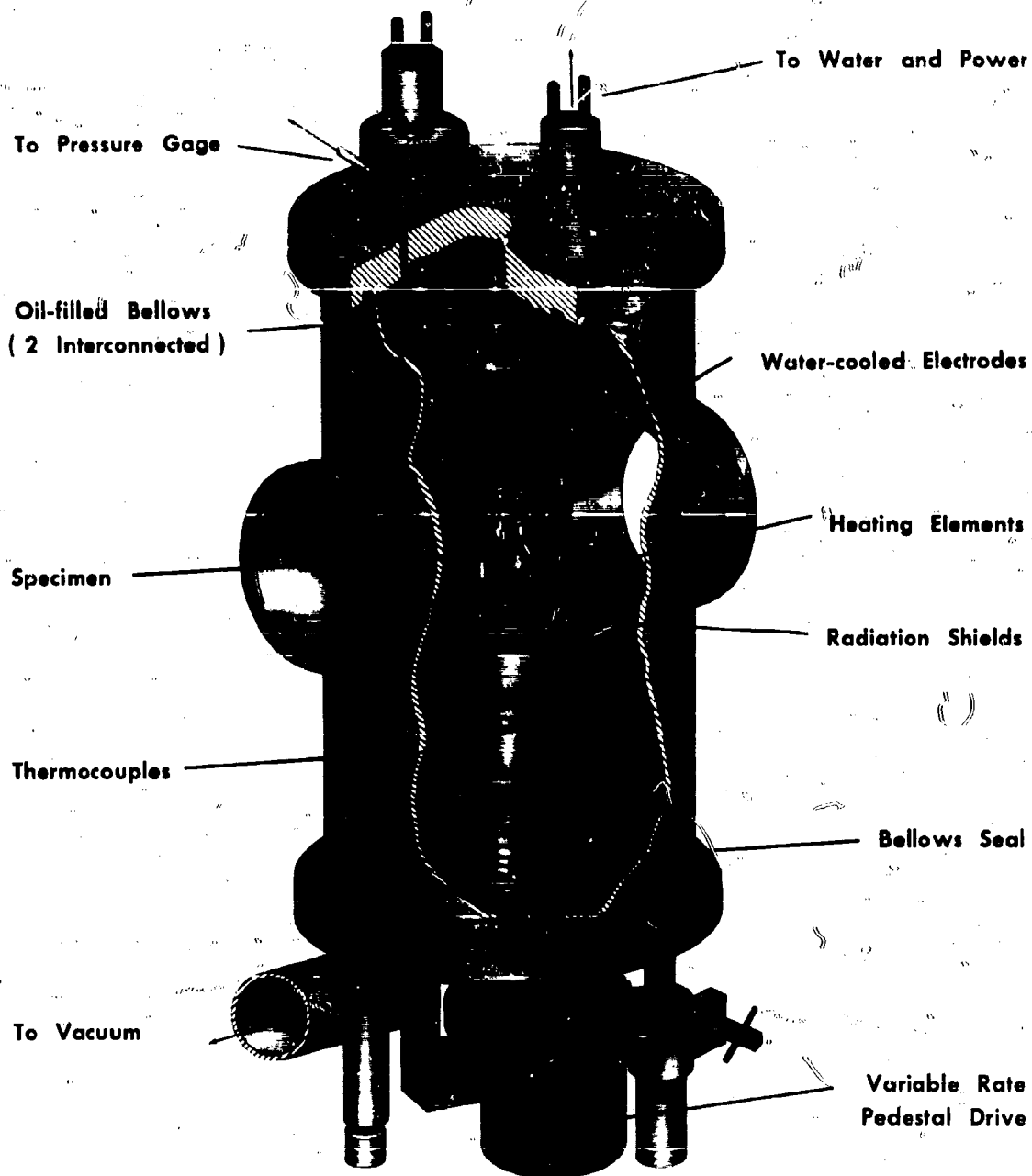
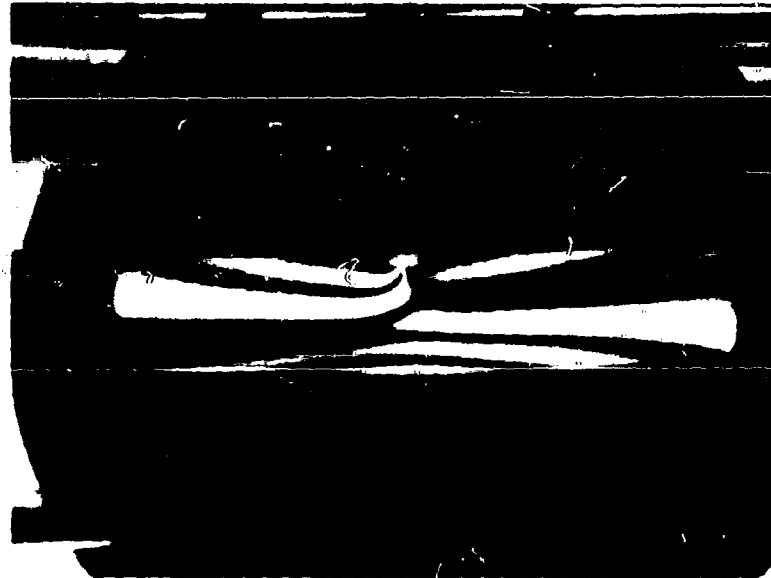
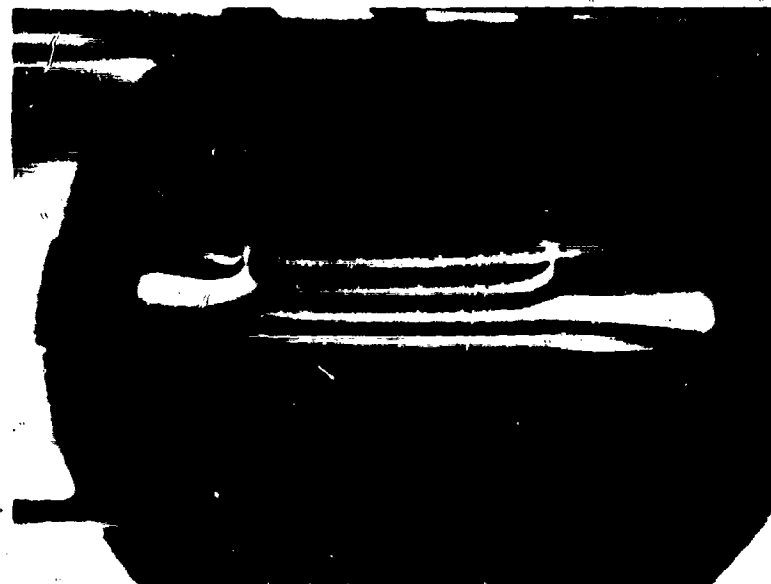


**Figure 1. HYDROSTATICALLY BALANCED HIGH-TEMPERATURE FLEXURAL STRENGTH APPARATUS**





c) Four-Point Loading



b) Three-Point Loading

Figure 2. PHOLOELASTIC MODELS OF STRESS IN 3-POINT AND 4-POINT LOADING

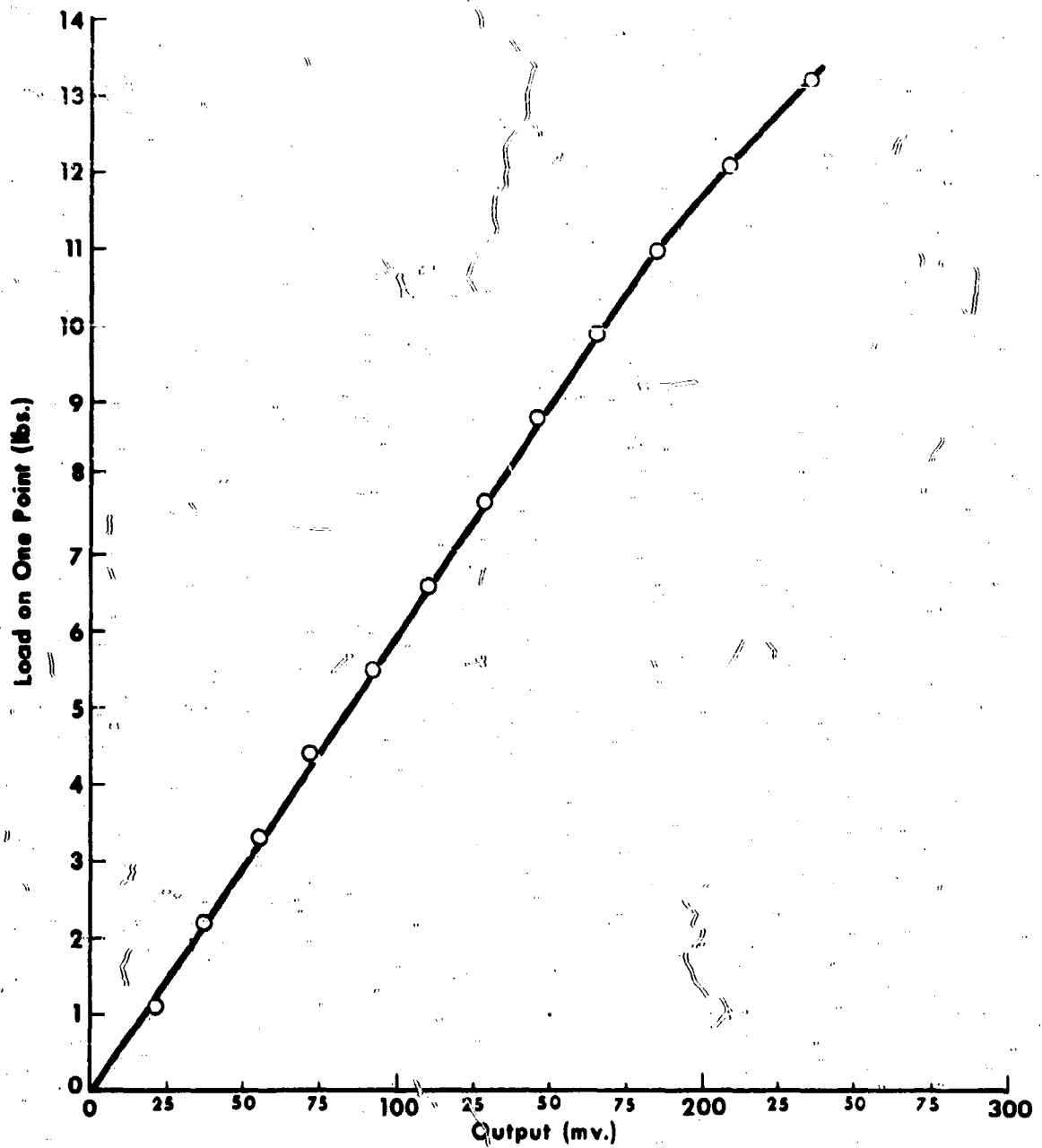


Figure 3. OUTPUT VERSUS LOAD

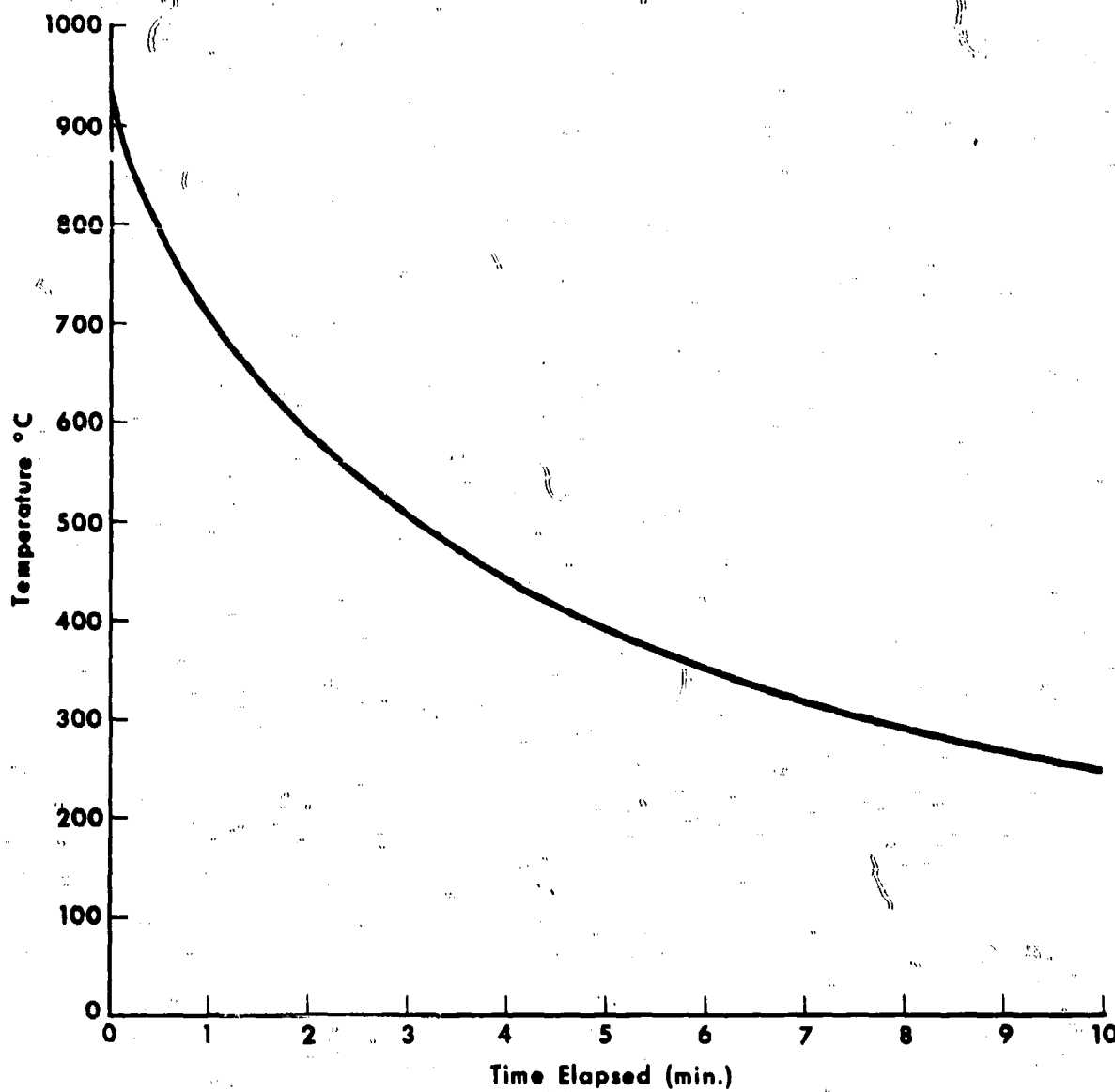


Figure 4. COOLING CURVE

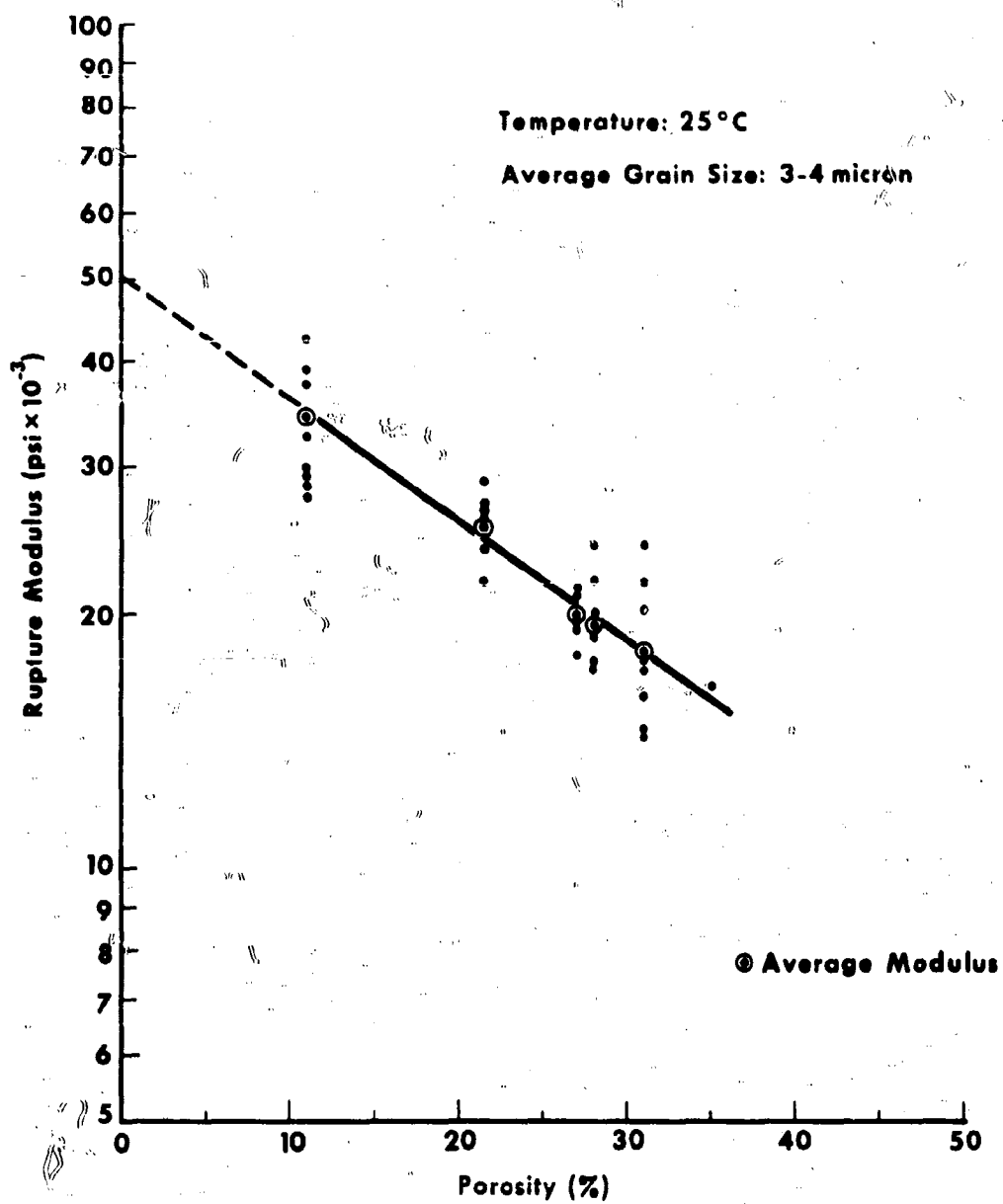


Figure 5. RUPTURE MODULUS VERSUS POROSITY FOR ZrC

**SECTION IX - PHYSIOCHEMICAL PROPERTIES OF SELECTED THERMIONIC EMITTER MATERIALS.****A. I. Kaznoff****L. N. Grossman****E. W. Hoyt****LIST OF ILLUSTRATIONS**

<b><u>Figure No.</u></b>	<b><u>Title</u></b>	<b><u>Page No.</u></b>
<b>1</b>	<b>Saturation Current Density Versus Sublimation Rate for <math>YB_6</math></b>	<b>9-13</b>
<b>2</b>	<b>Saturation Current Density Versus Sublimation Rate for <math>EuB_6</math></b>	<b>9-14</b>
<b>3</b>	<b>ZrC Spectral Emission Versus Time after Flashing</b>	<b>9-15</b>

**IX. PHYSIOCHEMICAL PROPERTIES OF SELECTED THERMIONIC EMITTER MATERIALS** - A. I. Kaznoff  
L. N. Grossman  
R. W. Hoyt

**A. Introduction**

During the course of the experimental work discussed throughout preceding sections of this report it became necessary to establish or review data on the physiochemical properties of the materials system being investigated. This section contains a discussion of the related work of the above nature which was performed during the contract period.

**B. Physiochemical Properties of Boride Thermionic Cathode Materials**

**1. Synthesis of  $YB_6$  and  $EuB_6$**

Through experience it has been established that the best technique of preparing single-phase  $YB_6$  is by the following reactions:

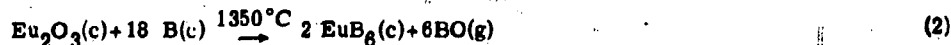


Other routes can be used and are being used at various laboratories. This synthesis was usually performed in a graphite crucible (coated with BN) in a vacuum induction furnace. In general the synthesis of one phase borides is difficult because the Y-B system has many intermediate phases such as  $YB_2$ ,  $YB_4$ ,  $YB_6$ ,  $YB_{12}$ . The latter three frequently occur together and considerable high temperature homogenization is necessary for stoichiometry control. Starting material purities are as follows:

B      99.6 - 99.9 per cent

$Y_2O_3$     99.9 + per cent

High temperature synthesis and fabrication improve the purity of the final product because most of the impurities are volatile at the high temperatures and vacuo used in their preparation. This is true for both  $YB_6$  and  $EuB_6$ . In the case of  $EuB_6$  the following synthesis was adopted.



The reactants are mixed in the weight ratio of 2:1 for  $Eu_2O_3:B$ . The reaction is carried out in BN crucibles in a tantalum resistance furnace in vacuo. In the case of  $YB_6$  and  $EuB_6$  synthesis, powders of about 325 mesh are used.

The oxide-boron route for  $\text{EuB}_6$  synthesis is relatively simple because the Eu-B system has only one reported stable intermediate phase:  $\text{EuB}_6$ . Attempts to synthesize other borides such as  $\text{EuB}_4$  have ended in failure.

The product  $\text{YB}_6$  and  $\text{EuB}_6$  are in the form of powder compacts which can be reduced to 325 mesh size quite readily for the hot pressing fabrication steps.

## 2. Fabrication of the Hexaborides

The powder hexaborides are fabricated into dense bodies by hot pressing in vacuum. The particular geometry fabricated is dictated by the end use of the material. The following are typical specimen shapes and sizes fabricated:

- a. 1/2 inch diameter pellets 1/8 - 1/4 inch thick for emission properties measurements, grain growth, sublimation, etc.
- b. 1/4 inch diameter rods up to 1-1/2 - 2 inches long for physical measurements, thermal and electric conductivities and total hemispherical emission.

The pellets are hot-pressed in graphite dies (Graphitite G) coated with boron nitride at temperatures ranging between 1500 - 1700 C. Nominal pressures are 4000-6000 psi and pressing times of 10-15 minutes. This method is highly successful with  $\text{YB}_6$ ; in the case of  $\text{EuB}_6$  the pellets are frequently cracked. Pellets of L/D ~ 1 are less susceptible to cracking in the case of  $\text{EuB}_6$ . A pellet of this type is cut into thin samples (1/8 inch thick) by means of an ultrasonic cutter using a boron carbide or silicon carbide slurry. Slicing of  $\text{YB}_6$  can be easily accomplished with cut-off blades (SiC or diamond wheels) while ultrasonic cutting has been found to yield the best results with  $\text{EuB}_6$  which has a tendency to chip and crack. Borides prepared in this manner have high densities: 92 - 96 per cent of theoretical density.

The 1/4 inch rods are more difficult to fabricate in the lengths required for measurements. Graphite dies are unsuitable because of large differences in thermal expansion (and interfacial reactions) which causes cracking of the specimen. Successful fabrication was accomplished by the use of molybdenum dies with tungsten plungers. The specimen has to be machined out of the die to prevent breakage. Evidence of reaction with Mo was noted.

Further fabrication steps are usually accomplished by ultrasonic techniques:

- a. Fabrication of washer geometries for sublimation and grain growth studies.
- b. Drilling half-body holes for temperature determination.

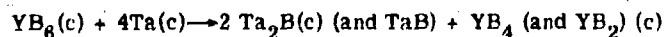
The surfaces of the specimens are generally finished by grinding, polishing, and ultrasonic cleaning.

### 3. Bonding Studies

In order to utilize the borides as emitters, it is desirable to bond these materials to refractory metal substrates. Such composites can then be fabricated into practical diode geometries or laboratory emission studies equipment. Tantalum and molybdenum were selected as substrate materials.  $YB_6$  was bonded to these materials by powder metallurgy techniques. This was accomplished by hot pressing the powders (325 mesh size) in a graphite die. The operation made use of an induction heated hot press at 1700 C - 2000 C and 5000 - 10,000 psi for a duration of 10-15 minutes. A sound bond was made between  $YB_6$  and tantalum. The reaction layer between the two materials was found to be primarily  $Ta_2B$  and  $TaB$  by x-rays. Bonding in the same manner to molybdenum was statistically less successful and the reaction zone between the two materials was less defined.

Bonding of  $EuB_6$  to Ta and Mo by powder metallurgy techniques was relatively unsuccessful. This was attributed to the strong reaction between the materials with the liberation of europium metal at the interface. Frequently a bond could be made but interfacial separation occurred after several hours in air at room temperature.

Bonding to cups of tantalum machined from solid stock was successful for  $YB_6$  and  $EuB_6$ . The borides were bonded as powders to the solid tantalum under the same conditions used in the other bonding studies. These composites are being used for electron emission studies. In order to gain more information on interfacial reactions between the hexaborides and tantalum powder compacts of the materials were hot-pressed. X-rays showed that the product was  $Ta_2B$  and  $TaB$ . The rare earth volatilized at the high temperatures and vacuum maintained in the experiment. Excess of tantalum was used and the fine powders used (325 mesh) allowed rapid and complete reaction. In practical configuration it can be postulated that in the case of  $YB_6$  the following reaction may take place at the Ta- $YB_6$  interface:





These reaction products are solids. It is, of course, noted that some yttrium is volatilized during the process. This appears to be the case when pressing  $YB_6$  in molybdenum dies. However, vapor or liquid formation with  $YB_6$  is not as dominant as in the case of  $EuB_6$ .

In the case of  $EuB_6$ , the following reaction appears very plausible:



Thus, one of the products is a liquid with a very high vapor pressure at the bonding temperature which results in bond weakness. Elemental europium is easily oxidized in air which can lead to interfacial bonding failures through the oxidation of europium metal in air.

#### 4. Sublimation Studies

One of the most important considerations in the use of a cathode is the evaluation of material loss as a function of temperature which in turn can be correlated with saturation currents obtainable from these materials.

In order to study this Langmuir type experiments were carried out. Pellets of  $YB_6$  were cut ultrasonically to form washers. The typical dimensions were 0.5 inch O.D., 0.25 inch I.D., 0.050 - 0.125 inch thick. These were supported by tungsten rods with point contacts. The material was placed in an induction heated vacuum furnace equipped with a copper, water cooled, concentrator. The temperature capability of the furnace is in excess of 2700 C. Measurements were carried out in the temperature range of 1550 - 2000 C. Experiments showed that the specimens had a tendency to crack at temperatures in excess of 1900 C. Over 20 determinations were made in the above temperature range. Examination of the specimens after heating revealed that the surface changed from a characteristic blue-black of  $YB_6$  to reddish-gold, typical of the  $YB_4$  phase. X-rays confirmed the fact that the surface layer was  $YB_4$  and the substrate was  $YB_6$ . Sublimation tests around 1600 C showed a gradual decrease in the rate of loss of material which settled to a constant rate in a period of several hours.

This is interpreted to be the result of build-up of the porous  $YB_4$  layer. Higher temperature runs did not exhibit this behavior as a steady state was achieved in time intervals measured in minutes. The presence of a surface layer of  $YB_4$  on  $YB_6$  was also observed by E. Hoyt (1) in previous sintering studies of  $YB_6$  powder compacts. In order to obtain true temperature of the heated  $YB_6$  specimens a black body hole was drilled in the specimen.

Surface temperatures and hole temperatures were measured in the range of 700 - 1900 C which allowed the determination of true temperatures in the sublimation studies. Spectral emission of 0.80 (at 0.65 microns) was determined. This is at variance with the 0.70 value reported by (2), G. A. Kudintseva. The weight loss can be represented by the following equation:

$$w \frac{\text{gms}}{\text{min cm}^2} = \frac{A}{\sqrt{T}} e^{-E/T}$$

where  $A = 8.36 \times 10^5$   $E = +37,400$  ( $\Delta H = 74,300$  k cal)

This equation cannot be used to obtain thermodynamic data as the surface area was established macroscopically and the true surface area could be greater by as much as one or two orders of magnitude. Furthermore, the presence of the adherent surface layer of  $YB_4$  does not allow an unequivocal interpretation. The weight loss equation represents, therefore, the steady state weight loss of 95 per cent dense  $YB_6$  in the range of 1600 - 2000 C. Several Knudsen cell determinations have been carried out but the results are too meager at this time. The formation of  $YB_4$  was confirmed in the effusion studies in the range of 1600 - 1700 C.

Since the hexaborides are highly susceptible to oxidation, with the formation of borates, at temperatures above 1000 C a good vacuum is essential in all sublimation studies. Borate formations may give low sublimation rates at low temperatures and higher than normal rates at high temperatures by the volatilisation of boron oxides. Low temperature runs in a poor vacuum showed that  $Y_2O_3$  formed on the surface. At higher temperatures only  $YB_4$  was formed.

The results of this study justify the conclusion that the following reaction occurs at high temperatures.



Collected sublimate appeared to be predominantly amorphous boron. Boron is the major constituent by spectroscopic examination and yttrium is very strong. Free boron was not detected in the solid samples after sublimation tests. Higher borides such as  $YB_{12}$  were also absent. Since gaseous species such as  $MB_6$  and  $MB_4$  have never been reported, it is reasonable to assume the vapor species are predominantly elemental boron and yttrium, with the former dominating the latter. Similar sublimation runs have been made on  $EuB_6$  specimens.

The weight loss can be represented by the following equation:

$$w \left( \frac{\text{gms}}{\text{min cm}^2} \right) = \frac{A}{\sqrt{T}} e^{-E/T}$$

where  $A = 3.03 \times 10^6$   $E = +39,000$

These sublimation studies indicated that the volatilization proceeds by the following reaction:



Spectral emission is not available at this time. No surface reaction product similar to  $\text{YB}_4$ , in the case of  $\text{YB}_6$  sublimation, has been observed. This confirms again earlier observations of E. W. Hoyt (1).

The results of these investigations point out very large differences in the volatilization behavior of the hexaborides. Lafferty (3) pointed out that  $\text{LaB}_6$  loses lanthanum metal when heated in vacuum. Samsonov (4) erroneously assumes that  $\text{SrB}_6$  volatilizes as  $\text{SrB}_6(\text{g})$ , and reports his Langmuir experiments on 90 per cent dense material as a thermodynamic determination of the heat of sublimation based on the above assumption. The main conclusion that needs to be drawn at this time is that no generalization can be made for hexaborides, even for hexaborides of the lanthanides.

The correlation of saturation emission current with sublimation rate for  $\text{YB}_6$  is shown in Figure 1. This material needs considerable space charge neutralization for the high current densities as surface ionization of cesium cannot be used to achieve this. Similar data for  $\text{EuB}_6$  is given in Figure 2. The high work function of  $\text{EuB}_6$  suggests that this material could be used in a cesium diode. The electron emission data was taken from Samsonov (5).

##### 5. Compatibility of the Hexaborides with Cesium

In order to evaluate the potential of utilizing the borides in cesium thermionic converters, tests were carried out to check if these materials are attacked by cesium.

Preliminary results on a test run at 1000 C for 350 hours are now available. The cesium pressure was nominally 1.82 torr (300 C). The following samples were tested:

2(two) composite specimens  $\text{YB}_6$  - Ta

1(one)  $\text{YB}_6$  pellet

1(one) composite  $\text{YB}_6$  - Mo

1(one) composite  $\text{EuB}_6$  - Ta

The results showed that the borides were not attacked by cesium. All of  $YB_6$  composites failed at the interface. The  $EuB_6$  - Ta composite remained sound. This was probably a result of a specially designed tantalum support. X-rays showed the presence of  $Y_2O_3$  at the interfaces of  $YB_6$  - Ta. This leads to the supposition that reaction between these materials is possible at 1000 C. The reaction products (Y metal) caused the interfacial failure. This failure actually was observed during the disassembly of the compatibility test chamber in vacuum dry box (under argon) so that the separation was caused during the test and not as a result of subsequent exposure to air. The results to date indicate that the borides have good possibilities in cesium converters but that the bonding of borides to refractory metals is not satisfactory although the soundness of  $EuB_6$  - Ta indicated that these problems may be circumvented, at least partially, by appropriate design of the composite structure. The test also showed that all tantalum surfaces were carburized. The cesium test chamber was constructed of the following materials:

- a. Contact with liquid cesium
  - 1) 304 S.S.
  - 2) OFHC copper  
(nickel plated on the exterior)
- b. Contact with cesium vapor
  - 1) 304 S.S.
  - 2) Inconel
  - 3) Tantalum

The mechanism of carbon transport has not been established.

The carbon sink was tantalum as  $Ta_3C$  formation was observed and confirmed by x-rays. The mode of transport is at the moment obscure. The test chamber components were all carefully cleaned and baked before the introduction of liquid cesium. The procedures followed closely paralleled those used in the electronic tube manufacture.

#### 6. Summary of Physicochemical Properties

Some of the basic properties of  $YB_6$  and  $EuB_6$  are given below:

	<u><math>YB_6</math></u>	<u><math>EuB_6</math></u>
Weight Per cent Boron	42.19	29.8
Crystal Structure	cubic	cubic
Lattice parameter	4.128	4.178
Density ( $\frac{gms}{cc}$ )	3.75	4.95
Melting point or peritectic	2600°C(P)	2200°C

	<u>YB<sub>6</sub></u>	<u>EuB<sub>6</sub></u>
Color	Blue-violet	Blue
Electrical resistivity micro ohm-cm at 298°K	10.4	3100
Richardson-Dushman	$2.31 \times 10^{-4}T$	$5.0 \cdot 2 \times 10^{-4}T$
Work function $\phi_{120}$ (ev)	(1200-1450°K)	

## 7. References

1. E. W. Hoyt, unpublished experimental data on boride sintering.
2. G. A. Kudintseva, B. M. Tsariv, Radiotekhnika i Elektronika 3, 428 (1958).
3. J. M. Lafferty, J. Appl. Phys. 22, 299 (1951).
4. G. V. Samsonov, I. I. Serebryakova, A. S. Bolyar, Zhur. Neorg. Khim, 6, 2243-8, October 1961.
5. G. V. Samsonov, L. Y. Markovski, A. F. Zhigach, M. G. Valiashko, "Boron, Its Compounds and Alloys". Akad. Sci. Ukr. SSR, Kiev 1960.

## C. Oxidation and Evaporation Characteristics of Carbide and Boride Materials

The following analysis and estimate of oxidation and evaporation characteristics of carbides and borides served as a guide for the high temperature experimental measurements involved in this program.

At sufficiently low temperature, a clean reactive surface will become oxidized at a rate determined by the arrival rate of oxygen at the surface. This sets the maximum rate of oxide formation. The true rate of formation is less than the oxide arrival rate by the rate of decomposition (evaporation) of the oxide. The foregoing argument implies that at sufficiently low temperatures, the rate of formation is independent of material; i. e. as long as an oxide-former is heated in oxygen, the rate of formation of the initial oxide layer is solely a function of pressure (at sufficiently low temperature).

The arrival rate of oxygen molecules near room temperature and at a pressure P(mm Hg) is given by kinetic theory roughly as

$$\frac{N}{T} \left( \frac{\text{molecules}}{\text{cm}^2 \text{ sec}} \right) \approx 10^{20} P_{\text{mm}} \quad (1)$$

For example, at  $10^{-6}$  mm Hg, a surface  $1 \text{ cm}^2$  will be impinged upon  $10^{16}$  times in about 100 seconds. If this surface reacts with oxygen, and if the "accommodation coefficient" for the surface is unity, a

monolayer of oxide will form within 100 seconds. In order for a surface to survive 1000 seconds with negligible monolayer formation, a vacuum of about  $10^{-8}$  mm Hg is required by this analysis.

The rate of reaction product build-up on ZrC in a dynamic vacuum of  $5 \times 10^{-7}$  torr can be seen qualitatively in Figure 3. To obtain this data, the specimen was flashed to 2400 K and then cooled in less than 10 seconds to about 1400 K. The increase in spectral emission with time is indicative of the formation of an optically thick layer of reaction product on the ZrC surface. From the preceding analysis, it is seen that a layer about  $10^3$  monolayers thick is optically thick at  $0.65\mu$ .

The maximum rate of departure of an oxide from surface is given by the total decomposition pressure (or vapor pressure) of the oxide. The stable oxides exhibit a vapor pressure above  $10^{-6}$  mm Hg, above some temperature which lies between 1800 K and 2200 K. For example, the vapor pressure of  $ZrO_2$  exceeds  $10^{-6}$  mm Hg above  $2000\text{ K} \pm 100\text{ K}$ ; therefore, a clean ZrC surface should remain clean above  $2000\text{ K} \pm 100\text{ K}$  in a pressure of  $10^{-6}$  mm Hg of oxygen. The maximum rate of departure of a thick oxide layer is given by Knudsen's formula:

$$G = 44 \cdot 10^{-6} \sqrt{\frac{M}{T}} P \left( \frac{\text{gm}}{\text{cm}^2 \text{ sec}} \right) \quad (2)$$

where

$G$  is the mass of evaporating species

$M$  is the average molecular weight of evaporating species

$T$  is the temperature (K), and

$P$  is the total decomposition pressure of the evaporating compound at the temperature  $T$ .

It is clear from the above formula that flashing to high temperature is not necessarily a cure-all if considerable oxide is present; the time at high temperature is an important factor.

For practical application with the subject materials, the following general rules should apply:

1. Oxides (or borates) will form at a rate given roughly by equation (1) at temperatures above room temperature and such that the vapor pressure of the oxide is less than that of oxygen in the system.
2. The oxides or borates will decompose at temperatures such that the vapor pressure of the oxide is greater than that of oxygen in the system. The maximum rate of weight loss is given by equation (2).

Experimental evidence of temperatures sufficiently high to decompose three oxides has been obtained in this laboratory:  $ZrC$  "cleans up" above 2100 K in  $10^{-6}$  mm Hg vacuum;  $YB_6$  and  $EuB_6$  "clean up" above 2000 K in  $10^{-4}$  to  $10^{-5}$  mm Hg. The rate of clean up has not been tabulated.

From the stability of the product oxides, it appears that one should be able to clean up UC,  $(U, Zr)C$ ,  $UC_2$ ,  $ThC$ , and  $ThC_2$  above 2100 K in a vacuum of  $10^{-6}$  mm Hg. The length of time one must remain at that temperature is dependent on the amount of oxide present; that is, on the length of time the specimen has been exposed to  $10^{-6}$  mm Hg of oxygen at oxidizing temperatures (i.e. approximately 400 K to 1900 K).

The evaporation rates of some bulk materials are given below:

Material	Evaporation Rate
$YB_6^*$	$W \left( \frac{\mu m}{min \text{ cm}^2} \right) = \frac{8.36 \times 10^5}{\sqrt{T}} e^{-\left(\frac{37,400}{T}\right)}$
$EuB_6^{**}$	$W \left( \frac{\mu m}{min \text{ cm}^2} \right) = \frac{3.03 \times 10^6}{\sqrt{T}} e^{-\left(\frac{37,000}{T}\right)}$
$UC_2$	$\log P_U (\text{atmos}) = -\frac{30,600}{T} + 6.36$
$ZrC$	$\log P_{Zr} (\text{atmos}) = -\frac{38,600}{T} + 7.73$
$(U_{0.9}Zr_{0.1})C$	$\log W \left( \frac{mg}{cm^2 \text{ sec}} \right) = -\frac{30,500}{T} + 9.7$
$(U_{0.2}Zr_{0.8})C$	$\log W \left( \frac{mg}{cm^2 \text{ sec}} \right) = -\frac{30,300}{T} + 8.3$

The thorium carbides will lose weight a little faster than their UC counterparts.

\* $YB_6$ : This material when exposed to vacuum at high temperature sublimates quite readily. Our Langmuir experiments gave the following result:

$$W \frac{\text{gms}}{\text{min cm}^2} = \frac{8.36 \times 10^5}{\sqrt{T}} e^{-\frac{37400}{T}}$$

YB<sub>3</sub> does not sublime congruently. YB<sub>4</sub>, reddish-gold material, builds up on the surface at high temperatures (above 1500 C and probably at lower temperatures). Our studies showed that YB<sub>4</sub> formed as a porous layer on the surface. It was visible in about 1/2 hour at 1500 C and in a matter of minutes at 2000 C. Initial sublimation rates at the lower temperatures were higher in the initial stages due to the sublimation of impurities from the borides. High temperature sublimation rates were fairly constant with time. Our experiments were run under a nominal vacuum of 10<sup>-5</sup>-10<sup>-6</sup> torr. True pressure could exceed these values by a factor of ten. These pressures are unsatisfactory because residual oxygen caused oxidation of the surface of YB<sub>3</sub>. A layer of Y<sub>2</sub>O<sub>3</sub> formed. At high temperatures this did not occur and only YB<sub>4</sub> was observed on the surface.

The spectral emission from YB<sub>3</sub> (with a YB<sub>4</sub> layer) is around 0.80 at 0.85 microns. The room temperature electrical resistivity is about 10 micro ohms cm. The material is metallic and the Wiedemann-Franz ratio may be used for hi-temperature extrapolation and approximation of the thermal conductivity. The electron emission data is reported as

$$J = AT^2 e^{-\phi/T}$$

$$A = 20 \quad \phi = 2.22 \text{ volts}$$

Measurements were made up to about 1750 K. At high temperatures used in emission studies it can be expected that some interfacial reaction between YB<sub>3</sub> and Ta will occur. Liberation of Y metal may occur.

**\*\*EuB<sub>6</sub>:** This material sublimates congruently. Therefore no compositional changes on the surface can be expected due to sublimation. A possibility of contamination by Europium metal film on the surface exists as EuB<sub>6</sub> will react with Ta at high temperatures. The sublimation rate determined here is as follows.

$$W \frac{\text{gms}}{\text{min cm}^2} = \frac{3.05 \times 10^6}{\sqrt{T}} e^{-39000/T}$$

The electrical resistivity at room temperature is about 3100 micro ohms-cm. EuB<sub>6</sub> is far more brittle than YB<sub>6</sub>. It is also less stable in a mechanical sense at high temperatures. We found that washers of EuB<sub>6</sub> fractured when 1900 C was exceeded. The reported work function is about 5.0 e.v.



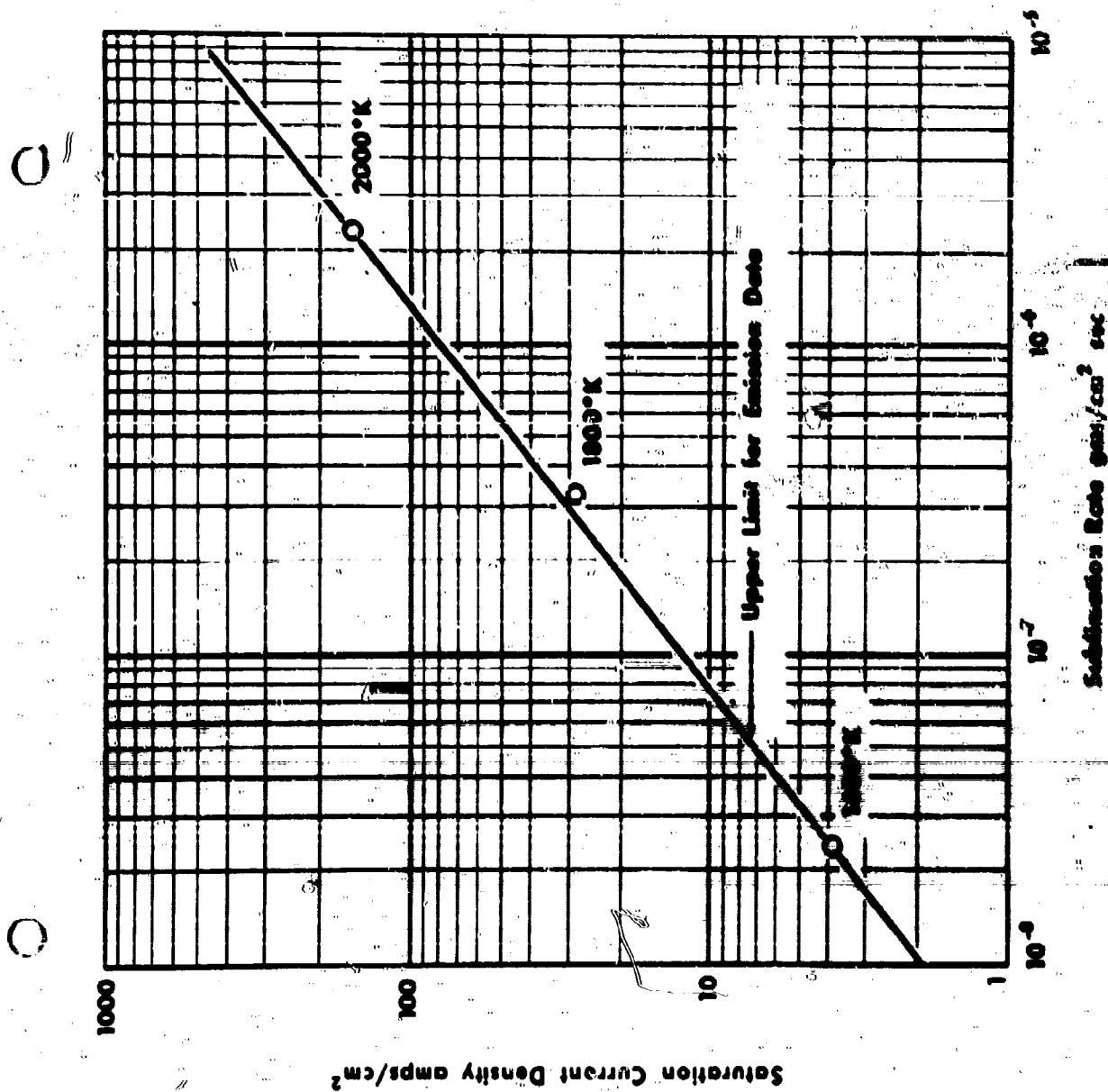


Figure 1. SATURATION CURRENT DENSITY VERSUS SUBLIMATION RATE FOR YB.

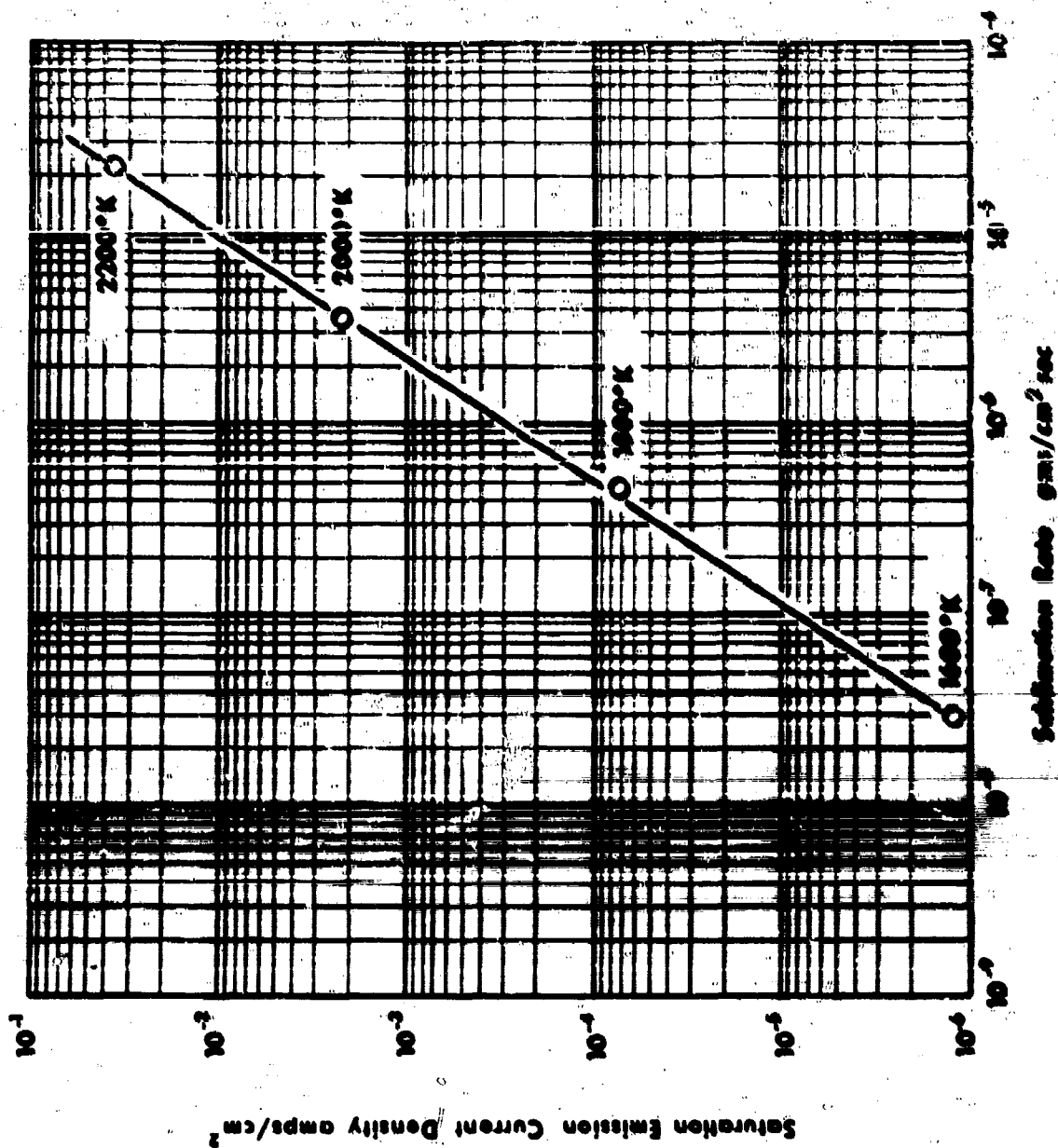


Figure 7. SATURATION CURRENT DENSITY VERSUS SUBLIMATION RATE FOR E-9.

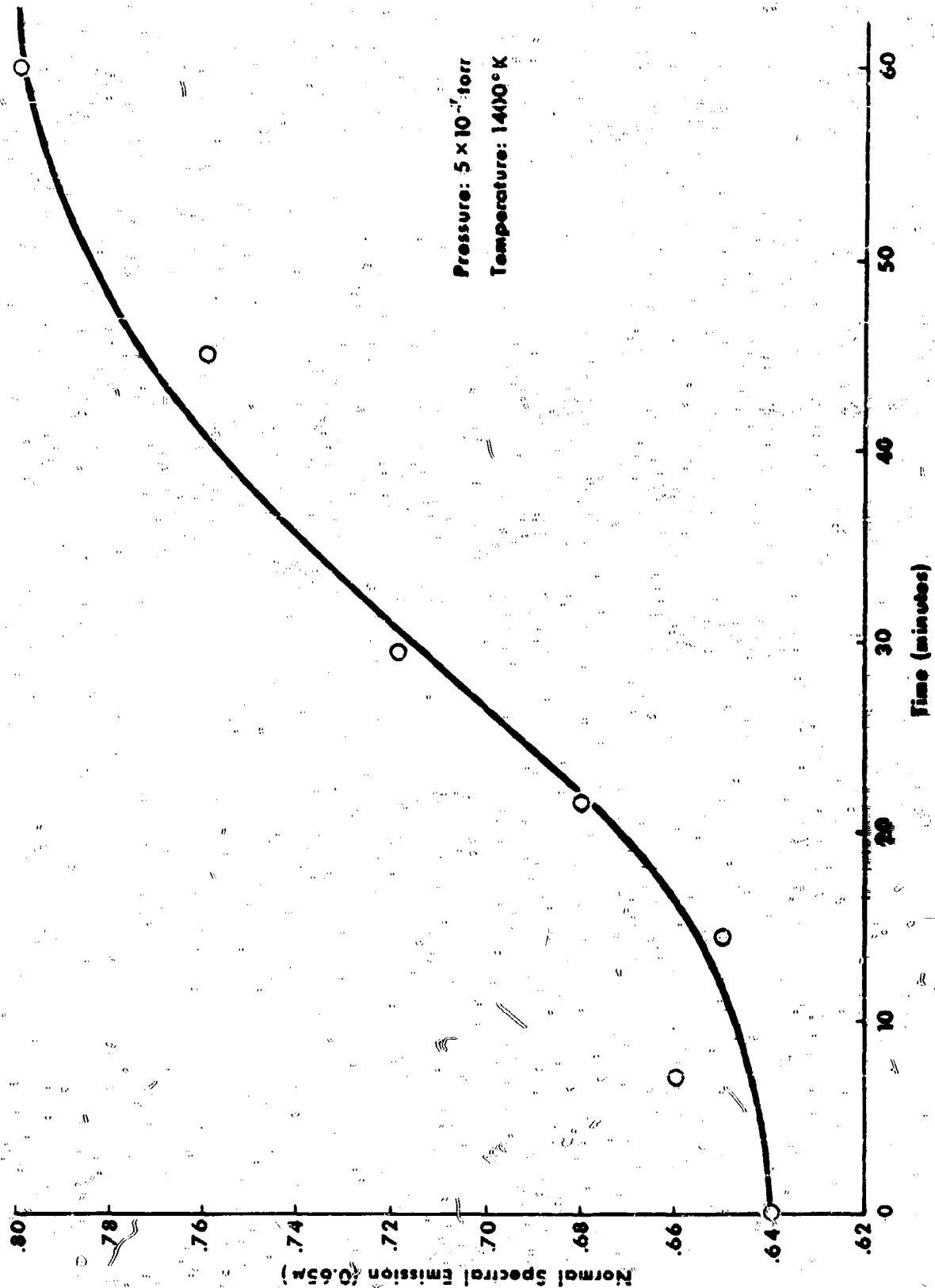


Figure 3. ZnC SPECTRAL EMISSION VERSUS TIME AFTER FLASHING

**X. ACKNOWLEDGMENTS**

The authors gratefully acknowledge the continuing interest and support of the program by Dr. John Huth of the Advanced Research Project Agency and Dr. B. Rosenbaum of the U. S. Bureau of Ships. We would also acknowledge the special assistance given by many Vallecitos Atomic Laboratory personnel --- to Dr. L. P. Bupp and A. N. Holden for their managerial support, encouragement, and review -- to Dr. R. Rollins, D. R. Lewis, P. Waskevich and W. V. Cummings for technical assistance, metallographic services, chemical analysis, and x-ray diffraction analyses respectively and to J. R. Balch, J. G. Wilson, F. Ziskind, R. E. Blood, and S. D. Harrington for continued technician assistance throughout the course of the program.

**UNCLASSIFIED**

**UNCLASSIFIED**